40517

National Library of Canada / Bibliothèque nationale du Canada

CANADIAN THESES ON MICROFICHE / THÈSES CANADIENNES SUR MICROFICHE

NAME OF AUTHOR/*NOM DE L'AUTEUR* MR REX C.H. TSE

TITLE OF THESIS/*TITRE DE LA THÈSE* Studies of the strength of rough rock surfaces in shear

UNIVERSITY/*UNIVERSITÉ* U. of Alberta

DEGREE FOR WHICH THESIS WAS PRESENTED/ *GRADE POUR LEQUEL CETTE THÈSE FUT PRÉSENTÉE* M. Sc.

YEAR THIS DEGREE CONFERRED/*ANNÉE D'OBTENTION DE CE GRADE* 1979

NAME OF SUPERVISOR/*NOM DU DIRECTEUR DE THÈSE* DR D.M. Cruden

Permission is hereby granted to the NATIONAL LIBRARY OF CANADA to microfilm this thesis and to lend or sell copies of the film.

The author reserves other publication rights, and neither the thesis nor extensive extracts from it may be printed or otherwise reproduced without the author's written permission.

L'autorisation est, par la présente, accordée à la BIBLIOTHÈQUE NATIONALE DU CANADA de microfilmer cette thèse et de prêter ou de vendre des exemplaires du film.

L'auteur se réserve les autres droits de publication; ni la thèse ni de longs extraits de celle-ci ne doivent être imprimés ou autrement reproduits sans l'autorisation écrite de l'auteur.

DATED/*DATÉ* 3rd Nov. 78 SIGNED/*SIGNÉ* (Rex Tse)

PERMANENT ADDRESS/*RÉSIDENCE FIXÉ* 7708 - 82 AVE.
EDMONTON T6C 0X9
ALBERTA CANADA

NL-91 (3-74)

National Library of Canada

Cataloguing Branch
Canadian Theses Division

Ottawa, Canada
K1A 0N4

Bibliothèque nationale du Canada

Direction du catalogage
Division des thèses canadiennes

NOTICE

The quality of this microfiche is heavily dependent upon the quality of the original thesis submitted for microfilming. Every effort has been made to ensure the highest quality of reproduction possible.

If pages are missing, contact the university which granted the degree.

Some pages may have indistinct print especially if the original pages were typed with a poor typewriter ribbon or if the university sent us a poor photocopy.

Previously copyrighted materials (journal articles, published tests, etc.) are not filmed.

Reproduction in full or in part of this film is governed by the Canadian Copyright Act, R.S.C. 1970, c. C-30. Please read the authorization forms which accompany this thesis.

THIS DISSERTATION
HAS BEEN MICROFILMED
EXACTLY AS RECEIVED

AVIS

La qualité de cette microfiche dépend grandement de la qualité de la thèse soumise au microfilmage. Nous avons tout fait pour assurer une qualité supérieure de reproduction.

S'il manque des pages, veuillez communiquer avec l'université qui a conféré le grade.

La qualité d'impression de certaines pages peut laisser à désirer, surtout si les pages originales ont été dactylographiées à l'aide d'un ruban usé ou si l'université nous a fait parvenir une photocopie de mauvaise qualité.

Les documents qui font déjà l'objet d'un droit d'auteur (articles de revue, examens publiés, etc.) ne sont pas microfilmés.

La reproduction, même partielle, de ce microfilm est soumise à la Loi canadienne sur le droit d'auteur, SRC 1970, c. C-30. Veuillez prendre connaissance des formules d'autorisation qui accompagnent cette thèse.

LA THÈSE A ÉTÉ
MICROFILMÉE TELLE QUE
NOUS L'AVONS REÇUE

THE UNIVERSITY OF ALBERTA

Studies of the Strength of Rough Rock Surfaces in Shear

by

© Rex Tse

A THESIS

SUBMITTED TO THE FACULTY OF GRADUATE STUDIES AND RESEARCH

IN PARTIAL FULFILMENT OF THE REQUIREMENTS FOR THE DEGREE

OF Master of Science

DEPARTMENT OF Civil Engineering

EDMONTON, ALBERTA

SPRING, 1979

THE UNIVERSITY OF ALBERTA

FACULTY OF GRADUATE STUDIES AND RESEARCH

The undersigned certify that they have read, and recommend to the Faculty of Graduate Studies and Research, for acceptance, a thesis entitled Studies of the Strength of Rough Rock Surfaces in Shear submitted by Rex Tse in partial fulfilment of the requirements for the degree of Master of Science in Civil Engineering

.....
D.M. Cruden, Supervisor

.....
N.R. Morgenstern

.....
B. Stimpson

Date Oct. 16, 1978

Tó my Mother and Father

ABSTRACT

Extensive laboratory studies have been carried out to investigate the shear strength properties of two artificially prepared rough rock surfaces -- Tyndall Stone and Standstead Granite.

Barton's peak shear strength envelope criterion for rough rock surfaces (Barton, 1973 and 1976) and a power law fit may be used to describe the distribution of experimental shear strength data. However Barton's maximum total friction angle (70 degrees) criterion (Barton, 1976) would underestimate the measured friction angles of highly dilatant surfaces. Angles as high as 82 and 87 degrees have been obtained for the limestone and granite surfaces respectively. Total friction angles are composed of the basic friction angle of the rock and the geometrical components of the rock surface which is termed the i-angle. The i-angle depends on the degree of surface roughness, normal stress and the strength of the rock. The ranges of i-angles exhibited by the rock surfaces vary from about 56.50 to 33.50 degrees for the granite surfaces and 48.50 to 14.50 degrees for the limestone surfaces.

Results from the shear tests also show that both the shear stiffness and stress- drop at peak strength increase with effective normal stresses. The values of the peak dilation angle for both rock surfaces remain almost steady with normal stresses but begin to decrease linearly at a

stress level of 4000 kPa. The "suppressed pressure" corresponding to zero dilation is estimated to be 7250 kpa. Rough surfaces which have previously been subjected to shear would have apparent peak strength values between peak and ultimate strengths. During simple and stage-loading direct shear tests, rough surfaces become smoother and flat surfaces become rougher because of wear. This causes non-dilatant surfaces to exhibit higher shear strength in staged testings. The ultimate friction angle of a surface does not have a unique value. It depends upon the initial surface roughness, stress level and the post peak shearing mechanism. For unweathered rock surfaces, the ultimate friction angles will have larger values than that of basic friction angles.

Characterization of surface roughness shows correlation with frictional behavior modelled by the effective i-angle of a rock surface. Peak strength has been successfully predicted by using the Z2 characterization correlation (Z2 = Root-mean-square of the first derivative of a surface profile). Arctan(Z2) estimates Patton's(1966) effective first order irregularity and is equivalent to the joint roughness coefficient (JRC) (Barton, 1973).

The frictional component of a rock surface may be a time-dependent parameter. The short-term standard laboratory peak shear strength may decrease with time and eventually reach the long-term (creep) condition. The apparent shear

strength at a time T may be a function of the elasped time and the initial peak shear strength.

Two conventional direct shear box machines have been modified for this investigation. Results of the 4 shear creep tests have shown the following.

(a) the validity of prediction of peak strength of rough rock surfaces based on roughness studies;

(b) the successful application of creep machines in shear creep studies;

(c) the possibility of a "by-pass" mechanism in rough rock surface where the short-term laboratory peak strength may actually be by-passed in a long term condition;

(d) the existence of two distinct shear creep zones: the decelerating creep zone and the accelerating creep zone.

Further research into the behavior of shear strength of rock surfaces both in the labortory and in situ is needed and particular emphasis should be placed on the time-dependent deformation and shear strength characteristics of natural discontinuities.

ACKNOWLEDGEMENTS

I would like to express my sincere gratitude to my supervisor, Dr.D.M. Cruden, for suggesting the research topic, and for his guidance, encouragement and moral support during the preparation of this thesis.

Gratitude is extended to Drs.N.R. Morgenstern and B. Stimpson for their comments and constructive discussions during the final stages of my thesis work.

Financial support provided by the N.R.C. and the Civil Engineering Department is appreciated.

Computer programming assistance provided by R. Howells is gratefully acknowledged. In particular, J. Harder from the Computer Centre is thanked for the significant contribution she made in implementing the initial stages of the computer program used in the rock surface profile studies.

I wish to thank Messrs. O. Wood and A. Muir for their help in preparation of the testing apparatus.

Useful discussions on some of the experimental results with I. Bruce, P. Kaiser and S. DA Fonturna are much appreciated.

I also wish to thank I. Bruce, F. El Nahhas, A. Gale, B. Kjartanson and D. Mageau for their friendship during the past two years. Moreover, their insight into the shear creep

problem is appreciated.

A. Gale and R. Stewart are acknowledged for having proof read some of the chapters in this thesis.

I am deeply grateful to my parents for their financial and moral support throughout my studies in Canada.

I also want to acknowledge the debt I owe to Lila Cheung for her understanding and moral support throughout the thesis work.

Last but not the least, I would like to thank D. Tanaka for typing part of the thesis.

TABLE OF CONTENTS

CHAPTER		Page
I.	INTRODUCTION	
	1.1 Natural Creep	1
	1.2 Creep in Soil	3
	1.3 Creep in Rock	5
II.	THE SHEAR STRENGTH OF ROCK SURFACES	
	2.1 LITERATURE REVIEW	12
	2.1.1 Rock Discontinuities	12
	2.1.2 Shear Tests on Discontinuities	13
	2.1.3 Shear Failure Criterian	17
	2.1.4 Shear Mechanism and Shear Strength Envelopes	18
	2.1.5 Barton's Peak Shear Strength Envelope	26
	2.2 SAMPLE PREPARATION	36
	2.2.1 Types of Rock	36
	2.2.2 Sample Size and Initial Orientation	37
	2.2.3 Sample Requirements	40
	2.2.4 Artificial Rock Surfaces	45
	2.3 LABORATORY TESTING PROGRAM	47
	2.3.1 Apparatus and Testing Environment	47
	2.3.2 Material Constants	49
	2.3.3 Tilting Tests	60
	2.3.4 Test Procedure	64
	2.3.5 Observations during Shear Tests	66
	2.3.6 Interpretation of Shear Test Observations	72
	2.4 TEST RESULTS	78
	2.4.1 Peak Shear Strength	78
	2.4.2 Shear Stiffness	90
	2.4.3 Peak Dilation Angle	91
	2.4.4 The Effects of Stress History on Peak Strength	95
	2.4.5 Stress Drop	98
	2.4.6 Effects of Normal Stress on Relative Stress Drop	100
	2.4.7 Ultimate Shear Strength	102
	2.5 SUMMARY OF CHAPTER II	107
III.	SURFACE ROUGHNESS STUDY AND PREDICTION OF THE EFFECTIVE GEOMETRIC i-ANGLE	
	3.1 Introduction	111
	3.2 Definitions of Surface Roughness	111

TABLE OF CONTENTS

CHAPTER		Page
	3.3 Measurements of Surface Profiles	115
	3.4 Degitization of Surface Profiles	117
	3.4 Computations of Surface Parameters	118
	3.6 Correlation between JRC and Surface Parameters	121
	3.7 JRC values of Tested Rock Surfaces	129
	3.8 Prediction of Effective i-angles of Sheared Surfaces	135
	3.9 Summary of Chapter III	152
IV.	CREEP IN SHEAR IN ROCK	
	4.1.1 Shear Creep Hypothesis	156
	4.1.2 Analysis of Hypothesis	156
	4.2 CREEP APPARATUS	158
	4.2.1 Creep Machines	158
	4.2.2 Air System	159
	4.2.3 Data Acquisition	161
	4.3 CREEP STUDY ON GRANITE SURFACES	165
	4.3.1 Shear Tests in Creep Machines	165
	4.3.2 Setting up a Creep Test	167
	4.3.3 Creep Test	168
	4.3.4 Observation During Creep	169
	4.4 RESULTS AND ANALYSIS	171
	4.4.1 Creep Test 1	171
	4.4.2 Creep Test 2	175
	4.4.3 Creep Test 3	181
	4.4.4 Creep Test 4	188
	4.4.5 Variation of Shear Resistance	197
	4.4.6 Increment Versus Single Creep Tests	200
	4.5 SUMMARY OF CHAPTER IV	210
V.	CONCLUDING REMARKS	213
	REFERENCES	217
	APPENDIX A DESIGN OF LOAD CELLS	228
	APPENDIX B DERIVED RESULTS OF DIRECT SHEAR STRENGTH TEST ON ARTIFICIALLY PREPARED TYNDALL STONE AND STANDSTEAD GRANITE SURFACES	239
	APPENDIX C RESULTS OF TWO SURFACE CHARACTERIZATIONS (Z2 AND SF) FOR THE SURFACE PROFILES OF TYNDALL STONE AND STANDSTEAD GRANITE SURFACES	242

THE TOTAL FRICTION
ANGLE,ARCTAN(PEAK/NORMAL STRESS) VERSUS
THE LARGEST VALUE OF ARCTAN(Z2) MEASURED
ON THE ROCK SURFACE(TYNDALL STONE) 245

THE TOTAL FRICTION
ANGLE,ARCTAN(PEAK/NORMAL STRESS) VERSUS
THE LARGEST VALUE OF ARCTAN(Z2) MEASURED
ON THE ROCK SURFACE(STANDSTEAD GRANITE) 246

LIST OF TABLES

Table		Page
2.1	Basic friction angles of various unweathered rocks obtained from flat and residual surfaces (Barton and Choubey, 1977)	31
2.2	Values of uniaxial compression strength of Tyndall Stone and Standstead Granite obtained from different methods	51
2.3	Results of the basic friction angles of Standstead Granite and Tyndall Stone surfaces prepared from different methods	58
2.4	Results of direct shear strength test on artificially prepared Tyndall Stone surfaces	79
2.5	Results of direct shear strength test on artificially prepared Standstead Granite surfaces	80
2.6	Results of the analysis of variance of the power law function in describing the direct shear strength data of the Tyndall Stone surfaces	87
2.7	Results of the analysis of variance of the power law function in describing the direct shear strength data of the Standstead Granite surfaces	88
2.8	Values of the mean ultimate friction angle of Tyndall Stone surfaces	105
2.9	Values of the mean ultimate friction angle of Standstead Granite surfaces	106
3.1	Values of three surface parameters for Barton and Choubey's ten standard surface profiles of different JRC values	120
3.2	Results of regression analysis of Barton and Choubey's ten standard surface profiles with eight surface parameters	123
3.3	Results of run tests	130
3.4	Ratios of predicted i-angle to measured i-angle for the Standstead Granite and Tyndall Stone surfaces	140

LIST OF TABLES (Continued)

Table		Page
3.5	Values of measured mean i-angle corresponding to the predicted i-angles equal to or greater than 36.5 and 39.5 degrees for the Tyndall Stone and Standstead Granite surfaces respectively	143
3.6	Comparison between the measured i-angles and the predicted i-angles at low normal stress levels (345kpa and 1035kpa for Tyndall Stone and Standstead Granite surfaces respectively)	146
4.1	Results of direct shear strength test on Standstead Granite surfaces in creep machine	166
4.2	Comparison between the % fluctuation of supply air-load from the bellofram and the % fluctuation in the measured shear resistance for creep tests	199
4.3	Summary of 4 shear creep test results	208

LIST OF FIGURES

Figure		Page
1.1	Generalized creep curve	6
2.1	Systems for shear testing	14
2.2	Failure envelope for specimens with flat surfaces	20
2.3	Failure envelope for multiple inclined surfaces	20
2.4	An example of a discontinuity illustration first-and second-order irregularities (Deere et al; 1967)	22
2.5	Ladanyi and Archambault's equation for peak strength of rough surfaces	27
2.6	Peak shear strength results obtained from direct shear tests performed on tension fractures in brittle model materials (Barton, 1971)	27
2.7	Barton's equation for peak strength of rough joint surfaces	30
2.8	Roughness profiles showing the typical range of JRC values (Barton and Choubey, 1977)	33
2.9	Initial orientation of the Tyndall Stone and Standstead Granite samples	38
2.10	The specially designed clamp for cutting the 2x2 samples into 2x1 samples	43
2.11	Procedures of fractured rock surface preparation	43
2.12	Shear load versus displacement curves showing the stress-drop characteristics for samples prepared from different methods	46
2.13	Direct shear box for testing shear strength of rock surfaces	48
2.14	Shear load versus displacement curves for single and stage-loading tests	57
2.15a	Geometry of block on inclined plane	62
2.15b	Conditions for sliding and toppling of a block	

LIST OF FIGURES (Continued)

Figure		Page
	on an inclined plane (De Freitas and Watters, 1973)	62
2.16	Typical rock surfaces after shear	67
2.17a,b	Typical load versus displacement and vertical versus horizontal displacement curves of artificially prepared Tyndall Stone surfaces	68
2.17c,d	Typical load versus displacement and vertical versus horizontal displacement curves of artificially prepared Standstead Granite surfaces	69
2.18	The frictional components of rock blocks subjected to shear	73
2.19a	Peak shear strength results obtained from direct shear tests performed on tension fractured surfaces of Tyndall Stone	81
2.19b	Peak shear strenght results obtained from direct shear tests performed on tension fractured surfaces of Standstead Granite	82
2.20	Shear stiffness - normal stress characteristics for (a) Tyndall Stone and (b) Standstead Granite surfaces	92
2.21	The effect of normal stress on dilation angle during shear for (a) Tyndall Stone and (b) Standstead Granite surfaces	94
2.22	The effects of stress history on peak shear strength results for (a) Tyndall Stone and (b) Standstead Granite surfaces	96
2.23	Stress drop - normal stress characteristics for (a) Tyndall Stone and (b) Standstead Granite surfaces	99
2.24	The ratio of peak to ultimate strength as a function of normal stress for (a) Tyndall Stone and (b) Standstead Granite surfaces	101
2.25	Ultimate shear strengths for (a) Tyndall Stone and (b) Standstead Granite surfaces	103

LIST OF FIGURES (Continued)

Figure		Page
2.26	Relationship between the ultimate friction angle and the normal stress for (a) Tyndall Stone and (b) Standstead Granite surfaces. The centre points indicate the mean angle, and the intervals the 95% confidence limits of the means.	108
3.1	A typical graphical output of a rock surface on the Watanbe X-Y plotter	
3.2	Relationship between the JRC and Z2 parameters for Barton and Choubey's 10 standard rock surface profiles	124
3.3	Relationship between the JRC and arctan(Z2) parameters for Barton and Choubey's 10 standard rock surfaces profiles	125
3.4	Relationship between the JRC and log(Z2) parameters for Barton and Choubey's 10 standard rock surface profiles	126
3.5	Relationship between the JRC and SF parameters for Barton and Choubey's 10 standard rock surface profiles	127
3.6	Relationship between the JRC and log(SF) parameters for Barton and Choubey's 10 standard rock surface profiles	128
3.7	Barton's empirical law of friction in graphical form for (a) Tyndall Stone and (b) Standstead Granite surfaces	132
3.8a	Comparison between peak shear strength results of Tyndall Stone surfaces and Barton's peak strength envelope criterion for rock surfaces	133
3.8b	Comparison between peak shear strength results of Standstead Granite surfaces and Barton's peak strength envelope criterion for rock surfaces	134
3.9	Effective i-angles predicted from arctan(Z2) log($\sigma c/\sigma n$) compared with the measured values obtained from conventional shear box tests on (a) Tyndall Stone and (b) Standstead Granite surfaces. (Z2 parameter is the largest value)	137

LIST OF FIGURES (Continued)

Figure		Page
3.10	Effective i-angles predicted through the log (Z2) correlation compared with the measured values obtained from conventional shear box tests on the Tyndall Stone surfaces. The Z2 parameter is the (a) mean and (b) largest value.	142
3.11	Representative direct shear strength tested Tyndall Stone surfaces showing the degree of shear damage with normal stresses	148
3.12	Representative direct shear strength tested Standstead Granite surfaces showing the degree of shear damage with normal stresses	149
3.13	Cracking at the end region of a specimen	151
4.1	Effect of time on friction of rock surfaces	157
4.2	The modified direct shear box for shear creep tests	160
4.3	The creep frame arrangement	160
4.4	The creep machine	162
4.5	The air system control board	162
4.6	The data acquisition system	164
4.7	Creep specimens after failure	164
4.8	Results of creep test #1	173
4.9	Results of creep test #2 (stage 1)	176
4.10	Results of creep test #2 (stage 2)	177
4.11	Results of creep test #2 (final stage)	178
4.12	Results of creep test #3 (stage 1)	183
4.13	Results of creep test #3 (stage 2)	184
4.14	Results of creep test #3 (final stage)	185
4.15	Results of creep test #4 (stage 1)	190
4.16	Results of creep test #4 (stage 2)	191
4.17	Results of creep test #4 (stage 3)	192

LIST OF FIGURES (Continued)

Figure		Page
4.18	Results of creep test #4 (final stage)	193
4.19	Complete shear stress-displacement history for creep test #1	203
4.20	Complete shear stress-displacement history for creep test #2	204
4.21	Complete shear stress-displacement history for creep test #3	205
4.22	Complete shear stress-displacement history for creep test #4	206
4.23	Shear strength-time plot of rough Standstead Granite surfaces	209

CHAPTER I

Introduction

1.1 Natural Creep

Time-dependent strain or creep is a process which affects to some extent not only all loose aggregates, but also all solids. Unlike elastic deformations, creep may be defined as the slow change in shape or deformation in a body which takes place continually as a consequence of constant shear stresses. In nature the shear stresses which are an essential condition of creep are primarily a result of the force of gravity. Natural creep processes, which are occasionally combined with slides take place in snow, glaciers, soil and rocks (Haefeli, 1953).

Rupture processes often occur on rock slopes with stratification parallel to the slope. A tragic example of creep process is the rock slide which occured on 2nd, September, 1806 where a 30m thick conglomerate layer, inclined at approximately 24 degrees, which lay on marly sandstone with intercalations of a bituminous marl layers 2-3m thick slipped down to the valley at Arth-Goldau, Switzerland (Haefeli, 1953). This was the largest rock slide recorded in Swiss history; it claimed 457 lives, 2 churches, 11 houses and 200 stables and barns were destroyed (Heim, 1882).

Depending on the roughness and friction condition of

the discontinuities, the creep of the upper stratification above the critical joint sets takes place either with, or without any sliding movement over the rigid rock layers below. The creep movement may take decades or centuries (Haefeli, 1953).

Terzaghi (1953) described two types of creep in rock: skin creep and mass creep. Skin creep refers to slow movements which are confined to the zone of seasonal variations of temperature and moisture. This kind of rock creep leads to the well known phenomenon of outcrop curvature. Mass creep causes deep seated deformations of mountain slopes. In many cases these slow motions started after the retreat of the glaciers of the last ice age as a consequence of ice erosion. If there was no further disturbance of the stress-field, the slopes appear to be stable today. However, creep movements are found at many places in the Alps and other mountain systems or faults all over the world (Ampfeier, 1939; Haefeli, 1953; Scholz, 1972; Osborn, 1975 and others).

If creep processes are accompanied by the final rupture of the structural material, the rupture may occur abruptly after a certain amount of creep deformation has developed. This is detrimental to engineering structures and may even cause loss of life. The following topics have been emphasized (Bieniawski, 1970): (i) the determination of the significance of time-dependent rock deformation, (ii) the

evaluation and predictability of time-dependent behavior of rock with special attention to rupture, and (iii) the assessment of time-dependent changes in the rock fabric and whether such changes can be used to predict impending time-dependent rock failure in situ.

Unfortunately these topics are not fully understood. Hence the stability of engineering works and natural slopes can not yet be evaluated realistically. In fact, it does not even appear possible to state with any degree of certainty under what conditions the influence of time ought to be considered. A knowledge of the effect of creep therefore, will be very important in obtaining a better understanding of geological processes and physical processes within manmade structures. Only careful laboratory creep research and field observations can furnish a better insight to the problem.

1.2 Creep In Soils

The process of soil creep in shear has been studied in the laboratory by many researchers; the tests led to well known creep curves in the co-ordinate system of time-shear strain (or time-deformation). These curves exhibit no time effects at low shear stresses. For stresses exceeding some limiting value it is customary to divide these curves into three sections: primary creep (decelerating), secondary creep (steady, at a constant rate) and tertiary creep

(accelerating). Sometimes the absence of the steady state creep zone with a constant strain rate was observed depending on the soil structure and reorientation of soil particles attained during the tests (Bishop, 1966; Ter-Stepanian et al, 1973).

In the early thirties Terzaghi (1931) was probably the first to emphasize the time-dependent effect in shear strength of clays. After that numerous theories, equations and rheological models were offered to account for the soil behavior, during shear creep. A review of these theories and their creep analysis is given in various published works (Vyalov, 1959; Scott and Ko, 1969; Suklji, 1969; Tsytovich, 1973 and others).

Some investigators (Murayama and Shibata 1961; Christensen and Wu, 1964; Andersland and Akili, 1967; Mitchell et al, 1968 and others) employed the Eyring theory (Eyring, 1936) of rate process to study the rheological properties of clays and frozen soils. The theory was based on the idea that the strain process consists of mutual displacements of flow units by surmounting energy barriers. The application of this theory of rate process proved sucessful in the study of homogenous continuous media, such as asphalt, polymers, or granular media in which the strength of bonds between particles is comparable to the strength of the particles themselves such as metal or concrete. However, the application of this theory to such

disperse discrete media as soils would cause certain difficulties arising from the influence of the soil structure where the strength of the bonds is essentially less than that of the grains themselves. In view of this, Ter-Stepanian (1975) proposed another rheological model describing the mechanical behavior of creep in clay during shear based on the concept of visco-plastic properties of the soil.

1.3 Creep In Rocks

The strength and deformation behavior of rocks are time-dependent. Even 60 years ago, creep was observed in rocks (Michelson, 1917). Griggs (1936, 1939, 1940) showed that rocks and minerals exhibited creep behavior and generalized creep curves into three sections: primary creep, secondary creep and tertiary creep as shown in figure 1.1. In the first zone (OA) the deformation or creep strain increases rapidly, but the strain rate decreases. Eventually the strain rate becomes constant over a section AB. Finally the strain rate begins to increase again at B and the strain rapidly increases until fracture occurs at C.

Some of the work on creep in rocks published prior to 1964 has been summarized in review papers by Murrell and Misra (1962) and Robertson (1963). Other papers have been published by Scholz (1968), and Hobbs (1970). More recently, papers have been published by Cruden (1970, 1971, 1974),

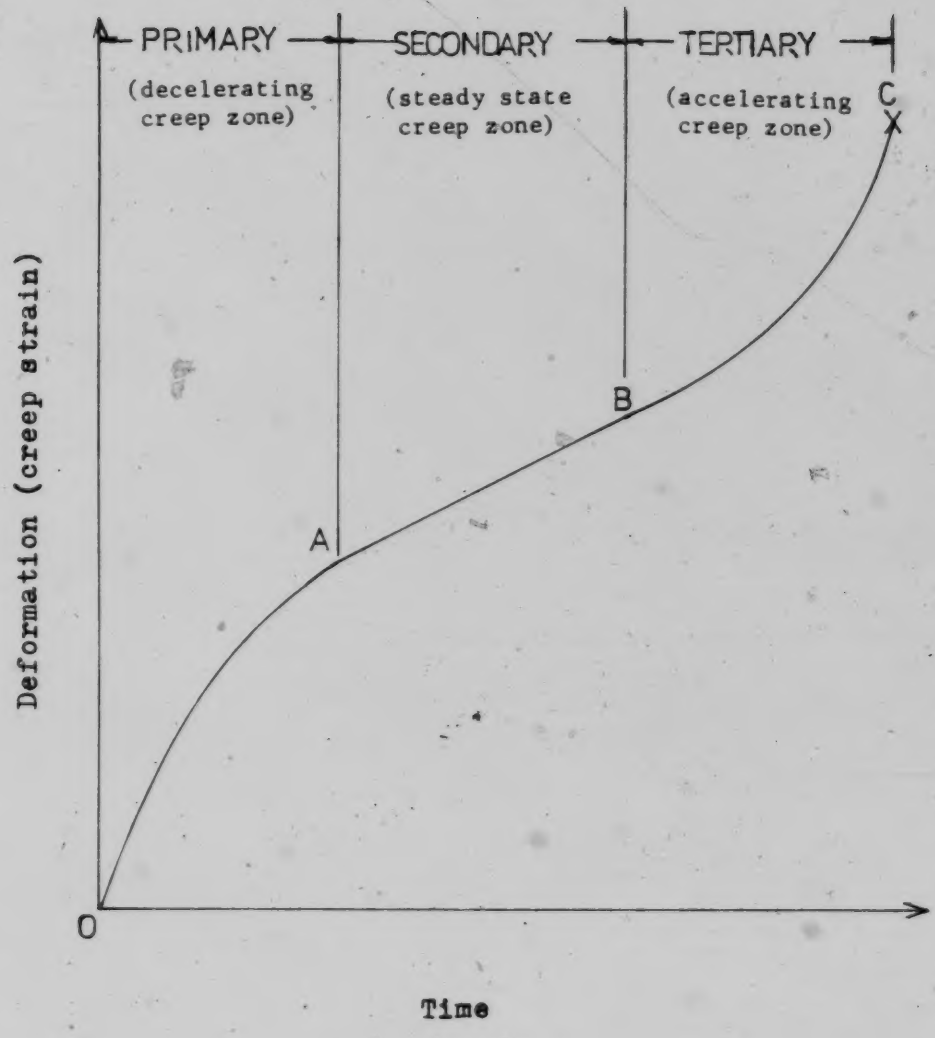

Figure 1.1 Generalized creep curve

Warwersik (1972), Afrouz and Harvey (1974), and others. Their studies of time-dependent behavior in rock have been primarily conducted in the laboratory. Most of these laboratory investigations and the corresponding stress-strain-time relationships developed have been uniaxial in nature. However some works have been conducted to evaluate creep behavior in triaxial tests (U.S. Army Corps of Engineers, 1963; Sample et al 1973). Also some attempts have been made to gain insight into time-dependent problems by utilizing rheological models (Winkle, 1970; Emery, 1971).

The empirical approach appears to have the widest acceptance in representing the creep of rocks (Robertson, 1963). In this approach, displacement is measured with time and load under controlled conditions. Subsequent creep expressions are developed to describe the physical behavior of rocks by selecting some suitable parameters from the experimental data. The total strain E (elastic plus creep) for a certain uniaxial stress may be represented by the following general equation (Robertson, 1963)

$$E = Eo + Ep(t) + At + Et(t)$$

where E = the total strain

Eo the instantaneous elastic strain

Ep(t) = the primary creep

At = the steady state or secondary creep

Et(t) = the tertiary creep

t = the time

There are several creep equations for rocks published in Boresi and Deere (1963), Obert and Duvall (1967), Farmer (1968), Winkle (1970), Hobbs (1970), Cruden (1971), Jaeger (1972), Nair et al (1973), Afrouz and Harvey (1974), and others.

Creep may eventually lead to rupture; such creep rupture is usually defined as failure of the rock material under a stress condition that is less than the applicable peak strength measured in the standard laboratory tests. Current engineering practice is to ignore or approximate this time dependency in the analysis of rock problems such as rock slope stability and tunnelling in rocks.

The problem in tunnel construction is so called "rock squeezing" (Terzaghi, 1946; Jaeger, 1972). Examples of failure due to this problem would include: the El-Colegio Tunnel in Columbia; Kamui Tunnel in Japan; and North Tauein Tunnel in Austria (Lane, 1975). Even in strong rocks, rock squeezes have been found in excavations (Feld, 1966, Lo and Morton, 1975). Without methods for the analysis of creep, creep rupture and squeezing ground, design procedures for engineering structures must be based on high factors of safety or the experience gained from previous failures. However interest in the rock squeezing behavior in underground structures has gained impetus in the last few years all over the world.

The problem of creep in rock slope stability and other

engineering structures, such as dam construction on rock foundations, is the static and dynamic frictional behavior of the discontinuities within the rock masses. Not withstanding a great deal is known at the present about the mechanical properties of rock from the great number of large scale direct shear tests that have been performed on irregular rock surfaces at various sites throughout the world, the number of published papers with complete descriptions of the tests is still very small. This refers particularly to the lack of data concerning the time-dependent frictional behavior in shear of the rock discontinuities. One report on shear creep was given by Deiterich (1972). He stated:

> " . . . . . Sliding on clean rough-ground surfaces is initially stable for this range. However, as powdered rock debris accumulates on the slip surface, stick slip becomes the dominant mode of sliding. The coefficient of static friction of surfaces with gouge exhibits a highly time-dependent behavior. Static friction increases with the logarithm of the time that adjacent blocks remain in stationary contact ..... This behavior may be significant in understanding the mechanisms of earthquake foreshocks, aftershock, and fault creep."

He attributed the increase of coefficient of friction with time to compaction of gouge on some nondilatant surfaces prepared on porous sandstone, quartzite, graywacke, and granite. These are probably the first indications of time-dependence and creep in frictional phenomena and since many fault surfaces are covered with gouge, this is of considerable importance in rock mechanics.

The question is raised as to whether dilatant rock surfaces would creep in shear. No other published data on this problem was known to the author at the time this thesis was written. The remaining chapters of this thesis report on the investigation of the time-dependent frictional behavior on rough rock surfaces conducted in creep machines which had been modified from direct shear boxes.

A hypothesis of shear creep in rock is presented in this thesis and it attempts to explain a shear failure along a discontinuty subjected to time effects. The manifestation of time effects on frictional behavior are the occurrence of irreversible time-dependent shear deformations recognized as shear creep and a corresponding reduction of the peak shear strength towards the long-term strength of the discontinuity.

With this in mind, an empirical approach is carried out to investigate the shear strength properties of some rough rock surfaces with emphasis on creep. In order to carry out a shear creep investigation, it is necessary to raise the shear stress on the specimen to a known percentage of the short-term laboratory shear strength of the rock surface. Thus a reliable non-destructive method of estimating the peak shear strength of the rock surface has to be developed. It appears from the literature (Krahn, 1974) that "rock surface roughness characterizations" may predict the frictional behavior of rock specimens with reasonable

accuracy. Since roughness characterization lends itself to experimental verification, it was decided to run some conventional direct shear box tests on the rock surfaces to confirm this method. This leads to structuring the thesis as follows:

(1) Chapter 2 is devoted primarily to the determination of shear strength parameters and the study of some related experimental results.

(2) Chapter 3 describes the results of rock surface analysis and characterization in prediction of i-angles. Validity of the prediction criterion tested by the measured shear strength values presented in chapter 2.

(3) Chapter 4 presents the hypothesis of shear creep in rock, and the proof of this hypothesis is demonstrated from the results of the creep tests.

The conclusions of this thesis are presented in Chapter 5.

CHAPTER II

The Shear Strength of Rock Surfaces

2.1 Literature Review

2.1.1 Rock Discontinuties

The stability of discontinuous rock masses is controlled by the frictional characteristics and the orientation of the discontinuities within the near surface of the earth. These surfaces and planes of weakness, which in nature separate masses of rock into blocks, include types such as bedding planes, joints, faults, shears, cleavages, contacts, gneissosities, schistosities or veins. (Cruden, 1976).

In addition to natural discontinuities, artificial surfaces can be constructed in the laboratory. One can introduce a rough or smooth surface in a sample of the actual rock by splitting the rock in a Brazillian test, point-load test machine (Broch and Franklin, 1972), by diamond sawing (Coulson, 1972; Krahn, 1974) or producing a planar shear failure in a triaxial test. Moreover, surfaces prepared from artificial materials such as plaster of Paris or similar kinds have been used by several workers (Patton, 1966; Lajtai, 1969; Barton, 1971 and others).

Shear failures in rock masses frequently take place along discontinuities. Therefore the specification of shear strength parameters for discontinuities is of fundamental

concern to engineers who are charged with designing rock slopes or rock foundations for heavy structures.

2.1.2 Shear Tests on Discontinuities

The common types of test used for the determination of shear strength parameters are: the direct shear test, triaxial or multiaxial test and torsion shear test as shown in figure 2.1 (Jaeger, 1971).

The direct shear test is frequently employed in the laboratory and also in the field since, it is a natural way to test properties of discontinuities. The main advantages of the direct shear test in the field are the ability to measure the shear resistance in any desired direction along potentially critical discontinuities and its adaptability to field conditions. Tests can be conducted in trenches, adits, tunnels and even calyx drill holes (Zeigler, 1972).

In the laboratory, conventional shear boxes either built for use in soil mechanics or specially constructed have been used extensively for testing surfaces. Some specific direct shear machines are described by Krsmanovic and Langof (1964) Edvokimov and Sapegin (1967), Hoek (1970), Goodman and Ohnisi (1973), and others.

In the simplest form of the direct shear test, a sample is cemented in a shear box, using a sulfur capping compound, epoxy, or sulfaset. The surface of discontinuity is

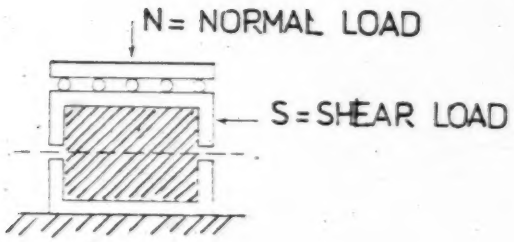

(a) Direct shear test

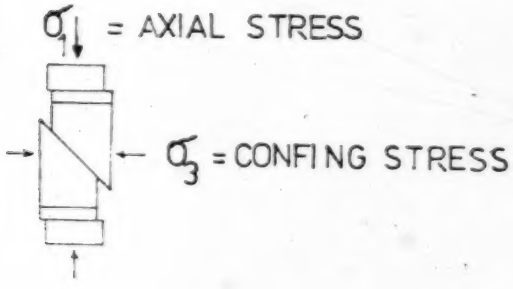

(b) Triaxial shear test

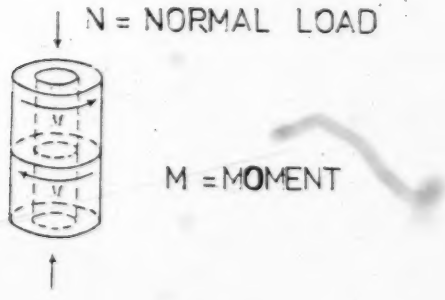

(c) Torsion shear test

Figure 2.1 Systems for shear test

coincident with the plane of shearing and a gap of about one centimetre or more depending on the irregularity of the surface, is left unbonded between the upper and lower boxes.

The sample is then subjected to a load perpendicular to and another load parallel to the predetermined failure discontinuity. These loads are termed the normal load, N, and the shear load, S, respectively, as shown in figure 2.1a.

The normal and shear stresses are obtained from the normal and shear loads, dividing each by the test surface area which has been measured before shear. These loads are assumed to be distributed uniformly over the test surface. This assumption is not much in error (Kutter, 1971).

The normal load is applied first and is generally held constant until the sample fails under an increasing shear load. The normal load is applied by a hydraulic ram, air cushion; screw, coil spring or dead weight hanger with or without lever system while the shear load is gradually applied through a screw, a hydraulic ram or driving gear unit. The choice of the loading device for both normal and shear loads depends on the size of the sample (Evdokimov and Sapegin, 1967; Coulson, 1970; Kenty, 1970; Rengers, 1971; Goodman and Ohnishi, 1973).

The desired normal load can be placed on the sample all at once as rapidly as possible or gradually, in stages or

increments. It should remain centered over the contact area (area between the load cap and the upper half sample) all the time. Its set up should provide the top half sample with free vertical movement to allow over-riding of the irregularities during shear. Friction produced between the normal load mechanism and test sample should be minimized. This is often accomplished by placing steel roller bearings between the test sample and loading device (Figure 2.1a).

Besides measuring normal and shear loads usually by proving rings, load cells or gages, both horizontal and vertical displacements of the sample should be measured. These measurements are usually recorded mechanically by dial gages or electrical gages, either the resistance or induction (LVDT) type.

The induction type is preferable since they are moisture proof. Measurements made by this type can be recorded on x-y-y' recorders to give smooth, continuous curves of shear resistance versus displacement and vertical deformation versus displacement plots.

Contraction and dilation of the sample during shear is one of the main interests in shear strength tests. Therefore, devices measuring vertical movement should be placed near the surface wherever readings may be influenced by internal compression or expansion of the test sample. A number of workers have used four gages to measure movements of the four corners of the top half sample; in this way, any

sample rotation during shear can be measured (Coulson, 1970; Noonan, 1972; and others).

The shear testing environment should be controlled. In most cases, the sample displacements are small so that temperature effects on the sample, shear boxes and measuring devices are important. The moisture condition desired on the surface during shearing should be considered too since the effects of moisture on a clean surface are not always predictable. Moisture on the surface may act either as a lubricant or antilubricant, depending on the surface mineralogic composition, rate of shearing and surface roughness (Horn and Deer, 1962; Mitchell, 1976). Deere et al (1967) also pointed out that the influence of pore water pressures within the irregularities along the surfaces is not understood.

2.1.3 Shear Failure Criteria

Before the direct shear test is begun, one should determine how shear failure will be defined. Having established the failure criteria, the variables that must be observed during the test and the point at which the test can be discontinued.

Different failure criteria have been discussed by Ruiz and Camargo (1966), Ruiz et al (1968) and others. Common failure criteria are:

(a) Peak load criterion: the peak shear load that can be

mobilized during shearing,

(b) Ultimate load criterion: the ultimate constant shear load required to produce continued displacement,

(c) Displacement criterion: the shear load mobilized at a particular horizontal displacement.

(d) Dilatance or Inversion criterion: the shear stress corresponding to the point at which the vertical displacement changes from downward to upward, that is from contraction to dilation.

2.1.4 Shear Mechanism and Shear Strength Envelope

Once the failure criterion is chosen the shear stress and normal stress at failure are used to determine a failure envelope, a curve joining all points on the shear stress versus normal stress plot. The resulting failure envelope is termed the shear strength envelope of the rock surface since the shear stress measured is the total frictional resistance or strength offered by the surface. The shear frictional resistance, on clean planar joints, can be defined by the expression (Patton, 1966):

$$S = N \tan \phi_b \qquad (2.1)$$

where S = Shear force

N = Normal force and

ϕ_b = the basic friction angle of the material as determined on flat unweathered rock surfaces (Figure 2.2)

In most cases, naturally occurring discontinuities exhibit surface irregularities which contribute additional shearing resistance. To demonstrate the effects of surface irregularities, Patton (1966) ran direct shear tests on plaster of paris samples to determine the mechanism of shear along a rock surface.

A sample was cast with a set of regular inclined surfaces (teeth) at the angle, i, measured with respect to the shear direction as illustrated in figure 2.3.

The peak and ultimate shear strength envelopes were constructed from test results. The shear failure at low normal loads, line OA in figure 2.3, is associated with vertical displacement or dilation produced by the upper block sliding up the inclined teeth as the shearing progressed. The sliding frictional resistance can be defined by the expression (Patton, 1966):

$$S = N \tan (\phi b + i) \qquad (2.2)$$

where i = angle of inclination of the teeth

The riding of surface irregularities over one another can take place only if the upper joint system dilates. At high normal loads, the failure mode changes. Dilation is suppressed with the teeth being sheared cff near their bases. When this happens, the shear strength will exhibit an apparent cohesion C. The line AB (figure 2.3) represents the failure envelope obtained from tests run at high normal loads and is inclined at the same angle as the basic

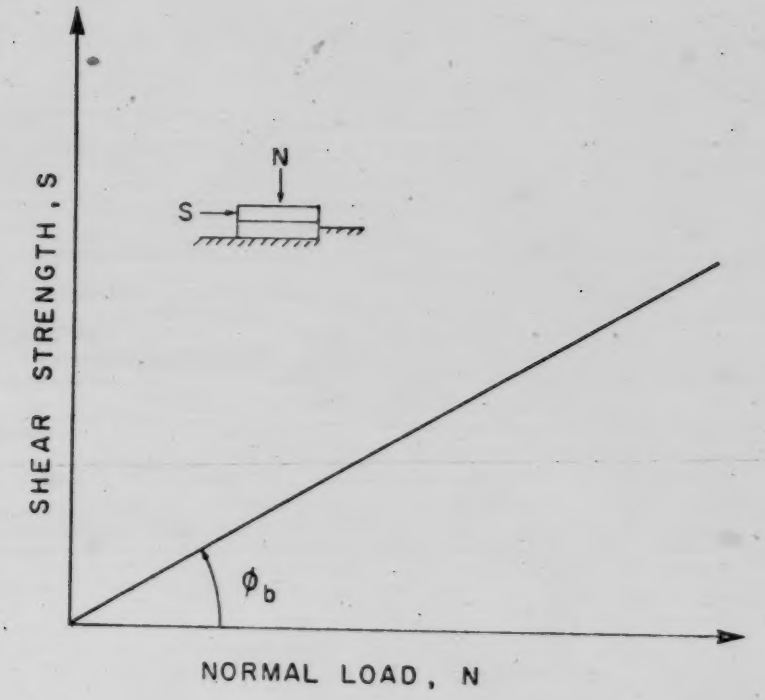

Figure 2·2 Failure envelope for specimens with flat surfaces

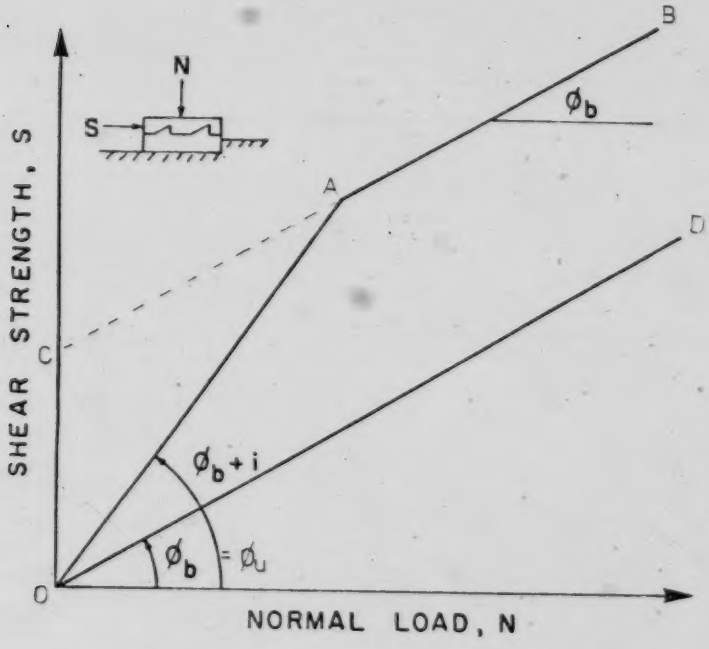

Figure 2·3 Failure envelope for multiple inclined surfaces

friction angle. This strength envelope can be defined by the expression (Patton, 1966):

$$S = C + N \tan \phi b \qquad (2.3)$$

By continuing displacement beyond the peak, the ultimate shear load is reached. Line OD in figure 2.3 is a typical ultimate shear strength envelope and is defined by the same expressions 2.1. In this case, the ultimate angle, ϕu is taken approximately to be the same value as the basic friction angle, ϕb for flat surfaces.

The vertical distance between line OAB and OD represents the shearing resistance lost with displacement and contributed by the teeth.

Combining expressions 2.2 and 2.3, that is joining the envelopes OA and AB in figure 2.3 allows definition of the shear strength over the whole normal load range and results in a bilinear failure envelope. The abrupt change in slopes at point A is related to change in the mode of failure; that is from failure due to sliding up the slopes of teeth to shearing through them.

For natural discontinuities there may be a large range of inclination angles of irregularities, as illustrated in figure 2.4.

Expression 2.2 contains the i-angle which is the effective inclination of the irregularities with respect to the average dip of the discontinuity in question. This angle

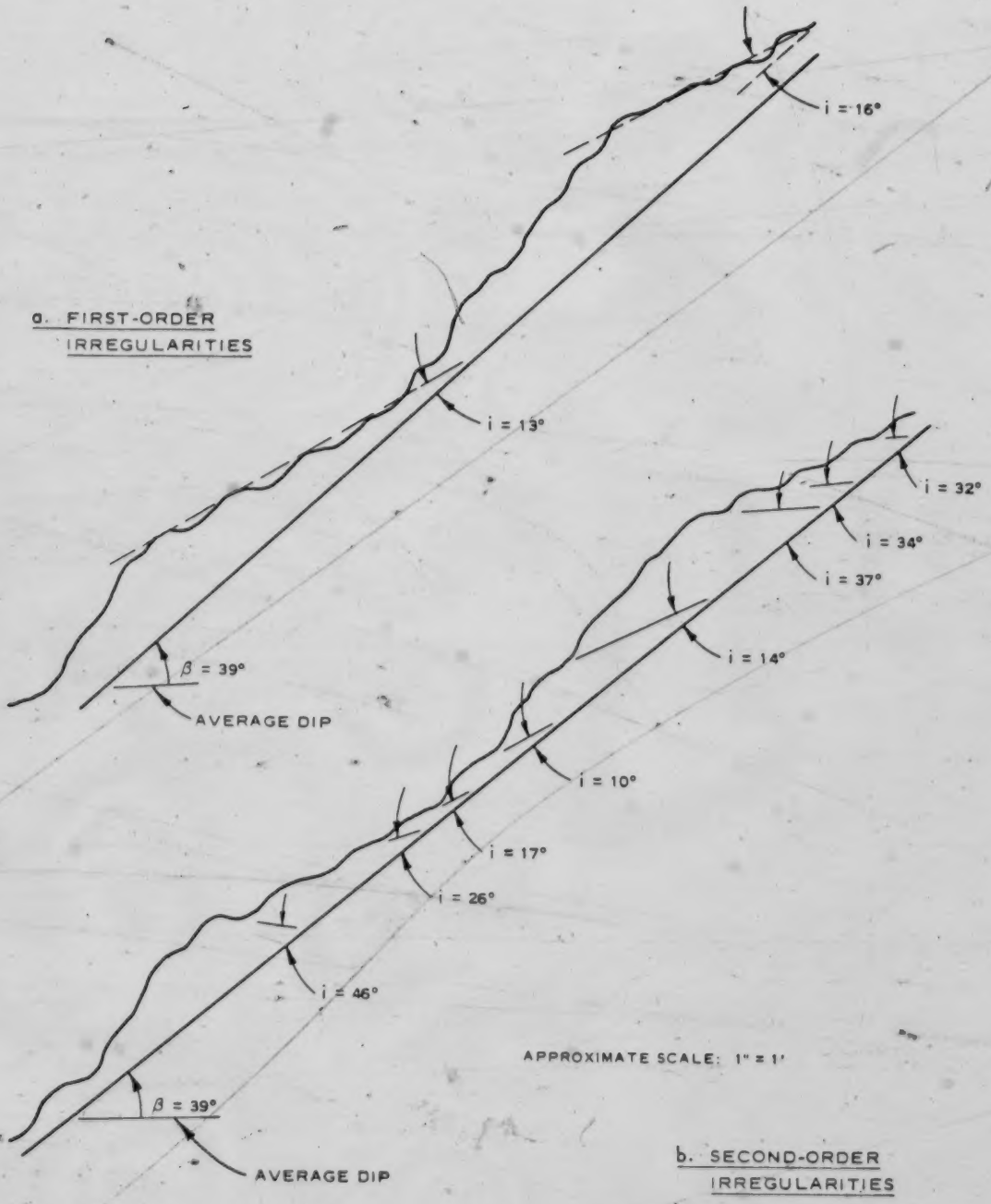

Figure 2.4 An example of a discontinuity illustrating first- and second-order irregularities (Deere et al., 1967)

is usually determined from field observations. Estimating the effective angle can be quite difficult. However, studies by Patton of over 300 rock slopes indicated that the first order irregularities shown in figure 2.4a control the shear strength along the discontinuities. The second-order irregularities shown in figure 2.4b are sheared off through progressive failure (Deere et al 1967). Schneider (1976) modified the geometric friction law or the bilinear model into a material law which described the frictional resistance and the dilation behavior at large deformations in their dependence upon the normal load and material strength.

Schneider's material law for shear strength envelope can be defined by the expression:

$$\tau = \sigma \tan(\phi b + io\, e^{-k\sigma}) \qquad (2.4)$$

τ = peak shear stress

σ = normal stress

where io = the maximum dilation angle at zero effective normal stress

k = a material coefficient which depends upon the material strength (Schneider, 1976)

Ladanyi and Archambault (1970) proposed an expression for the peak shear strength of rough joint surfaces, based on energy considerations of combined friction, dilatancy and interlocking of irregularities. Their general peak shear strength envelope can be defined by the expression:

$$\tau = \frac{\sigma(1 - as)(\dot{V} + \tan \emptyset b) + as\ \tau r}{1 - (1 - as)\dot{V} \tan \emptyset b} \qquad (2.5a)$$

where as = the proportion of the discontinuity surface which is sheared through projections of intact rock material

$\dot{v}$ = the dilation rate dV/dH at peak shear strength; V and H are the vertical and horizontal displacement at peak respectively.

τr = the shear strength of the intact rock material

At very low normal stress level when almost no shearing through asperities take place, as = o and $\dot{v} = \tan i$, expressions 2.5a reduces to expression 2.2. At very high normal stresses, the sample behaves like intact block material, as = 1 and expression 2.5 a reduces to $\tau = \tau r$.

Ladanyi and Archambault suggested that τr, the shear strength of the material adjacent to the joint surfaces, can be represented by the equation of a parabola in accordance with the proposal by Fairhurst (1964).

$$\tau r = \frac{\sigma_c \sqrt{1 + n} - 1}{n} \left(1 + n\frac{\sigma}{\sigma_c}\right)^{0.5} \qquad (2.5b)$$

where σ_c = the uniaxial compressive strength of the rock material adjacent to the joint surface.

n = the ratio of uniaxial compressive to uniaxial tensile strength of the rock material.

n is approximately equal to 10 as suggested by Hoek (1968).

Expression 2.5a, while it may be conceptually correct, includes parameters like as and $\dot{V}$ which are not easy to measure even under laboratory conditions. In order to overcome this problem and to make their equation generally useful, Ladanyi and Archambault carried out a large number of shear tests on prepared rough surfaces and, on the basis of these tests, proposed the following empirical relationships:

$$as = 1 - (1 - \frac{\sigma}{\sigma_c})^L \qquad (2.5c)$$

$$\dot{V} = (1 - \frac{\sigma}{\sigma_c})^k \tan i \qquad (2.5d)$$

where K and L are constants which have the following values:

K=4 and L=1.5 for sliding on a single rough discontinuity,

K=5 and L=(2/nr)^3 tan i, where 2 < nr < 5 denotes the numbers of rows in a failure zone when the equation is applied to the failure of a mass of interlocking rock blocks

Once the parameters τr, as and $\dot{V}$ have been defined, the equations 2.5b, 2.5c and 2.5d are substituted into equation 2.5a with N=10, K=4 and L=1.5, and dividing through by the uniaxial compressive strength σc, one obtains the expression:

$$\frac{\tau}{\sigma_c} = \frac{\frac{\sigma}{\sigma_c}(1-\frac{\sigma}{\sigma_c})^{1.5}\left\{(1-\frac{\sigma}{\sigma_c})^4 \tan ie + \tan \phi b\right\} + 0.232\left\{1-(1-\frac{\sigma}{\sigma_c})^{1.5}\right\}(1+10\frac{\sigma}{\sigma_c})^{0.5}}{1-\left\{(1-\frac{\sigma}{\sigma_c})^{5.5} \tan ie \tan \phi b\right\}} \qquad (2.5)$$

While this equation may appear complex, it will be noted that it relates the two dimensionless groups τ/σ_c and σ/σ_c and that the only unknowns are the effective angle of irregularities, i and the basic friction angle, ϕ_b.

Figure 2.5 shows that Ladanyi and Archambault's equation 2.5 with $\phi_b=30°$ and $i=20°$ gives a smooth transition between Patton's equation 2.2 for dilatcn of a regular rough surface and Fairhurst's equation 2.5b for the shear strength of the rock material adjacent to the surfaces.

2.1.5 Barton's Peak shear Strength Envelope

An alternate approach to the problem of peak shear strength envelope of rough surfaces was proposed by Barton (1971, 1973, 1976) who ran direct shear tests on a variety of artificial tension fractures generated from brittle model materials (Barton, 1970). Two methods for presenting the shear results on these clean surfaces were suggested and are shown in figure 2.6. The solid lines extrapolated through the scatter of data are the best-fit lines obtained by the method of least squares. A dotted line is drawn in each diagram, involving a small rotation from the best fit line. The dotted lines show the following relationships:

$$\tau = \sigma \tan (2\theta d + 30) \qquad (2.6a)$$

$$\theta d = 10 \log (\sigma_c/\sigma) \qquad (2.6b)$$

where θd = the dilation at peak

The basic friction angle ϕ_b for the model materials

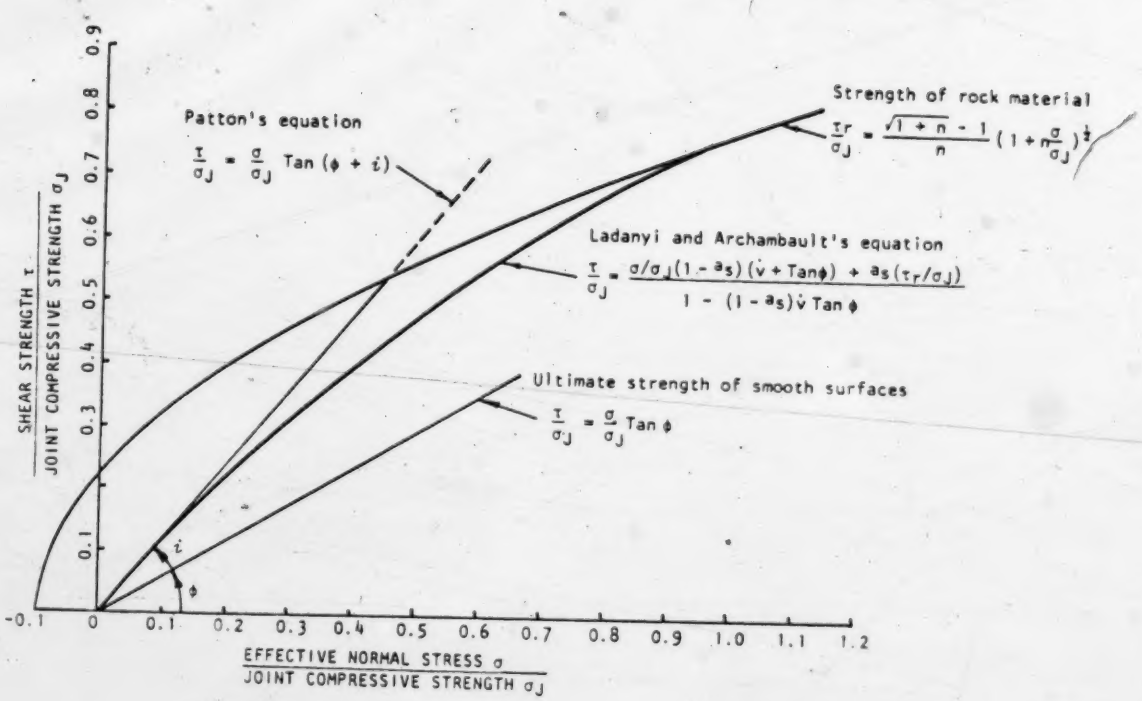
Patton's equation
$\frac{\tau}{\sigma_J} = \frac{\sigma}{\sigma_J} \text{Tan}(\phi + i)$
Strength of rock material
$\frac{\tau_r}{\sigma_J} = \frac{\sqrt{1+n} - 1}{n}\left(1 + n\frac{\sigma}{\sigma_J}\right)^{\frac{1}{2}}$
Ladanyi and Archambault's equation
$\frac{\tau}{\sigma_J} = \frac{\sigma/\sigma_J(1-a_s)(\dot{v} + \text{Tan}\phi) + a_s(\tau_r/\sigma_J)}{1 - (1-a_s)\dot{v}\,\text{Tan}\phi}$
Ultimate strength of smooth surfaces
$\frac{\tau}{\sigma_J} = \frac{\sigma}{\sigma_J}\text{Tan}\phi$
SHEAR STRENGTH $\frac{\tau}{\text{JOINT COMPRESSIVE STRENGTH } \sigma_J}$
EFFECTIVE NORMAL STRESS $\frac{\sigma}{\text{JOINT COMPRESSIVE STRENGTH } \sigma_J}$
-0.1 0 0.1 0.2 0.3 0.4 0.5 0.6 0.7 0.8 0.9 1.0 1.1 1.2
0.1 0.3 0.4 0.5 0.6 0.7 0.8 0.9
i
ϕ

Figure 2.5 Ladanyi and Archambault's equation for peak strength of rough surfaces

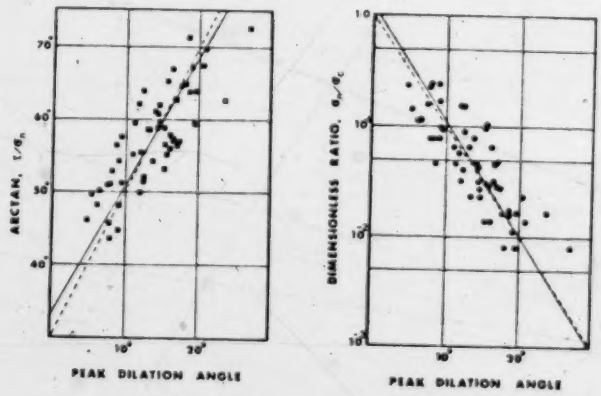

Figure 2.6 Peak shear strength results obtained from direct shear tests preformed on tension fractures in brittle model materials (Barton,1971)

ranged from 28.5° to 31.5° and $\phi b = 30°$ was used. Combining expression 2.6a and 2.6b, one obtains the approximate peak strength envelope for the model tension joint. (equation 2.6 c).

$$\tau = \sigma \tan (20 \log(\sigma c/\sigma) + 30) \qquad (2.6c)$$

Barton found that for low and medium stress levels (100 - 10,000 kPa), expression 2.6c gave a close approximation to the peak strength of interlocking rough surfaces, tension fractures and artificial faults. Moreover this expression could be modified to incorporate the effects of different degrees of surface roughness.

At the smoothest end of the spectrum, the logarithmic function describing the additional shear strength contributed by the surface roughness must obviously disappear, leaving the linear function which is the same form as the expression 2.1 ($\tau = \sigma \tan \phi b$). On the other hand, the coefficient (20) appearing in expression 2.6c defined the roughest end of the spectrum.

Surfaces of intermediate roughness were found to have intermediate values of the coefficient. Barton (1976) suggested the following general expression for peak strength envelope of rough surfaces:

$$\tau = \sigma \tan (JRC \log (JCS/\sigma) + \phi b) \qquad (2.6)$$

where JRC = joint roughness coefficient, representing a sliding scale of roughness which varies from approximately 20 to 0,

JCS = joint wall compressive strength; same as the unconfined compressive strength σ_c of the rock if the joint is unweathered, but may reduce to 1/4 σ_c if the joint walls are weathered.

The form of expression 2.6 for different values of JRC is illustrated in figure 2.7 (after Hoek 1976).

Notice that Barton's equation is based on three rock parameters the joint roughness coefficient (JRC), joint wall compressive strength (JCS) and basic friction angle (Øb). All these parameters can be measured in the laboratory and in the field.

The basic friction angle can be estimated with the help of the data listed in Table 2.1 unless the surfaces are strongly weathered.

If the surfaces are completely unweathered then the JCS will be equal to the uniaxial unconfined compressive strength of the rock material. The point load strength tests on rock core or irregular lumps as described by Broch and Franklin (1972) provide an alternate means to estimate the JCS. In most cases, however, discontinuity walls are weathered to some extend. Therefore, the JCS will be lower than σ_c. The relevant value is then measured using a Schmidt hammer applied directly to the exposed surface walls (Barton and Choubey, 1977). The Schmidt hammer is a simple device for recording the rebound of a spring loaded plunger after

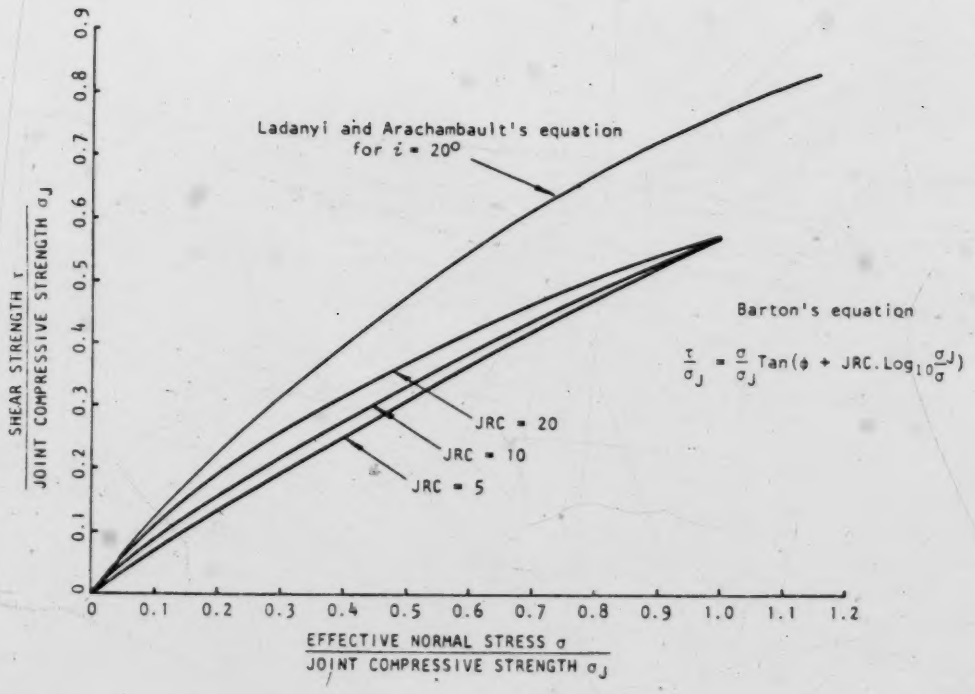
Ladanyi and Arachambault's equation
for i = 20°
Barton's equation
$\frac{\tau}{\sigma_J} = \frac{\sigma}{\sigma_J} \text{Tan}(\phi + \text{JRC}.\text{Log}_{10}\frac{\sigma_J}{\sigma})$
JRC = 20
JRC = 10
JRC = 5
SHEAR STRENGTH τ / JOINT COMPRESSIVE STRENGTH σJ
EFFECTIVE NORMAL STRESS σ / JOINT COMPRESSIVE STRENGTH σJ
0 0.1 0.2 0.3 0.4 0.5 0.6 0.7 0.8 0.9
0 0.1 0.2 0.3 0.4 0.5 0.6 0.7 0.8 0.9 1.0 1.1 1.2

Figure 2.7 Barton's equation for peak strength of rough joint surfaces

Rock type	Moisture condition	Basic friction angle ϕ_b	Reference
A. Sedimentary Rocks			
Sandstone	Dry	26—35	Patton, 1966
Sandstone	Wet	25—33	Patton, 1966
Sandstone	Wet	29	Ripley & Lee, 1962
Sandstone	Dry	31—33	Krsmanović, 1967
Sandstone	Dry	32—34	Coulson, 1972
Sandstone	Wet	31—34	Coulson, 1972
Sandstone	Wet	33	Richards, 1975
Shale	Wet	27	Ripley & Lee, 1962
Siltstone	Wet	31	Ripley & Lee, 1962
Siltstone	Dry	31—33	Coulson, 1972
Siltstone	Wet	27—31	Coulson, 1972
Conglomerate	Dry	35	Krsmanović, 1967
Chalk	Wet	30	Hutchinson, 1972
Limestone	Dry	31—37	Coulson, 1972
Limestone	Wet	27—35	Coulson, 1972
B. Igneous Rocks			
Basalt	Dry	35—38	Coulson, 1972
Basalt	Wet	31—36	Coulson, 1972
Fine-grained granite	Dry	31—35	Coulson, 1972
Fine-grained granite	Wet	29—31	Coulson, 1972
Coarse-grained granite	Dry	31—35	Coulson, 1972
Coarse-grained granite	Wet	31—33	Coulson, 1972
Porphyry	Dry	31	Barton, 1971b
Porphyry	Wet	31	Barton, 1971b
Dolerite	Dry	36	Richards, 1975
Dolerite	Wet	32	Richards, 1975
C. Metamorphic Rocks			
Amphibolite	Dry	32	Wallace et al., 1970
Gneiss	Dry	26—29	Coulson, 1972
Gneiss	Wet	23—26	Coulson, 1972
Slate	Dry	25—30	Barton, 1971b
Slate	Dry	30	Richards, 1975
Slate	Wet	21	Richards, 1975

Table 2.1 Basic friction angles of various unweathered rocks obtained from flat and residual surfaces(Barton and Choubey,1977)

its impact with a surface. The rebound value is then converted to an estimate of compressive strength using the method described by Miller (1965) who found a reasonable correlation between the rebound number and the unconfined compressive strength of the rock. The only unknown parameter is the jcint roughness coefficient or JRC.

If one or more direct shear tests have been performed the JRC can be computed by back analysing the shear test data. Thus, rearranging the expression 2.6,

$$JRC = \frac{\tan^{-1}(\tau/\sigma) - \phi b}{\log(\frac{JCS}{\sigma})}$$

Alternatively the JRC also can be estimated. This can be accomplished by comparison of the roughness of the discontinuity in question with the comprehensive set of natural joint roughness profiles given in figure 2.8 (after Barton and Choubey (1977).).

Barton and Choubey used expression 2.6 to predict the peak strength of eight different types of natural discontinuities. The mean value of the predicted peak shear strength angle, arctan (τ/σ) for the 100 surfaces tested in the direct shear tests was estimated to 0.5 degree.

They suggested that the equation 2.6 could be used in three different ways:

(i) curve fitting to experimental peak strength data

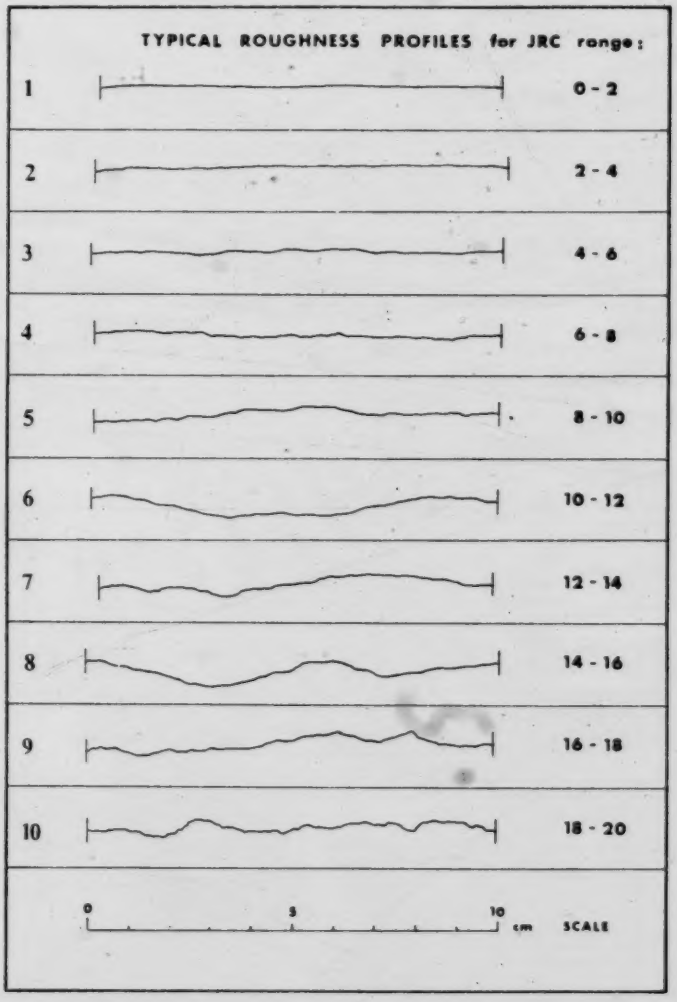

Figure 2.8 Roughness profiles showing the typical range of JRC values (Barton and Choubey, 1977)

(ii) extrapolation of experimental peak strength data and

(iii) prediction of peak strength of rock surfaces.

Notice that Barton's equation has the same form as Patton's, although they employ different failure criteria. Barton's equation can be written as:

$$\tau = \sigma \tan (iB + \phi b)$$

$$\text{where } iB = JRC \log (JCS/\sigma) \qquad (2.7)$$

Thus Barton's effective i-angle or iB is a function of the surface roughness (JRC), the material constant of surface Walls (JCS) and the effective normal stress level (σ).

Arctan (τ/σ) = 70 was the suggested maximum allowable shear strength for design purposes. Therefore, the maximum i-angle could be 40 degrees if the $\phi b = 30°$. However, the value of ϕb for most smooth unweathered rock surfaces in fact lies between 25° and 35° as can be seen in Table 2.1. The corresponding range of i-angle, for design purposes in rock mechanics, would be between 0 and 45 degrees.

For comparison with Barton's equation, Ladanyi and Archambault's equation for i=20 is plotted on the figure 2.7. From this figure one can conclude that Barton's equation is in close agreement with Ladanyi and Archambault's (for i = JRC = 20) at very low normal stress levels. As the stress level increases, the strength envelopes diverge. The difference in shear strength

predicted by these two methods is due to the alternate sources of shear strength assumed as $\sigma/\sigma c=1$, Barton's equation reduces to $\tau = \sigma \tan \phi b$ which means that the strength at high normal stresses is due to the basic friction on the smooth rock surfaces whereas, Ladanyi and Archambault's equation reduces to $\tau = \tau r$, the shear strength of the rock material adjacent to the surface.

Barton's equation tends, therefore, to be more conservative than Ladanyi and Archambault's at higher normal stress levels. However, if required, these strength envelopes can be brought into coincidence by adjusting the contribution of the intact material at failure. This adjustment is not recommended since Barton's original studies were carried out at very low stress levels and his equation is probably most applicable in the range $0.01 < \sigma/\sigma c < 0.3$, which generally operate in rock slope engineering, whereas Ladanyi and Archambault's equation was intended for more general use.

Barton's equation is a very useful tool in rock slope stability analysis and it is highly recommended by Hoek and Bray (1977) for the above specified range of stress levels.

Note that the Patton's equation, Schneider's equation, Ladanyi and Archambault's equation and Barton's equation for shear strength envelopes for rock discontinuities all include the basic friction angle and the effective inclination of rock surfaces. The complexity of their

equations reflect the difficulty of including the shearing resistance offered by the effective surface irregularities which primarily control the shear mechanism and the forms of failure envelopes.

One of the purposes of this thesis is to test the validity of Barton's equation for peak shear strength of two types of rock surfaces. Some direct shear tests have to be carried out in order to fulfil this goal. It is the author's intention in the rest of this chapter to present the experimental data from laboratory direct shear tests.

2.2 Sample Preparation

2.2.1 Types of Rock

Two rock types were of interest for this study: one a soft material and the other hard. The soft type, a limestone, was Tyndall Stone whereas the hard type, an igneous rock, was Standstead Granite. The choice of these rocks primarily depended on their availability and their two extremes of hardness.

A slab of Tyndall Stone of size 50 cm x 76 cm by 5.7 cm thick (about 20" x 30" by 2.25") was purchased from J.F.C. Masonry Supplies Ltd., Edmonton. About four weeks elapsed from the time it was quarried to the time it was ordered. Tyndall stone is quarried by Gillis Quarries Ltd., at Garson, Manitoba, about thirty miles north east of Winnipeg. The deposit at Garson was opened in 1895, but since the

nearest railway point was at Tyndall the stone became known as Tyndall Stone.

Two slabs of Standstead Granite were purchased from Alberta Granite Marble & Stone Co. Ltd., Edmonton. One slab measured 30 cm x 30 cm by 5.7 cm thick (about 12" x 12" by 2.25") and the other 60 cm x 91 cm by 5.7 cm thick (about 24" x 36" by 2.25"). The age of these slabs is unknown but according to the best estimate of the suppliers, it was about two to three months old. Standstead Granite is quarried by the ADRU Granite Company, at Beebe, Quebec.

The three slabs were sent to Alberta Granite Marble & Stone Co. LTD. for cutting into 15.24 cm (6 in.) square blocks and these blocks were termed the 6x6 blocks.

2.2.2 Sample Size and Initial Orientation

Before the slabs were cut into square blocks, numbers were marked on each slab as illustrated in figure 2.9. In this way, blocks could be matched to the original shape of the slabs after cutting.

In figure 2.9, type 1 represents Tyndall Stone whereas type 2 and type 3 represent the big and small slabs of Standstead Granite respectively. The numeral characters designation chosen is for ease of computer program input and output of data. Therefore, any subsequent designation will be numeral.

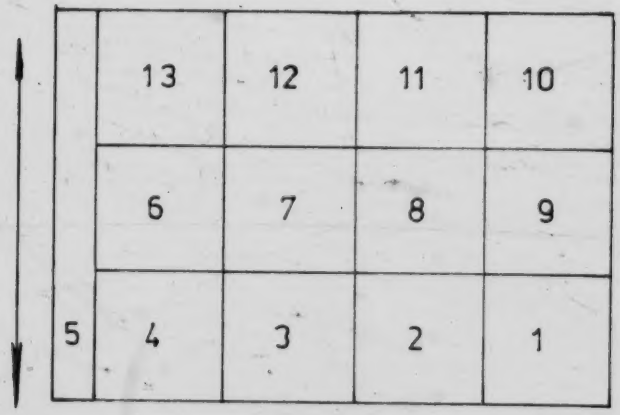

7	6	1
8	5	2
9	4	3

2x2 samples

Type 1 Tyndall Stone slab (6x6 blocks)

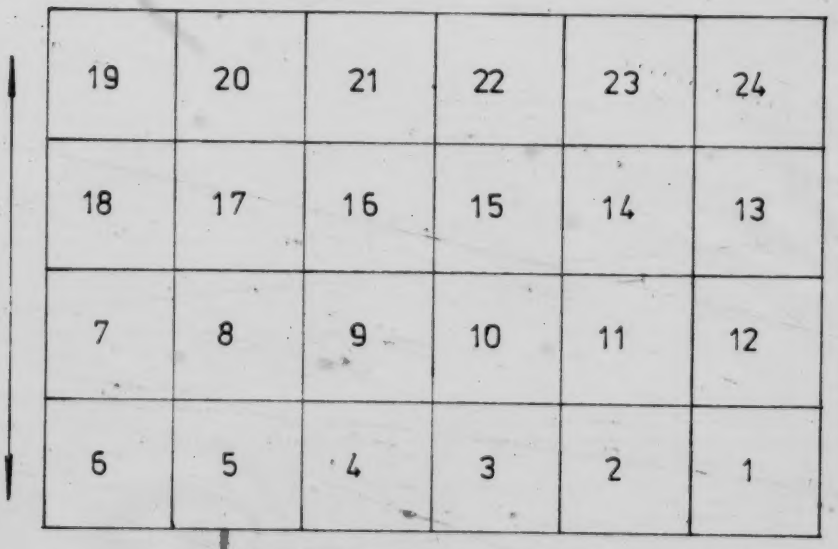

7	6	1
8	5	2
9	4	3

2x2 samples

Type 2 Standstead Granite slab (6x6 blocks)

36	25	24	13	12	1
35	26	23	14	11	2
34	27	22	15	10	3
33	28	21	16	9	4
32	29	20	17	8	5
31	30	19	18	7	6

Direction of shearing

Type 3 Standstead Granite slab (2x2 samples)

Figure 2.9 Initial orientation of the Tyndall Stone and Standstead Granite samples

The 15.24 cm square blocks were cut into small 5.08 cm (2") square samples, all having a thickness of 5.7 cm. These square samples were termed the 2x2 samples. Again the initial orientation of these samples were noted as illustrated in figure 2.9.

The purpose of sampling designation by numerals is three-fold: (a) the ability to characterize a large number of samples, (b) the indication of the direction of shearing of the samples, denoted by arrows in figure 2.9, and (c) the investigation of any changes in strength within the slab.

Direction of shear is of importance since the planar nature of the discontinuities and the widely varying characteristics of the irregularities causing the shear strength along a discontinuity may be highly anisotropic (Deere et al 1967).

The cutting took a great deal of time. With the permission of the Mineral Engineering Department, University of Alberta, two diamond saw machines, model-J3, manufactured by the Highland Park Manufacturing Co. California, were used for this purpose. In addition, some cutting was done in the Civil Engineering Department using a Northland concrete saw manufactured by Oxford Machine and Welding Co. Ltd. of Edmonton, Alberta.

In all cases when using the diamond saws water was employed as a cutting fluid. It also served as a cooling

agent.

Once the 2x2 samples were cut, they were washed cleaned and dried. If samples were not square, they were sanded to a snug fit in the 2x2 shear boxes.

Some of the 2x2 samples of each type of rock were finally cut into "half samples". The orginal plan area remained the same but the thickness was cut into halves. The half samples were termed the 2x1 samples.

The 2x1 samples were cut using the Northland machine together with a specially designed clamp, illustrated in figure 2.10. With the clamp six 2x2 samples could be cut into halves at the same time to give smooth cutting edges. The lower halves were denoted by 1 and top halves by 2.

The reason for using 2x1 samples will become apparent in the next section.

2.2.3 Sample Requirements

The sample sizes and the method of production of rock surfaces were determined by:

(A) Availability of machines : the size of the surfaces governed by the dimensions of the direct shear boxes available and their (shear and normal stress) capacity,

(B) Sample reproducibility: a good controlled procedure is needed in order that the same kind of samples can be

reproduced at any time. This also includes the reproducibility of surface roughness.

(C) Shear stress drop: the rock surfaces must be rough enough to have distinct peak and ultimate resistances in a shear load versus horizontal displacement plot.

(A) Availability of Machines:

The ultimate goal of this study is to investigate the time-dependence of frictional behavior in shear. The machines available for this purpose were conventional soil shear boxes modified for shearing rock surfaces. These machines are termed the creep machines. The creep study will be presented in Chapter IV.

Since the creep machines are limited to a certain range of stress levels, the samples should be prepared with this in mind. Half samples are encouraged. The sample would be sheared in the same direction shown in figure 2.9. The side with a smaller area would be sheared in the horizontal position parallel to the fractured surface which was induced artificially (B), whereas with the 2x2 samples the shearing surfaces would be on the larger area.

The 2x2 samples were used to evaluate the basic friction angles of the two rocks considered and also for the study of (C).

(B) Sample Reproducibility

Both types of rock slabs can be purchased at anytime from the suppliers and can be transformed into 2x2 or 2x1 sample sizes as described above.

The 2x1 samples were cast into 5.08 cm square samples for snug fit in the the shear boxes. The casting procedure is illustrated in figure 2.11.

They were cast in F-181 sulfaset which is a fast grouting cement, yellow in colour, manufactured by Randustrial Corporation, of Cleveland, Ohio. Each half was cast separately leaving a space between the halves for the fractured surface.

After casting was completed, a continuous notch (figure 2.11d) about 0.3 cm deep was cut along the four sides between the two halves (figure 2.11c) using a portable diamond saw. Some 2x2 samples were notched in the same manner.

The purpose of a continuous notch was to define an exact right angle rectangular area which could be easily measured using calipers. Moveover the notch could provide a wedge for a chisel (section C).

Up to this point, there were three types of samples prepared, VIZ.; 2x2 samples with notches, 2x1 cast samples with notches and 2x1 half samples.

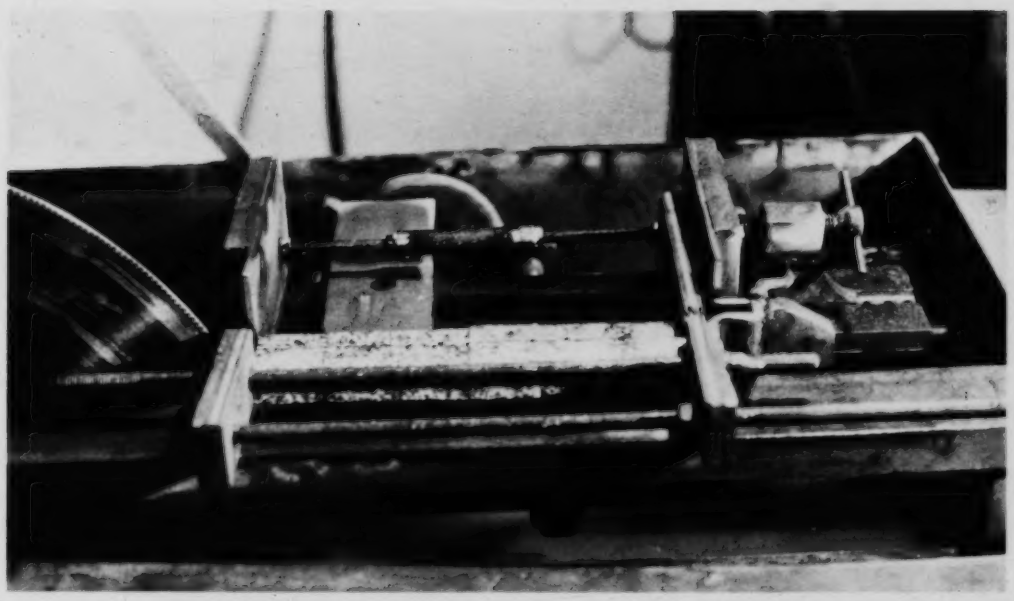

Figure 2.10 The special design clamp for cutting the 2x2 samples into 2x1 samples

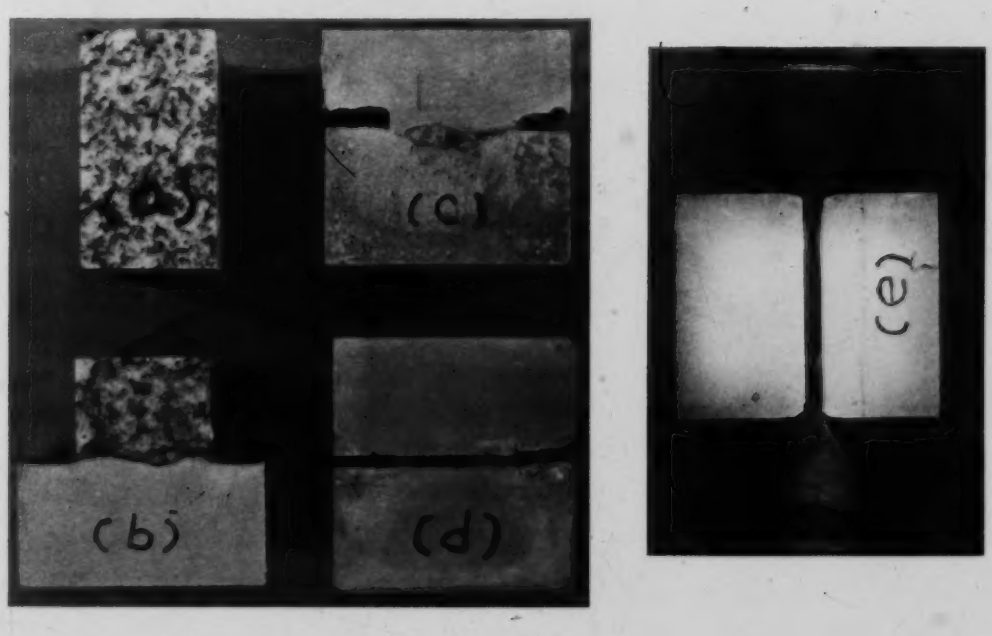

Figure 2.11 Procedures of fractured rock surface preparation

(C) Shear Stress Drop

The stress drop of a surface is the difference between peak and ultimate shear strengths. This difference reflects the resistance offered by surface asperities. Therefore, a good control of constructing a rock surface would govern the corresponding degree of roughness of asperities induced which in turn controls the amount of stress drop if the surface were sheared.

Three methods were employed to artificially prepare the rock surfaces, (a) sandblasting with #30 grits for different lengths of time (for the 2x1 half samples), (b) chisel splitting (for the 2x2 samples with notches and (c) point load strength machine splitting with edge blades (for the 2x1 cast samples with notches).

Using methods (a) and (b), samples were prepared at the Alberta Granite Marble & Stone Co. Ltd. whereas those from method (c) were prepared in the University of Alberta (figure 2.11e). The point load testing machine was borrowed from the Mineral Engineering Department. It was a RM-730 model point load tester manufactured by the Soiltest Inc. Evanston, Illinois. These prepared surfaces were then tested in a 89 kN direct shear machines. (This machine will be described in detail later in this chapter) The tests were run dry at a rate of horizontal deformation of 0.052 cm/min. The shear load versus displacement curve was recorded on a Honeywell model 540 x-y-y' recorder. The results of these

tests are shown in figure 2.12.

The results indicate that the surfaces prepared using the sandblast technique do not give distinct peak and ultimate shear load values whereas surfaces prepared in the other ways yielded distinct peak and ultimate shear load values. While the chisel splitting method satisfies the stress drop criterion, the shear loads required to produce the drops are very high as shown in figure 2.12. This range of shear load is outside the capacity of creep machines (maximum 8.9 kN shear load).

In view of this, the method employing the point load splitting machine for artificial rock surface preparation was adopted. Besides, the sample requirements were satisfied and this method gave a good control of the surface roughness reproducibility.

2.2.4 Artificial Rock Surfaces

After the choice of preparing rock surface was made, more than a hundred tensile fractured surfaces from the 2x1 cast samples were constructed (figure 2.11e) for each type of rock. Each surface was marked with the appropriate numeral characters. For example a surface labelled 5.3.8.1 means that it is from a half sample (5), the sample is from the small slab granite (3), the original 2x2 sample location is denoted by an eight (8) as shown in figure 2.9 and finally it is the lower half of a 2x2 sample (1).

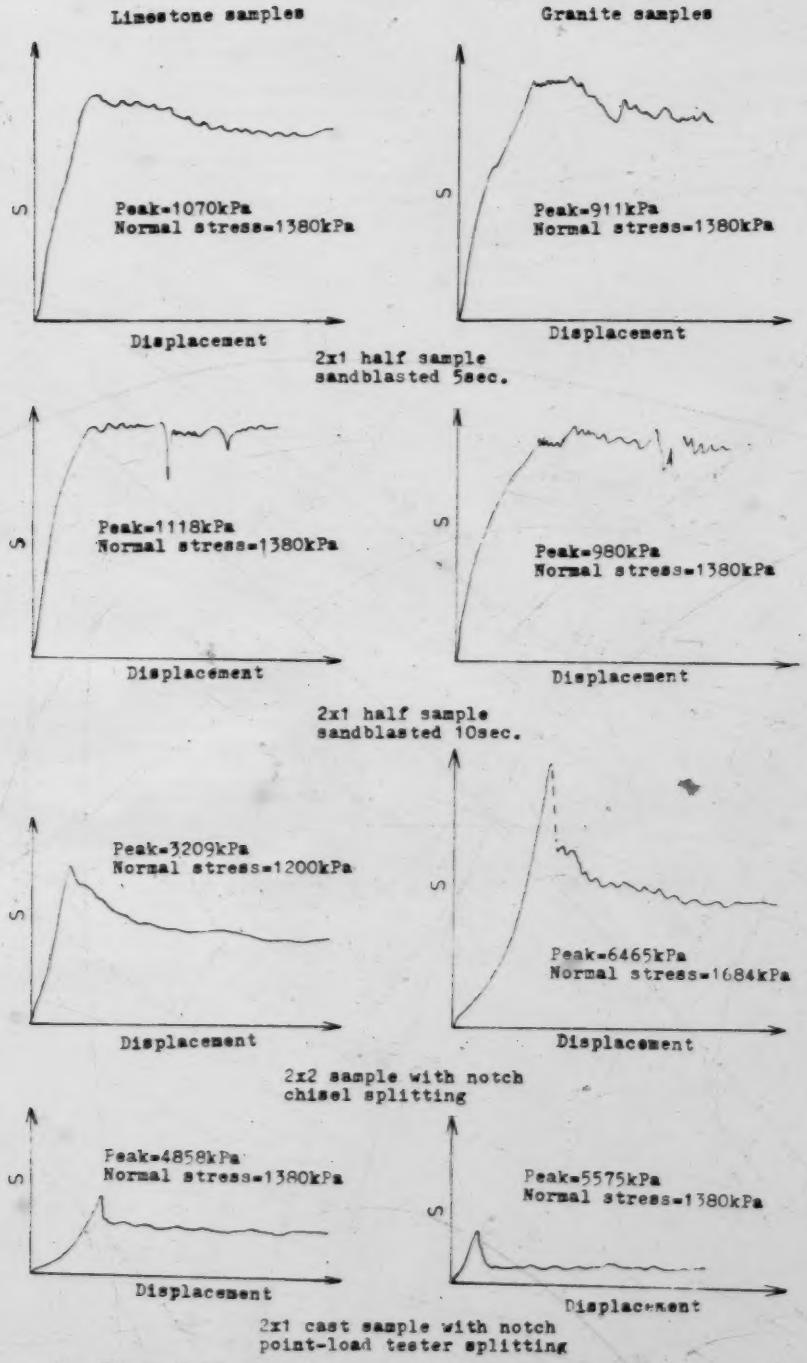

Figure 2.12 Shear load versus displacement curves showing the stress-drop characteristics for samples prepared from different methods

All the rock surfaces were then stored in a temperature and humidity controlled room.

2.3 Laboratory Testing Programme

2.3.1 Apparatus and Testing Environment

The direct shear machine used for shear strength tests was specially built at the University of Alberta for testing rock specimens. The machine has a shear capacity of 89 kN.

All the moving parts are made of stainless steel. While the upper shear box "travels" above the lower one, it has two brackets bolted together, one at each end of the box and these brackets are connected by two steel rods to four arms which are welded to the supporting steel block lying below the lower shear box. The detailed arrangement of the shear box is illustrated in figure 2.13.

The friction between steel rods and brackets and arms in minimized by small bearing rings. Slip bearings are places in between the lower shear box and the supporting steel block so that the shear box can move relative to the stand without much friction. The lower shear box is driven by a steel rod connected to the gear box (not shown in the figure) whereas the upper shear box is hooked up to a load cell which records the shear force.

The upper shear box is allowed to translate only. In this way, both sample toppling in the shear direction and

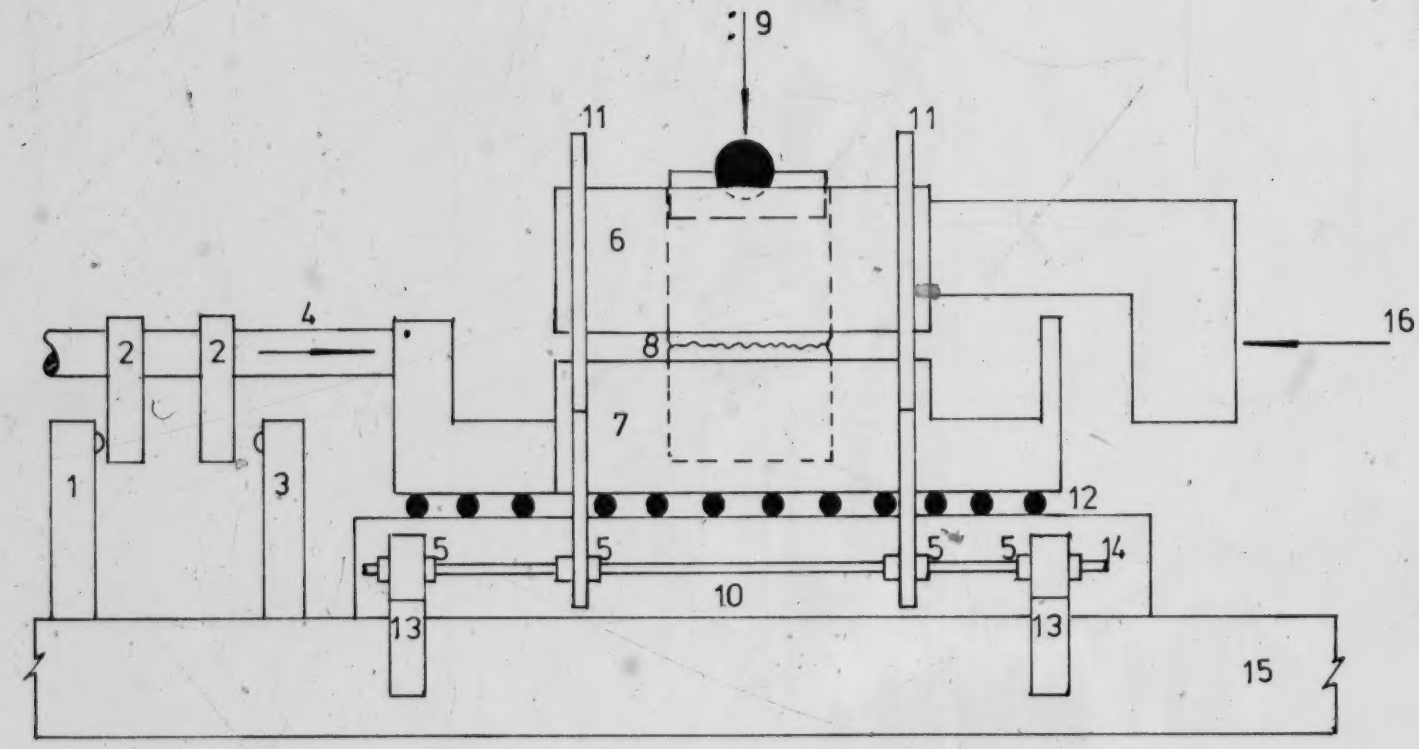

1.stop swith 2.adjustable clamps 3.reverse switch 4.shearing force 5.bearing rings
6.upper box 7.lower box 8.rock surface 9.normal load 10.supporting block
11.brackets 12.steel ball bearings 13.arms 14.steel rod 15.stand 16.load cell

Figure 2.13 Direct shear box for testing shear strengths of rock surfaces

sample tilting, sideways during shear, are precluded.

Five load cells (one 4.5 kN, two 11.12 kN and two 22.24 kN capacity) were designed and calibrated. They were used at different stress levels. The design of the load cells can be found in the appendix A.

The vertical and horizontal displacements were measured by linear voltage displacement transducers (LVDT). Both displacements and shear load were recorded on the x-y-y' recorder which could plot vertical displacement versus horizontal displacement and shear load versus horizontal displacement graphs at the same time.

All tests performed were done in a temperature and humidity controlled environment. The temperature was at 20°±1°C with a relative humidity of 50 percent.

The prepared samples were stored in the same environment. A minimum of two weeks was allowed for samples to come to an equilibrium condition with the surroundings before they were sheared.

2.3.2 Material Constants

(A) Uniaxial Compressive Strength, σ_c

Three methods were employed to compute the uniaxial compressive strength (σ_c) of Tyndall Stone and Stanstead Granite; (i) conventional compression test on cylindrical Samples (ii) the point load strength test and (iii) the

Schmidt hammer index test.

(i) Conventional Compression Test

Three cylindrical Tyndall Stone and two cylindrical Standstead Granite specimens were cored from the 15.24 cm square blocks. The ends were then finished, at right angles to the long axis of the sample. This was done by positioning the specimen in a RM-830 Rock Specimen Holder polishing the ends using a lapping machine employing #400 grit lapping compounds. In their final form, the specimens were about 2.3 cm in diameter and 5.0 cm in length. Thereafter, these specimens were tested in a compression testing machine in the Mineral Engineering Department. It was Universal Testing Instrument, Model-TTD manufactured by the Instron Corp., Canton, Mass. Both the load frame and load cell had a 89 kN capacity.

The loading rate was 0.508 cm/min. The measured failure loads of the specimens were then divided by the corresponding cross sectional areas to obtain the uniaxial strengths of the rocks. The results of these tests are listed in table 2.2.

(ii) Point Load Strength Test

The point load strength test for strength classification of rock materials described by Brock and Franklin (1972) is an alternate method to compute σc.

	TYNDALL STONE	STANDSTEAD GRANITE
	Uniaxial compression strength MPa	Uniaxial compression strength MPa
Cylinder test	35.91 39.01 76.87	119.33 95.24
Point-load strength test	76.99 77.99	142.27 147.17 137.36 121.66 132.45
Schmidt hammer index test	66.90	144.00
Supplier information	62.87	

Table 2.2 Values of uniaxial compression strength of Tyndall Stone and Standstead Granite obtained from different methods

Five granite and two limestone samples were prepared using a diamond saw. They were rectangular prisms with the average height being 5.7 cm and the width 4.2 cm. Using the point load strength method, the compressive strength of the two rocks were determined. The results are listed in table 2.2.

(iii) Schmidt Hammer Index Test

Miller (1965) suggested the suitability of the Schmidt hammer to estimate the unconfined compressive strength (σ_c) of rock. The Schmidt hammer is a simple device for recording the rebound of a spring loaded plunger oriented normal to a rock surface after impact with that same surface. Miller found a reasonable correlation between the rebound number (range 10 to 60) and the unconfined compressive strength of the rock. However, a better correlation was obtained when he multiplied the rebound number by the dry density of the rock:

$$\log (\sigma_c) = 0.00088\,\gamma R + 1.01 \qquad (2.8)$$

where σ_c = unconfined compressive strength (Mn/m^2)

γ = dry density of rock (kN/m^3)

R = rebound number

Using the Schmidt hammer method, five tests of each rock were made. The results are given below:

Tyndall Stone : $\gamma = 23.90\ kN/m^3$ (152 pcf)

R = 40, 37, 44, 38, 35

Mean R = 38.8

σ_c = 66.90 MN/m²

Standstead Granite : γ = 26.10 kN/m³ (166 pcf)

R = 52, 54, 49, 48, 45

Mean R = 50

σ_c = 144.00 MN/m²

The above results together with the compressive strength of Tyndall Stone obtained from the suppliers are also listed in table 2.2

As shown in table 2.2, the average uniaxial compressive strengths obtained from the cylinder tests are less than those obtained from other methods. These lower values may be explained due to faulty preparation of the ends of the sample- their not being parallel. Buckling failure of some specimens was observed in the tests. Therefore, unless the ends of the specimens are very carefully prepared the strengths are too low. Other possible factors affecting the results in the uniaxial compression are discussed by Coates (1970).

The compressive strengths from the point load strength test for the granite specimens fall within a range of values between 122 MPa and 147 MPa having a mean of 136 MPa. The average value for the same rock from the Schmidt hammer test is 144 MPa which lies within the range of the point-load

strengths. This good agreement in strength between these two methods can not be found in the Tyndall Stone specimens where the strength values from both methods are greater than the compressive strength obtained from the supplier.

In view of this, for the purpose of this study, the value of σ_c for the Tyndall Stone is taken to be 62.87 MPa (9112 psi) and that for the Standstead Granite 136 MPa (19740 psi).

(B) Basic Friction Angle ϕ_b

As noted earlier, the peak strength envelope equations for rock discontinuties include the basic friction angle, ϕ_b. Ideally, this quantity should be determined by direct shear testing on flat artificially prepared surfaces.

Patton (1966) suggested using rough sawn rock surfaces and Coulson (1972) employed surfaces prepared with #80 grit (silicon carbide grits) whereas Barton (1971) used surfaces prepared by sandblasting technique.

Shear tests for the determination of ϕ_b should be carried out over a range of normal stress levels to ensure that a linear relationship between shear strength and normal stress with zero cohesion is obtained. This precaution is necessary because the shear strength at very low normal stresses can be influenced by extremely small asperities on the sample surface.

In this study, surfaces were prepared using (i) a diamond saw, (ii) 40x dry sand paper and (iii) sandblasting methods. The 5.08 cm square (2x1 half) samples were used for each type of rock. Five series of samples were prepared employing each method of surfaces preparation. Therefore, there was a total of 30 samples.

Before the actual shear tests were carried out, the samples were tested on a tilt table. The angle (α), measured between the tilt table and the horizontal reference plane, at which the upper half sample started to slide was recorded and was used tc ccmpare with the ϕb.

Samples tested in the tilt table were then sheared in the 89kN direct shear machine described earlier (4.5 kN load cell was used). Four of each of the similarly prepared samples were sheared at different normal stresses and the remaining sample was tested by stage-loading. All tests were run dry at a rate of horizontal deformation of 0.052 cm/min.

A stage-test was achieved by initially allowing the sample to deform horizontally until the shear load ceased to increase then, the normal load was increased and the test continued until the shear load had once more levelled off. In this way, the sample was step-loaded to the highest desired normal load. The advantage of such a test is that only one sample is needed to define the shear strength envelope of the rock surface considered.

After shearing, upon removing the samples from the shear box, surface damage features such as rock flour and polished areas were observed. All surfaces suffered some degree of damage during shearing and the damage was marked in the stage-loading failure surfaces. In general, damage increased with normal pressure.

Typical shear load versus displacement curves for single and stage-loading tests are shown in figure 2.14. From these curves, the shearing resistance corresponding to the joint where the shear load began levelling off was noted at each normal load. The shear and normal loads were then divided by the initial area to obtain values of the respective stresses. Once the stresses had been computed, their angles of friction, [arctan (peak/normal)] were tabulated, as shown in table 2.3, together with the results from the tilt tests. The following points can be made from study of these results:

(a) There is no systematic variation of the basic friction angle, ϕ_b with normal stress for both single and stage-loading direct shear tests within each method of surface preparation.

(b) The difference in ϕ_b obtained in the various direct shear tests between methods of surface preparation is significant. This might be the results of different degree of surface roughness from various methods of surface preparation. The computed mean ϕ_b from the stage-loading tests is higher than that from the

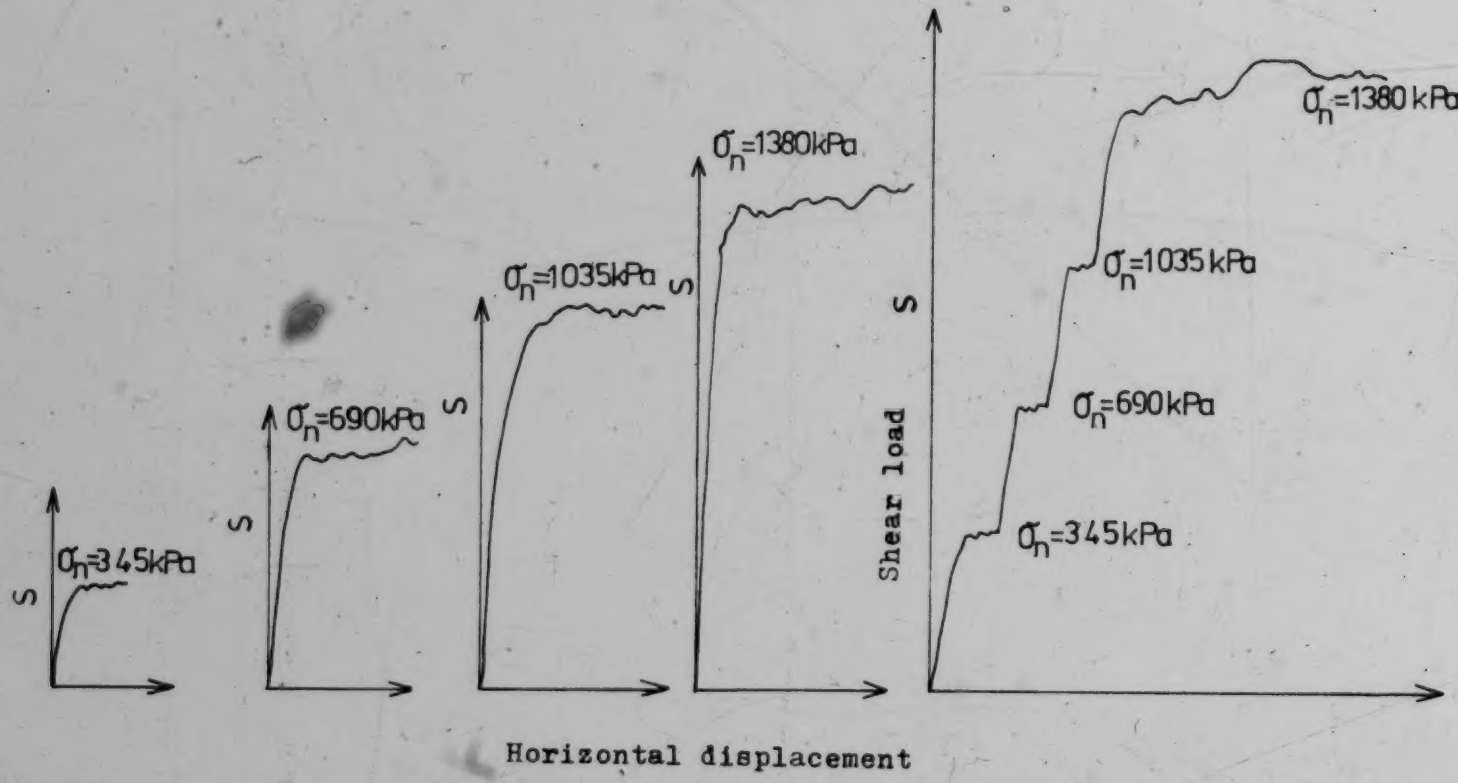

Figure 2.14 Shear load versus displacement curves for single and stage-loading tests

Surface preparation	Rock type	TILT TEST: Mean failure angle N=0.05 to 0.1kPa	S.D.	DIRECT SHEAR SINGLE-LOADING TEST: Basic friction angle Øb N=345 kPa	N=690 kPa	N=1035 kPa	N=1380 kPa	Mean Øb	S.D.	DIRECT SHEAR STAGE-LOADING TEST: Basic friction angle Øb N=345 kPa	N=690 kPa	N=1035 kPa	N=1380 kPa	Mean Øb	S.D.
Diamond saw cut	G	27.00 ±2.83	2.09	32.13	31.23	34.29	36.35	33.50 ±3.50	2.29	40.97	39.06	38.41	36.71	38.78 ±2.38	1.76
	L	31.70 ±3.01	2.22	44.10	40.75	41.54	40.37	41.69 ±2.26	1.67	44.66	43.66	41.72	42.08	43.03 ±1.85	1.37
Dry, sand paper size 40x (60 sec)	G	27.80 ±3.78	2.79	36.24	34.46	34.47	39.24	36.10 ±3.05	2.25	32.09	33.19	34.11	34.36	33.43 ±1.38	1.02
	L	42.00 ±1.72	1.27	44.63	36.35	30.38	43.29	38.66 ±8.95	6.60	43.63	40.75	40.55	41.06	41.50 ±1.94	1.43
Sand-blast	G	33.50 ±3.94	2.91	28.40	28.83	31.73	33.05	30.50 ±3.05	2.25	32.52	32.52	33.42	33.54	33.00 ±0.75	0.55
	L	43.50 ±2.87	2.12	34.10	30.93	35.45	33.41	33.50 ±2.56	1.89	38.05	35.82	36.58	34.32	36.20 ±2.10	1.55

N=normal stress
G=Standstead Granite surfaces
L=Tyndall Stone surfaces
S.D.=standard deviation of the mean angle
±95% confidence limits on the mean

Table 2.3 Results of the basic angles, Øb of Standstead Granite and Tyndall Stone surfaces prepared from different methods

single-loading tests. (except in the case of the Standstead Granite surfaces prepared from the dry sand paper method).

(c) In general, the standard deviations of the mean ϕb are lower in the stage-loading than in the single-loading tests. In a stage-loading test, only one sample is employed whereas in the other several individual samples are tested. The difference in individual microscopic surface roughness is reflected in the higher values of the standard deviations of the mean ϕb.

(d) There is a significant difference between the mean failure angle, α obtained from the tilt tests and the ϕb obtained from the direct shear tests at the low normal stresses.

(e) For both types of rock, the sandblasting method gives the lowest mean ϕb in the single-loading tests. Moreover, by comparing the mean ϕb from the single-loading tests with the values in table 1 for both rocks, one sees that the ϕb obtained from the sandblasted surfaces fall in the suggested range of the basic friction angles of various unweathered rocks listed in the literature.

In view of these results, the values chosen for this study are $\phi b = 33.5$ degrees for the Tyndall Stone and $\phi b = 30.5$ degrees for the Standstead Granite. The 95% confidence limits for these mean ϕb are 30.94 to 36.06 degrees and

27.45 to 33.55 degrees for the limestone and granite respectively.

2.3.3 Tilting Tests

Upon the completion of sample preparation, each fractured sample was labelled to differentiate the top half (T) from the botton half (B). It was then subjected to a tilt test. The tilting apparatus was described in detail by Bruce (1978). It is a simple inclined-plane friction apparatus in which a sample is positioned with the bottom half clamped on the plane while the top half is subjected to slide relative to the bottom half when the plane is tilted. When the top half begins to slide, the angle of inclination of the plane is noted. The angle is termed angle .

Since a surface would be sheared in the direction as shown in figure 2.9, it could be sheared in two ways, either uphill or downhill along the irregularities. The corresponding strength obtained would be different. Therefore, two tilt tests were performed for each surface by tilting it in the "forward" and then "backward" directions. The small angle (α) and the direction of motion were denoted by arrows which indicated the way the surface would finally be sheared in the direct shear box.

All the tilted surfaces failed in toppling; the top half rotated about its lowest point of contact with the bottom half. Toppling failure was seen both in the forward

and backward directions. The range of α for 95 granite surfaces was between 52 and 85 degrees with a mean value of 59.8 degrees. The range of α for 90 limestone surfaces was between 56 and 75 degrees with a mean value of 60.3 degrees.

DeFreitas and Watters (1973) studied the toppling failure mechanism by considering a block of rock resting on an inclined plane as illustrated in figure 2.15 a. The block has a height h and base length b. It is assumed that the force resisting downward movement of the block is due to friction only.

When the vector representing the weight W of the block falls within the base b, sliding of the block will occur if the inclination of the plane ψ (same as α in a tilt test) is greater than the angle of friction ϕ. However, when the block is tall and slender (h>b), the weight vector W can fall outside the base b and, when this happends, the block will topple.

The conditions for sliding and toppling of a block on an inclined plane are given in figure 2.15b. The four regions in this diagram are as follows:

Region 1 : $\psi < \phi$ and $b/h > \tan\psi$, the block is stable and will neither slide nor topple.

Region 2 : $\psi > \phi$ and $b/h > \tan\psi$, the block will slide but it will not topple.

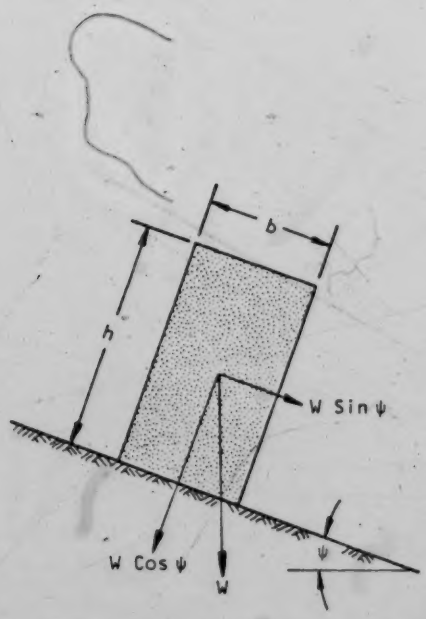

Figure 2.15a Geometry of block on inclined plane

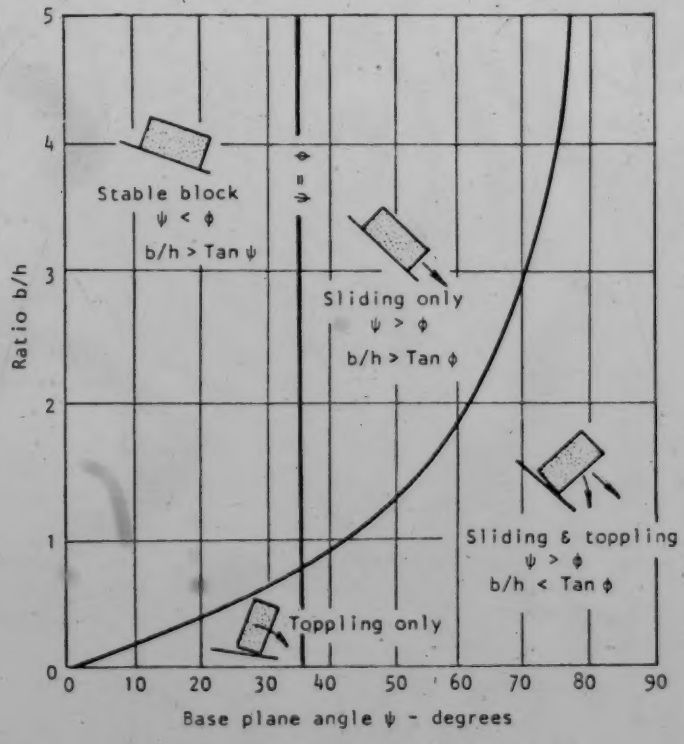

Figure 2.15b Conditions for sliding and toppling of a block on an inclined plane (De Freitas and Watters, 1973)

Region 3 : $\psi < \phi$ and $b/h < \tan\psi$, the block will topple but it will not slide.

Region 4 : $\psi > \phi$ and $b/h < \tan\psi$, the block can slide and topple at the same time.

The criterion of region 3 was applied to the results of tests on rock surfaces performed in the tilting apparatus. Since these rock surfaces toppled, they had to satisfy (i) $\alpha < \phi$ and (ii) $b/h < \tan\psi$. The dimensions for the top halves were measured and fcund, on average, to be b = 5.08 cm and h = 3.05 cm. The arctan (b/h) was 59 degrees which was less than the mean values of α for both rock surface; therefore, $b/h < \tan\alpha$ was satisfied. No visible damage to the surface irregularities was observed after the tilt tests. This might be due to the very small effective normal pressure generated by the self weight W of the top half sample. In general, the pressure was less than 1 kPa. The shear mechanism at this low stress level would be controlled by the "sliding-up" mode (Patton, 1966).

A lower bound on the angle of friction in figure 2.15b would then be the effective angle of inclination plus the basic friction angle. That meant $\phi = i + \phi b$ and $\phi = \alpha$ which satisfied the other requirement for failure in toppling.

Using the results of basic friction angles of rocks in last section (ϕb=33.5, Limestone; ϕb=30.5 Granite) and the ranges of α, one could compute the approximate ranges of

effective angles of inclination of two types of rock surfaces. For the limestone surfaces the range would be between 22.5 and 41.5 degrees whereas between 21.5 and 54.5 degrees for the granite surfaces. Surfaces having these i-angles are very rough as might be expected from the fresh tensile fractures of natural rocks. The effects of surface roughness on shear strength of these surfaces is clearly very important. Detailed studies of surface roughness and their relationships with the peak strength of rock surfaces will be presented in the next chapter.

2.3.4 Test Procedure

The testing environment was the same as described earlier. The direct shear apparatus is illustrated in figure 2.13. The shear load was applied by a gear box chain drive assembly powered by an electric motor. The normal load was applied with a dead weight lever arm arrangement. The vertical and horizonal deformations were measured with LVDT. The shear load was measured with a load cell. The LVDT and load cell outputs were fed and calibrated to the axes of the x-y-y' recorder which permitted magnification of the load-displacement and vertical-horizontal displacement curves.

The five load cells designed were calibrated in compression and were assumed to give the same calibration factors in tension.

Each surface was airblown to make sure it was clean,

the direction of shear was checked, the intial shear area was measured and the desired normal load was computed before the machine and the sample were assembled. The normal load was then applied and the initial reading on the x-y-y' recorder noted. When the set-up was completed, horizontal deformation of the sample was started and continued until the total deformation was approximately 0.7 cm (which was about 15 percent of length of the surface in the direction of shear). At this point, the normal load was held constant and the direction of shear displacement reversed till the shear box was back in its initial position. This was done automatically by the reversal switch. Both the reversal and on-off switches were set in between the driving gear box and the shear box as illustrated in figure 2.13. The two metal plates which were clamped to the driving shaft could be adjusted to any desired positions as to when the shear experiment reversed or stopped.

The upper shear box was fixed relative to the stand while the lower half advanced or reversed relative to the upper box.

All tests were run dry at a rate of deformation of 0.052 cm per minute and all experiments were begun with new rock samples. In this way, a total of 48 granite and 46 limestone surfaces were sheared. The effective normal stresses used varied from 173 kPa to 6900 kPa.

Upon removing the samples from the shear box after the

test, it was noticed that the actual area of contact had been very small. The approximate percentage of area of contact for the limestone sheared surfaces was about 5 to 30% whereas for the granite surfaces 5 to 20% was observed. A typical sheared surface of each type is illustrated in figure 2.16.

During every shear box test performed, a sharp cracking sound was heard, with higher intensity during testing of granite samples. The occurrence of the cracking sound coincided with the attaining of the highest shear load as recorded on the load-displacement graph.

2.3.5 Observations During Shear Tests

For each of the shear tests run, two curves, the load versus displacement and vertical versus horizontal displacement were obtained directly on the x-y-y' recorder. Typical curves are illustrated in figure 2.17a,b,c,d in which diagrams a and b represent curves for a limestone surface and diagrams c and d for a granite surface.

Both load-displacement curves (diagrams b and d) for the two types of rock surfaces had common characteristics. The shear force gradually increased to a peak as denoted by a point A and fell sharply with increasing deformation. The peak was then followed by considerable fluctuations but at larger displacements, the shear force decreased at a decreasing rate and finally tended to an ultimate value as

Figure 2.16 Typical rock surfaces after shear

Speed=0.052 cm/min.
Rock surface=51932
Normal stress=3450kPa
Shearing area=9.88 sq.cm.
Scale: load 1cm=2882.46N
vert. 1cm=0.018cm
hori. 1cm=0.14cm

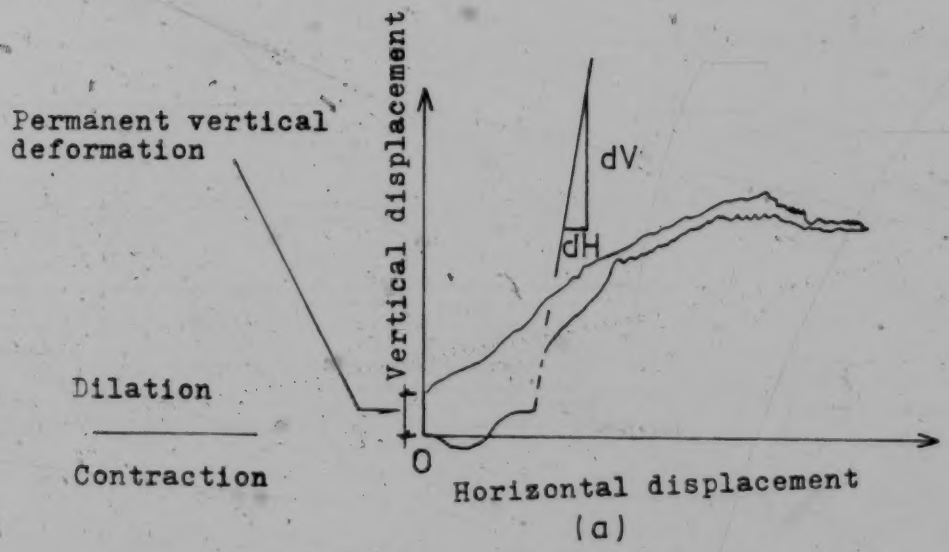

(a)

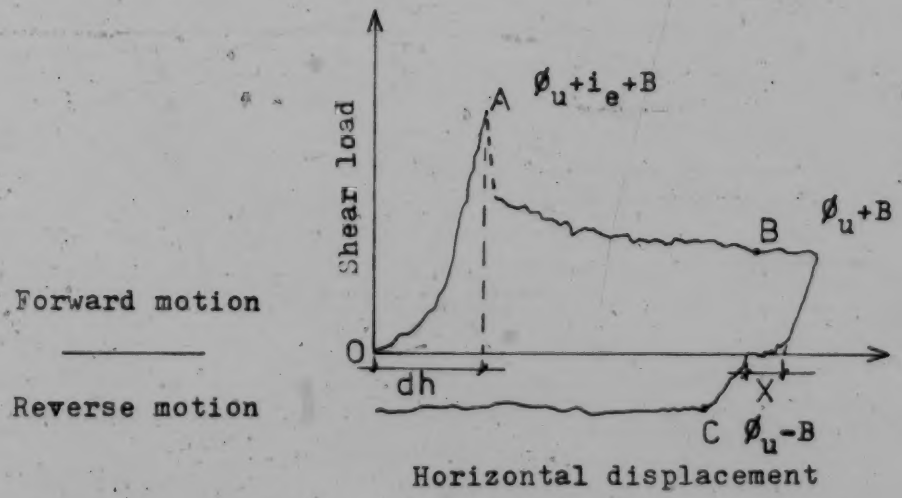

(b)

Figures 2.17a,b Typical load versus displacement and vertical versus horizontal displacement curves of artificially prepared Tyndall Stone surfaces

Speed=0.052 cm/min.
rock suface=5341
Normal stress=3450kPa
Shearing area=9.11 sq.cm.
Scale: load 1cm=2882.46N
vert. 1cm=0.018cm
hori. 1cm=0.14cm

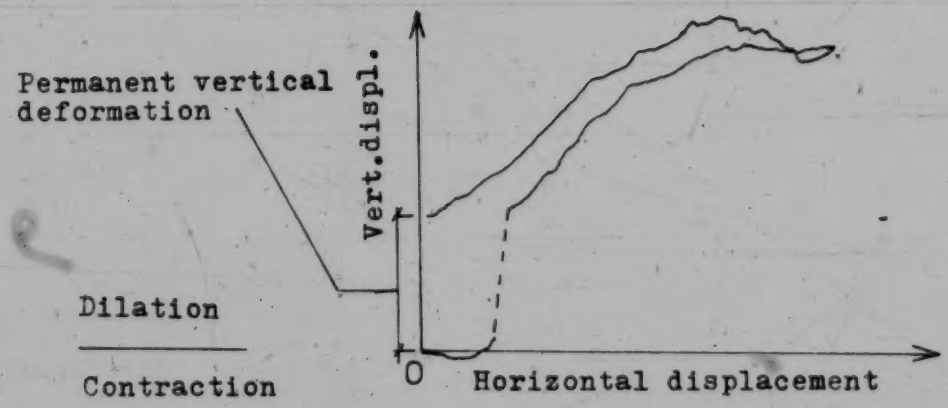

(c)

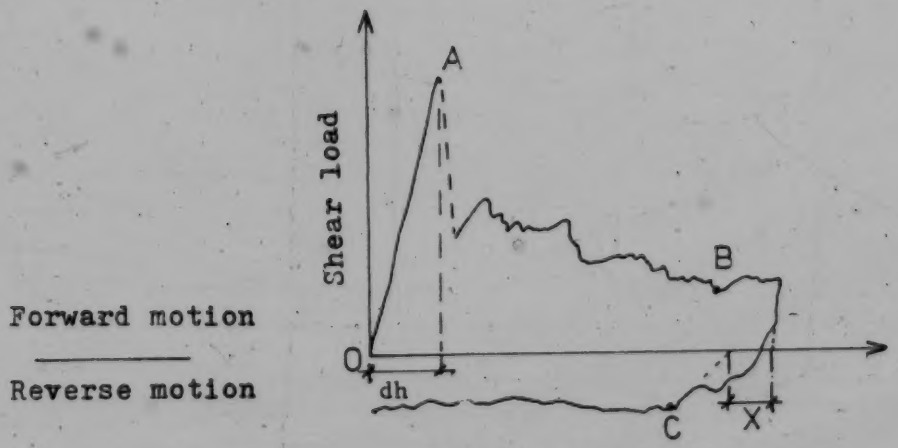

(d)

Figures 2.17c,d Typical load versus displacement and vertical versus horizontal displacement curves of artificially prepared Standstead Granite surfaces

denoted by a point B. This was termed the post peak value.

The reverse post peak value was then taken at a point when the sample had returned to the same position as it was at the point B. Since there was some compliance in the machine, this meant that the reverse post peak value was read at a point C, to the left of point B. The amount of compliance in the machine was denoted by an X.

In most cases, the fall in shear force after the peak was so rapid that the machine was unable to follow it. This phenomenon is expected for tightly interlocked rock surfaces (Jaeger 1971).

A dotted path was constructed from the point A to the rest of the curve to show the sudden failure of the sample. The horizontal deformation corresponding to the peak was denoted by dh.

The portion of curve above the reference line at the orgin represented the sample in forward motion whereas the portion below represented the reverse motion. The load cell was in compression when the sample was in forward motion and tension when the sample reversed.

As in the vertical-horizontal curves (diagrams a and c) again both types of rock surfaces showed some common features. Theoretically the upper half block would begin to rise relative to the bottom half when the horizontal deformation was started unless the normal force was high

enough that dilation was suppressed. However, due to the difficulties of obtaining perfect seating of the surface, some vertical displacement curves would begin with contraction first as the horizontal deformation commenced. Later on, after a small horizontal displacement the seating was overcome and the top half began to dilate gradually. Dilation continued until it reached a point where the sample failed suddenly, the vertical displacement jumped so rapidly that the machine was unable to follow it. Then dilation continued with deformation at a decreasing rate. Considerable fluctuations were also measured here. This appeared to be the result of the rupture of asperities.

In most shear tests the dilation rate became almost zero or negative at the ultimate deformation. When the sample began in the reverse motion, no great change in the vertical deformation was recorded for a short duration and appeared to be the result of the slack in the system. Upon overcoming the slack, the sample began to contract until it had returned to its initial position. As seen in diagrams a and c, the reversed protion of the curve were high above the advanced portion. The difference between the reverse and forward curves could be the thickness of the detritus of broken asperities induced during shear, as a permanent vertical displacement was obtained at the original position.

The peak dilation angle (θd) for a shear test is equal to the instantaneous inclination dv/dh (dv = vertical

displacement, dh = horizontal displacement at failure) of the shearing path at peak load, relative to the mean plane. Barton (1973) suggested that it is a very powerful phenomenological parameter of shear strength, since for a given normal stress it represents the minimum energy path between a sliding up and a shearing through mode of failure.

In this study, the dilation angle was taken to be the slope of the dotted path in diagram a or c, which represented the instantaneous shearing path at the peak strength relative to the mean plane of the rock surface. Therefore, the shear strength value and dilation angle were corrected to the mean plane. For flat surfaces, the mean plane is the surface of contact whereas for rough irregular surfaces, it is taken to be the plane that yields a zero value for the sum of the amplitudes or heights of the asperities above and below it. (Detailed consideration of mean planes will be presented in the next chapter).

2.3.6 Interpretation of Shear Test Observations

The question was raised as to how the shear parameters are corrected to the mean plane. Let us put this question aside for the present being and consider some simple sliding blocks as illustrated in figure 2.18.

The two flat, clean half rock blocks (diagram a) slide on each other along the mean plane under a shear load S and a normal load N. The frictional component is described by S

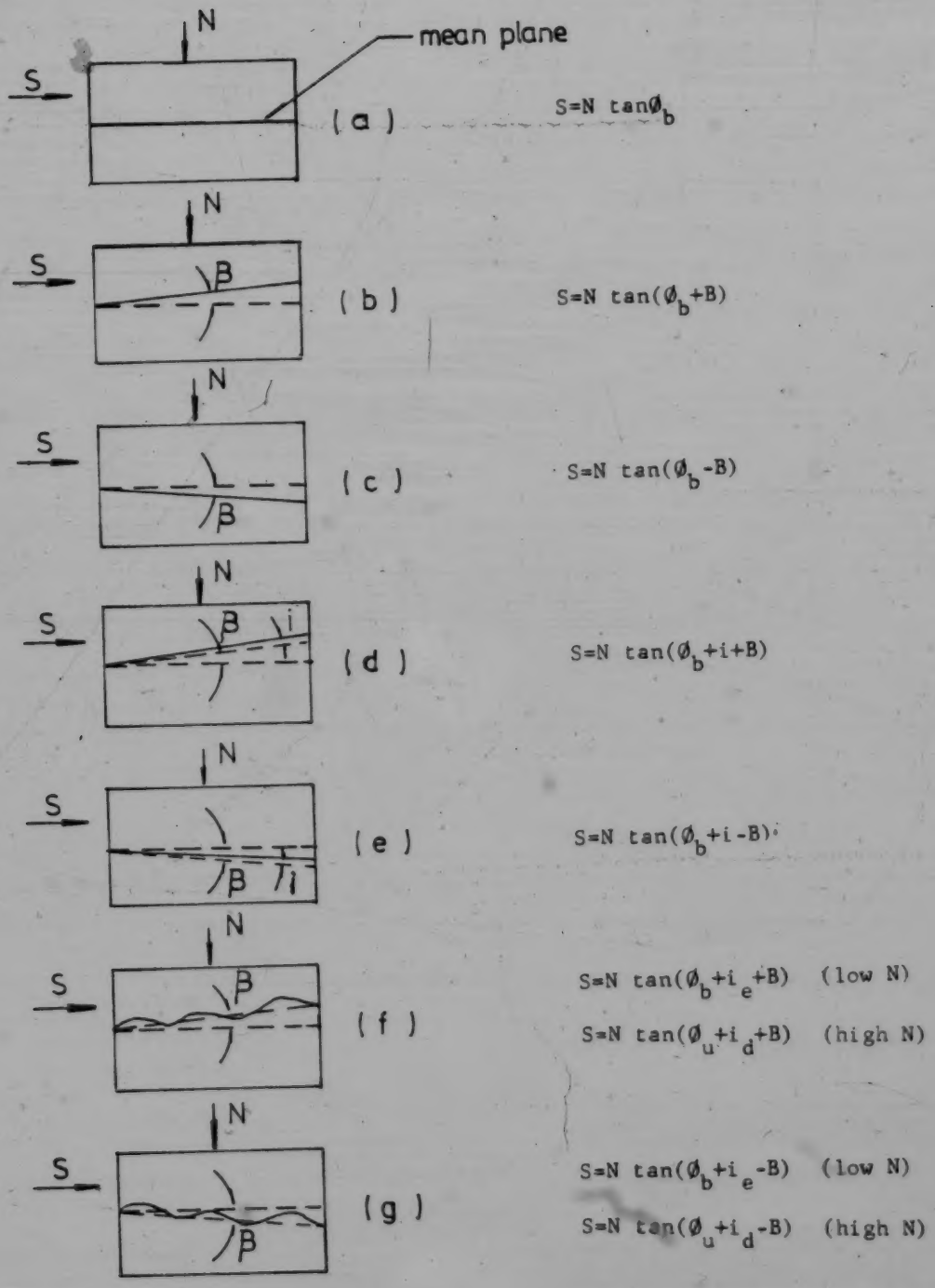

Figure 2.18 The frictional components of rock blocks subjected to shear

= Ntan Øb. If the mean plane is "tilted" an angle of B "against" the shear load, the frictional component will be described by S = Ntan (Øb + B) as shown in diagram b, while if tilted an angle B "away" (diagram c) from the mean plane, then S = Ntan(Øb - B). If a regular asperity with an inclination of angle i is superimposed on the rock surface of diagram b, the frictional component will be described by S = Ntan (Øb + i + B) as shown in diagram d; superimposed on the rock surface of diagram C, then S = Ntan (Øb + i - B) as shown in diagram e.

However, if a set of irregular asperities is superimposed on the rock surface of diagrams b, as illustrated in diagram f, the resulting frictional component will be described by S = Ntan (Øb + ie + B) at low normal loads, where ie is the effective inclination of the asperities (Patton, 1966). Hence no damage of asperities will occur. When the normal load increases, damage to the asperities results the friction resistance will be described by S = Ntan (Øu + id + B) where Øu is termed the ultimate frictional angle obtained after large shearing displacements have occurred (Krahn, 1974) and id is the average effective inclination of asperities, which have not been damaged or sheared off with displacement. The degree of damage or thus the magnitude of id depends upon the effective normal load and because id varies, a curved strength envelope is expected.

The value of ϕu for natural discontinuities is not equal to that of the basic friction angle, ϕb. The ϕb determined on flat artificially prepared surfaces is intended to be a unique value for the rock in question (table 2.1). The ultimate friction angle is determined on rock surfaces from a forward and a reversal shear test or both. The magnitude of ϕu depends upon the initial surface conditions as well as the degree of surface damage after the test. Therefore, the ϕu does not posses a unique value for a particular rock, but can be smaller or greater than the basic friction angle (Krahn, 1974).

To complete the general picture of figure 2.18 the same set of irregularities as illustrated in diagram g is superimposed on the rock surface of diagram C, the friction will be described by $S = N\tan(\phi b + ie - B)$ at low normal loads and $S = N\tan(\phi u + id - B)$ as the normal load increases. The purpose of figure 2.18 is to give a general idea of how the corrected mean plane is chosen in order to interpret shear data. With this idea in mind, the interpretation of figure 2.17 will be easy. The point A in the load-displacement curves represents the peak strength contributed by the individual frictional resistance from ϕu, id and B. Along the post peak curve, the id term disappears with large horizontal deformations.

Therefore, the point B represents the resistance contributed by ϕuf plus angle B, where ϕuf is the ultimate

friction angle in the forward motion. Similarly using the same argument described earlier in figure 2.18; diagrams C, e and g, the point C along the reversal post peak curve represents the resistance contributed by the difference between ϕ_{ur} and B, where ϕ_{ur} is the ultimate frictional angle in the reversal motion.

Since the broken small particles from the failed asperities of the surface and the remaining intact geometric components complicate the post peak strength, the mechanism of shearing along the post peak path and reversal post peak path is seldom known. In view of this and also for simplicity, the ultimate friction angle, was taken to be the average of ϕ_{uf} and ϕ_{ur}. They were set to be the same magnitude when B values were evaluated.

For example, let us use the results obtained from the shear test which had been performed on a limestone surface, numbered 51932, as shown in figure 2,17 a.b. The following are the experimental data:

Surface number = 51932
Surface area = 9.878 cm² (1.532 in²)
Normal stress = 3450 kPa (500 psi)
Rate of deformation = 0.052 cm/minute
Load cell used = 11.12kN - load cell
scale : Load (y) 1 cm 294.2 kg (648 lb)
Vertical displacement (y') 1 cm = 0.018 cm
Horizontal displacement (x) 1 cm = 0.14 cm

From curves:

dh = 1.603 cm dV = 2.00 cm dH = 0.31 cm

$y(\text{point A}) = \phi_u + i_d + B = 3.55\text{cm}$
$y(\text{point B}) = \phi_{ur}^{uf} + B = 1.50\text{cm}$
$y(\text{point C}) = \phi_{ur}^{uf} - B = 0.83\text{cm}$

Therefore:
$y(\phi_u) = (1.50+0.83)/2 \text{ cm} = 1.165\text{cm}$
$y(B) = (1.50-1.165) \text{ cm} = 0.335\text{cm}$
$y(\phi_u + i_d) = (3.55-0.335) \text{ cm} = 3.215\text{cm}$

Computation of shear strength parameters:
Peak strength before B correction(correction to the mean plane):
$= (3.55 \times 648)/1.532 = 1502.35\text{psi} = 10366.21\text{kPa}$
Peak strength after B correction:
$= (3.215 \times 648)/1.532 = 1360.57\text{psi} = 9387.93\text{kPa}$
Ultimate shear strength:
$= (1.165 \times 648)/1.532 = 493.03\text{psi} = 3401.87\text{kPa}$
Stress drop:
$= 1360.57 - 493.03 = 867.54\text{psi} = 5986.13\text{kPa}$
Dilation angle before B correction:

$$\theta_d = \tan^{-1}(dV/dH) = \tan^{-1}\left(\frac{2 \times 0.018}{0.31 \times 0.14}\right) = 39.67^\circ$$

B angle:

$$= \tan^{-1}\left(\frac{\text{Peak before B correction}}{\text{Normal stress}}\right) - \tan^{-1}\left(\frac{\text{Peak after B correction}}{\text{Normal stress}}\right)$$

$$= \tan^{-1}\left(\frac{1502.35}{500.00}\right) - \tan^{-1}\left(\frac{1360.57}{500.00}\right) = 1.77^\circ$$

Dilation angle after B correction:

$$\theta_d = 39.67^\circ - 1.77^\circ = 37.90^\circ$$

Failure time:

$$t_f = \frac{1.603 \times 0.14}{0.052} = 4.31 \text{ minutes}$$

Shear stiffness:

K_s = Peak shear strength/peak shear displacement

$$= \frac{9387.93}{1.603 \times 0.14} = 41831.96 \text{ kPa/cm}$$

Total friction angle:

$$\phi_T = \tan^{-1}\left(\frac{\text{Peak shear strength}}{\text{Normal stress}}\right)$$

$$= \tan^{-1}\left(\frac{1360.57}{500.00}\right) = 69.82^\circ$$

The above procedure for the computations of shear parameters was carried out for each shear experiment on the surfaces of limestone and granite samples. These manipulations were performed on the IBM 360 computer and the results are shown in table 2.4 for the limestone surfaces and tables 2.5 for the granite surfaces. Column 1 of these tables shows the location of the samples with respect to the original rock slabs. Column 2 shows the computed angles in degrees. Cclumn 3 shows the failure angles of samples from the tilting apparatus, in degrees. Column 4 shows the peak shear strength values of the rock surfaces after B correcting, in kPa (kN/m^2). Column 5 shows the range of the effective normal stresses, in kPa. Column 6 shows the average values of the ultimate strength after B corrections, in kPa. Column 7 shows the maximum dilation angles after B corrections in degrees and column 8 shows the peak deformations, in cm. Other derived parameters such as the time of failure, stress drop, shear stiffness of the rock surface and total friction angle are listed in appendix B.

2.4 Test Results:

2.4.1 Peak Shear Strength

The peak strengths, after B correction, were plotted against the effective normal stresses as shown in figures 2.19a,b, (diagram a, limestone; diagram b, granite surfaces). Note that at each stress level in these figures two to four rock surfaces were sheared and their peak

1	2	3	4	5	6	7	8
Rock sample	B angle	Tilt angle	Peak strength kPa	Normal stress kPa	Ultimate strength kPa	Angle of dilation	Peak travel cm
51842	1.03	64.0	1192.04	172.50	275.86	14.91	0.089
51421	0.84	58.0	1147.68	172.50	284.28	21.36	0.120
51111	1.95	58.5	906.73	172.50	321.75	20.25	0.042
51112	2.94	59.5	1293.82	345.00	424.97	13.00	0.251
51662	1.71	63.0	1603.15	345.00	447.60	13.58	0.183
511312	3.80	60.0	1269.32	345.00	551.86	13.03	0.157
51681	0.94	58.0	3192.15	517.50	593.19	51.18	0.151
51561	1.80	60.5	2329.72	517.50	673.03	16.66	0.057
51792	2.64	59.0	1637.85	517.50	591.40	17.53	0.110
51632	0.33	59.0	3361.40	517.50	484.24	37.59	0.057
51672	1.53	57.0	3565.44	690.00	1170.93	29.94	0.151
51742	1.43	58.5	2730.95	690.00	793.84	22.48	0.110
51152	2.88	63.0	2526.16	690.00	899.14	27.99	0.125
51841	2.37	59.0	3838.40	1035.00	1114.83	24.84	0.183
51562	3.21	61.0	2868.40	1035.00	1045.76	19.98	0.068
51791	0.96	62.0	4367.35	1035.00	1019.54	42.64	0.219
511510	1.70	59.5	3784.51	1035.00	1037.97	49.06	0.120
511022	7.38	60.0	1527.66	1035.00	1060.46	11.54	0.063
51451	1.43	61.0	2282.59	1380.00	1342.67	15.03	0.063
51342	7.66	60.0	2556.10	1380.00	1528.21	6.49	0.167
51381	2.65	61.0	3470.98	1380.00	1324.80	19.87	0.104
51692	1.50	60.0	3315.17	1380.00	975.87	39.10	0.167
51642	3.23	70.0	3954.94	1725.00	1574.92	22.65	0.157
51641	3.76	64.0	3765.19	1725.00	1272.01	31.77	0.214
51771	0.98	61.0	3747.46	1725.00	1229.65	29.89	0.188
511242	2.48	59.0	4674.06	2070.00	1594.66	34.62	0.292
51482	2.94	56.5	4263.23	2070.00	2634.14	46.51	0.287
51782	3.27	62.0	3821.50	2070.00	1674.15	23.04	0.146
51781	1.08	61.0	5127.66	2760.00	2009.21	39.52	0.188
51632	2.76	73.0	5023.75	2760.00	2184.26	24.92	0.287
51772	3.44	58.0	4852.70	2760.00	2274.72	28.65	0.178
511021	2.15	60.0	7950.87	3450.00	3227.06	36.63	0.162
51932	1.77	62.0	9387.93	3450.00	3401.91	37.90	0.224
511042	1.19	59.0	10009.28	3450.00	3074.36	30.28	0.157
51262	5.02	60.0	6471.51	4140.00	4475.61	40.78	0.224
51331	0.72	58.5	9763.64	4140.00	3819.36	29.02	0.178
511152	3.82	64.0	8603.75	4140.00	4540.41	35.85	0.167
51712	3.53	60.0	7990.06	4830.00	4955.03	37.07	0.167
51852	0.97	57.5	12522.67	4830.00	4574.70	39.63	0.198
511041	1.45	59.5	9232.82	4830.00	3884.35	18.72	0.167
51671	5.02	59.0	9688.36	5520.00	3547.43	14.88	0.193
51422	1.31	64.0	12451.12	5520.00	5538.77	17.61	0.271
511151	3.79	61.0	6948.57	6210.00	5998.72	8.92	0.167
51711	7.10	58.0	7617.67	6210.00	6325.57	5.50	0.172
51831	3.64	59.5	11386.31	6900.00	6880.47	15.52	0.209
51842	0.18	56.0	12451.88	6900.00	6180.26	16.84	0.178

Table 2.4 Results of direct shear strength test on artificially prepared Tyndall Stone surfaces

1	2	3	4	5	6	7	8
Rock sample	B angle	Tilt angle	Peak strength kPa	Normal stress kPa	Ultimate strength kPa	Angle of dilation	Peak travel cm
5392	0.40	54.0	1727.48	172.50	203.69	56.13	0.068
53281	0.06	57.5	4733.81	172.50	218.11	45.74	0.151
53211	0.58	56.0	1360.13	172.50	225.77	45.22	0.057
53352	0.24	63.0	1718.79	172.50	172.02	51.88	0.084
53332	0.26	62.0	4307.39	345.00	459.33	62.92	0.167
53151	0.32	64.0	3591.31	345.00	392.75	47.86	0.099
53331	1.08	54.0	2442.74	345.00	512.39	55.45	0.094
53162	0.61	55.0	2276.17	345.00	329.20	51.51	0.157
53161	2.18	56.0	1915.30	517.50	628.66	46.00	0.104
53181	0.71	54.5	3682.67	517.50	794.33	47.47	0.068
53182	1.36	59.0	2146.80	517.50	467.89	29.51	0.068
53152	0.0	56.0	8810.88	517.50	2065.86	41.56	0.115
53322	0.0	62.0	4452.91	690.00	643.77	53.53	0.084
5321	0.46	54.0	5719.55	690.00	697.45	38.32	0.084
5322	0.09	59.0	7668.59	690.00	649.84	54.91	0.110
53302	0.20	57.0	10540.37	1035.00	928.39	68.54	0.178
53342	0.0	75.0	7788.93	1035.00	913.15	55.00	0.219
53341	0.0	57.0	6417.07	1035.00	829.03	66.83	0.125
53132	0.0	57.0	5576.58	1380.00	1052.18	52.12	0.078
5382	0.57	60.5	7680.46	1380.00	1288.64	46.40	0.099
53351	0.15	58.0	9290.85	1380.00	1139.95	42.41	0.141
53242	1.46	72.5	5463.63	1725.00	1469.91	34.84	0.162
53241	0.23	69.0	8700.28	1725.00	1445.48	45.57	0.120
5361	0.28	58.5	7991.16	1725.00	1445.20	41.28	0.104
53132	0.51	57.0	7728.69	2070.00	1430.85	47.67	0.110
53131	2.07	58.0	6184.75	2070.00	2041.43	48.69	0.094
5381	0.47	56.0	11998.27	2070.00	1836.43	53.06	0.219
5351	0.74	58.5	7848.33	2760.00	2056.48	42.86	0.110
5352	0.85	63.0	9046.66	2760.00	2029.15	62.33	0.125
53172	0.89	66.0	11460.28	2760.00	2225.25	58.85	0.151
53171	1.18	57.0	10450.46	3450.00	2867.92	55.35	0.162
5341	0.57	64.0	12515.01	3450.00	2724.74	62.61	0.146
5342	0.71	64.0	11993.09	3450.00	3028.82	55.82	0.162
53272	0.44	59.0	11283.09	4140.00	3042.00	50.32	0.157
53271	1.05	60.5	9844.23	4140.00	2646.29	55.48	0.125
5371	1.75	57.0	12852.49	4140.00	3652.79	12.67	0.256
53141	1.57	55.0	12576.42	4830.00	3711.92	28.17	0.240
5332	2.60	58.5	9993.61	4830.00	4039.95	36.18	0.146
5372	2.83	62.5	12165.73	4830.00	4679.09	29.90	0.224
53252	0.80	53.5	14245.74	4830.00	3705.51	37.98	0.188
53311	1.96	61.5	13460.93	5520.00	4725.05	29.51	0.188
53312	4.53	61.0	10604.95	5520.00	5129.66	14.39	0.266
53321	1.55	54.0	11989.58	5520.00	3923.34	14.73	0.240
5331	1.14	57.5	16505.00	5520.00	4636.87	26.07	0.209
5391	0.54	56.0	13910.12	6210.00	4033.12	15.74	0.209
53191	1.33	57.5	13527.79	6210.00	3600.07	5.39	0.308
53192	0.82	59.0	17319.00	6900.00	5100.06	15.12	0.235
53142	2.97	55.5	14153.41	6900.00	5144.16	5.63	0.397

Table 2.5 Results of direct shear strength test on artificially prepared Standstead Granite surfaces

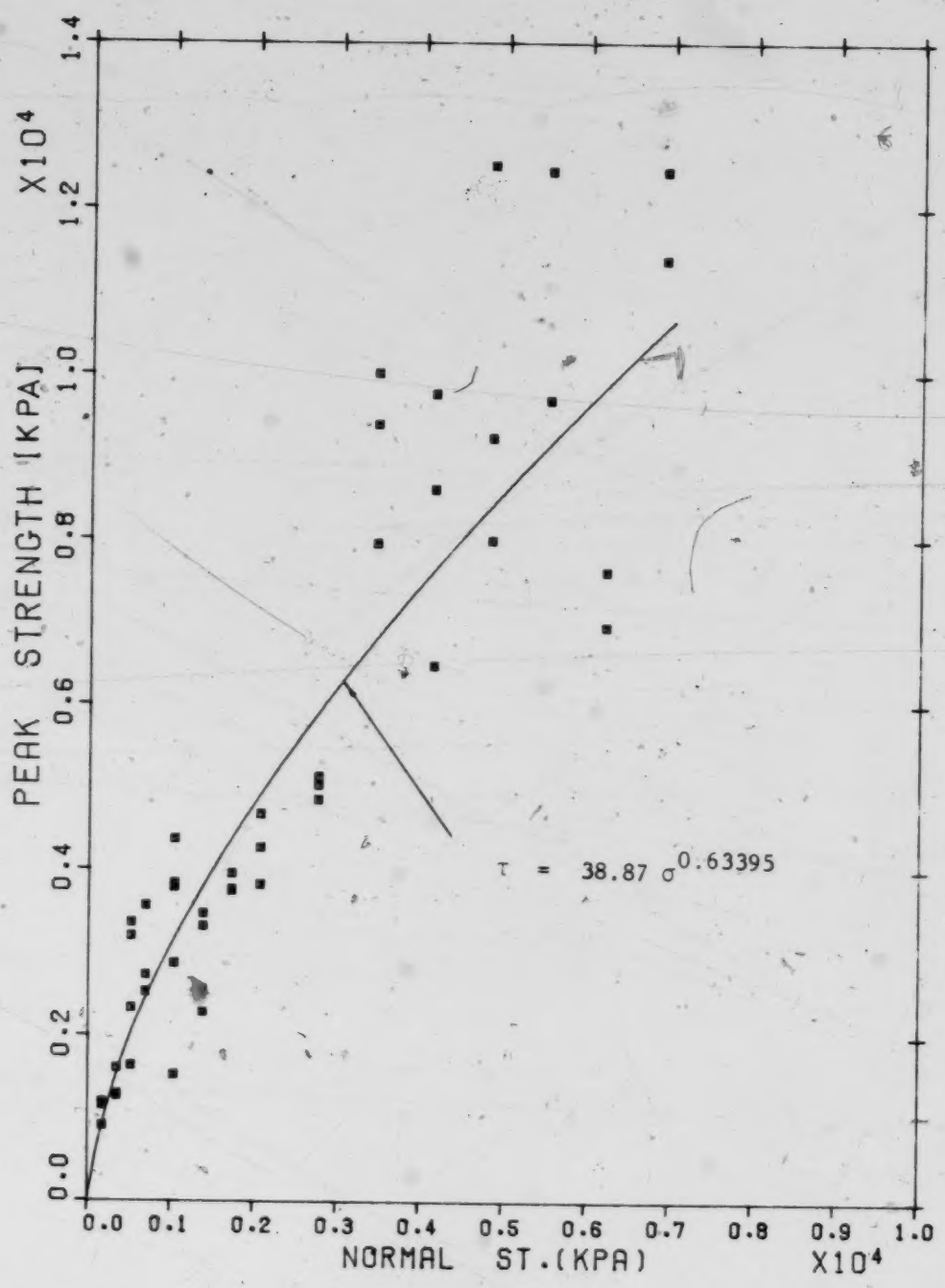

Figure 2.19a Peak shear strength results obtained from direct shear tests performed on tension fractured surfaces of Tyndall Stone

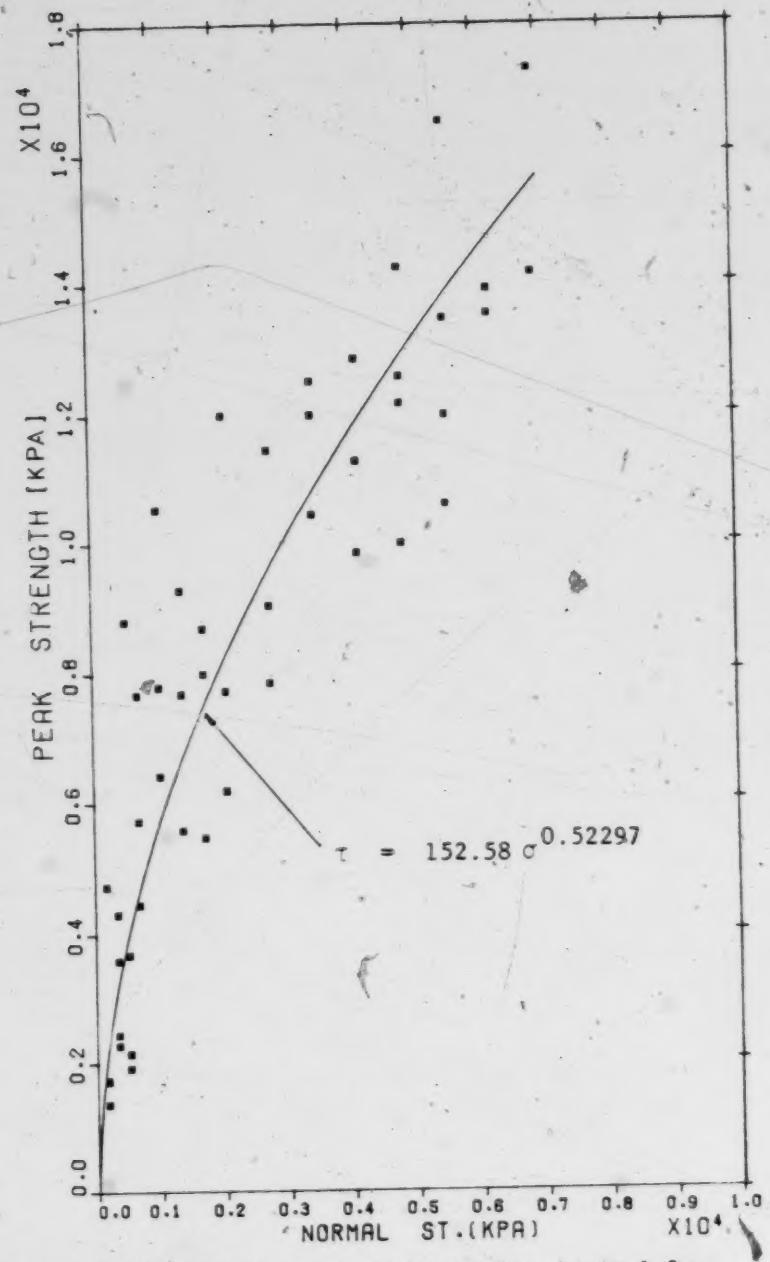

Figure 2.19b Peak shear strength results obtained from direct shear tests performed on tension fractured surfaces of Standstead Granite

strength values varied.

The total friction angles defined by the arctan (peak/normal stress) are found in excess of 80 degrees when the normal stress is below 170 kPa for the limestone surfaces and below 800 kPa for the granite surfaces. The value can be as high as 88 degrees and 82 degrees for the granite and limestone surfaces respectively. Other high values are reported in the literature (Goodman, 1964; Paulding, 1970; Rengers, 1971) but the total friction angles from the present study are higher than any of these values. This seems to be the result of the artificially fractured surfaces having a great degree of surface roughness.

No cohesion intercepts are found and this is expected for clean rough surfaces. In both strength diagrams, the data tend to follow a curve. A power law regression analysis was carried out for each of the strength plots. The fitted power curves are as follows (curves in figures 2.19 a,b): for the limestone surfaces

$$\tau = 38.87\ \sigma^{0.63395} \qquad (2.9)$$

with a correlation coefficient, R = 0.93 for the granite surfaces

$$\tau = 152.58\ \sigma^{0.52297} \qquad (2.10)$$

with a correlation coefficient, R = 0.89

The high values of R emphasize the curvilinear characteristics of strength envelopes of these rock surfaces.

Murrell (1965) and Maurer (1965) advocated the use of the power law in reporting results of shear tests. To determine if this type of function, a power law could be used to describe the experimental observations, a statistical analysis, a measure of goodnes of fit was undertaken. Equations 2.9 and 2.10 are transformed to the empirical regression lines 2.9a and 2.10a respectively:

$$\log \tau = \log 38.87 + 0.63395 \log \sigma \qquad (2.9a)$$

$$\log \tau = \log 152.58 + 0.52297 \log \sigma \qquad (2.10a)$$

i.e., the logarithm of the peak shear strength is a linear function of the logarithm of the effective normal stress.

These equations take the form

$$y = a + bx$$

The variable x or $\log \sigma$ is taken to be the independent variable, and the variable y or $\log \tau$, the dependent variable.

The theory of linear regression analysis may be considered as an extension of the analysis of variance. In the analysis of variance the hypothesis (equations 2.9a and 2.10a) is tested by comparing the variance within sets and between sets. The following procedure is taken from the valuable book by Hald (1952).

<u>Variation within each set of observation:</u> (i.e., variation of the experimental $\log \tau$ values at each normal stress level, $\log \sigma$). Corresponding to each value of the independent variable, the mean and the variance of the

values of the dependent variable are calculated i.e., corresponding to the independent variable x = xi, the mean

$$\overline{yi} = \frac{1}{ni} \sum_{v=1}^{ni} yiv \qquad i=1,2,3,\ldots\ldots\ldots\ldots,k$$

and the variance

$$Sli^2 = \frac{1}{ni-1} \sum_{v=1}^{ni} (yiv - \overline{yi})^2 \qquad fi=ni-1\ ,\ i=1,2,3,\ldots\ldots,k$$

The hypothesis of a constant variance, (scatter of the observed log τ values) for each piece of data from a homogeneous experiment (log σ level) is tested by comparing the variances $S11^2$, $S12^2$, $S1k^2$. If the hypothesis is not rejected, the k variances are combined to the estimate

$$Sl^2 = \frac{\sum_{i=1}^{k} fi\ Sli^2}{\sum_{i=1}^{k} fi} = \frac{\sum_{i=1}^{k} \sum_{v=1}^{ni} (yiv - \overline{yi})^2}{\sum_{i=1}^{k} ni - k}$$

Variation about the empirical regression line: Corresponding to each value of the independent variable set (xi), the estimate value (Yi) of the empirical regression line is calculated and the estimate variance of the regression line is

$$S2^2 = \frac{1}{k-2} \sum_{i=1}^{k} ni(\overline{yi} - Yi)^2$$

The hypothesis regarding the form of the regression

line is therefore tested by means of the variance ratio $V^2 = S2^2/S1^2$. If $S2^2$, is significantly larger than $S1^2$, the hypothesis of linearity must be rejected.

Once the procedure of analysis of variance was defined the peak and normal stress values in table 2.4 and 2.5 were manipulated employing the above procedure. The results are tabulated in tables 2.6 and 2.7 respectively. Based on the empirical equations 2.9a and 2.10a, the logarithm of the peak shear strength at each logarithm of normal stress level was computed. The next step was to test the hypothesis of a constant variance - the square of the standard deviation of the mean of log peak shear strength, within the experimental observations. The quickest test for heterogeneity of variance is Hartley's maximum F ratio (Hartley, 1950). In this test the ratio of the largest mean square of standard deviation to the smallest is taken providing that there are k estimates of variance and each has f degrees of freedom. If the ratio exceeds the tabular entry (Pearson and Hartly, 1966, Table 31), it is concluded that the variances are significantly different, and this conclusion will be wrong 5 percent of the time. This test assumes that all k of the estimating variances have f degrees of freedom. Hartley (1950) felt that the sensitivity of the test is not seriously dependent on this assumption and suggested using it as a rough test even if the fi are different, entering the table with f, the mean of the fi's.

Xi Log(σ_n) σ_n in kPa	ni Number of test	fi Degree of freedom	k Number of Xi level	$\bar{y}i$ Mean Log(τ) τ in kPa	Sli Stanard deviation of the $\bar{y}i$	Yi Empirical value of Log(τ)
2.2368	3	2	1	3.0312	0.0643	3.0076
2.5378	3	2	2	3.1401	0.0563	3.1985
2.7139	4	3	3	3.4030	0.1441	3.3101
2.8388	3	2	4	3.4636	0.0784	3.3893
3.0149	5	4	5	3.4888	0.1829	3.5009
3.1399	4	3	6	3.4567	0.0878	3.5802
3.2368	3	2	7	3.5822	0.0129	3.6416
3.3160	3	2	8	3.6272	0.0439	3.6918
3.4409	3	2	9	3.6989	0.0120	3.7710
3.5378	3	2	10	3.9590	0.0531	3.8324
3.6170	3	2	11	3.9117	0.0914	3.8826
3.6839	3	2	12	3.9885	0.0996	3.9251
3.7419	2	1	13	4.0407	0.0770	3.9618
3.7931	2	1	14	3.8618	0.0282	3.9943
3.8388	2	1	15	4.0758	0.0274	4.0233

$$S1^2 = \frac{\sum_{i=1}^{k} fi\ Sli^2}{\sum_{i=1}^{k} fi} = 0.009686$$

$$S2^2 = \frac{1}{k-2} \sum_{i=1}^{k} ni(\bar{y}i - Yi)^2 = 0.021475$$

$$V^2 = \frac{S2^2}{S1^2} = \frac{0.021475}{0.009686} = 2.17$$

Table 2.6 Results of the analysis of variance of the power law function in describing the direct shear strength data of the Tyndall Stone surfaces

Xi Log(σ_n) σ_n in kPa	ni Number of test	fi Degree of freedom	k Number of Xi level	$\bar{y}i$ Mean Log(τ) τ in kPa	Sli Standard deviation of the $\bar{y}i$	Yi Empirical value of Log(τ)
2.2368	4	3	1	3.3203	0.2414	3.3533
2.5378	4	3	2	3.4836	0.1328	3.5107
2.7139	4	3	3	3.5313	0.3023	3.6028
2.8288	3	2	4	3.7635	0.1181	3.6681
3.0149	3	2	5	3.9072	0.1086	3.7602
3.1399	3	2	6	3.8666	0.1120	3.8256
3.2368	3	2	7	3.8598	0.1075	3.8762
3.3160	3	2	8	3.9194	0.1464	3.9177
3.4409	3	2	9	3.9701	0.0830	3.9830
3.5378	3	2	10	4.0651	0.0409	4.0337
3.6170	3	2	11	4.0515	0.0579	4.0751
3.6839	4	3	12	4.0845	0.0637	4.1101
3.7419	4	3	13	4.1127	0.0817	4.1404
3.7931	2	1	14	4.1372	0.0085	4.1672
3.8388	2	1	15	4.1947	0.0619	4.1911

$$S1^2 = \frac{\sum_{i=1}^{k} fi\ Sli^2}{\sum_{i=1}^{k} fi} = 0.021344$$

$$S2^2 = \frac{1}{k-2} \sum_{i=1}^{k} ni(\bar{y}i - Yi)^2 = 0.010644$$

$$V^2 = \frac{S2^2}{S1^2} = \frac{0.010644}{0.021344} = 0.498$$

Table 2.7 Results of the analysis of variance of the power law function in describing the direct shear strength data of the Standstead Granite surfaces

The maximum k entry in the Hartley's table is 12 and for the present study k is 15 (tables 2.6 and 2.7). Therefore, it was felt that it would not lose any significance to divide each table into two halves; the first k being 7 and the second 8. The computed ratios and Hartley's ratios for the two rock surfaces are as follows:

Tyndall Stone surfaces:

First halve $(\frac{Sli(max)}{Sli(min)})^2 = 201$ Hartley's ratio = 333 (k=7, f=2)

Second halve $(\frac{Sli(max)}{Sli(min)})^2 = 69$ Hartley's ratio = 403 (k=8, f=2)

Standstead Granite surfaces:

First halve $(\frac{Sli(max)}{Sli(min)})^2 = 8$ Hartley's ratio = 333 (k=7, f=2)

Second halve $(\frac{Sli(max)}{Sli(min)})^2 = 296$ Hartley's ratio = 403 (k=8, f=2)

For both rock surface the computed ratios are less than the Hartley's table entries which indicates that the hypothesis of a constant variance is not rejected and the scatter of the observations is the same for each normal stress level considered.

The final step was to compute the values of the squares of S1 and S2 and they are shown in tables 2.6 and 2.7. The variance ratio, V^2 for the granite surfaces is 0.498

indicating that $S2^2$ is less than $S1^2$. The line having the smaller variance is a better fit to the data; therefore, the power law function, equation 2.10 can be used to describe the experimental results. As for the limestone surfaces, the variance ratio, V^2 is 2.217. Using the critical values of the F distribution, for the particular degrees of freedom (f=13, for $S2^2$; f=31, for $S1^2$) at hand, the upper 5 percent and 1 percent points were found to be 2.08 and 2.82 respectively.

The most common confidence level used in statistics is 5 percent (Action, 1959) but, because of the large amounts of data analysed, a 1 per cent level is used here.

Since V^2 is in between these F values there is less than 5 percent but more than 1 percent probability that the hypothesis of linearity is true. Therefore one cannot, with certainty, reject the power law function in describing the direct shear test results on the limestone surfaces.

2.4.2 Shear Stiffness:

Stiffness measures the amount of force necessary to produce equilibrium in a body undergoing differential displacement. It is an important parameter in finite element analysis of non-linear rock problems introduced by heterogeneities and discontinuities for which closed form solution methods are difficult and special (Goodman, 1976).

The stiffness of a rock surface is used to describe the overall stress-deformation characteristics. It is the mean gradient of the shear stress-shear deformation curve, taken up to the point of peak strength. It has the following form

$$Ks = \tau/dh$$

where Ks = the shear stiffness of a rock surface (kPa/cm)

dh = the peak shear deformation (cm)

Figures 2.20a,b show the shear stiffness versus normal stress (diagram a, limestone surfaces; diagram b, granite surfaces). In general the shear stiffness in diagram b increases with normal stress and becomes level off as the stress reaches about 3000 kPa. In diagram a, the increase in shear stiffness with the normal stress is obviously marked. It can be concluded that the shear stiffness of the rock surfaces in the present study is normal stress dependent.

2.4.3 Peak Dilation Angle

The peak dilation angle is the instantaneous slope of the shearing path at peak strength. The number of published reports on direct shear tests on rough rock surfaces concerning the variation of dilation angle with normal pressure is very small; Ripley and Lee (1961), Ladanyi and Archambault, Tsytovich et al (1970) and Barton (1971). They found that the peak dilation angle decreased exponentially with normal pressure. It is of interest to compare this

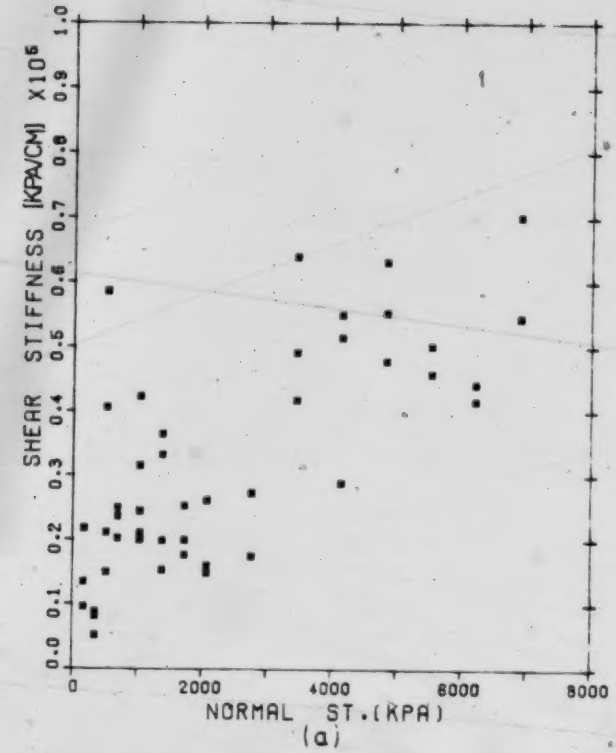

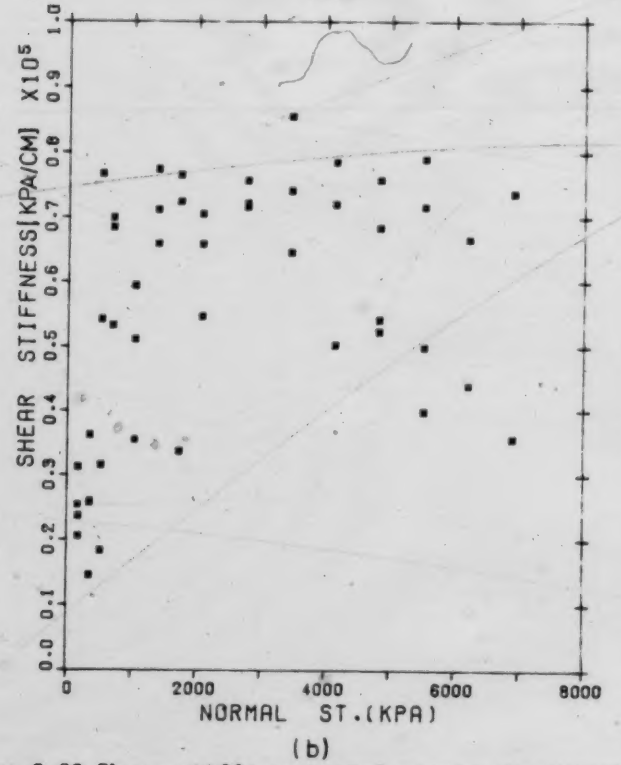

Figure 2.20 Shear stiffness-normal stress characteristics for (a)Tyndall Stone and (b)Standstead Granite surfaces

finding with the results obtained in this study.

Figures 2.21a,b, show the dilation angle versus normal stress plots (diagram a, limestone surfaces; diagram b, granite surfaces). Note that the data in these figures do not exhibit the exponential phenomenon but, tend to fall into two groups. The first has same average dilation angle independent of normal stress and the second displays a decrease in dilation angle with normal stress. This characteristic is found for both limestone and granite surfaces. The average values of dilation angle seem to be 30 and 50 degrees for the limestone and granite surfaces respectively. The data appear to converge above the lines having the average values as the normal stress increases but, up to about 4000 kPa where low dilation angles are found to be absent. Beyond the transition stress at 4000 kPa, the dilation angles appear to decrease linearly with stress. If the line is extrapolated to intersect the abscissa, the normal stress corresponding to zero dilation would be at 7300 kPa beyond which the dilatancy of rock surfaces would be totally suppressed.

The reasons for the absence of low dilation angles at the transition normal stress are unknown. As no other published data of similar kind were known to the author, a probable interpretation had to be made from limited information furnished by the data. It was felt that around the narrow range of the transition stress the rupture

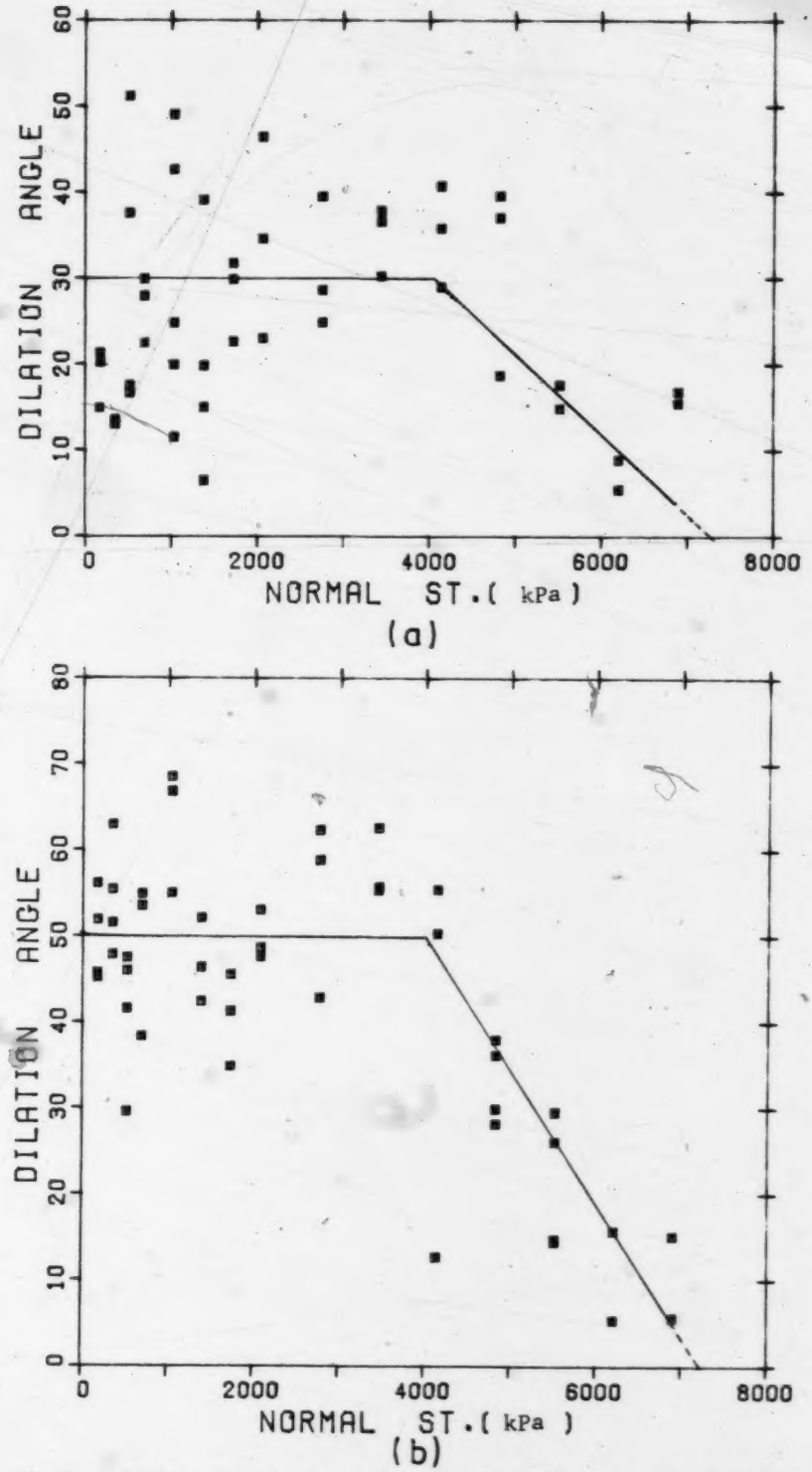

Figure 2.21 The effects of normal stress on dilation angle during shear for (a)Tyndall Stone and (b)Standstead Granite surfaces

behavior of specimens changed from a mode of involving the "riding up" or "riding up and shearing through" surface asperities to the onset of pure "shearing through" (Patton, 1966). Perhaps, the rocks surfaces begin to produce a regular set of inclinations.

Maximum values of dilation angle as high as 51 and 68 degrees were measured for the limestone and granite surfaces respectively.

2.4.4 The Effect of Stress History on Peak Strength

Some of the samples which had already been sheared at the low stress levels (170-518 kPa) were sheared again at higher stress levels (2070-4140 kPa) to investigate the effect of stress history on the peak strength of rock surfaces. As mentioned before, damage to surface irregularities was noticed on the sheared samples. For this reason, one would expect a lower strength for these "daughter" samples when sheared at high normal stresses.

Figures 2.22a,b show the experimental results (diagram a, limestone surfaces; diagram b, granite surfaces). The shaded envelope at the top of each diagram shows some of the average peak strengths of the samples sheared at high normal stresses, reproduced from figures 2.14a,b. These samples were termed the "parent" samples, meaning that no stress history was involved that each of them had not been previously sheared.

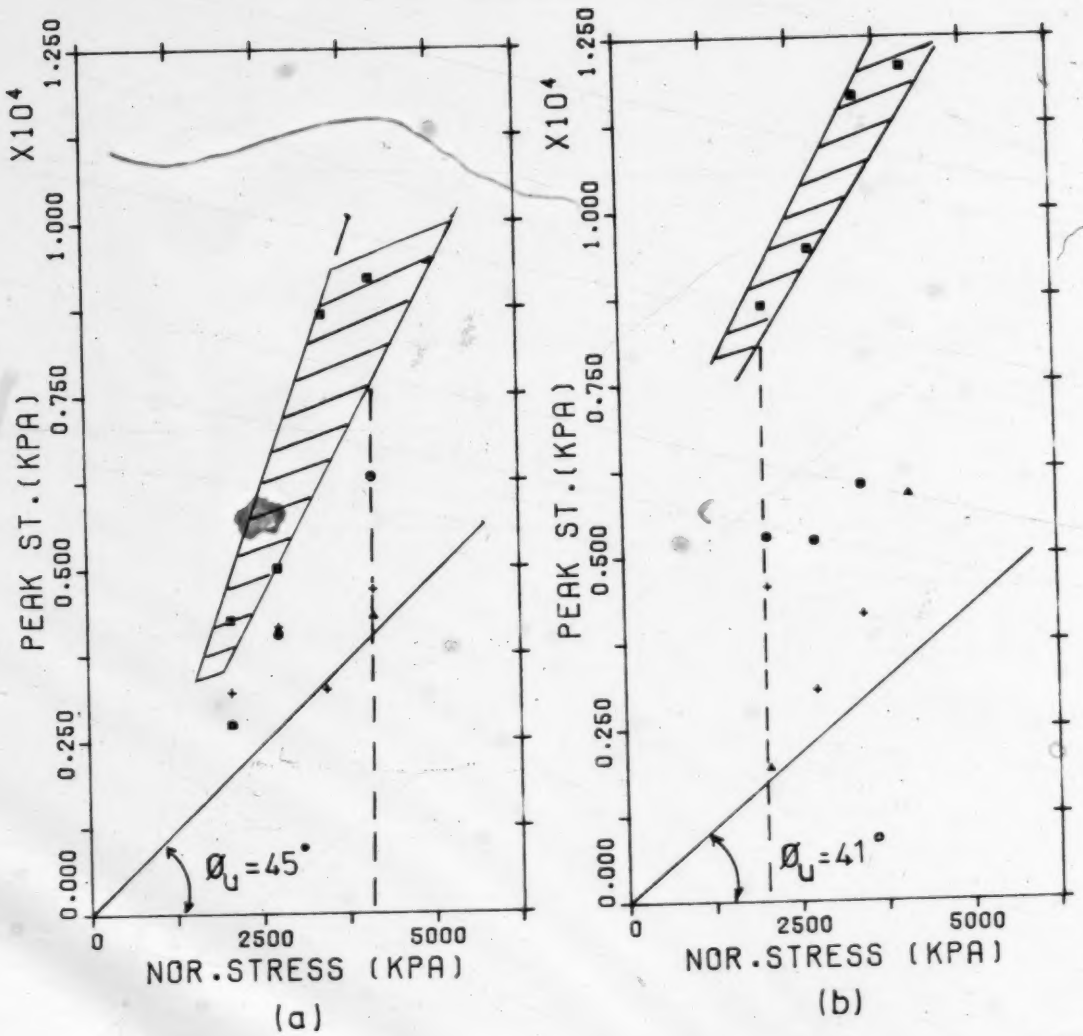

▪ =parent samples
o =daughter samples already sheared at 172.5kpa
▲ =daughter samples already sheared at 345.0kpa
+ =daughter samples already sheared at 517.5kpa

Figure 2.22 The effects of stress history on peak shear strength results for (a)Tyndall Stone and (b)Standstead Granite surfaces

Below the shaded envelope are the peak strengths of daughter samples; denoted by different symbols, each of which represents its normal stress history.

Note that the peak strengths of these daughter samples at a particular stress level, for example those along the vertical dotted lines in the diagrams, fall below the parental peak strengths. Decreases of as much as 50 percent were found, for both rock surfaces.

If two samples are sheared, one at a low normal stress level (say 172.5kPa), the other at a high normal stress level (say 517.5kPa), both within the low stress range, then if they are both sheared again at a high normal stress level (say 800.0kPa), it is expected that the former sample will have a higher peak shear strength. The reason for this result is that more damage to the asperities would be expected for the latter during the first shearing. However, this reasoning assumes two identical speciments having the same initial surface conditions. This phenomenon can not be found in figures 2.22 a,b, implying that initial surface condition also play an important role on the effect of the peak stress history.

The straight line in each diagram represents the estimated average ultimate strength envelope of the rock surfaces and it lies below the peak of daughter specimens. This suggests that only those tests performed on parent specimens will give reliable peak strengths. The peaks of

daughter specimens lie somewhere between peak and ultimate.

However, the peaks obtained from the direct shear stage-loading tests on the non-dilatant rock surfaces (section 2.3.2) have higher values than those from the single-loading tests. Upon comparing the surface damage on these non-dilatant surfaces with that of the sheared daughter surfaces, damage features like abrasive wear particles gouges, rock flour and some ploughing of the flat surfaces were observed. The surfaces became much rougher than they had been initially. During the parent shear tests on rough rock surfaces, the small steep asperities were damaged or partially sheared off first, leaving smoother surfaces for the daughter specimens.

It appears that during shearing, rough surfaces becoming smoother and flat surfaces rougher because of wear. Ohnaka (1975) also found that the frictional coefficient on flat surfaces increased with the amount of wear.

2.4.5 Stress Drop

For all the shear tests, distinct peak and ultimate shear stresses were measured. The stress drop for a particular normal condition is given by the difference of these shear stresses or simply the difference between the peak and ultimate envelopes (figure 2.3).

Figures 2.23a,b, show the experimental computed stress

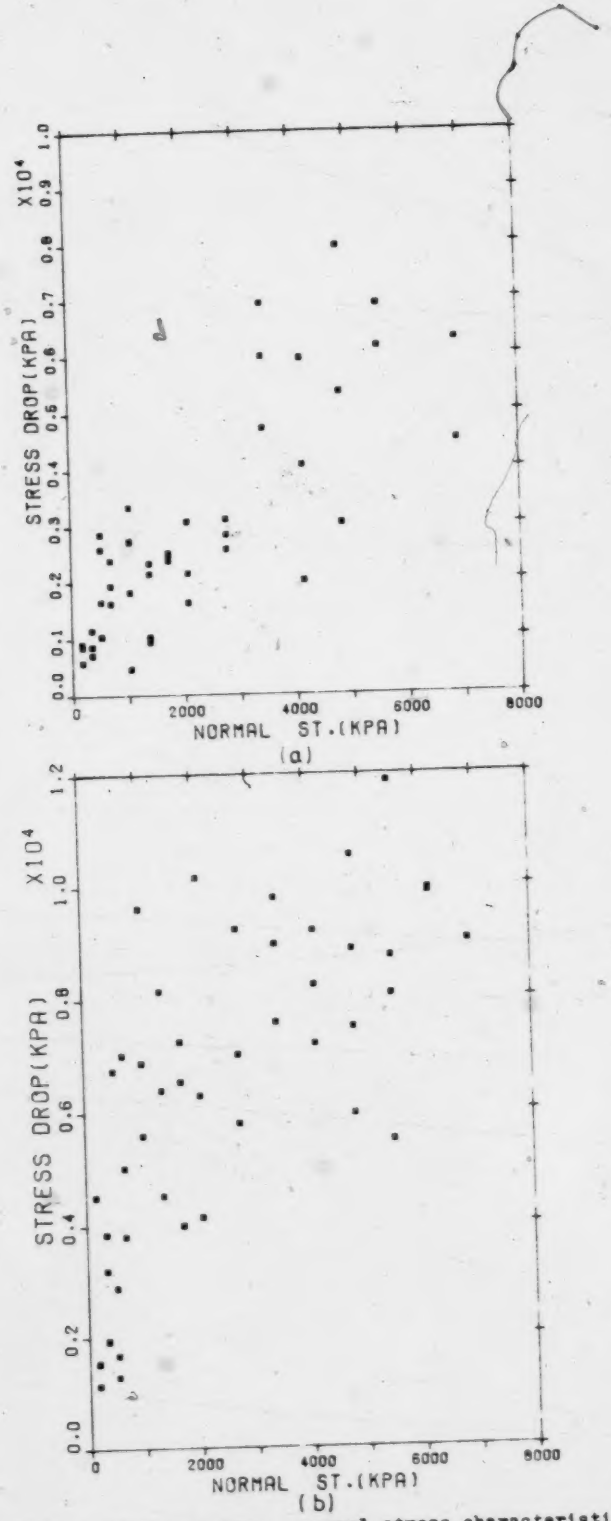

Figure 2.23 Stress drop - normal stress characteristics for (a)Tyndall Stone and (b)Standstead Granite surfaces

drop values versus the effective normal stresses (diagram a, limestone surfaces; diagram b, granite surfaces). The data are scattered but in general, the stress drop increases with normal stress. Some points are worthy of mention: (i) under low normal stress, the amount of stress drop is higher in the case of granite surfaces than limestone surfaces, (ii) difference in stress drop diverges with increase in normal stress and is more marked for the granite surfaces, and (iii) the amount of stress drop seems to reflect the dependence upon surface roughness. Therefore for a stronger material with a rough undulating surface testing at a high normal load, a great amount of stress drop would be expected. Moreover the energy released during the drop would be great. The energy dissipated indicated by the occurrence of a cracking sound appeared to be the result of brittle failure of the steep asperities.

2.4.6 Effect of Normal Stress in Relative Stress Drop

Another rock surface deformation characteristic is the relative stress drop from peak to ultimate strength. The effect of normal stress on the relative drop is illustrated in figures 2.24a,b (diagram a limestone surfaces; diagram b, granite surfaces).

The interlocking effect of asperities rock surfaces at low effective normal stress is clearly illustrated by the large ratio (6.9:1 and 21.7:1 for the limestone and granite

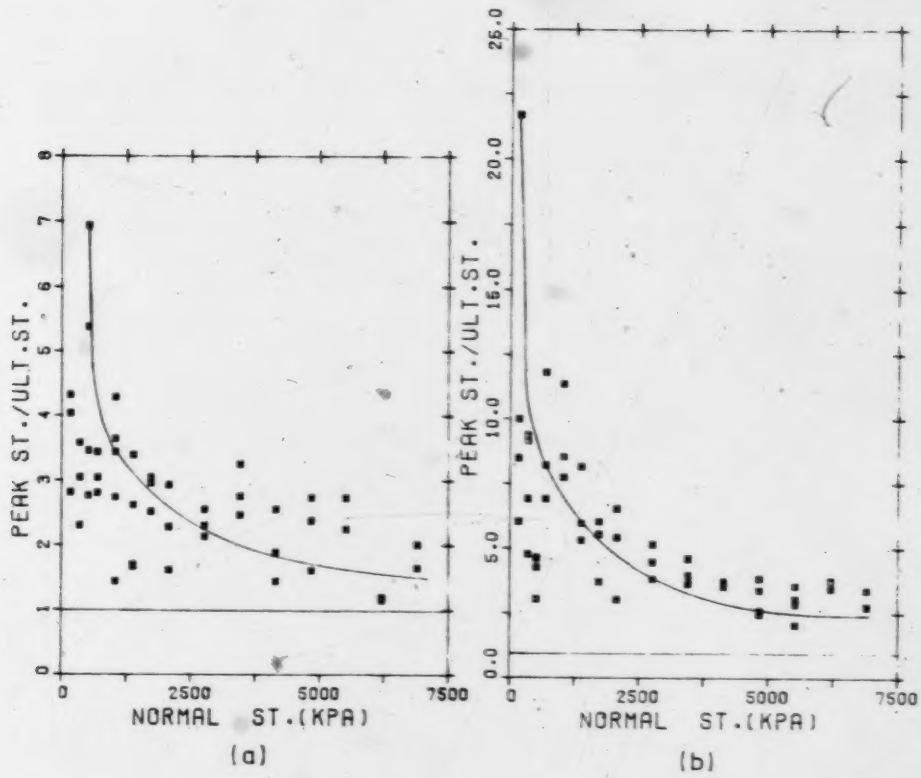

Figure 2.24 The ratio of peak to ultimate strength as a function of normal stress for (a)Tyndall Stone and (b) Standstead Granite surfaces

surfaces respectively) of peak to ultimate strength. The relative drops appear to become asymptopic to a ratio of 1:1 as the effective normal stress increases. One might expect this to happen at a very high stress when the presence of discontinuities has limited effect on the strength and deformation of rock.

2.4.7 Ultimate Shear Strength

When a rock surface is sheared to large strains, it will pass through a peak shearing resistance which will decline to a value where shear deformation can continue with essentially no change on shearing resistance. The resulting frictional resistance is termed the ultimate shear strength offered by the rock surface at large strains. As discussed in section 2.3.6 the ultimate shear strength of rock surfaces does not have a unique value. It depends on the pre-peak surface roughness and the post peak shear mechanism. Figures 2.25a,b, (diagram a, limestone surfaces; diagram b, granite surfaces) which show the ultimate values after B corrections versus normal stress, illustrate the phenomenon. Note that the data at each normal stress vary. Some scatter is found at the low range of normal stress but it increases greatly as the normal stress increases. One might expect this to happen at high stress when the shearing through mechanism is more prevalent and more asperity damage results.

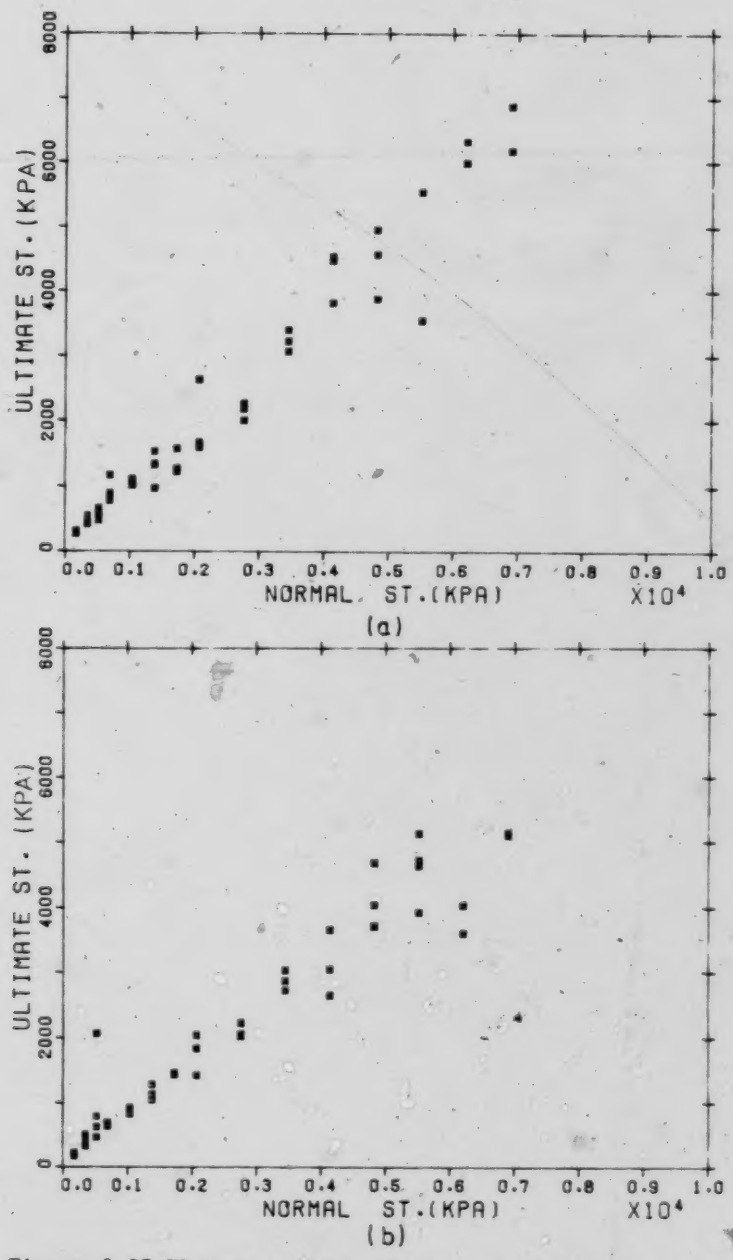

Figure 2.25 Ultimate shear strengths for (a)Tyndall Stone and (b)Standstead Granite surfaces

To each stress level, there corresponds a mean ultimate friction angle. Its standard deviation, its coefficient of variation and the 95 percent confidence limits on the mean angle were calculated and tabulated in table 2.8 for the limestone surfaces and table 2.9 for the granite surfaces. An estimate of the relative amount of scattering is given by the coefficient of variation (standard deviation/mean). As seen in these tables the coefficients do not have a consistent value and the standard deviations change with normal stress. To see whether the scatter (results within a normal stress and between normal stresses) is significant or the assumption of homoscedasticity within the ultimate strengths is valid the mean variances were tested by the Hartley's maximum F ratio test which had been mentioned before in section 2.4.1.

Results from this test indicated that the ratio of the largest variance (square of the standard deviation) to the smallest exceeded the tabular entry of the Hartley's table for the granite surfaces, but it was smaller for the limestone surfaces. In the other words the scatter in the ultimate strength in the hard rock depends on the stresses imposed but this is not the case in the soft rock.

Ohnaka (1975) found that the controlling mechansim of friction for uniform soft rocks such as limestone and marble was distinctly different from that for such rocks as granite and monzonite which contain various minerals of different

Normal stress σ_n kPa	Number of test	Mean ultimate friction angle ϕ_u	Standard deviation of mean ϕ_u	Coefficient of variation [standard deviation / mean]	95% confidence limits on ϕ_u
172.50	4	59.51	2.02	0.0339	57.14---61.88
345.00	3	53.76	3.72	0.0691	47.43---60.09
517.00	4	48.31	3.04	0.0629	45.27---51.35
690.00	3	53.66	5.34	0.0995	44.57---62.75
1035.00	5	45.55	0.96	0.0210	44.63---46.47
1380.00	4	42.80	5.35	0.1250	36.52---49.08
1725.00	3	38.09	3.75	0.0984	31.71---44.47
2070.00	3	42.80	7.85	0.1834	29.44---56.16
2760.00	3	37.96	1.75	0.0461	34.98---40.94
3450.00	3	43.13	1.45	0.0336	40.67---45.59
4140.00	3	45.85	2.74	0.0597	41.19---50.51
4830.00	3	42.66	3.52	0.0825	36.67---48.65
5520.00	2	38.91	8.74	0.2246	0.00---77.84
6210.00	2	44.77	1.07	0.0238	40.01---49.53
6900.00	2	43.38	2.17	0.0500	33.72---53.04

Table 2.8 Values of the mean ultimate friction angle, ϕ_u of Tyndall Stone surfaces

Normal stress σ_n kPa	Number of test	Mean ultimate friction angle ϕ_u	Standard deviation of mean ϕ_u	Coefficient of variation [standard deviation / mean]	95% confidence limites on ϕ_u
172.50	4	49.74	3.42	0.0687	45.73---53.75
345.00	4	50.37	5.39	0.1070	44.04---56.70
517.00	4	56.38	14.37	0.2548	39.50---73.26
690.00	3	43.86	1.25	0.0284	41.74---43.56
1035.00	3	40.66	1.72	0.0423	37.74---43.58
1380.00	3	39.97	2.88	0.0720	35.07---44.87
1725.00	3	40.11	0.27	0.0067	39.66---40.56
2070.00	3	40.27	5.10	0.1266	31.59---48.95
2760.00	3	37.29	1.38	0.0370	34.94---39.64
3450.00	3	39.77	1.49	0.0374	37.24---42.30
4140.00	3	36.77	4.43	0.1204	29.23---44.31
4830.00	4	39.75	3.10	0.0779	36.11---43.39
5520.00	4	39.72	3.13	0.0788	36.05---43.39
6210.00	2	31.55	2.05	0.0649	22.42---40.68
6900.00	2	36.59	0.16	0.0043	35.88---37.30

Table 2.9 Values of the mean ultimate friction angle, ϕ_u of Standstead Granite surfaces

hardness.

Figures 2.26a,b, show the relationship between the mean ultimate frictior angle and the effective normal stress (diagram a, limestone surfaces; diagram b, granite surfaces). The square points indicate the sample means, and the intervals of the 95% confidence limits of the population means. The straight line represents the estimated basic friction angle of the rock (section 2.3.2).

In general, the mean ultimate friction angle decreases with normal stress and tends to a consistent range of values. The estimated average ultimate friction angles were 45 and 41 degrees for the limestone and granite surfaces respectively. Comparing these to the corresponding basic friction angles of the rocks ($\emptyset b$=33.5, limestone; $\emptyset b$=30.5, granite) one finds the average ultimate friction angles are higher. This is expected for unweathered rock surfaces.

2.5 Summary Of Chapter II

(1) A laboratory direct shear machine which precludes sample toppling and sideways tilting was employed for the testing of shear strengths of two artificially fractured rock surfaces. These surfaces were carefully prepared, labelled and controlled environmentally, thereby satisfying the requirements of sample and roughness reproducibiltiy, and shear load capacity of

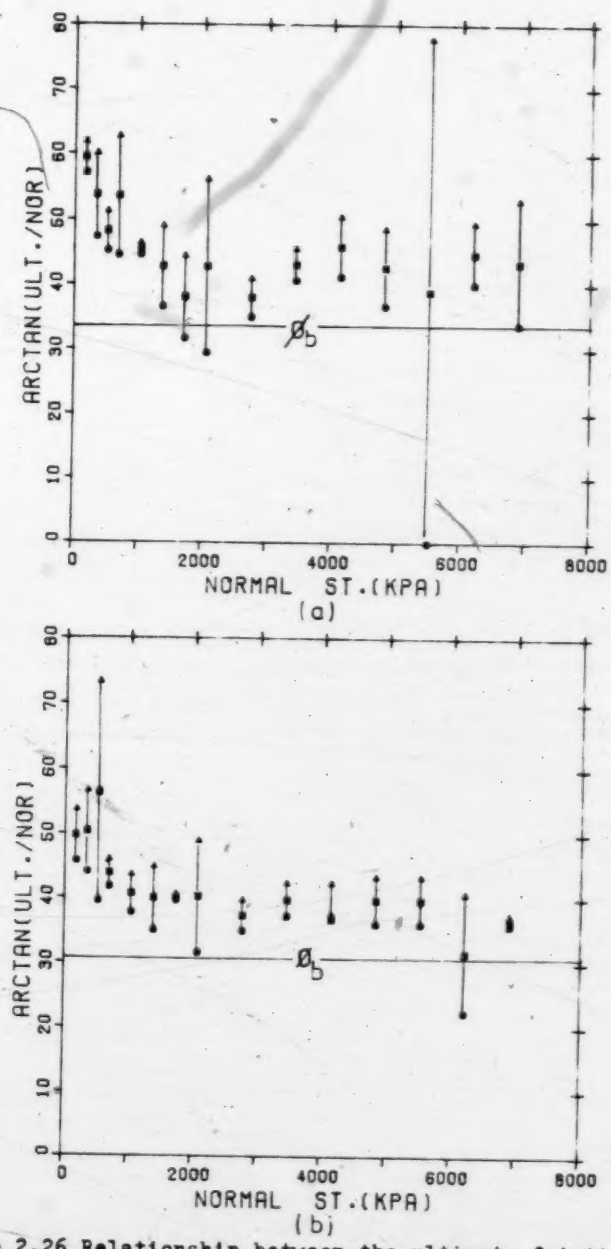

Figure 2.26 Relationship between the ultimate friction angle and the normal stress for (a)Tyndall Stone and (b)Standstead Granite surfaecs. The centre points indicate the mean angle, and the intervals the 95% confidence limits of the means.

the creep machines.

(2) The shear strength of rock surfaces is due to the frictional resistance offered by the geometrical irregularities of rock surfaces - the effective i-angle and the basic friction angle of the rock - ϕb. The i-angle is a material as well as a stress-dependent rock parameter.

(3) The point load strength method and the Schmidt hammer index test gave reasonable values of the uniaxial compressive strength of the rocks.

(4) Flat surfaces prepared using a sandblasting technique could be the best means to test for the basic friction angle of rock. The stage-loading test on one specimen would overestimate the shear strength because of additional wear induced from previous stages.

(5) The average angle from the toppling failure on the tilting apparatus for the rock surfaces was about 60 degrees, indicating very rough surface morphology.

(6) Sheared surfaces showed a small percentage of actual contact area during sliding and the amount varied with stress level.

(7) No cohesion intercepts were measured for the clean and tightly interlocking surfaces. The distribution of the shear strength versus normal stress plot, generally trended in the shape of curves as expected. A power law could be constructed to describe the experimental observations.

(8) The degree of dilatancy of the rock surfaces reflected the dependence upon the degree of surface roughness, the effective normal stress and the mineral composition of the rock. The measured dilation angles tended to converge to a narrow range of values as the normal stress increased up to the transition stress. Beyond this stress range the dilation angles seemed to decrease linearly with stress level.

(9) In general, the shear stiffness and stress drop of the rock surfaces increased with stress level and strength of the material.

(10) Shear strengths derived from stage-loading tests on rough rock surfaces were not reliable because of the unknown stress history and steep asperity damage. They tended to have values between peak and ultimate.

(11) The ultimate friction angle was not a unique value for a given type of rock surface. Its magnitude depended upon the post peak characteristics and the rock type in question. The estimated overall average ultimate friction angle was higher than the basic friction angle of the rock.

CHAPTER III

Surface Roughness Study and Prediction of the Effective Geometric i-Angle

3.1 Introduction

It is general knowledge that the shearing resistance along rock surfaces airses from two components: the frist being the frictional resistance resulting from two flat surfaces sliding over each other and the second component arising from the resistance to sliding offered by the geometric irregularities on the rock surfaces (Ripley and Lee, 1961; Patton, 1966; Barton, 1971; Coulson, 1972; Schneider, 1974; Krahn, 1974 and others). The former is known as the material parameter (ϕb), depending upon the strength of the rock and its mineral composition. The latter is termed the geometrical parameter (i-angle). Its magnitude depends upon the surface conditions such as the geometry of the surface roughness, degree of indentation and contact area (Schneider, 1974). The irregularity or roughness of the rock surfaces is the hardest quantity to estimate. Rengers (1970), Fecker and Rengers (1971) and Bruce (1978) described methods for its detailed measurement.

3.2 Definitions of surface roughness

Single mathematical surface characteristics have been

used by mechanical engineers in describing the finish on milled metallic surfaces. For example, many surface roughness instruments now in use employ an average deviation from the centre line. The centre line is the line about which roughness is measured. It is a line parallel to the general direction of the profile and within the limits of the profile-width cutoff such that the sums of the area contained between it and those parts of the profile which lie on either side of it are equal (ASA, 1955). A measure of the average deviation is the root mean square (RMS) defined by (ASA, 1955) the following equation.

$$RMS = \sqrt{\frac{1}{M}\int_{x=0}^{x=M} y^2 \, dx} \qquad \text{(units of length)} \qquad (3.1)$$

where: M = the number of discrete measurements of the amplitude
y = the amplitude of the roughness about the center line, a mean of zero amplitude
dx = the constant distance between two adjacent amplitude readings

In Britain, a similar method of determining the roughness is used. The roughness parameter is known as the centre line average (CLA). This average is defined by (ASA, 1955) as:

$$CLA = \frac{1}{L}\int_{x=0}^{x=L} |y| \, dx \qquad \text{(units of length)} \qquad (3.2)$$

where: L = the distance over which the average is taken

Using the RMS as the basic roughness characterization, Myers (1962) proposed three other parameters giving

numerical values to certain components of surface roughness: the RMS of the first derivative of the profile (Z2), the RMS of the second derivative (Z3), and the percentage excess of distance measured along the profile where the slope is positive over that where the slope is negative (Z4). These three parameters may be expressed in the following mathematical forms (Myers, 1962):

$$Z2 = \sqrt{\frac{1}{L}\int_{x=0}^{x=L} \left(\frac{dy}{dx}\right)^2 dx} \qquad \text{(dimensionless)} \qquad (3.3)$$

$$Z3 = \sqrt{\frac{1}{L}\int_{x=0}^{x=L} \left(\frac{d^2y}{dx^2}\right) dx} \qquad \text{(units of length}^{-1}\text{)} \qquad (3.4)$$

$$Z4 = \frac{\Sigma(\Delta xi)_{positive} - \Sigma(\Delta xi)_{negative}}{L} \qquad \text{(dimensionless)} \qquad (3.5)$$

where: Xi = the ith segment of L
$L = \sum(\Delta xi)\,positive + \sum(\Delta xi)\,negative$

Z2 was used in gauging the light-scattering properties of metallic surfaces, Z3 and Z4 as a measure of the degree of wear or rounding of asperities and directional lay, respectively. Myers (1962) correlated parameters RMS, Z2 and Z3 with the coefficients of friction on samples of cold-rolled steel discs with different finishes and found that the best relationship of friction was obtained with the Z2 parameter.

Krahn (1974), in his work on rock surface roughness found that there existed a linear relationship between the total friction angle and Z2 for some non-dilatant rock surfaces. Another possible approach in characterizing surface roughness is to consider the distribution of the asperity heights, in a representative profile, to be a random phenomenon. It is then analyzed on a statistical basis(Moore, 1969; Bendat and Piersol, 1970).

Two such statistical fuctions, the mean square values (MSV) and the autocorrelation function (ACF), are described in this study. These functions are defined (Bendat and Piersol, 1971) as follows:

$$MSV = \frac{1}{L}\int_{x=0}^{x=L} y^2\,dx \qquad \text{(units of length}^2\text{)} \qquad (3.6)$$

$$ACF = \frac{1}{L}\int_{x=0}^{x=l} f(x)\ f(x+\Delta x)\,dx \qquad \text{(units of length}^2\text{)} \qquad (3.7)$$

where: $f(x)$ = the amplitude of asperity height at the distance x along the length L
x = a constant distance lag

Salyes and Thomas (1977) proposed another surface parameter which is related simply to the ACF. This parameter is known as the structure function (SF) defined to be:

$$SF = \int_{x=0}^{x=L} (f(x) - f(x+\Delta x))^2 \qquad \text{(units of length}^2\text{)} \qquad (3.8)$$

The SF was used to quantify the variation in surface texture. Physically, the SF is independent of the mean plane, a property not shared by the ACF, and may be computed over only a portion of the profile without loss of significance (Sayles and Thomas, 1976).

It is the purpose of this chapter to investigate the physical significance of these eight surface parameters in their characterizations of the fractured surfaces of two natural rocks.

3.3 Measurement of Surface Profiles

The first step in attempting to characterize the roughness of a surface is to obtain traces of the surface profile. Therefore, before shear strength testing of the fractured surfaces took place, three profiles were run on the lower surface of each of the fractured surfaces (Section 2.2.4). The profiles were traced at equal distances from each other, each being parallel to the direction in which the sample would be sheared in the shear box.

These profiles were obtained using a roughness measuring device described by Krahn (1974). The device is a small frame on which an LVDT and a stylus arrangement are mounted. Vertical movement is sensed by the LVDT, the output from the LVDT being directly recorded on a Watanbe x-y plotter. About 600 profiles were traced. A typical graphical output is shown in Figure 3.1.

Figure 3.1 A typical graphical output of a rock surface on the Watanbe X-Y plotter
Horizontal scale 1: 0.185
Vertical scale 1: 0.332

The length of tracks was limited by the size of the plotter. For the particular problem at hand the horizontal scale was chosen to be 1 : 0.185 and the vertical amplification 1 : 0.332. The stylus, a keenly sharp pointed steel needle was attached to the LVDT which was mounted in a pickup that could be traversed across the surface by an electrically driven gearbox. The stylus was replaced whenever wear was observed at its tip. In this way, macro-roughness (Moore, 1969) of the rock surfaces could be measured. For most engineering and manufacturing surfaces macroscopic methods suffice and they are usually mechanical in nature (Selwood, 1962). On the other hand, physicists and physical chemists require fine-scale details of surfaces and often details of molecular roughness. These details are usually provided through use of optical techniques (Selwood, 1962).

3.4 Digitization of Surface Profiles

Once the surface profiles were obtained, the next step was to determine the trace of the mean plane. A ruler was used to aid in this process. A new coordinate system was then constructed, the abscissa coinciding with the trace of the mean plane, the ordinate as before. The directed distance between the new and old abscissa is termed the B correction.

The profiles, upon redrawing, were digitized together

with Barton and Choubey's ten standard roughness profiles. The ten standard profiles (Figure 2.8) were enlarged, having the same horizontal and vertical scales of 1 : 0.4. Discrete measurements of the amplitude (y-coordinate), relative to some datum established on the digitizing table, were made at regular intervals (x-coordinate).

This was done using a digitizer available at the Computer Centre, University of Alberta. Essentially, this device is an analog to digital converter. It records x and y coordinates of selected points when a curser is run over the analog signal and the recorded readings are stored in digital form on an output file - a 9-track magnetic tape. For the digitization of profiles at hand, the device was set to take a reading at intervals of 0.127 cm along the abscissa, the smallest interval possible. A total of twenty discrete amplitude measurements was then obtained for every 2.54 cm. To ensure that there were no erroneous results in the digitized files, all the digital profile data were retrieved and replotted on a Calcomp plotter. The Calcomp plotter output for the profiles consists of discrete points close enough to give the appearance of smooth curves. These computer plots were compared with the traced surface profiles. If any visible difference were noted the profile was then redigitized until the difference disappeared.

3.5 Computations of Surface Parameters

Once the surface profiles were in digital form, a computer program was written in order to read the data files from the magnetic tape. The coordinate readings were then converted into centimetres and translated to some appropriate datum relative to each profile. The datum was chosen so that the mean of all the readings (amplitudes) for a particular profile would be zero - the center line. Eight surface parameters, as discussed in Section 3.2 (Equations 3.1 to 3.8), were calculated for each profile. Since there were three profiles traced on each rock surface, the program would also compute the average and the largest values of the parameters for each surface; however, for Barton and Choubey's profiles, the two would be of the same value. All computing work was performed on an IBM-360 computer.

The computation of parameters was a relatively simple matter. For example, to compute the Z2 parameter with equal intervals (Dx), one simply sums the squares of the differences in adjacent y-coordinates over the entire length (L). This number is divided by the product of the number of intervals (M) and the square of interval, the sqare root of the quotient then being taken. In discrete form, Z2 may be expressed as:

$$Z2 = \sqrt{\frac{1}{M(Dx)^2} \sum_{i=1}^{M} (y_{i+1} - y_i)^2}$$

The results of the computations for Barton and Choubey's profiles are shown in Table 3.1, those of the rock

JRC	Z2	Z4	SF
0.4	0.09614	0.07998	0.00489
2.8	0.13941	0.20985	0.01061
5.8	0.15088	0.09439	0.01226
6.7	0.18535	-0.03125	0.01834
9.5	0.19612	0.45481	0.02047
10.8	0.21115	-0.19464	0.02369
12.8	0.24620	0.23050	0.03138
14.5	0.27939	-0.07867	0.04253
16.7	0.31294	0.22959	0.04911
18.7	0.39718	0.01717	0.07898

Table 3.1 Values of three surface parameters for Barton and Choubey's ten standard surface profiles of different JRC values

surfaces in the Appendix C.

3.6 Correlation Between JRC and Surface Parameters

The first column in Table 3.1 shows the values of the JRC corresponding to the profiles in Figure 2.8. These values were back-calculated from experimental data (Barton and Choubey, 1977). The rest of the columns in this table show the important values of three different surface parameters.

A linear regression analysis was carried out for each set of parameters with the back-calculated JRC values. The JRC values were taken to be absolute numbers since they were back-calculated from the test results. Therefore, the JRC was the independent variable and the surface parameter the dependence in the regression analysis. However, reversing of the variables in the relationship would have yielded the same statistical results(same correlation coefficients). In view of this, the regression equations, as shown in Table 3.2, express JRC values as functions of the surface parameters. The reasons for this arrangement will be apparent later in this chapter.

The tabulated values of the correlation coefficients (R) reflect the degree of dependence of the surface parameter on the JRC values. If the coefficient is near unity, in absolute value, strong dependence is indicated (Bejamin and Cornell, 1970). The results of the regression

analyses indicate that the joint roughness coefficient of a rock surface can be well predicted by the parameters, Z2 (R = 0.968) and SF (R = 0.919). The results of the Z4 correlation indicate that the profiles in Figure 2.8 are highly directional (Myers, 1962) since for this correlation, the value of the coefficient R is -0.838. As noted in Table 3.1, the sign of Z4 changes. A negative value indicates that a greater portion of the rock surface profile measured has a negative slope than positive slope. Surfaces with no directional property would have a value of Z4 of 0.

Because of the high correlation exhibited by the parameters Z2 and SF, additional linear regression analyses were carried out, this time using the arctan and/or logarithm of these two parameters. The results of analysis are shown together in Table 3.2. Again, high correlations are found, the highest being in logarithmic relationships with the JRC values (R = 0.986, log(Z2) correction; R = 0.984, log(SF) correlation). Figures 3.2 to 3.6 show curves depicting the relationships between the JRC and Z2, arctan (Z2), log (Z2), SF, and log (SF), respectively. The best fitting straight line (as determined by linear regression) was drawn through each set of data.

Although strong correlation between the JRC values and the two surface parameters (Z2 and SF) was obtained, the results of regression analysis do not indicate whether the deviations of the data in Figures 3.2 to 3.6 from the

REGRESSION EQUATION	CORRELATION COEFFICIENT R	
JRC= 2.37+ 70.97(RMS)	0.784	(3.9)
JRC= 2.76+ 78.87(CLA)	0.768	(3.10)
JRC=-4.41+ 64.46(Z2)	0.968	(3.11)
JRC=-6.84+ 4.06(Z3)	0.785	(3.12)
JRC=10.14- 2.68(Z4)	-0.838	(3.13)
JRC= 5.43+293.97(MSV)	0.690	(3.14)
JRC= 5.47+293.80(ACF)	0.688	(3.15)
JRC= 2.69+245.70(SF)	0.919	(3.16)
JRC=-5.05+ 1.20$\tan^{-1}$(Z2)	0.973	(3.17)
JRC=32.20+32.47Log(Z2)	0.986	(3.18)
JRC=37.28+16.58Log(SF)	0.984	(3.19)

Table 3.2 Results of regression analysis of Barton and Choubey' ten standard surface profiles with eight surface parameters

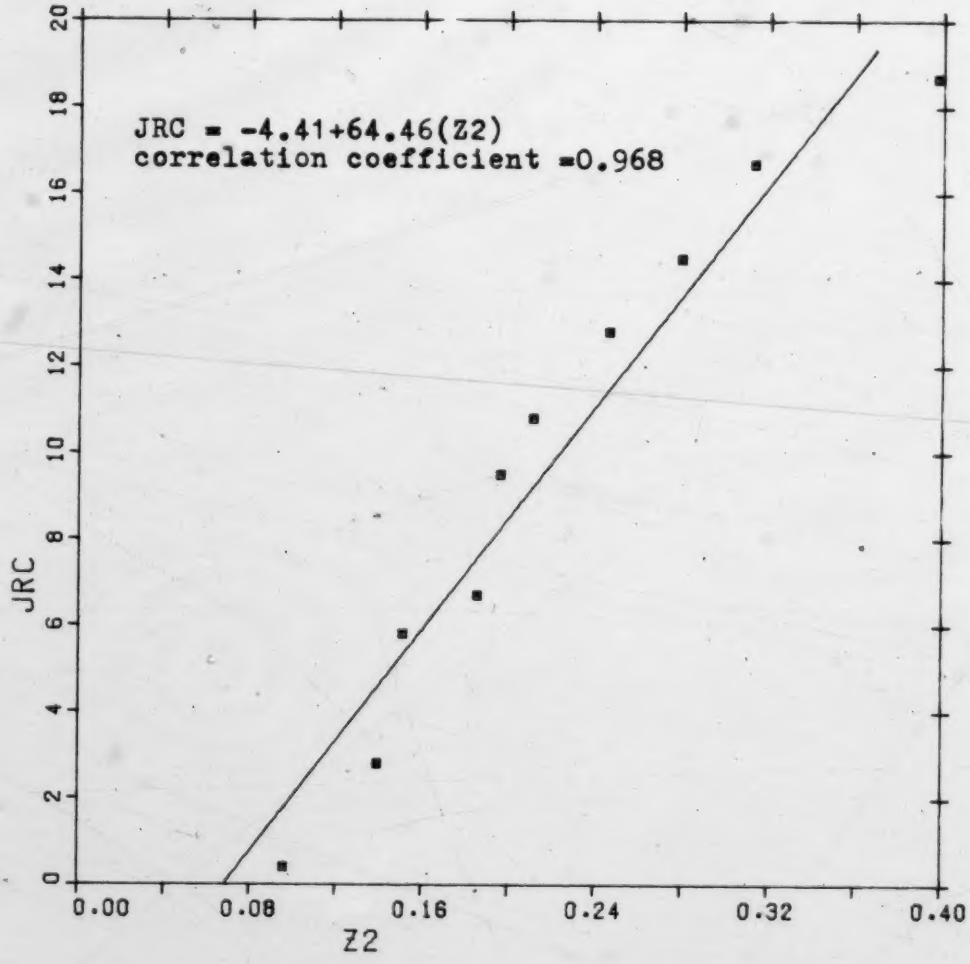

Figure 3.2 Relationship between the JRC and Z2 parameters for Barton and Choubey's 10 standard rock surface profiles

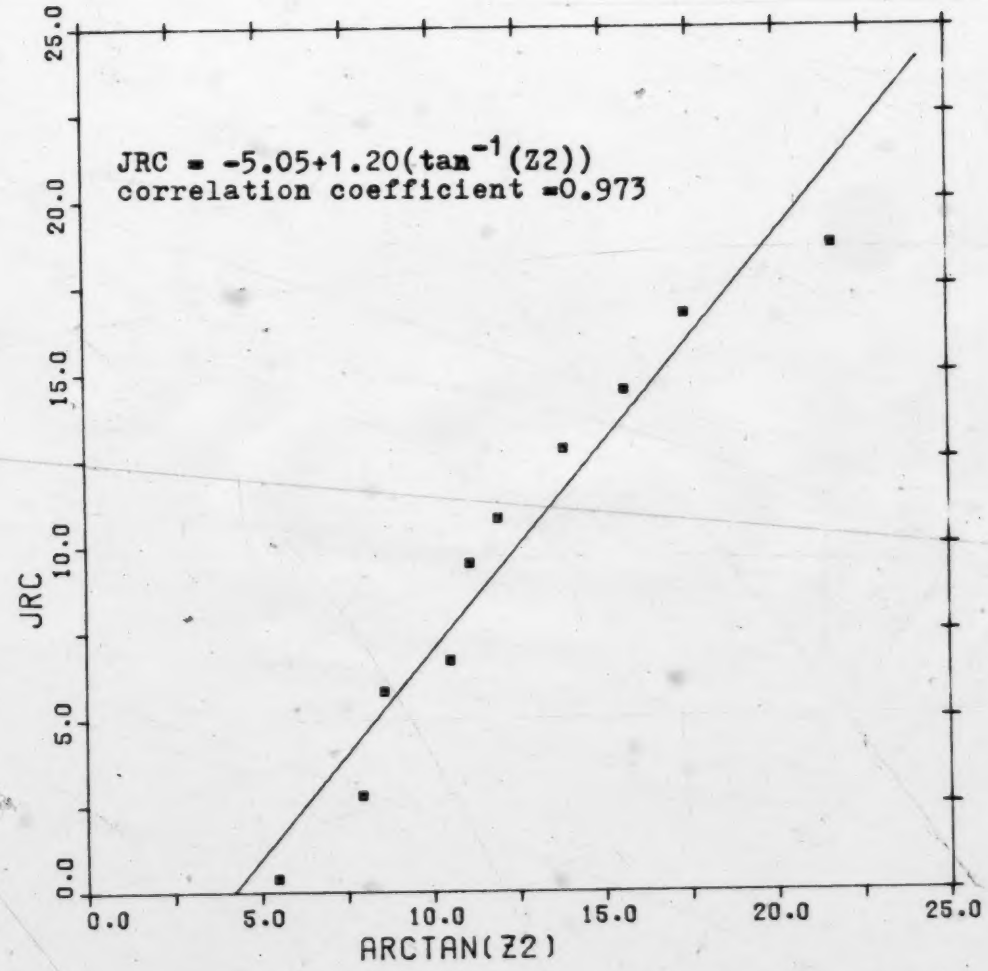

Figure 3.3 Relationship between the JRC and arctan(Z2) parameters for Barton and Choubey's 10 standard rock surface profiles

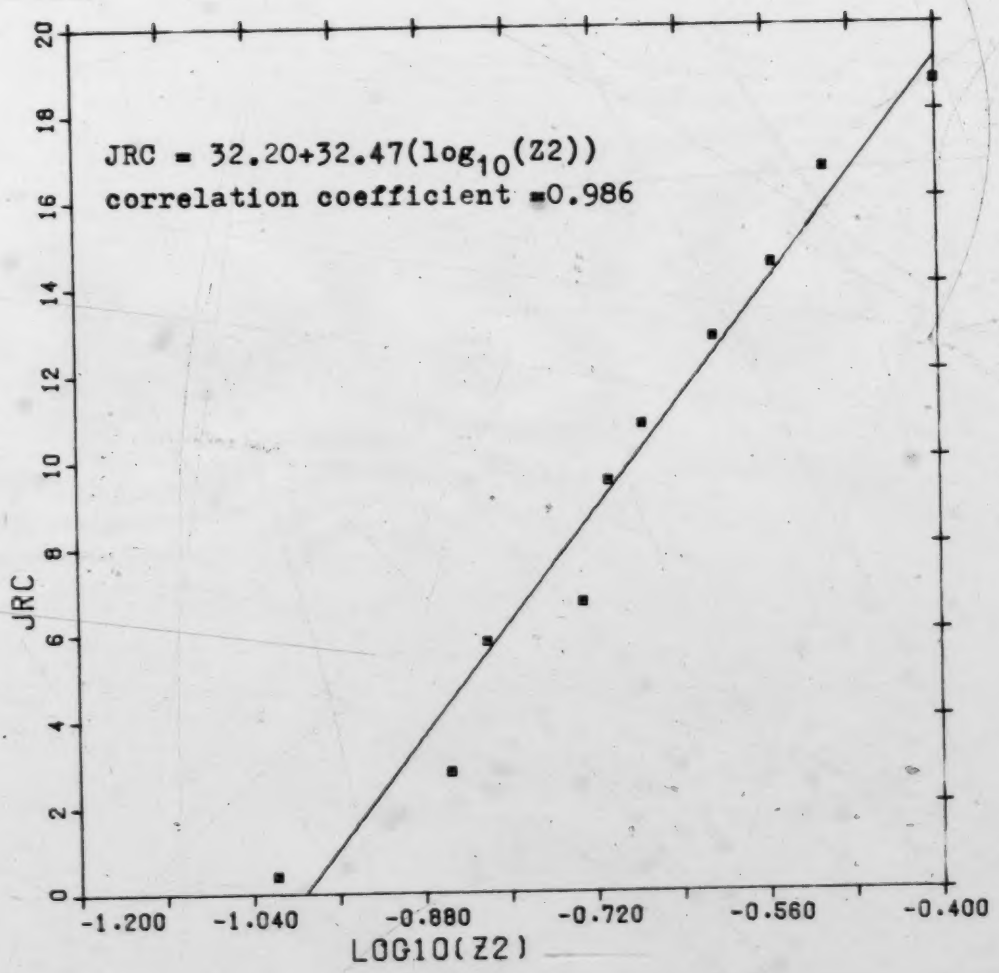

Figure 3.4 Relationship between the JRC and log(Z2) parameters for Barton and Choubey's 10 standard rock surface profiles

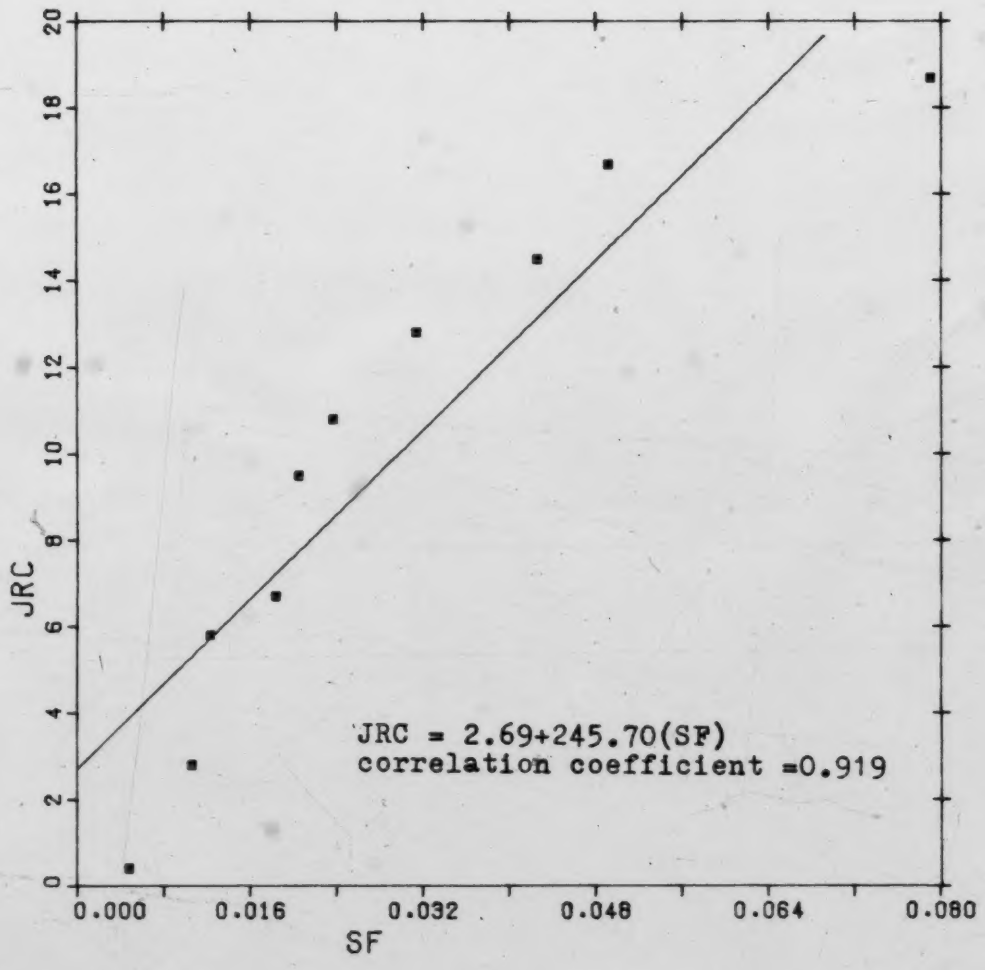

Figure 3.5 Relationship between the JRC and SF parameters for Barton and Choubey's 10 standard rock surface profiles

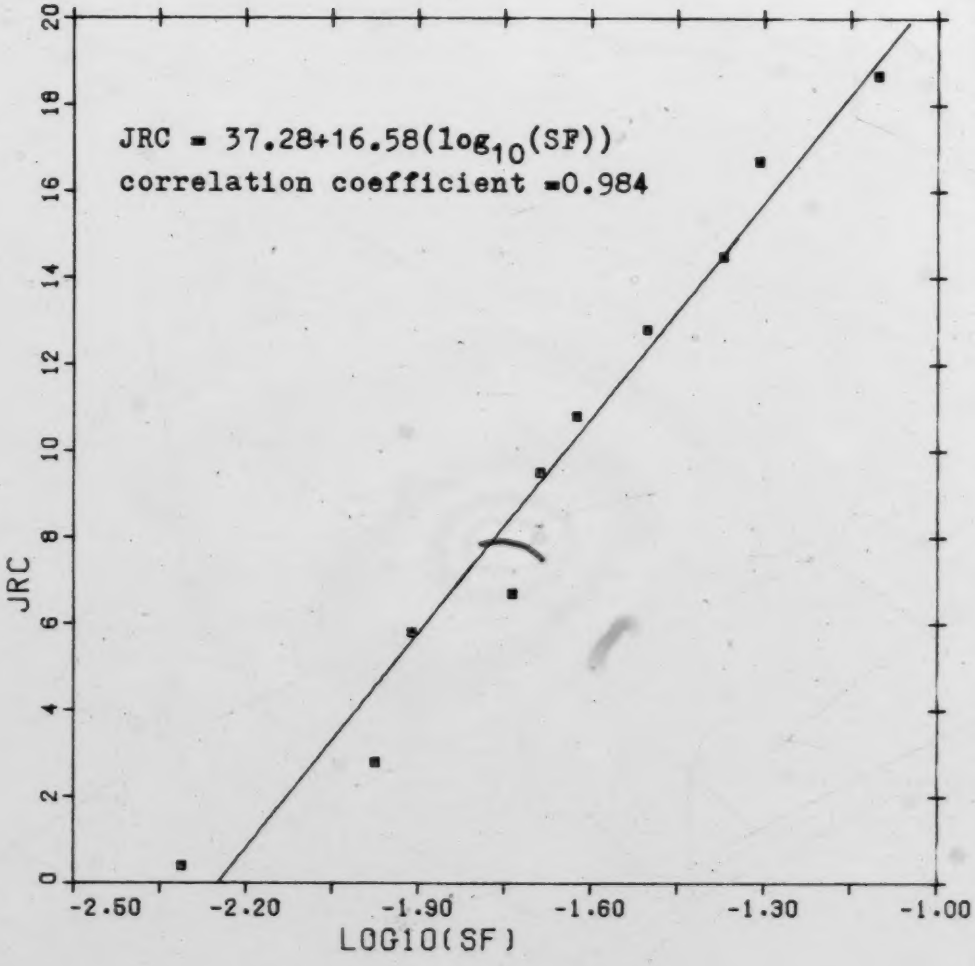

Figure 3.6 Relationship between the JRC and log(SF) parameters for Barton and Choubey's 10 standard rock surface profiles

regression lines are random. The theory of runs was used to test this hypothesis (Dixon and Massey, 1969).

To test this hypothesis, the regression line was taken as the median of the data points. Observations below the median were denoted by a minus sign and those above by a plus sign. Any set having the same sign occurring in a row is called a run. If the number of runs of plus and minus signs is greater or smaller than might be expected by chance, the hypothesis of random deviation from the regression line is rejected.

Let N1 be the number of occurrences of one type (for example, observations below the median) and N2 the number of occurrences of the other type (observations above the median). Let U equal the total number of runs among the N1 and N2 observations and let p be the percentile of the distribution of U (values of P are tabulated by Dixon and Massey (1969) Table). In this manner, the values of N1, N2, U and P for each of the figures 3.2 to 3.6 were obtained. They are listed in Table 3.3. Since the percentile of the distribution (P) of U for each plot is between 2.5 and 97.5, there is no reason to reject, at the 5 percent level of significance, the hypothesis that the deviations of the data have been drawn at random from a single population or over the regression line.

3.7 JRC Values of Tested Rock Surfaces

	N1	N2	U	P
JRC VS. Z2	4	6	5	40.5
JRC VS. $\tan^{-1}$ (Z2)	4	6	5	40.5
JRC VS. Log(Z2)	3	7	6	83.3
JRC VS. SF	4	6	5	40.5
JRC VS. Log(SF)	3	7	6	83.3

N1=Number of observation below the median

N2=Number of observation above the median

U=Total number of runs

P=The percentile of the distribution of U

Table 3.3 Results of run tests

The empirical law of friction of rock surfaces, relating arctan (Peak/normal stress) to lcg (compressive strength of the rock/normal stress) as developed by Barton (1976) in graphical form was used to investigate the range of JRC values encountered on the sheared rock surfaces. These plots are illustrated in Figures 3.7a,b, (Diagram a for the limestone surfaces; Diagram b for the granite surfaces). On each diagram three lines were constructed and the basic friction angle of each rock (Section 2.3.2) was used as the ordinate value. The two solid lines covered the range including the extremes, the dotted line indicating the mean value of surface roughness of the sheared surfaces. These boundary lines plus any straight line falling in between the range would represent Barton's shear strength envelopes for rock surfaces (equation 2.6) of different JRC values. The magnitude of the JRC is the slope of any of these lines.

For limestone surfaces, the range of the JRC values was found to be between 12.5 and 31.1 having a mean value of 21.9. The range corresponded to the slopes of the boundary lines. As for the granite surfaces, the range was between 17.9 and 29.5 having a mean value of 23.9. These JRC values are much greater than the maximum value (20) found by Barton for the roughest class of rock surfaces.

Barton's equation for the peak shear strength of the sheared surfaces is plotted in Figures 3.8a,b, (Diagram a

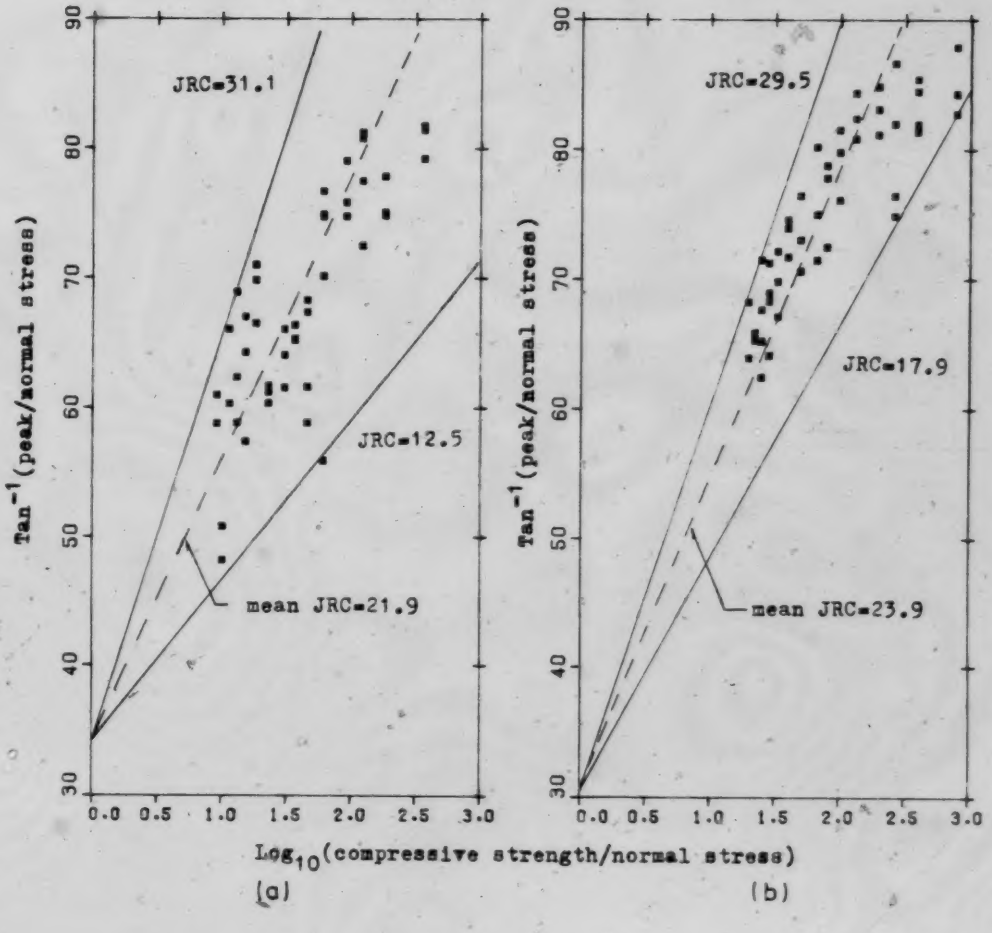

Figure 3.7 Barton's empirical law of friction in graphical form for (a)Tyndall Stone and (b)Standstead Granite surfaces

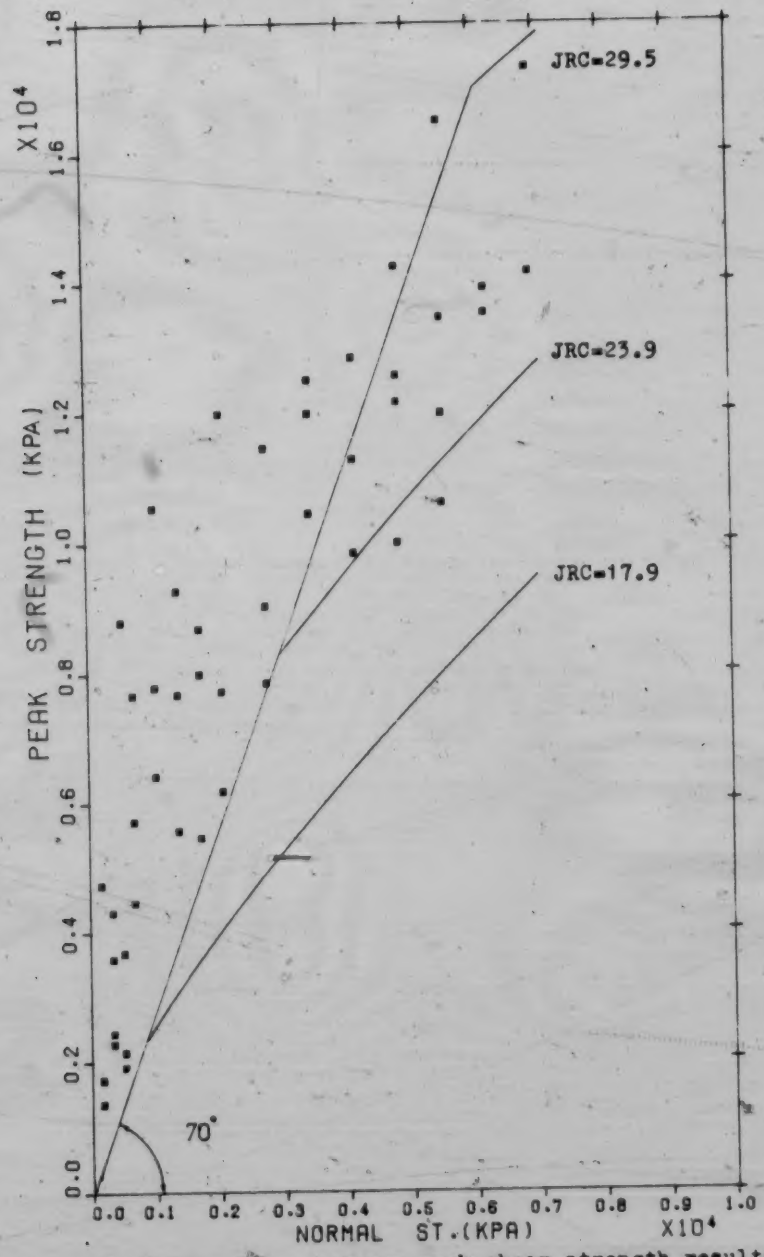

Figure 3.8b Comparison between peak shear strength results of Standstead Granite surfaces and Barton's peak strength envelope criterion for rock surfaces

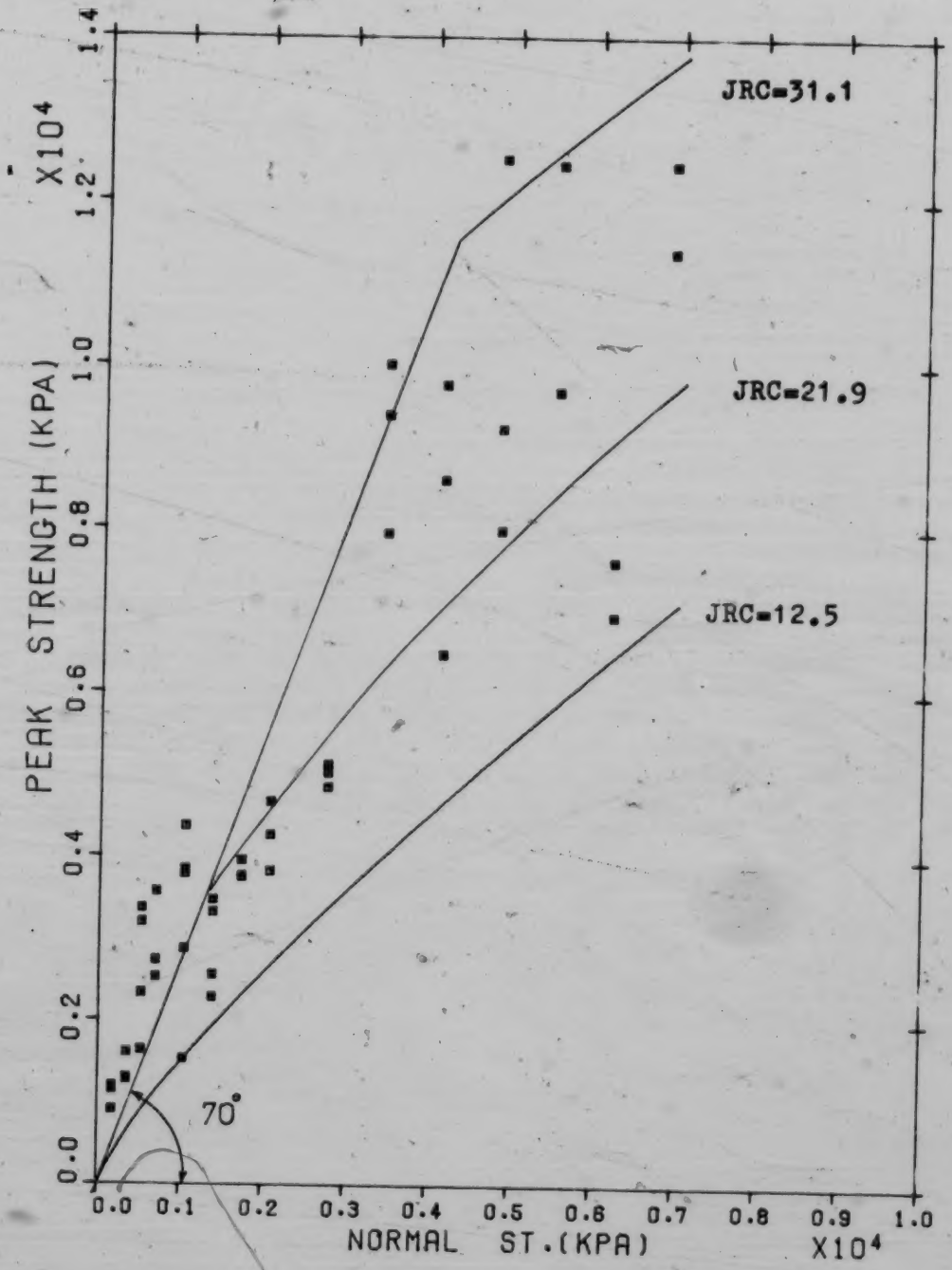

Figure 3.8a Comparison between peak shear strength results of Tyndall Stone surfaces and Barton's peak strength envelope criterion for rock surfaces

for limestone surfaces; Diagram b for granite surfaces) with the corresponding range of the measured JRC values. On each diagram a straight line inclined at an angle of 70 degrees was drawn through the origin. This line represents the maximum design shear strength envelope as suggested by Barton (1976). Note that a great number of data points fall outside and to the left of this design envelope, especially among those representing results of tests on granite surfaces at normal stresses below 3000 kPa. This indicates that the shear strength of these rock surfaces would be underestimated if the Barton's design shear strength criterion were employed.

3.8 Prediction of Effective i-Angles

One significant feature of the Z2 surface parameter (equation 3.3) is that the mean i-angle is denoted by the arctan (Z2). Conceptually, it has the same meaning as Patton's effective i-angle or the first order irregularities of a rock surface. Therefore the regression equations 3.11, 3.17 and 3.18 actually correlate the effective i-angle, Patton (1966) and JRC, Barton (1973).

The experimentally determined i-angles of the rock surfaces were taken to be the difference between the total friction angle, defined by arctan (Peak/normal stress), and the basic friction angle of the rock. The predicted i-angles were computed using Barton's equation for i-angles (Equation

2.7) by substituting computed values for the JRC and log (compressive strength of the rock/normal stress) terms.

The JRC values were computed from the measured surface parameters, (Z2 and SF) from the roughness profiles (discussed in Section 3.5) and the regression equations 3.11, 3.16, 3.17, 3.18 and 3.19.

The values of arctan (Z2), as shown in Figure 3.3, were close to the proposed range of JRC values shown in Figure 2.8. It was felt that another possible correlation might be obtained by setting the JRC value equal to the arctan (Z2) of a surface profile.

$$JRC = \tan^{-1}(Z2) \qquad (3.20)$$

Therefore, graphs of a total six possible relationships between predicted and measured i-angles were computed for each of the two surface parameters.

Since the average and largest values of the parameters (Z2 and SF) were computed for each rock surface, a total of twelve possible predicted i-angles were plotted against the measured value. Two types of rock surfaces had been considered, which meant twenty-four plots were investigated for correlation.

Two typical plots are shown in Figures 3.9a,b, (Diagram a for the limestone surfaces; Diagram b for the granite

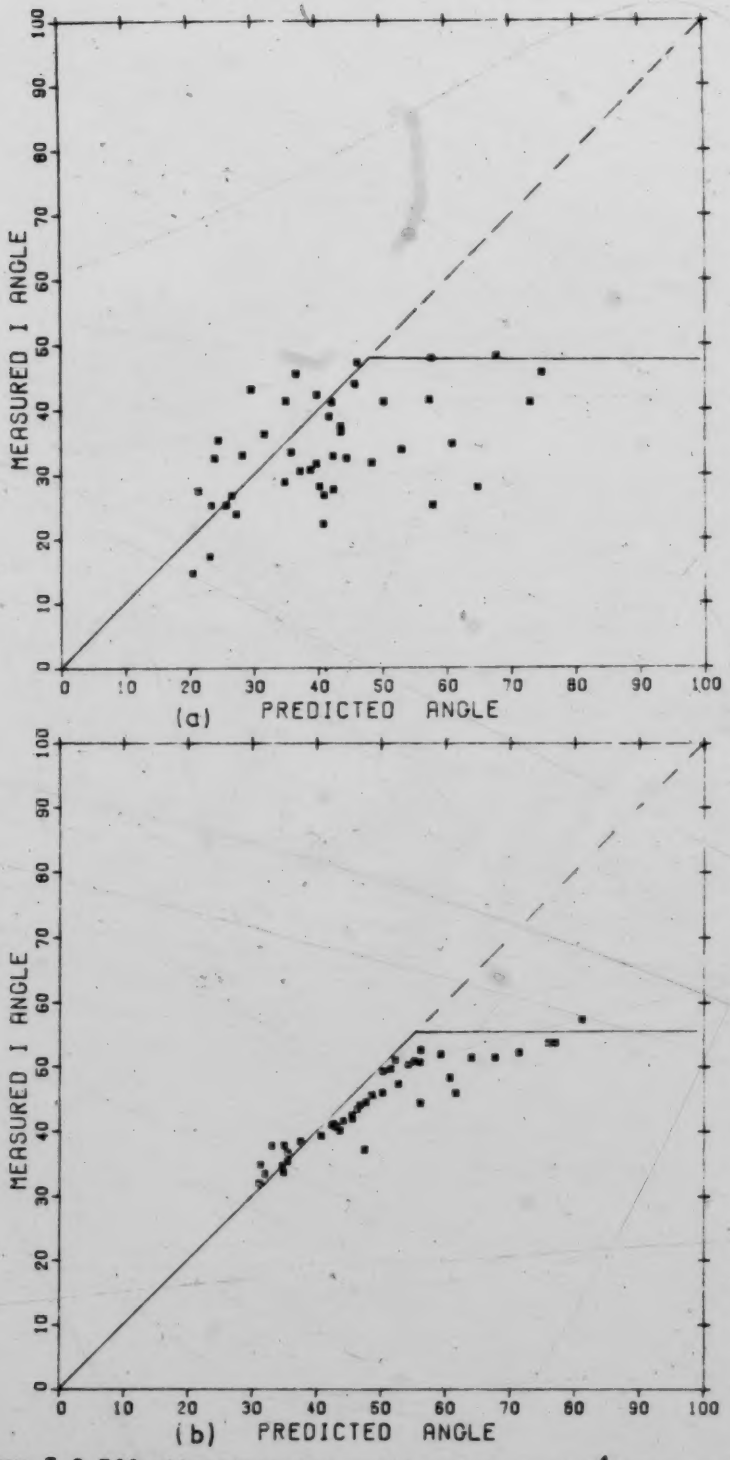

Figure 3.9 Effective i-angles predicted from $\tan^{-1}(Z2)\log(\sigma_c/\sigma_n)$ compared with the measured values obtained from conventional shear box tests on (a)Tyndall Stone and (b)Standstead Granite surfaces.(Z2 parameter is the largest value)

surfaces). In these diagrams the measured i-angles are plotted against the predicted values equal to arctan (Z2)*log (compressive strength of the rock/normal stress) in which the Z2 are the largest values. The straight line on the diagram is the 45 degree line. Any data falling on this line indicate equality of predicted and measured values. A majority of these diagrams show that the data divide into two groups - the first falling close to the 45 degree line and the second departing from this line. The narrow regions or the breaks in the curves where the data departed correspond to predicted i-angles having values between 50 and 55 degrees. The normal stresses yielding these predicted numbers are in the range of 1035 kPa for the granite surfaces and 345 kPa for the limestone surfaces.

Those data belonging to the second group overestimate the values of i-angle. Values as large as 80 degrees were found while the measured i-angles tend to an upperbound. These measured upperbound values at the breaks were 52 ± 1 degree for the granite surfaces and 48 ± 1 degree for the limestone surfaces.

Each of the twenty-four diagrams were placed in one of these two groups: the first being data having predicted values less than 55 degrees (normal stress greater than 1035 kPa, granite surfaces; 345 kPa limestone surfaces) and the second group equal to or greater than 55 degrees.

In each group of data, the ratio of predicted to

measured i-angles was calculated. A ratio of unity means equality of predicted and measured values. Both the mean and standard deviation of these ratios were also computed and are tabulated in Table 3.4.

Note that in this table, for both types of rock surface the mean of the ratios (Predicted/Measured) as found by the SF correlations (Methods E and F) is far from unity. Hence, SF correlations can not be used for the prediction of effective i-angles of rock surfaces.

The mean ratios based on the average values of the surface parameters as calculated from group one data are less than those based on the largest. Therefore, greater predicted i-angles will be obtained when the largest value of the parameter is used for the estimate of JRC value. The predicted i-angles based on the largest values overestimate the measured i-angles (most of the mean ratios greater than unity). However, the granite surfaces, the predicted i-angles based on the average value of the parameters underestimate the measured i-angles (mean ratios less than unity) whereas the i-angles of the soft rock are overestimated when the average values were used. In the case of the granite surfaces at normal stress level greater than 1035 kPa, where the mean ratio is 1.03 with a standard deviation of 0.0752, the best estimate of i-angles is found by setting the JRC value equal to arctan (Z2). As for the limestone surfaces, the best estimate of i-angles at stress

		GROUP ONE (Predicted i-angles $<55^{o}$)			GROUP TWO (Predicted i-angles $\geq 55^{o}$)		
	Methods of correlation	Number of test	Mean ratio	Standard deviation	Number of test	Mean ratio	Standard deviation
Standstead Granite surfaces (biggest Z2 and SF for correlation)	A	29	1.03	0.0752	13	1.26	0.1302
	B	27	1.07	0.1107	15	1.30	0.1513
	C	30	1.04	0.0882	12	1.29	0.1304
	D	36	0.90	0.0781	6	1.15	0.0570
	E	42	0.33	0.0488			
	F	42	0.39	0.0640			
Standstead Granite surfaces (average Z2 and SF for correlation)	A	35	0.95	0.1035	10	1.32	0.1419
	B	34	0.95	0.1100	11	1.38	0.1959
	C	35	0.95	0.1162	10	1.33	0.1720
	D	39	0.85	0.0975	6	1.18	0.0914
	E	45	0.29	0.0490			
	F	45	0.34	0.0699			
Tyndall Stone surfaces (biggest Z2 and SF for correlation)	A	35	1.13	0.2775	8	1.71	0.4057
	B	34	1.15	0.3188	9	1.94	0.5943
	C	34	1.12	0.2924	9	1.77	0.4510
	D	40	1.02	0.2699	3	1.29	0.0914
	E	43	0.34	0.1029			
	F	43	0.39	0.1400			
Tyndall Stone surfaces (average Z2 and SF for correlation)	A	41	1.09	0.3137	2	1.26	0.0031
	B	40	1.07	0.3345	3	1.57	0.5388
	C	40	1.07	0.3345	3	1.57	0.5388
	D	43	0.95	0.2409			
	E	43	0.31	0.0926			
	F	43	0.33	0.1334			

A--JRC=$\tan^{-1}$(Z2) correlation, B--JRC and Z2 correlation, C--JRC and $\tan^{-1}$(Z2) correlation, D--JRC and Log(Z2) correlation, E-- JRC and SF correlation, F--JRC and Log(Z2) correlation

Table 3.4 Ratios of predicted i-angle to measured i-angle for the Standstead Granite and Tyndall Stone surfaces

level greater than 345 kPa is through log (Z2) correlation (Figure 3.10). The mean ratios based on the largest and average values of the Z2 parameter are 1.02 and 0.95, respectively. However, their standard deviations (0.2699 and 0.2409) are very high compared with those for the granite surfaces.

Barton (1976) suggested that the total friction angle ϕ' cannot exceed 70 degrees, implying the effective i-angle cannot exceed 70 minus ϕb. This criterion was taken to compare with the average measured i-angles of the surfaces at low stress level. That meant to investigate the difference between the mean measured values and the suggested maximum i-angles, 36.5 degrees (70 - 33.5) for the limestone surfaces and 39.5 degrees (70 - 30.5) for the granite surfaces.

To do this, the means and the standard deviations were computed for the measured i-angles which corresponded to the predicted values equal to or greater than 36.5 and 39.5 degrees for the limestone and granite surfaces, respectively. The computation was carried out only on data from plots based on Z2 parameter correlation (Methods A and D in Table 3.4) since the SF correlation, in the prediction of i-angles, were proved to be unreliable. Results of the computation are listed in Table 3.5.

As noted in that table, the mean measured i-angles obtained from the granite surfaces based on the two methods

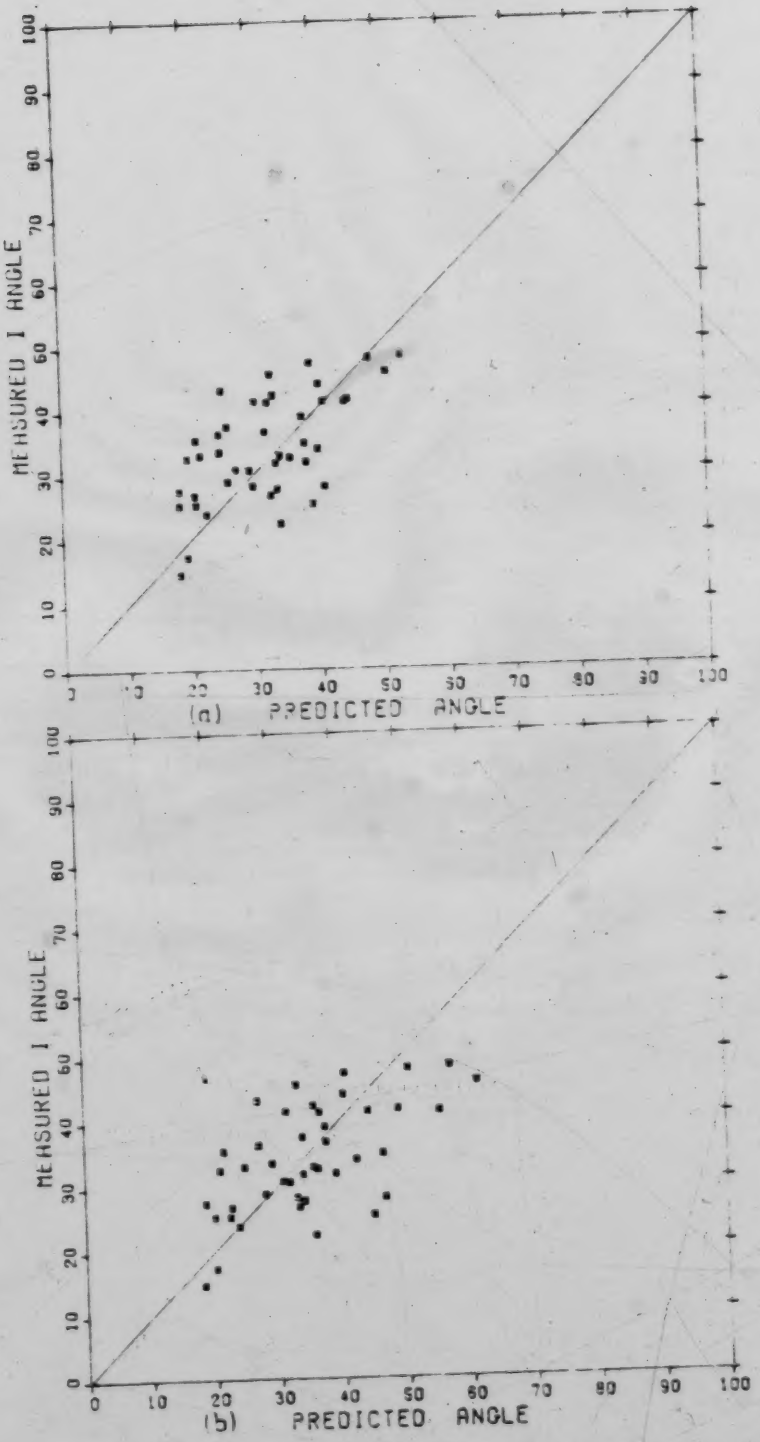

Figure 3.10 Effective i-angles predicted through the log(Z2) correlation compared with the measured values obtained from conventional shear box tests on the Tyndall Stone surfaces. The Z2 parameter is the (a)mean and (b)largest value.

	TYNDALL STONE SURFACES				STANDSTEAD GRANITE SURFACES			
Method	A	A'	D	D'	A	A'	D	D'
Number of test	28	20	16	13	32	30	22	19
Measured mean i-angle (degree)	36.33	36.22	39.25	40.25	46.94	49.11	49.57	51.87
Standard deviation	7.50	8.10	6.98	6.88	5.13	4.91	3.72	3.51

A JRC=$\tan^{-1}$ (Z2) correlation ,Z2 being the biggest value
A' JRC=$\tan^{-1}$ (Z2) correlation ,Z2 being the average value
D Log(Z2) correlation ,Z2 being the biggest value
D' Log(Z2) correlation ,Z2 being the average value

Table 3.5 Values of measured mean i-angle corresponding to the predicted i-angles equal to or greater than 36.5 and 39.5 degrees for the Tyndall Stone and Standstead Granite surfaces

of correlation - JRC = arctan (Z2) and log (Z2) correlations are greater than 39.5 degrees. However, the mean angles for the limestone surfaces based on the JRC = arctan (Z2) correlation just fell below the suggested maximum of 36.5 degrees. Therefore, at low stresses, there is not a significant difference between the experimental average i-angles of the soft rock surfaces and those based on Barton's maximum angle criterion. The above does not hold for the hard granite surfaces.

In Section 2.3.2, the estimated range of i-angles from the tilting experiments was found to be between 23 and 42 degrees for the soft rock and between 22 and 55 degrees for the hard. In general, the mean values in Table 3.5 fall within these ranges indicating that the tilting test could be used to estimate the i-angles at low stress levels.

Patton (1966, page 512) stated:

> "...Three general conclusions can be drawn from the results of the tests on plaster specimens: (1) failure envelcpes for specimens with irregular failure surfaces are curved, (2) changes in the slope of the failure envelope reflect changes in the mode of failure, and (3) changes in the mode of failure are related to the physical properties of the irregularities along the failure surface."

Thus, it might be possible to relate the breaks in the plots of measured versus predicted i-angles to changes in the mode of failure. (That is a change from the sliding up mode to the onset of shearing through the bases of asperities.)

According to this criterion, there would be a constant i-angle below the stress of 345 kPa and 1035 kPa for the limestone and granite surfaces, respectively. Table 3.6 summarizes, below these normal stresses, the means and standard deviations of the measured i-angles and the predicted angles based on the parameter Z2 relationships.

The measured means for the limestone and granite surfaces are 44.96 and 52.62, spectively. In general, compared with these measured means, the mean predicted i-angles obtained by the JRC = Arctan (Z2) correlation (Expression 3.20) are much too low whereas those from the arctan (Z2) correction (Expression 3.17) are much too high. The results of the log (Z2) correlation (Expression 3.18) seem very promising. Bearing in mind the errors due to the testing programme and roughness studies, one would conclude that the phencmenon of a changing mode of failure might be responsible for the occurrence of break points in the curve. Since the predicted i-angles through the log (Z2) correlation are based on Equations 2.7 and 3.18 the onset of the crushing of asperities depends upon the degree of roughness (Z2), the stress level (σ), and the material strength of the irregularities (σc). This explained why the breaks in the curves for the two rocks occurred at different normal levels.

This hypothetical interpretation of the breaks can be compared with what occurred experimentally. The sheared

Method of obtaining i-angles	TYNDALL STONE SURFACES						STANDSTEAD GRANITE SURFACES					
	A			B			A			B		
	Number of test	Mean i angle	Standard deviation	Number of test	Mean i angle	Standard deviation	Number of test	Mean i angle	Standard deviation	Number of test	Mean i angle	Standard deviation
Experimental results	5	44.96	3.37	5	44.96	3.37	16	52.62	2.68	16	52.62	2.68
$i=\tan^{-1}(Z2)$ correlation	5	25.11	2.88	5	21.87	1.43	16	25.40	1.98	16	28.82	4.30
$\tan^{-1}(Z2)$ correlation	5	61.48	9.65	5	53.49	6.04	16	64.26	9.40	16	62.92	10.90
Log(Z2) correlation	5	52.48	6.81	5	47.21	4.84	16	54.80	7.40	16	53.74	7.90

A-- Z2 being the biggest value
B-- Z2 being the average value

Table 3.6 Comparison between the measured mean i-angles and the predicted i-angles at low normal stress levels(345kPa and 1035kPa for Tyndall Stone and Standstead Granite surfaces respectively)

surfaces were examined and pictures of representative specimens taken. These pictures are shown in Figures 3.11 and 3.12 arranged in order of increasing magnitude of normal stresses. Some specimens at particular stress levels are missing because they were used for the study of stress history effects on peak strength (Section 2.4) before the pictures were taken. The granite surfaces can be observed to have suffered a very small amount of damage to the tips of some relatively steep irregularities theoretically effective between a normal stress of 0 to 1035 kPa. Above 1035 kPa these small asperities failed before displacements could occur along them. At a normal stress of 1725 kPa, some larger asperities became effective. Above 1725 kPa these larger asperities began to fail before displacements could occur. Between a normal stress of 6210 kPa and 6900 kPa new cracks were observed on the surface walls.

In a similar manner, the soft rock surfaces began to have suffered damage to the steep asperity tips between a normal stress of 0 and 172.5 kPa. At a normal stress as low as 345 kPa larger asperities became effective. Above 1380 kPa these larger asperities began to fail. It was observed that new cracks were induced in the surface walls at stress levels of 2760 kPa and above 4830 kPa.

Generally speaking, study of these sheared surfaces indicated changes in the mode of failure at stresses corresponding to those at which the breaks occurred.

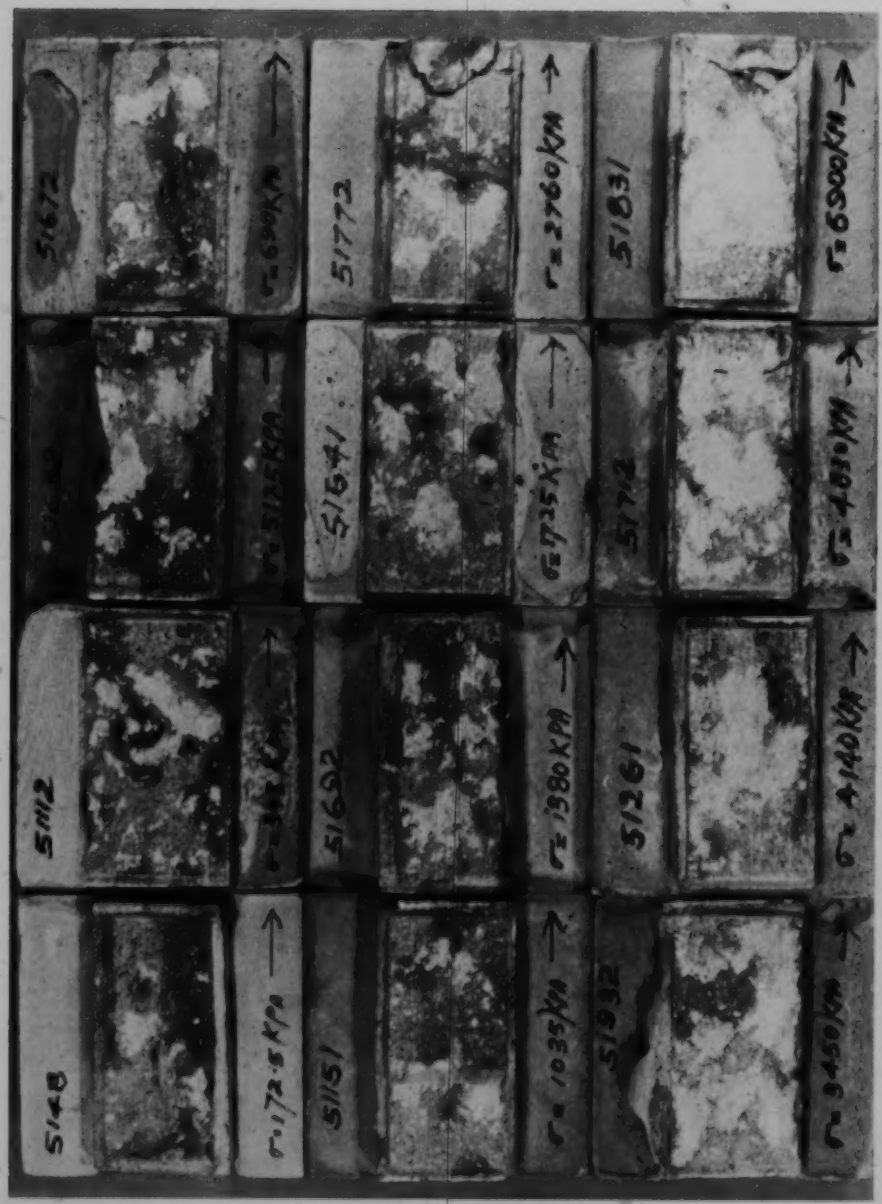

Figure 3.11 Representative direct shear strength tested Tyndall Stone surfaces showing the degree of shear damage with normal stresses

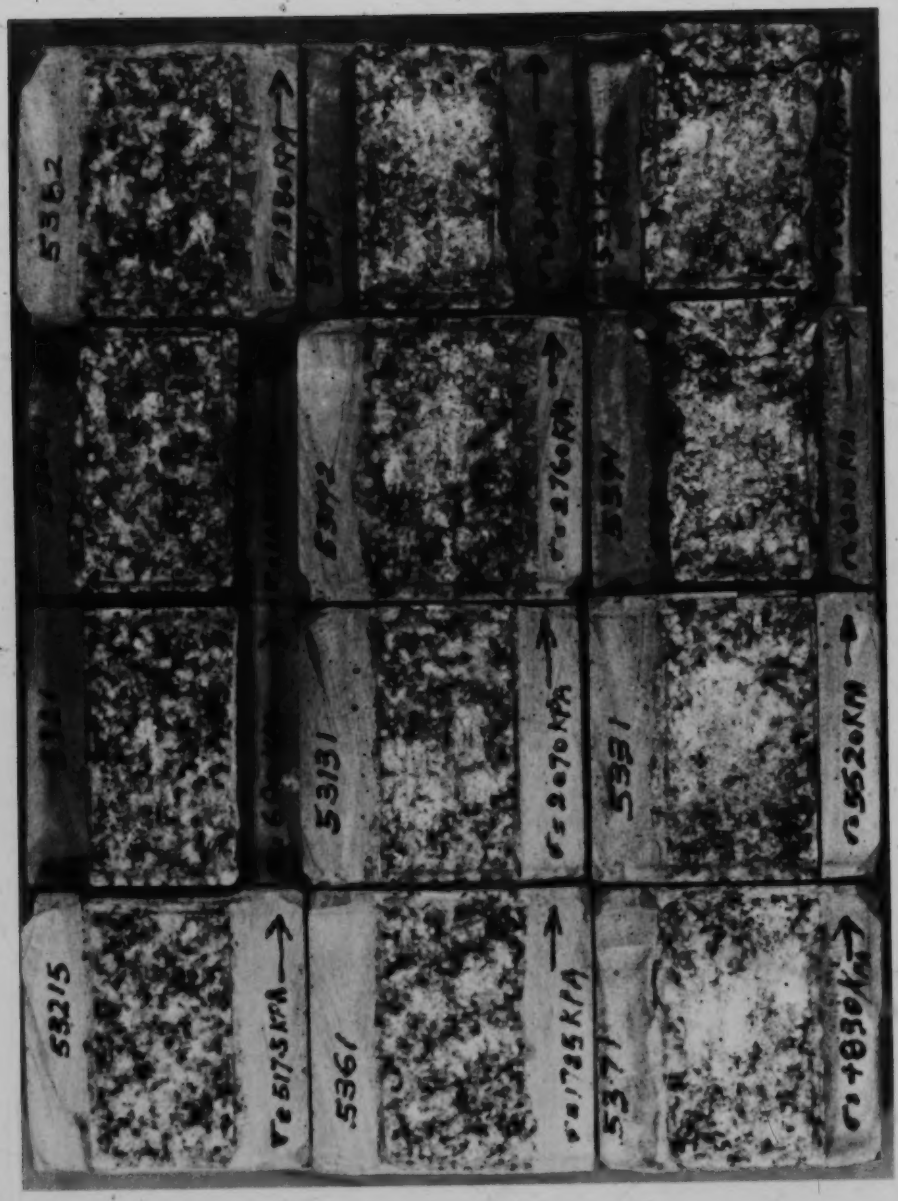

Figure 3.12 Representative direct shear strength tested Standstead Granite surfaces showing the degree of damage with normal stresses

However, the transition is more distinct in the case of the granite than limestone surfaces. Once again, this explains why the location of the break in the curve was more marked in the hard rock than the soft (figures 3.9a,b,).

Cracking of the surface wall was observed only in the lower half of the specimens at very high normal stresses and occasionally at a stress between 2760 and 4830 kPa if the containment (amount of sulfaset) of specimen was inadequate. The mode of cracking seen at the far end of a specimen (Figure 3.13), sheared through from the wall down to the sulfaset, indicates a concentration of stress at the contact of sulfaset and the sample.

In a discussion of the results of stress distribution studies in direct shear test samples, Kutter (1971, p.6) stated:

> "...The results show a relatively uniform shear and normal stress distribution in the central 70% of the shear plane and a reduction in shear stress together with a sharp increase in normal stress at the end regions of the shear plane."

According to this type of analysis, it was felt that the stress field at the end regions of the cracked specimens was a function of the changes in the dimension of containment and the shear load direction. Rotation of the top halves of the samples would not be possible since the shearbox was originally designed to restrain sample rotation. Moreover, upon examining the top halves after

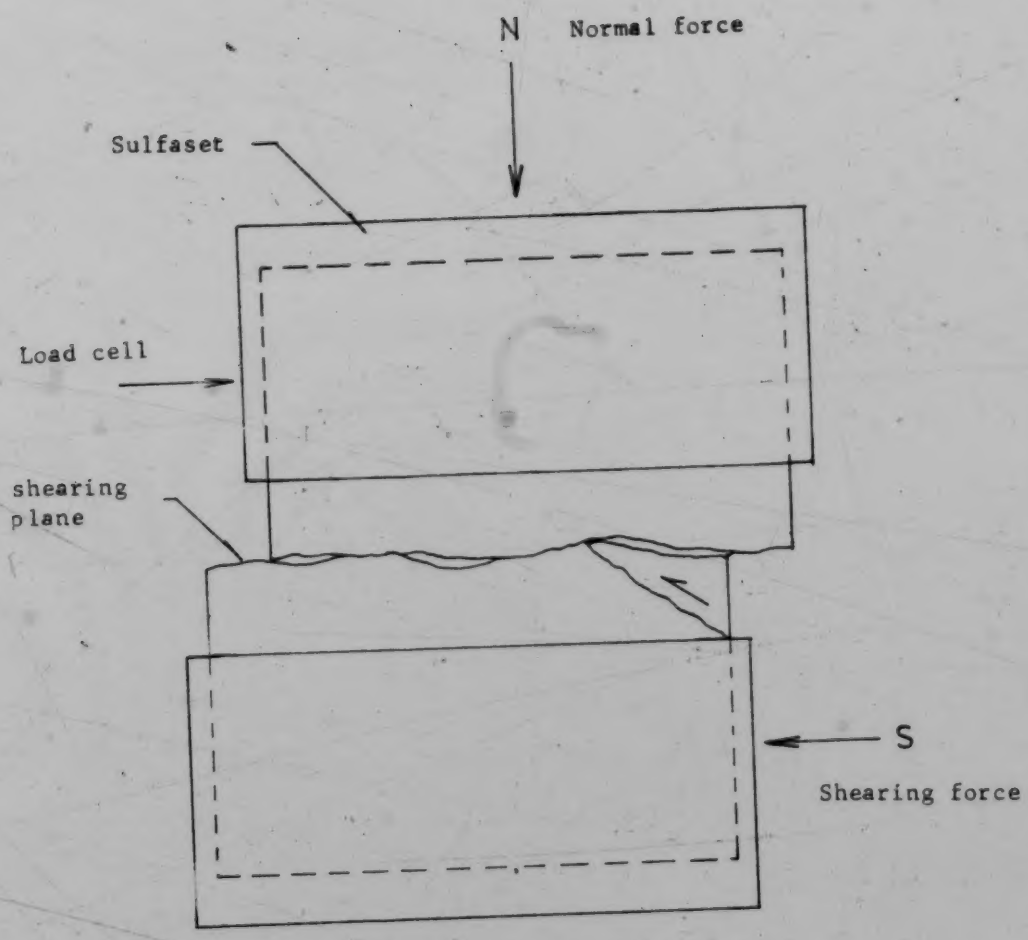

Figure 3.13 Cracking at the end region of a specimen

shearing, no marks of stress concentration indicating sample rotation were observed.

In summary, it was felt that the effective i-angles of the fractured surfaces were better predicted in the Standstead Granite than in the Tyndall Stone. Therefore, the following expressions are recommended for this purpose of prediction of i-angles for the hard rock:

$$i = \tan^{-1}(Z2) \times \log(\sigma_c/\sigma) \qquad \sigma \geq 1035\text{kPa} \quad (3.21)$$

$$i = (32.20+32.47 \times \log(Z2)) \times \log(\sigma_c/\sigma) \qquad \sigma < 1035\text{kPa} \quad (3.22)$$

These two equations will be employed in the next chapter for the study of time-dependent frictional behavior of the granite fractures.

3.9 Summary of Chapter III

(1) To determine the peak shear strength of a rock surface, one must ascertain those values of the basic friction and i-angles. Frictional resistance arising from the surface irregularities (i-angles) renders the estimation of the peak strength difficult. The study of surface irregularities is therefore necessary.

(2) Eight surface characteristics (RMS, CLA, Z2, Z3, Z4, MSV, ACF, and SF) have been discussed as possible indicators of the frictional properties of different surface geometries.

(3) Three profiles for each of the fractured surfaces were traced. These profiles, along with Barton and Choubey's ten standard profiles were digitized for the computation of the eight surface parameters.

(4) Regression analysis on the ten standard profiles yielded good linear relationships between the joint roughness coefficient, JRC and two surface parameters; the root mean square of the first derivative of the profile (Z2) and the structure function (SF). Additional analysis proved that the arctan and logarithm of these two parameters gave higher correlation coefficients. Moreover, results from the run tests on these regression data showed that the deviations of the data from linearity had been distributed at random over the regression lines.

(5) Using Barton's expression for i-angles and the computed JRC values based on the Z2 and SF correlations, the predicted i-angles for the sheared surfaces were calculated for the two types of rock surfaces. Results from the statistical analysis of the predicted i-angles and the measured values from the experimental data indicated the prediction of the effective i-angles for the fractured surfaces was better estimated in the Standstead Granite than in the Tyndall Stone. The best estimate was found when the JRC term in Barton's equation for the i-angles was set equal to the arctan (Z2), Z2 being the

largest value of the traced profiles cn a Standstead Granite surface. The prediction of i-angles for the Tyndall Stone surfaces could be best estimated by the log (Z2) correlation.

(6) For both types of rock surfaces considered the predictien of i-angles based on the structure function (SF) correlations seemed unreliable.

(7) The peak shear strength values for both rock surfaces were scattered. This variation in strength might be the result of different initial surface irregularities. The range of roughness was such as to yield JRC values from 12.5 to 31.1 and 17.9 to 29.5 for the limestone and granite fractured surfaces, respectively.

(8) Results frcm roughness studies indicated that the effective i-angle (arctan(Z2)) attributed to Patton's work (1966) correlated with the joint roughness coefficient, JRC attributed to Barton's work (1973). At high stresses, they would be the same value.

(9) The curves in the measured versus predicted i-angle plots could be approximated by two straight lines. The abrupt changes in the i-angles of these lines represented the onset of significant amounts of crushing of asperities. The amcunts of crushing depended primarily on the degree of surface roughness (Z2), stress level (n) and material strength of the surface walls (c). The stresses corresponding to the

breaks in the curves were found to be at 345 kPa and 1035 kPa for the Tyndall Stone and Standstead Granite, respectively. Below these stresses, a constant i-angle was assumed.

CHAPTER IV

CREEP IN SHEAR IN ROCK

4.1.1 Shear Creep Hypothesis

The following hypothesis is based on the observations on creep of during compression (Bishop, 1966; Cruden, 1971; Ter-Stepanian et al 1973; Campanella and Vaid, 1974 and others).

Under conditions of constant shear load at a particular normal load, the peak shear strength of a rough surface is reduced with time. The frictional shear resistance resulting from the rock surface is a time-dependent parameter and there exists a critical value of shear stress below which the time effect is not detrimental. This value corresponds to the long term strength of the rock surface. The manifestation of this behavior is the occurrence of irreversible time - dependent shear deformations recognized as shear creep.

4.1.2 Analysis of Hypothesis

The foregoing hypothesis of shear creep in rock could be illustrated graphically as shown in figures 4.1a,b,c. Diagram a shows what would result if the rock surface were loaded to a particular constant shear stress, and for a period of time subjected to that constant stress, time-dependent irreversible plastic strain, Ep, would accumulate

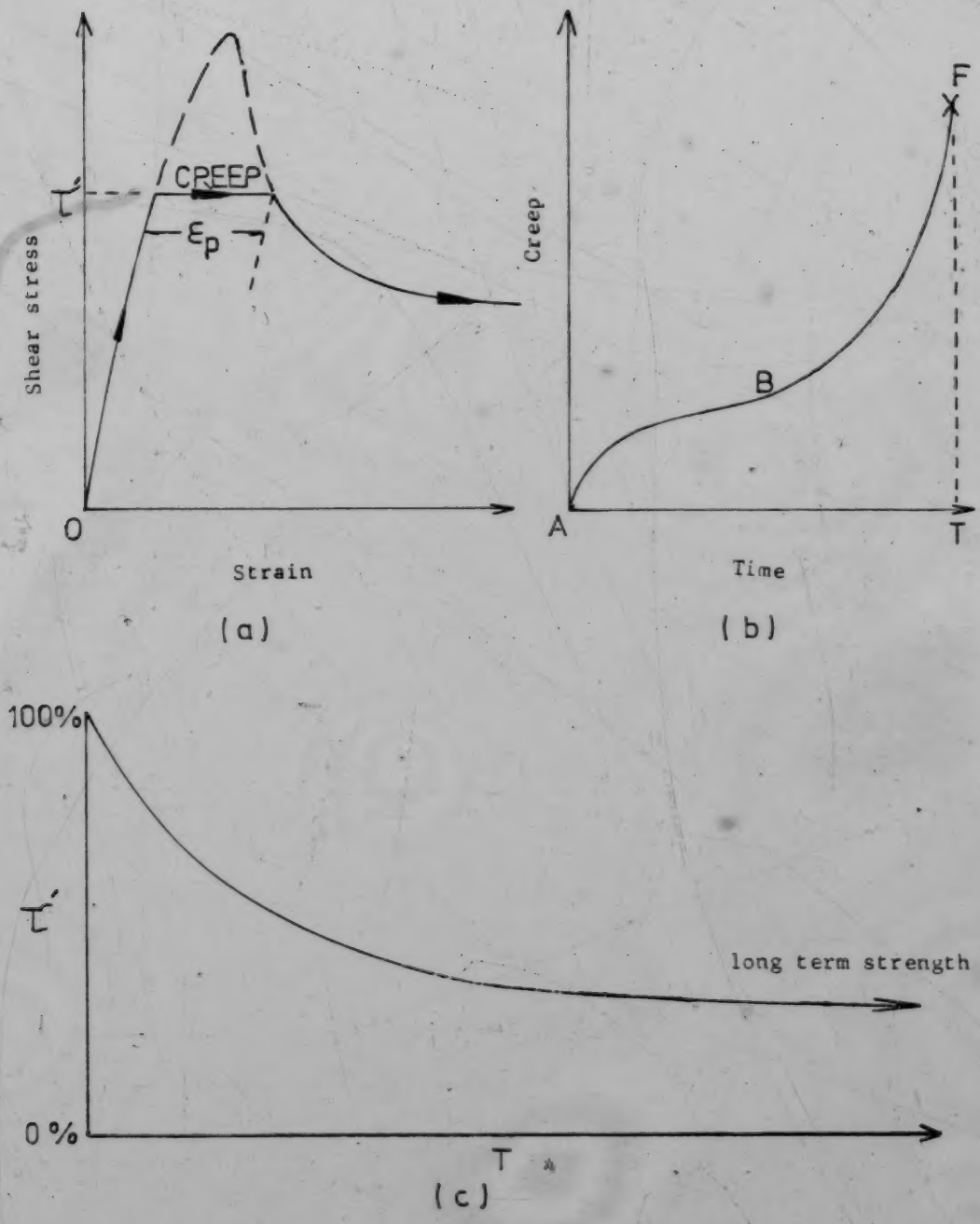

Figure 4.1 Effect of time on friction of rock surfaces

due to creep before failure along the ultimate stress-strain path. Diagram b shows the assumed shear creep curve which would be represented by two terms corresponding to the decelerating (path AB) creep and accelerating (path BF) creep. The difference in time, T between points A and F in diagram b, would represent the "age" of the particular constant shear stress. Diagram C indicates what would be the relationship between the shear strength of the rock surface and its "age" if the hypothesis were true. The curve in this diagram would tend to a constant stress value as denoted by the long term strength of the rock surface. The hypothesis lends itself to labortory tests.

4.2 Creep Apparatus

4.2.1 Creep Machines

Two conventional soil direct shear machines were modified for the purpose of shear creep study. Each had a shear capacity of 8.9kN. The square shear box (figure 4.2) made of stainless steel was designed in such a way that the lower (1) and upper (2) boxes were connected together by brackets (3) and steel rods (4) with bearing rings (5) so that the lower box could travel smoothly relative to the "fixed" upper box.

The upper box was again attached to a load cell by a coupling yoke (6) on which stood a light aluminum rod (7). This rod was used for the vertical LVDT arrangement; in this

way, the measurements of vertical deformation of the creep specimen were made relative to the shear box itself rather than to the bench of the machine as had been done conventionally.

The lower box which travelled on steel ball bearings had a small creep frame attached to one side near the gear box (figure 4.3). This cantilevered creep frame was assembled with two 1 cm. diameter steel rods, each encased in a 1.7 cm. diameter steel tube for reinforcement against bending. While one end of each rod was screwed to the side of the lower shear box, the other end was bolted to an aluminum block. This block was the loading platform for the constant shear load which was transmitted from a 30.48 sq. cm. bellofram manufactured by Diaphragm Air Cylinder Co. Burlington, Mass.

The bellofram was bolted onto a steel bracket which in turn was welded onto the bench of the direct shear machine. The driving steel shaft from the bellofram was guided through an additional support having a steel bearing ring the same diameter as the shaft. The arrangement of the bellofram and creep frame was designed to transmit horizontally the creep load to the shearing plane of the specimen. Figure 4.4 illustrates the general arrangement of the creep machine.

4.2.2 Air System

Figure 4.2 The modified direct shear box for shear creep tests

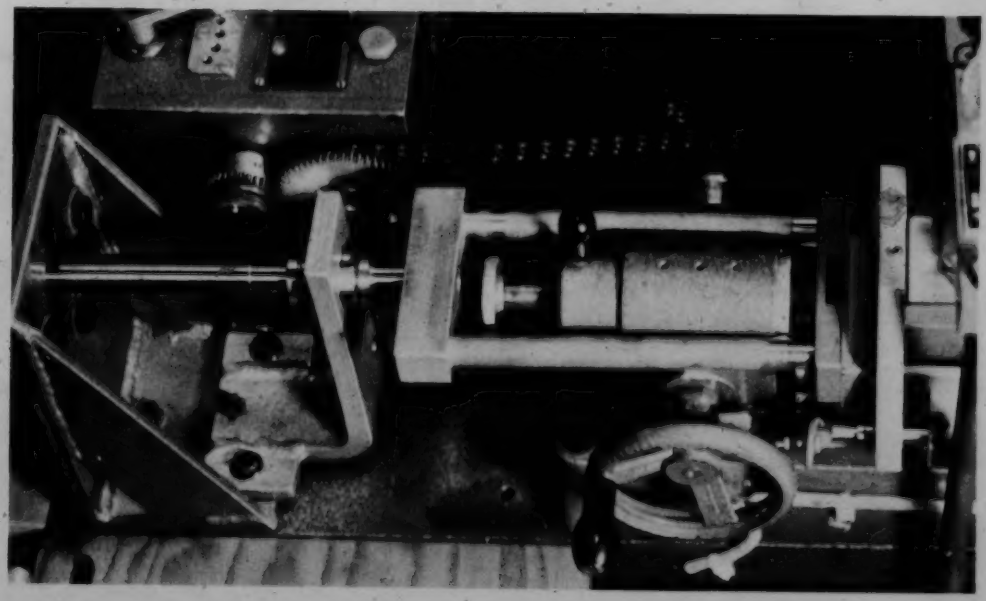

Figure 4.3 The creep frame arrangement

The bellofram was run by compressed air which was regulated manually from a control board as shown in figure 4.5. The inlet air supply line (T valve at the top of figure 4.5) was under a constant air pressure of 1300 kPa. This pressure supply was distributed to two regulators, one for each creep machine. The regulators were operated independently from one another by turning the appropriate controlling knob (clockwise motion indicated increasing pressure), and the approximate regulated line pressure was read on the pressure gauge. The regulated pressure was transmitted to the bellofram as well as to a transducer (centre gauge in figure 4.5) where readings of the pressure were taken. The transducer was shared between two regulators by means of two separate switches; that meant if a reading was required for a regulator, the switch connecting the regulator would be open to the transducer while the other switch remained closed (and vice-versa).

The diaphragm inside the bellofram had a constant cross sectional area of 30.48 square cm.; therefore, if the regulated pressure were X N/m^2, a constant force of 0.003048 X N would have been obtained. This constant force was controlled by a 3-way switch (outlet to the air, inlet to the diaphragm and close condition) located at the end of the bellofram. When the switch was in the close position the compressed air would neither release to the atmosphere nor engage in the bellofram. However, if the switch was turned to the diaphragm, an instantaneous horizontal force would be

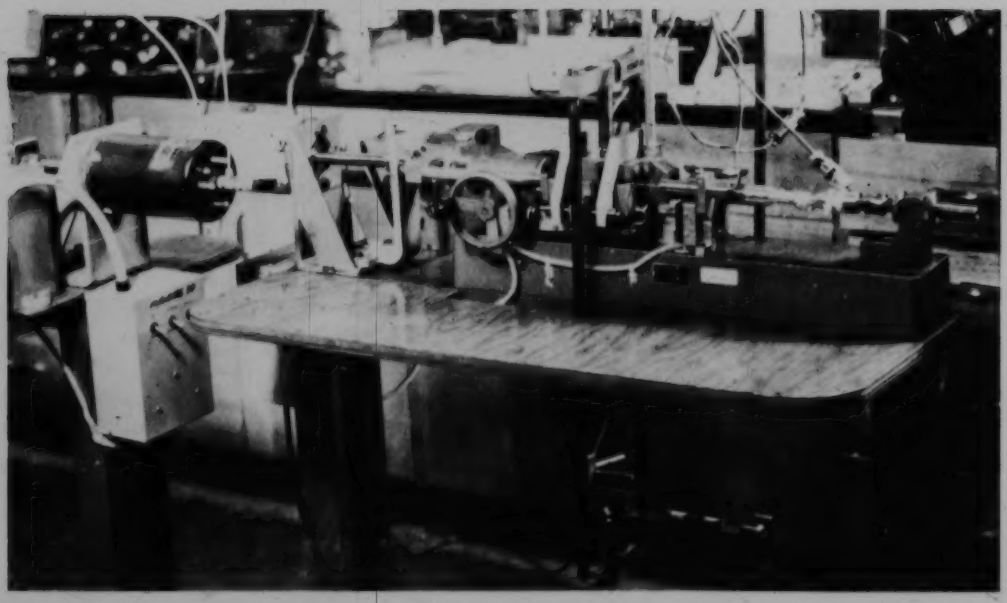

Figure 4.4 The creep machine

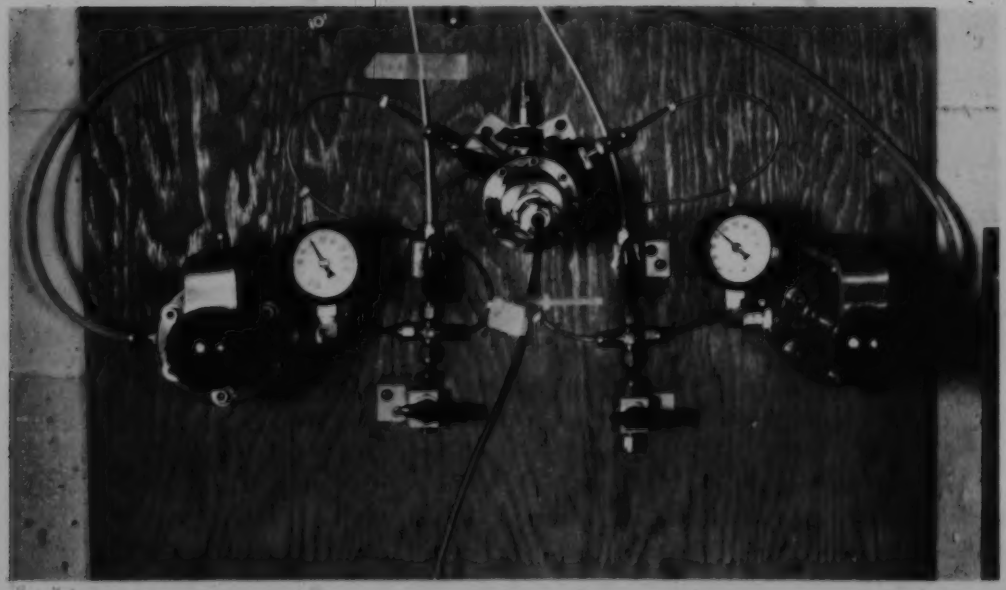

Figure 4.5 The air system control board

obtained. When this happened, the driving shaft from the bellofram would engage the creep frame in front, which in turn would transmit and sustain the force onto the shearing plane of a specimen.

4.2.3 Data Acquisition

Electronic data-gathering methods (figure 4.6) were employed in creep tests, with the exception of room-temperature and humidity measurements during testing (where manual recording was used). The remote-controlled data acquisition system employed was a multichannel Fluke #2200A datalogger manufactured by John Fluke MFG. Co. LTD. Mountlake Terrace, Washington. This system in itself could have variable sampling time and a printed output, was in conjuction with a Techtran-#8410 digital cassette recording unit manufactured by Techtran Industries Inc., Rochester, New York. Displacements were measured by linear voltage displacement transformers (LVDTS), shear loads were measured by load cells, and air pressure was measured by a transducer. These measurements were calibrated and recorded in milli-volts. All electronic measuring devices were recalibrated after each creep test performed to eliminate error due to zero point drift or to sensitivity alteration.

Upon completion of a given creep test the digital cassette tape was transcribed to the IBM 360 computer, and processed by computer programs to yield both printed and

Figure 4.6 The data acquisition system

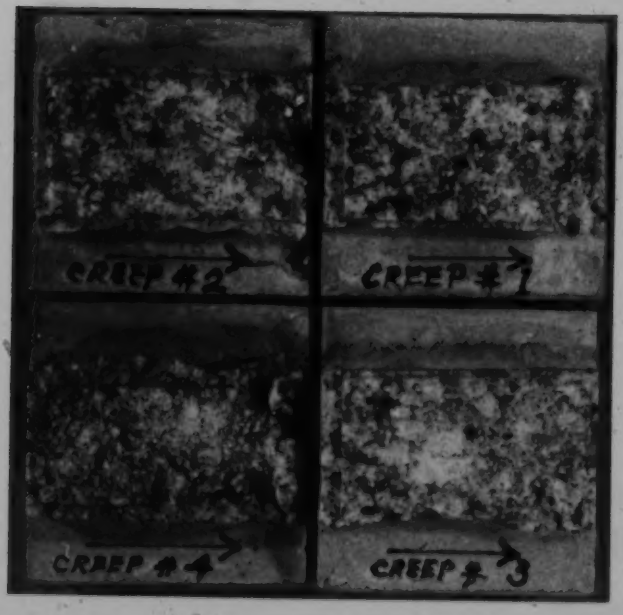

Figure 4.7 Creep specimens after failure

graphical output.

4.3 Creep Study on Granite Surfaces

4.3.1 Shear Tests in Creep Machine

Creep machines could be used in either a shear strength test or a creep test. In a creep test, the conjunction of the creep frame with the gear box was employed (section 4.3.3). Three granite surfaces were sheared in one of the creep machines. The tests were run dry at 0.061 cm/min, as close as possible to the rate 0.052 cm/min at which all the shear strength tests (chapter 2) were performed in the 89kN direct shear machine.

The test results are tabulated in table 4.1 together with the predicted values based on the expression 3.21. The normal stress, 1035 kPa, employed was the maximum allowable level because of the limitation of shear capacity of the creep machine and rough rock surfaces in question. The predicted i-angles for these three specimens did not vary much; they were close to 52 degrees. Two specimens underestimated the actual peak (ratio of predicted to measured i-angles less than unity) while the other slightly overestimated (ratio greater than unity). These ratio were used to compare individually with those performed in the 89kN direct shear machine; in this way one could investigate the significant difference in shear strength testings in different direct shear machines.

Rock surface	Z2	Normal stress kPa	Predicted i-angle degree	Predicted peak strength kPa	Measured i-angle degree	Measured peak strength kPa	Ratio of predicted i-angle / measured i-angle
53122	0.45645	1035	51.99	7855.78	52.77	8779.76	0.9852
53301	0.46183	1035	52.53	8470.99	52.50	8435.94	1.0005
53282	0.46506	1035	52.85	8886.64	53.35	9610.11	0.9906

Table 4.1 Results of direct shear strength test on Standstead Granite surfaces in creep machine

In section 3.8 (table 3.4), the estimate of the i-angle through the JRC=arctan(Z2) correlation gave a mean ratio (predicted to measured i-angle) of 1.03 with a standard deviation, S of 0.0752. Therefore, the mean ratio would have a confidence interval of 1.03 ± ts (where Student's t is a function of (a) the degree of freedom and (b) the significance level (Dixon and Massey, 1951)). For the particular problem at hand, the degree of freedom of 28 gave a t of 2.05 at 5% significance level. Thus the ratio would have a 5% confidence interval between 1.1842 and 0.8758. Note that the values of the ratio in table 4.1 fall within this interval indicating that there is no significant difference in measuring shear strength of granite rock surfaces despite testing them in different direct shear machines of different stiffness, shearing at different speeds (0.052 and 0.061 cm/min for the big and small machines respectively) and using different measuring techniques (x-y-y' recorder and data acquisition system for the big and small machines respectively).

4.3.2 Setting Up a Creep Test

From the geometry (area) and measured Z2 value of a rock surface, the estimated peak of the specimen was computed for a particular normal stress (expressions 2.6 and 3.21). A predetermined air pressure which would correspond to, say 75% of the predicted peak load was set up in the supply line up to the controlling 3-way switch of the

bellofram (meanwhile this switch was in the close position). The specimen was then assembled in the shear box. The next step was to apply the predetermined normal load and initialize the data acquisition and Techtran tape recorder.

4.3.3 Creep Tests

Upon completing the set up, the specimen was loaded in shear. The horizontal displacement which was applied through a variable gear arrangement powered by an electric motor was started at a speed of 0.061 cm/min. At the same time a "continuous" printed output from the data acquisition was set.

Since the recording device was shared with other research purposes, a single complete sampling printed output of all the channels took almost 10 seconds. Because of this, the readings of the channel (channel 7 for creep machine 1 and channel 8 for creep machine 2) corresponding to the particular load cell from the creep machine was monitored manually from each of the sampling printed outputs until it was noted that the load cell gave a reading between 74 to 75% of the predicted peak (the air pressure in the supply line was 75% for this particular test at hand); when this happened, the electric motor was shut down immediately while at the same time, the 3-way switch of the bellofram was turned to the inlet to diaphragm position. An instantaneous constant shear load of 75% was sustained on

the shearing plane of the rock surface. Continuous sampling (or at every 10 seconds) was set for the first 10 minutes of creep. After that the sampling time was increased in a sequence of every 1, 2, 5, 10, 20, 30, 60 and 90 minutes depending upon the magnitude of shear deformations.

Timing was critical. Firstly the load supplied by the motor should not exceed the already predetermined on line constant shear force; secondly the sudden impact on the specimen from the bellofram if the motor were shut down earlier before the load cell had reached the desired load should be avoided. In the first case, even though the load as measured by the load cell would eventually decrease and reach a value equal to that of the bellofram and then resume a creep test, it would complicate the stress history of the rock surface and introduce uncertainty in the interpretation of experimental results. However, when the motor were stopped too early, as in the latter case, resulting in a much smaller gear load than that of the bellofram, the rock surface would have been subjected to an impact shear force; again this would complicate the stress history.

To overcome these difficulties, experience in good coordination with the whole system and practice of "stopping and starting" the test is necessary.

4.3.4 Observations During Creep

Once the specimen was on its way to deform under the

constant shear force, measurements were taken at an interval of every cne minute (the smallest interval obtained in the data acquisition system) for the first half hour. During this period, the rapid increase in creep was noted. After that, creep deformaticn was observed to slow down with time and the interval of measurements was increased to every 2 minutes then 5, 10 or more minutes depending upon creep magnitudes. The reasons for the increase of observation interval were two-fold: first eliminating a large number of unnecessary data points without losing the general trend of the creep deformation and second the avoidance of changing the Techtran recording tape at an inconvenient time. A maximum observation interval could be obtained as long as 90 minutes.

Reaching the maximum sampling time usually took two to four days, this depended on the initial amount of constant shear force. Observations based on the printed output information and manual readings of environmental conditions showed: time-dependent deformation had occurred; the deformation was increasing at a very slow rate; a constant air supply in the bellofram was maintained; small but considerable fluctuations in vertical, horizontal and load cell readings were occuring and room temperatures were maintained at 20±1°C while the humidity was kept at 50%.

When the creeping specimen had reached a more or less steady shear deformation which usually took weeks or months,

the shear force was increased to the next creep stage. This was done by turning the appropriate air regulator on the control board in a clock-wise motion and at the same time a "continuous" printed output was monitored until the next desired constant shear force was reached. Then the technique of sampling data was repeated. The whole procedure was also repeated for another creep stage unless the specimen failed.

When a creep failure happened, it was usually preceded by decreasing shear resistance (readings of load cell decreased) and increasing dilation and shear deformation for a short duration compared with the total time of a test.

A total of 4 creep tests were performed on 4 individual new granite rock surfaces (two at a normal stress of 690 kPa; others at 1035 kPa) and all of which ended in creep failure.

It was noticed that at the same normal stress level, a more significant amount of asperity crushing had resulted in the shear creep failed specimens than in the shear strength tested specimens. The amount of damage increased with normal pressure and number of creep stages. Figure 4.7 shows the picture of these four creep failed specimens.

4.4 Results and Analysis

4.4.1 Creep Test 1

The first creep test was carried out on a rock surface

numbered 53121 with a Z2 value of 0.46750 and the initial cross-sectional area, Ao of 10.389 sq.cm. (Lo x W = 4.305 X 2.413 sq, cm., where Lo = the initial length and W = the width). The normal stress level was at 1035 kPa and the predicted i-angle (expression 3.21) was 53.10 degrees whereas the corresponding estimated peak based on Barton's equation (expression 2.6) was 9227.62 kPa. At the onset of shear creep, the constant shear force as supplied through the bellofram measured 8988.74 kPa when converted to stress. This corresponded to 97.41% of the estimated peak.

Upon completion of the test, the Techtran cassette tape was transcribed to the computer and processed by computer programs to give time in hours, vertical and creep deformation (Lc) in mm., and also creep strain. The strain was computed by dividing the current creep by the original length, Lo. The load, F as measured by a load cell was also converted to shear stress, by dividing it by the corrected area.

$$\tau = \frac{F}{(Lo-Lc)W} = \frac{F}{Ao-Lc \times W}$$

Once the data, in digital form, were in the computer, it was a relatively simple matter to yield graphical outputs which were processed by some simple plotting programs. The results of creep test 1 are shown in figure 4.8. The top

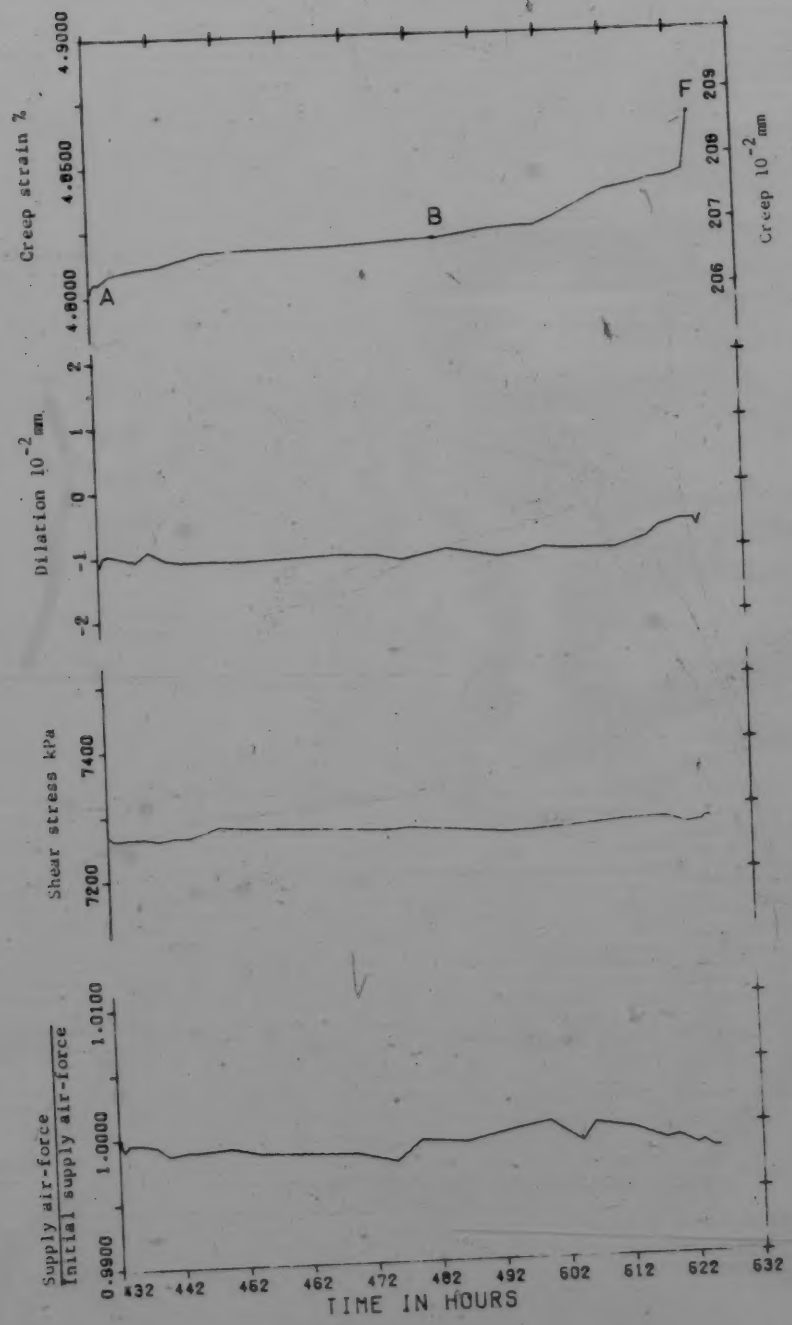

Figure 4.11 Results of creep test #2(final stage)

diagram is the creep versus time plot; the second is the vertical deformation (or dilation) during creep versus time plot; the third is the computed shear stress versus time plot whereas the bottom diagram is the ratio of air-load from the bellofram to the initial predetermined air force versus time plot. The last plot is omitted from some graphical presentations of experimental data as the air pressure transducer was shared between the two belloframs of the two creep machines. In all the 4 experiments, fluctuation in shear stress, dilation and creep strain are noted. Therefore, it is suggested in section 4.4.5 that the air-supply system did not maintain an absolutely constant feed. This might be the cause of fluctuations. Notice in the dilation plot, initially sample contraction was measured with considerable fluctuations. However as creep progressed, the specimen began to dilate at an increasing rate until it had reached the rupture stage, the dilation rate was increased dramatically as noted by the steep portion of the curve near creep rupture. A total of 0.004 mm. vertical deformation or dilation was measured prior to failure.

The creep curve showed 2 sections : the decelerating creep (AB) and the accelerating creep (BF). The intersection of the ordinate shows the total amount of elastic deformation of 8.310% before the onset of substained constant shear force. After that time-dependent deformations began starting at point A and then increased rapidly. Despite the fluctuations in general trend, the strain rate

decreased up to point B and thereafter increased until rupture at point F. Warning of rupture was indicated by the trend of increasing dilation in the region BF. The elasped time in the decelerating creep was about 3 times the elapsed time in the accelerating creep. The total amount of time-dependent strain was 0.075% which represented approximately 0.09% of the elastic deformation. The measured lifetime, T for this particular constant shear force (97.41%) was 82.42 hours which ccrresponded to the difference in time between points A and F.

4.4.2 Creep Test 2

The second creep specimen was 53361 with a Z2 value of 0.45201 and Ao of 10.069 sq. cm. (Lo x W = 4.290x2.347 sq. cm.) The i-angle (expression 3.21) was estimated 51.54 degrees for a normal stress of 1035 kPa and the corresponding predicted peak (expression 2.6) was 7409.07 kPa. The specimen underwent a total of 3 stages of constant force loading before final creep failure. The stresses corresponding to these constant forces were set to be 6643.90 kPa, 6950.98 kPa and 7268.98 kPa which represented 89.67%, 93.82% and 98.11% of the predicted peak respectively.

The graphical outputs of these 3 stages are shown in figures 4.9, 4.10 and 4.11 respectively. In stage 1 (figure 4.9), the early part of the dilation curve (second diagram)

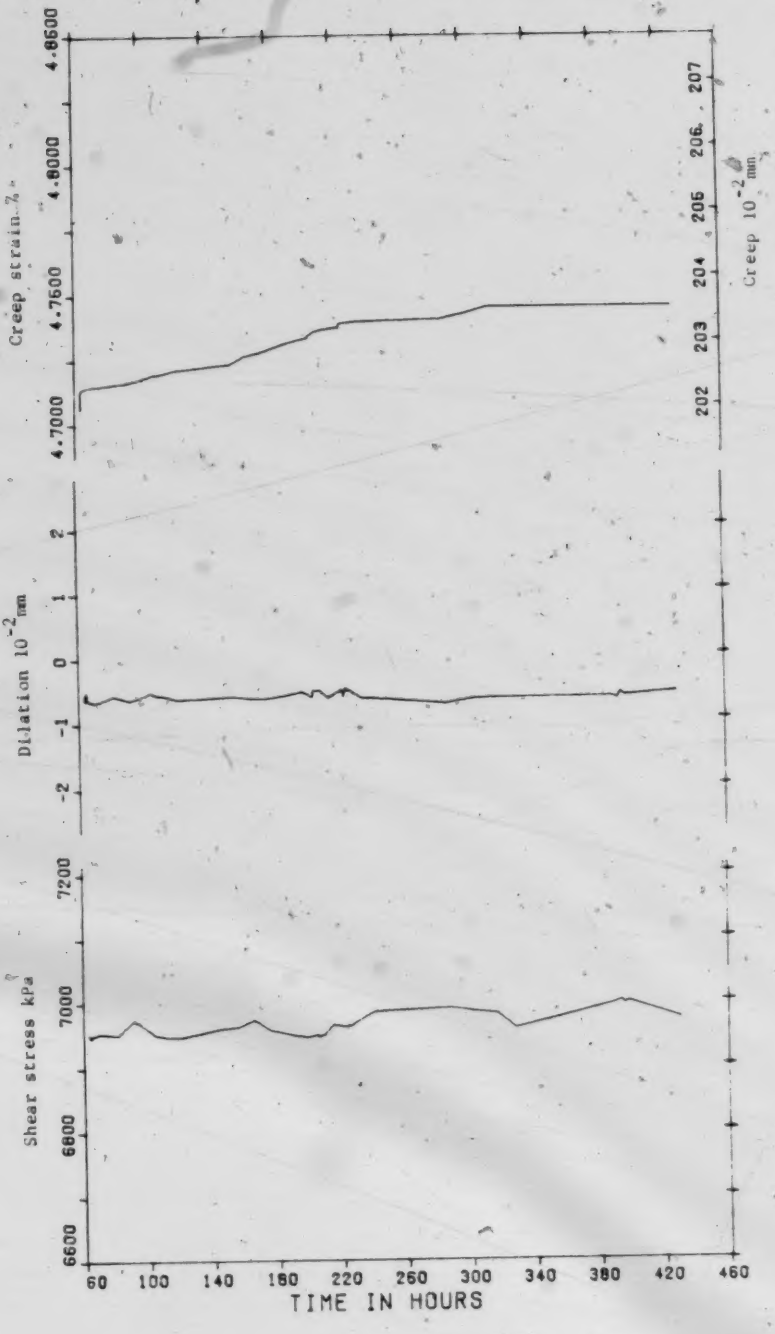

Figure 4.10 Results of creep test #2 (stage 2)

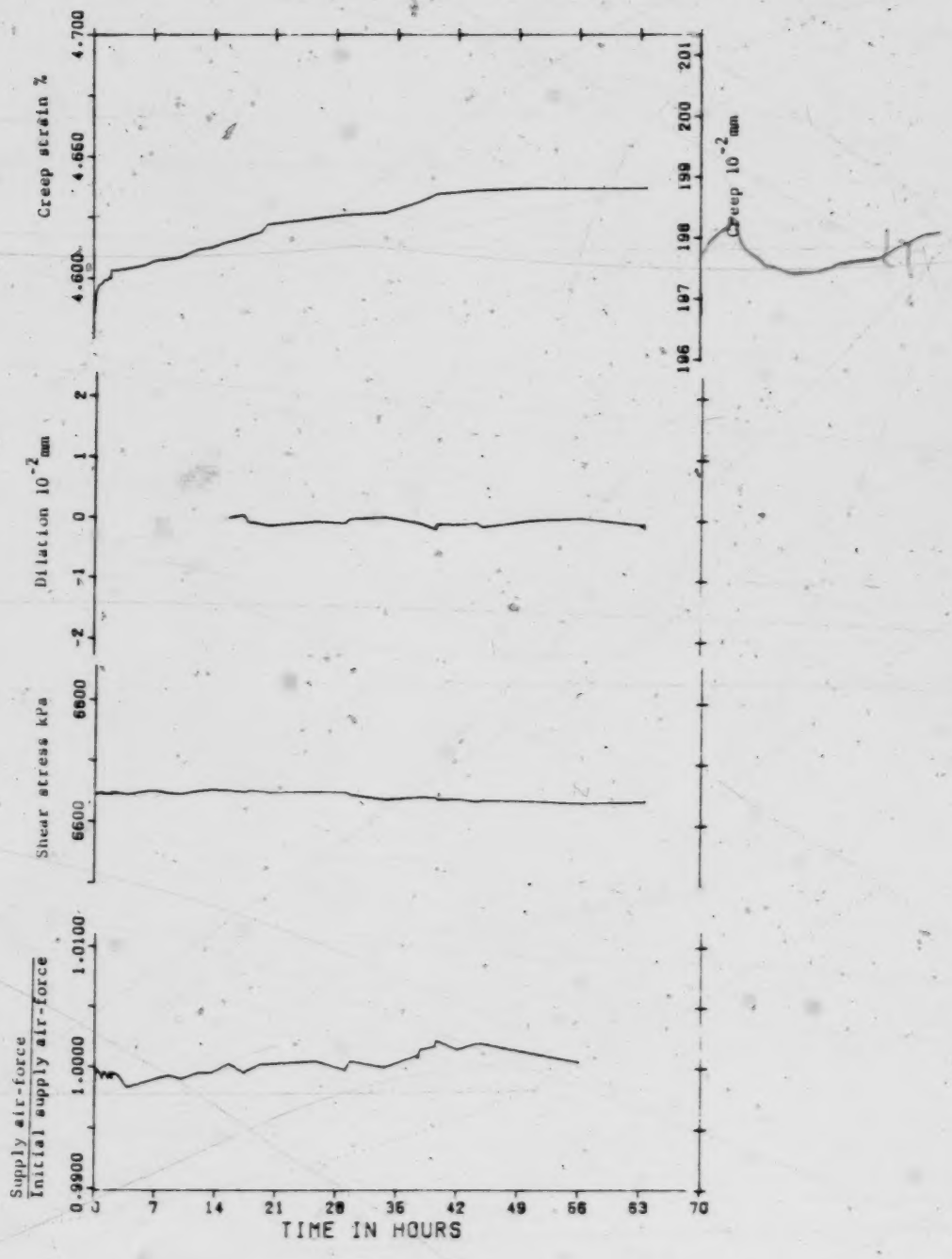

Figure 4.9 Results of creep test #2(stage 1)

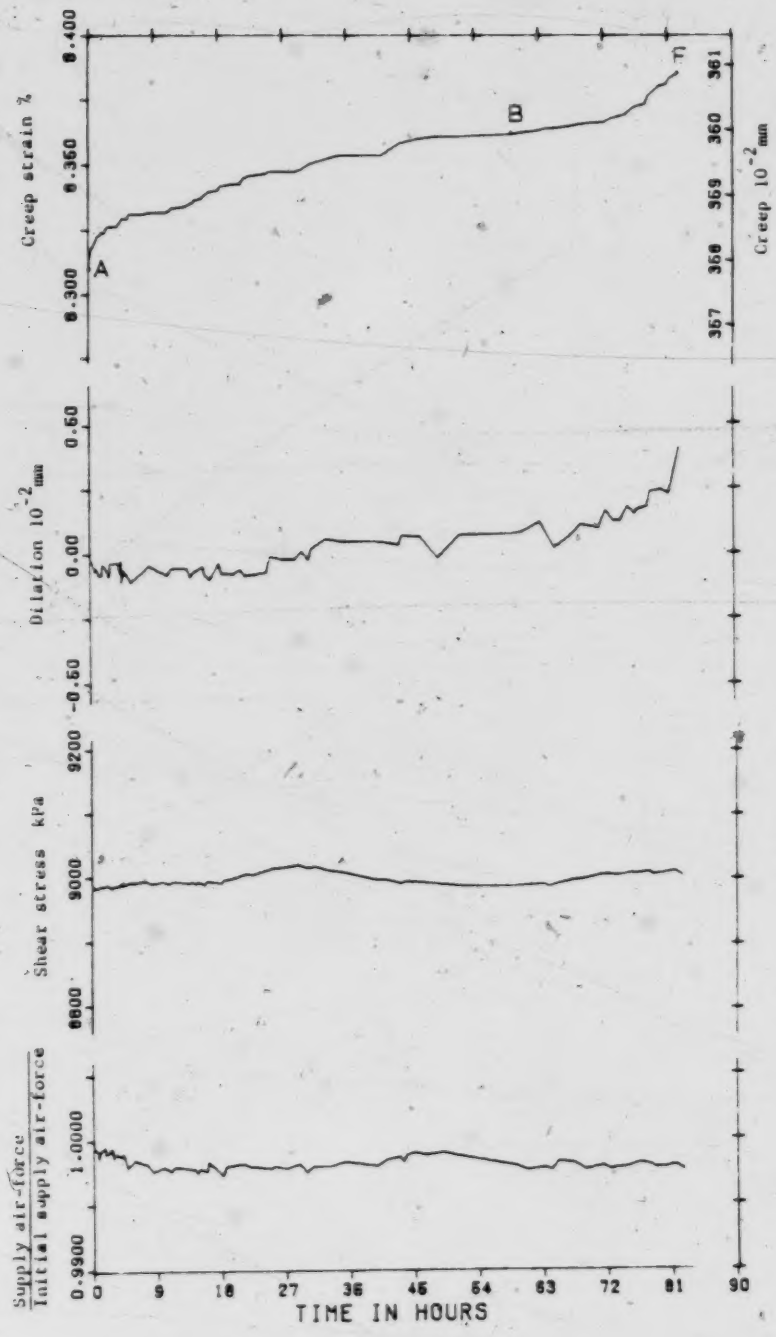

Figure 4.8 Results of creep test #1

had not been plotted due to the error of zero point drift of the LVDT. The measured shear stress during the test seemed to be quite constant at values of 6644.00 ± 5.00 kPa. The dilation curve also appeared to remain constant. The supply air-load (bottom diagram) showed some fluctuations. Careful examination suggested that the small abrupt charges in the shear resistance reflected jumps in the supply load curve. The percentage changes in the supply ranged from 0 to 0.4% above the mean or the predetermined feed. Again in the creep curve, the strain increased rapidly at the beginning but the rate decreased. Some occurrence of abrupt changes in slope indicated that the surface asperities were subjected to uneven distribution of internal stresses or the results of brittle failure of some steep asperities. The creep strain died down and became steady at a time of 40 hours. In this stage this initial elastic strain was 4.580% while the total amount of creep was 0.057% which represented 1.25% of the elastic deformation.

Upon reaching a steady deformation the shear force was increased to the next stage, 93.82% of the peak (figure 4.10). During the increase, an additional elastic strain of 0.069% was obtained and this seemed quite small a value as compared with 4.58% in stage 1. This might be the results of change in shear stiffness during creep (more discussion in section 4.4.6). At the same moment, the dilation contracted to a value of 0.006 mm and remained at this level during the rest of stage 2. The shear stress showed some fluctuations

roughly ±0.21% above the constant stress of 6950.98 kPa. The characteristics of creep curve also showed similarities as noted in stage 1. At first, the strain increased rapidly but the strain rate decreased. Eventually at a total elasped time of 320 hours, no appreciable increase in creep was noted. The total amount of creep deformation in this stage was 0.039% which represented 56% of the stage's additional elastic strain.

Upon reaching another steady creep strain the shear force was then increased to the third stage where the creep failure occurred. Figure 4.11 shows that further contraction of the specimen was observed at the completion of loading to a total value of 0.011 mm; however, it began to dilate gradually when creep had started. The dilation rate increased significantly at the end portion of accelerating creep. In spite of this, the final accumulative vertical deformations were still negative prior to creep failure. This seemed to be the results of seating of the specimen. No dramatical variations in shear resistance were observed. The maximum percentage fluctuation above the initial shear resistance was about ±0.14% as compared to ±0.13% above the mean supply air-load (bottom diagram).

The creep curve showed two stages of creep: the decelerating creep (AB) and the accelerating creep (BF). Rapid increase in creep rate was noted during approximately 1 to 2 hours prior to creep rupture at F as seen by the

steep creep curve. Again warning concerning creep failure was indicated by the trend of increasing dilation in the region BF. The additional elastic strain during this final stage was 0.057% and the total amount of creep deformation was 0.065% which represented 112.10% of the apparent elastic strain. The apparent elastic strain was less than that of stage 2 (0.057% and 0.069% respectively) even though the increase in stage loading in the final stage was greater (4.29% and 4.15% for the final and second stages respectively). This again gave important insights as how the apparent shear stiffness (shear stiffness occurred in a stage loading test) could affect the creep phenomenon (section 4.4.6). If one could ignore the effects of stress history prior to the final stage, the lifetime for this particular constant stress level (98.11%) would be the difference in time between points A and F in the creep curve and therefore, the creep life T would be 93.14 hours.

4.4.3 Creep Test 3

The third shear creep specimen was 53222 with a Z2 value of 0.50122 and Ao of 10.98 sq. cm. (Lo x W = 4.39 x 2.50 sq. cm.). The test was run at a normal stress of 690 kPa. The i-angle based on the log (Z2) correlation (expression 3.22) was estimated as 51.55 degrees and the corresponding predicted peak (expression 2.6) was 4942.97 kPa. Like creep test 2, the specimen underwent a total of 3 stages of constant force loading prior to creep failure. The

stresses corresponding to these constant forces were set to be 4361.75 kPa, 4623.27 kPa and 5324.75 kPa which represented 88.25%, 93.53% and 107.72% of the predicted peak respectively. Since the substained constant load at the final stage was beyond 100% of peak, it suggested that either the shear strength based on the expression 3.22 was underestimated or the increase in strength was primarily due to the change in the apparent shear stiffness in the stage loading creep test (section 4.4.6).

The graphical outputs of these 3 stages are shown in figures 4.12, 4.13 and 4.14 respectively. In stage 1 (figure 4.12) both shear stress and dilation plots showed considerable fluctuations indicating that the surface was not statically stable. The dilation curve tended to have an average value of 0.003 mm while the shear stress tended to increase slightly during the duration of this stage. At a time of 800 hours a sharp jump in shear stress followed by a sudden stress drop was measured. This jump seemed to be the results of brittle failure of some steep asperities. The creep increased rapidly at the beginning but the strain rate decreased. An extra strain of 0.025% was obtained from the sudden jump in shear stress at 800 hours. Having reached the jump the strain rate decreased once again. The initial elastic strain was 7.286% whereas the total amount of creep in this stage was 0.156% which represented 2.134% of the elastic strain.

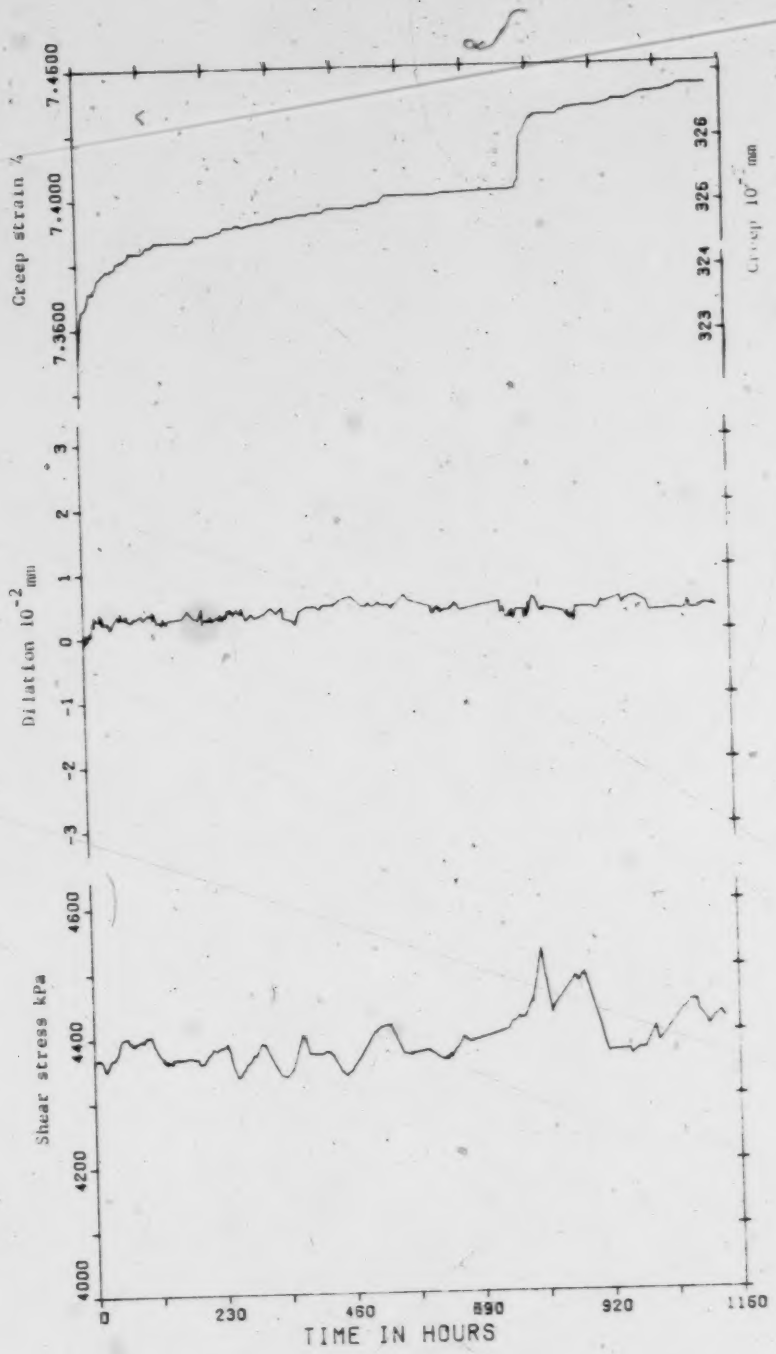

Figure 4.12 Results of creep test #3 (stage 1)

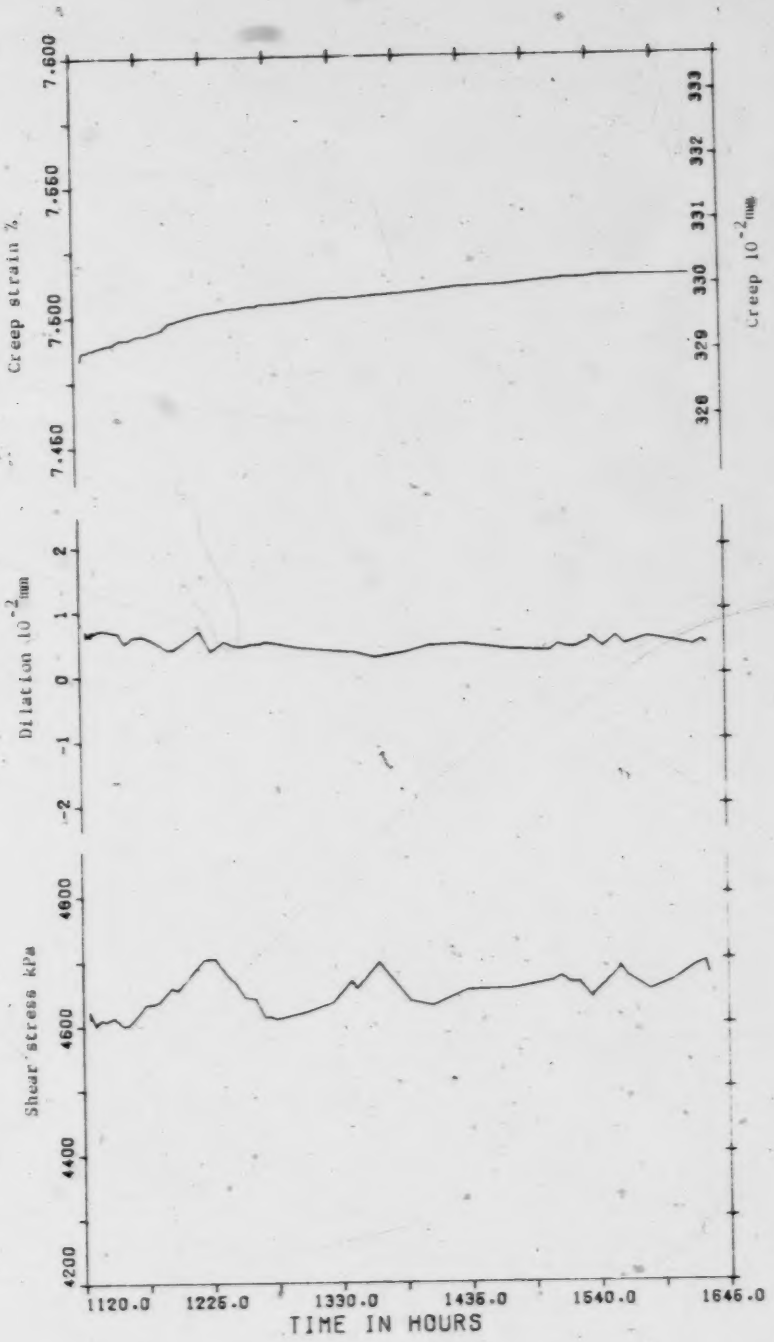

Figure 4.13 Results of creep test #3 (stage 2)

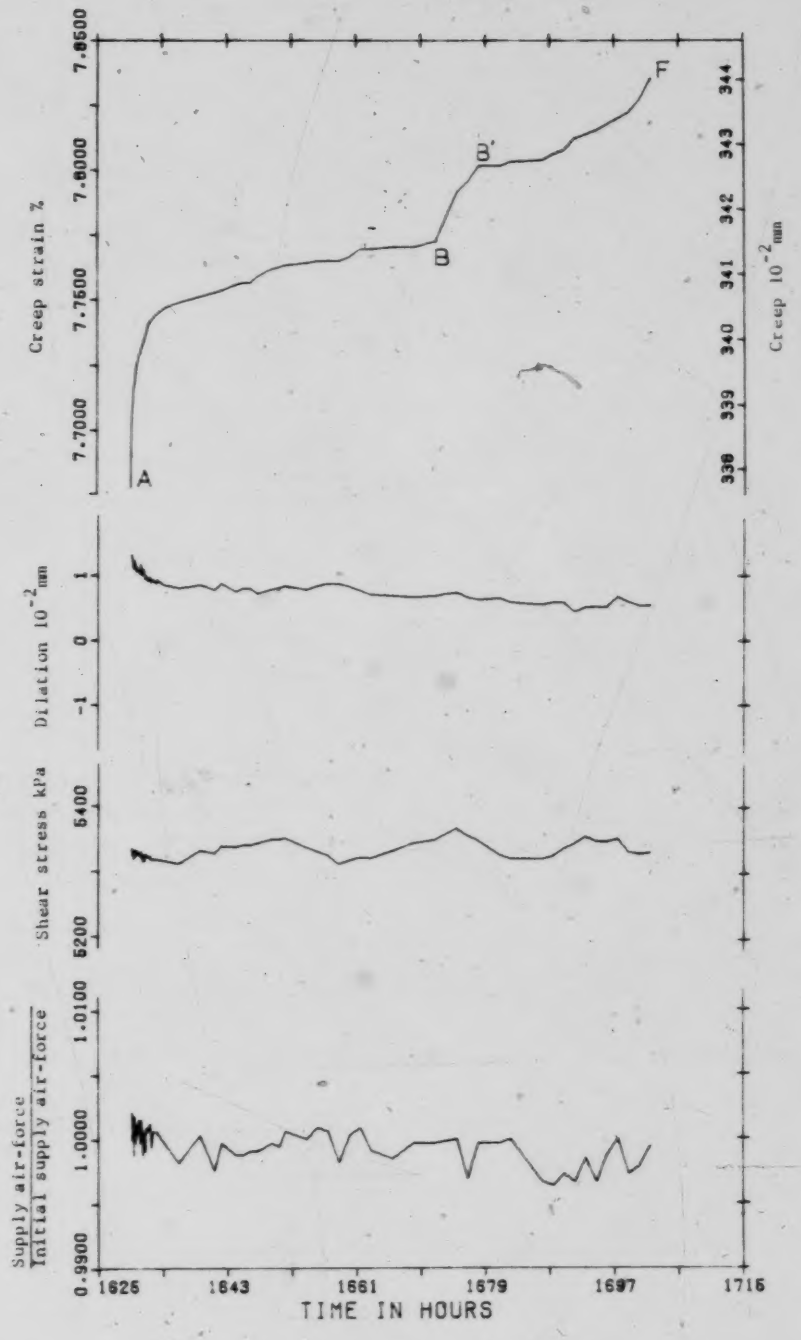

Figure 4.14 Results of creep test #3 (final stage)

In stage 2 (figure 4.13), an additional apparent elastic strain of 0.042% was obtained when the shear force was increased by 5.28%. Upon completion of the loading, both shear stress and dilation curves showed some fluctuations. Careful examination of these curves, showed that the variation in dilation reflected the changes in slopes of shear stress curve. In general, the dilation tended to decrease from 0.007 mm to 0.005 mm while the shear stress increased slightly during creep. Compared with that of stage 1, the creep strain of this stage increased only slightly for a short duration while the strain rate decreased dramatically for the rest of creep. The total amount of creep during this stage was 0.031% which represented 72.92% of the stage's apparent elastic strain.

In the final stage (figure 4.14), an additional apparent elastic strain of 0.163% was obtained when the shear force was increased by 14.19%. Subjected to this stage-loading, the specimen had gained in dilation from 0.005 mm (end of stage 2) to 0.013 mm. However as the creep progressed, the dilation rate decreased and eventually an accumulated vertical deformation of 0.007 mm was obtained prior to creep failure.

Although fluctuations were noted in both the shear stress and supply air-load curves during creep, yet the values at the beginning and end of creep did not vary much. The percentage variations were measured to be ±0.56% and

±0.29% above the mean values of shear stress and supply air-load respectively. The majority of abrupt changes in slopes in the shear stress curve could be related to jumps in the supply air-load. Those which did not appear in-phase might be due to "slack" in the creep system and measuring devices or perhaps due to the combined results of increasing normal stress because of suppressed dilation during creep rupture and brittle failure of steep asperities (more discussions in section 4.4.5).

The resulting final creep curve showed some special features. First of all, the creep strain increased exceptionally fast from point A and covered a creep strain of 0.05% within the first one hour. Secondly, at point B where the accelerating creep might be supposed to begin, a sharp jump in strain rate had occurred along path BB' (top diagram). At point B' the creep resumed its conventional speed. Then the creep strain rate increased again until it had reached the point F where the creep failure occurred.

Reasons for the sudden jump in creep (BB' in figure 4.14) were not known exactly but there was a disturbance during the time between B and B' plus some time after point B' caused by 2 events; (i) three hours power shut down and (ii) effects of heating coming from lighting systems when pictures of creep machines were taken. However, the shear stress, dilation and supply air-load curves did not show any significant changes. This causes uncertainty in the

accurracy of data beyond point B. Notwithstanding these interruptions, the rock specimen eventually reached creep failure.

The total amount of creep strain was 0.157% which represented 96.32% of the final stage apparent elastic strain. The lifetime T of this stage for this particular constant stress and disregarding any effects due to stress history and changes in apparent shear stiffness was estimated to be the difference in time between points A and F; this would be 72.37 hours.

As mentioned earlier in this section, the peak may have been underestimated. However, with an engineering judgement, one could back-calculate a reasonable percentage of peak for the constant force substained during the final stage by comparing the lifetimes T of all the creep tests performed. Table 4.3 summaries the amounts of shear force and their corresponding T values for the final stages. From this table, apparently both the Z2 value and the measured T for creep test 3 were in between creep tests 2 and 4, it appeared reasonably enough to suggest that the uncertain percentage of peak would lie in between 98.11% and 98.65%, say a value equal to 98.40% was chosen for this constant shear force.

4.4.4 Creep Test 4

The final shear creep specimen was 53291 with a Z2

value of 0.55241 and Ao of 8.80 sq. cm. (Lo x W = 4.31 x 2.04 sq. cm). The i-angle (expression 3.22) was estimated 54.70 degrees and the corresponding predicted peak (expression 2.6) was 8216.99 kPa the test was carried out at a normal stress level of 690 kPa. This time, the specimen underwent a total of 4 stages of constant force loading prior to creep failure. The stresses corresponding to these forces were set to be 4219.89 kPa, 5859.02 kPa, 7461.08 kPa and 8105.83 kPa which represented 51.35%, 71.30%, 90.80% and 99.04% of the predicted peak respectively.

The graphical outputs of these 4 stages are shown in figures 4.15 to 4.18 respectively. It was the intention of this final creep test to investigate if a rough rock surface would also show time-dependent frictional behavior at a low constant shear force; therefore, in stage 1, the shear force was kept at 51.35%, the resulting horizontal deformations did confirm the possibility of creep at a low stress level. Notice in figure 4.15 (top diagram), the creep curve illustrated a quite distinct decelerating creep phenomenon. The initial elastic strain was 2.92% and the total amount of creep was 0.099% which represented 3.39% of the elastic strain.

According to Patton's theory (1966), rock surfaces would dilate at low normal loads. However, results from stage 1 showed the opposite. The specimen initially contracted to about 0.002 mm at the end of shear test. The

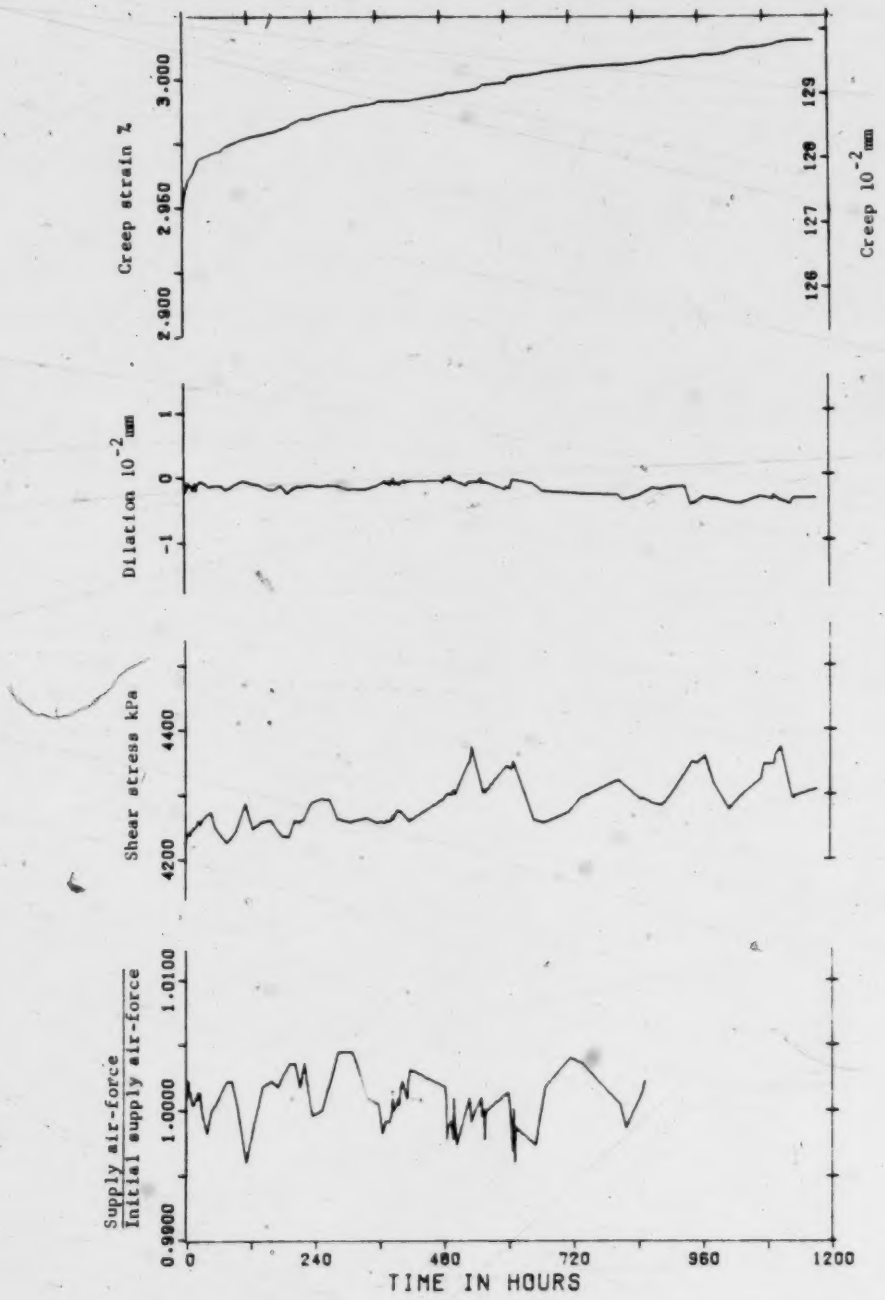

Figure 4.15 Results of creep test #4 (stage 1)

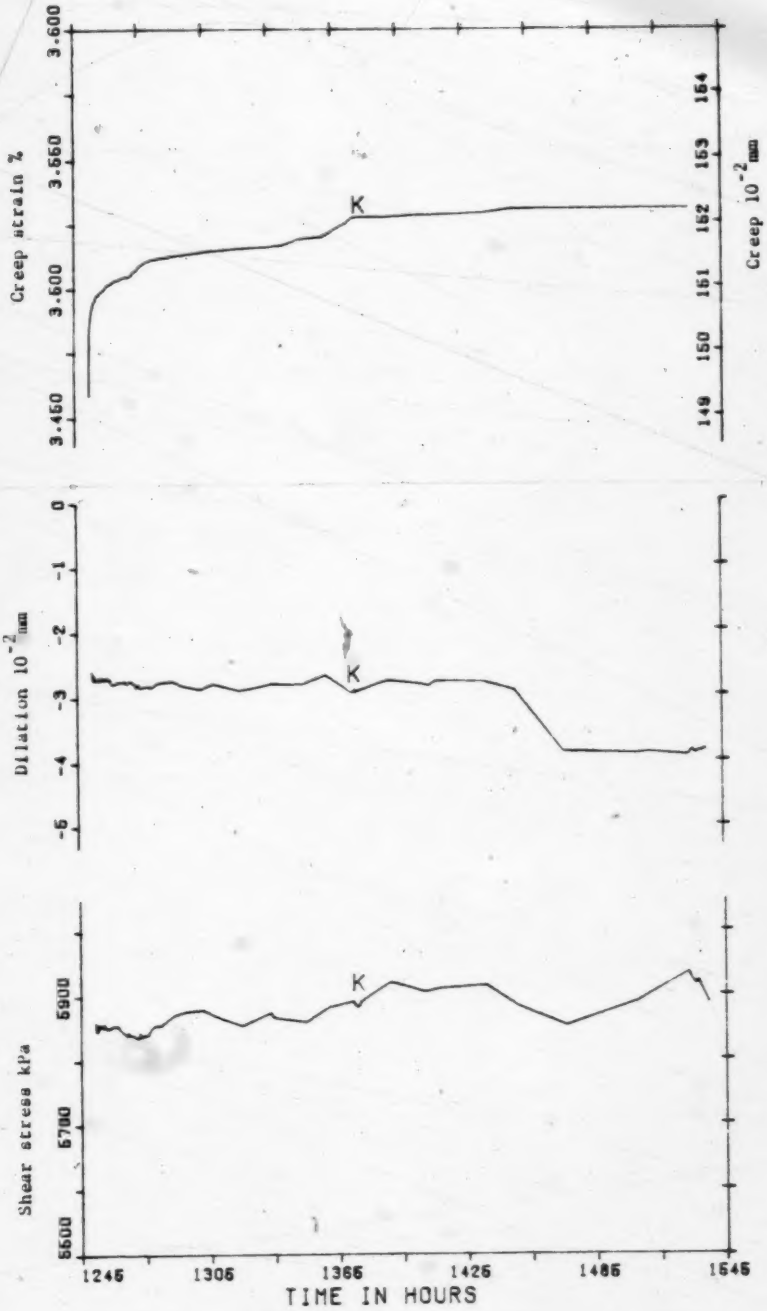

Figure 4.16 Results of creep test #4 (stage 2)

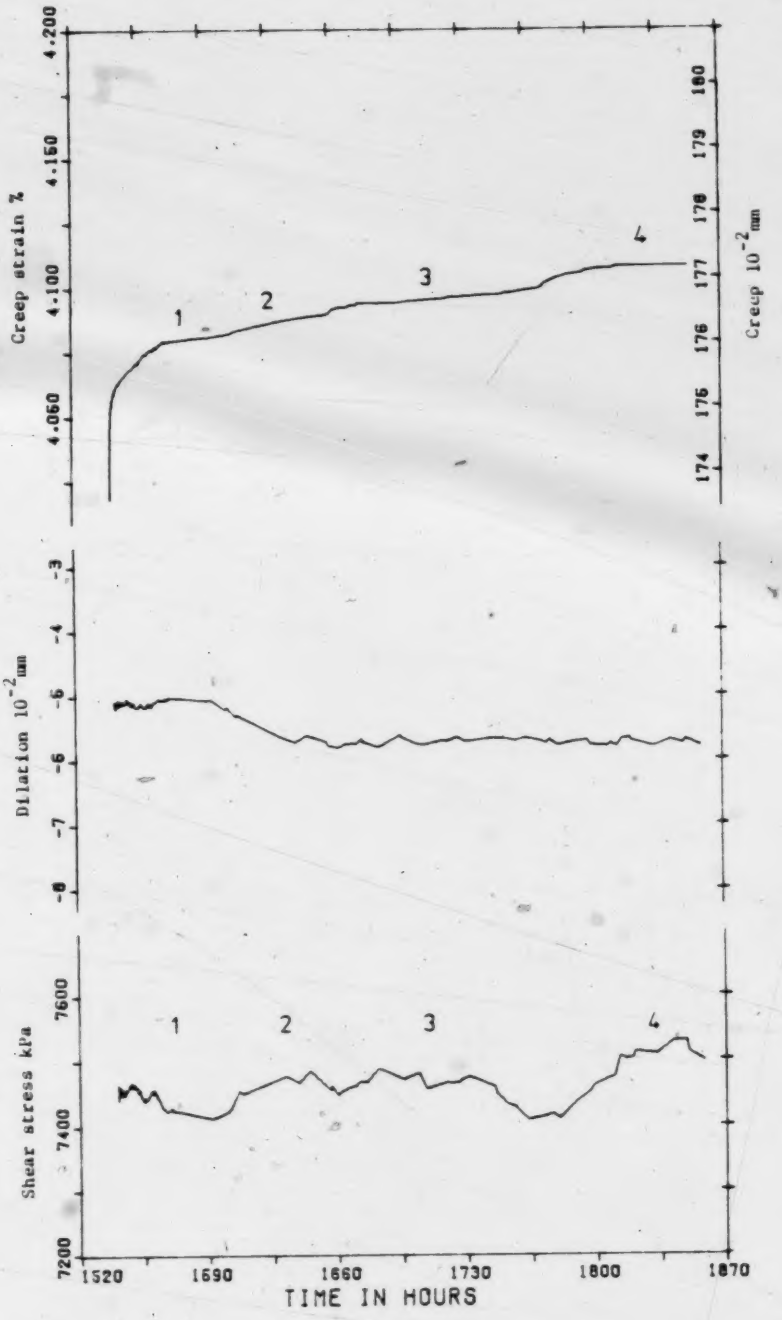

Figure 4.17 Results of creep test Ø4 (stage 3)

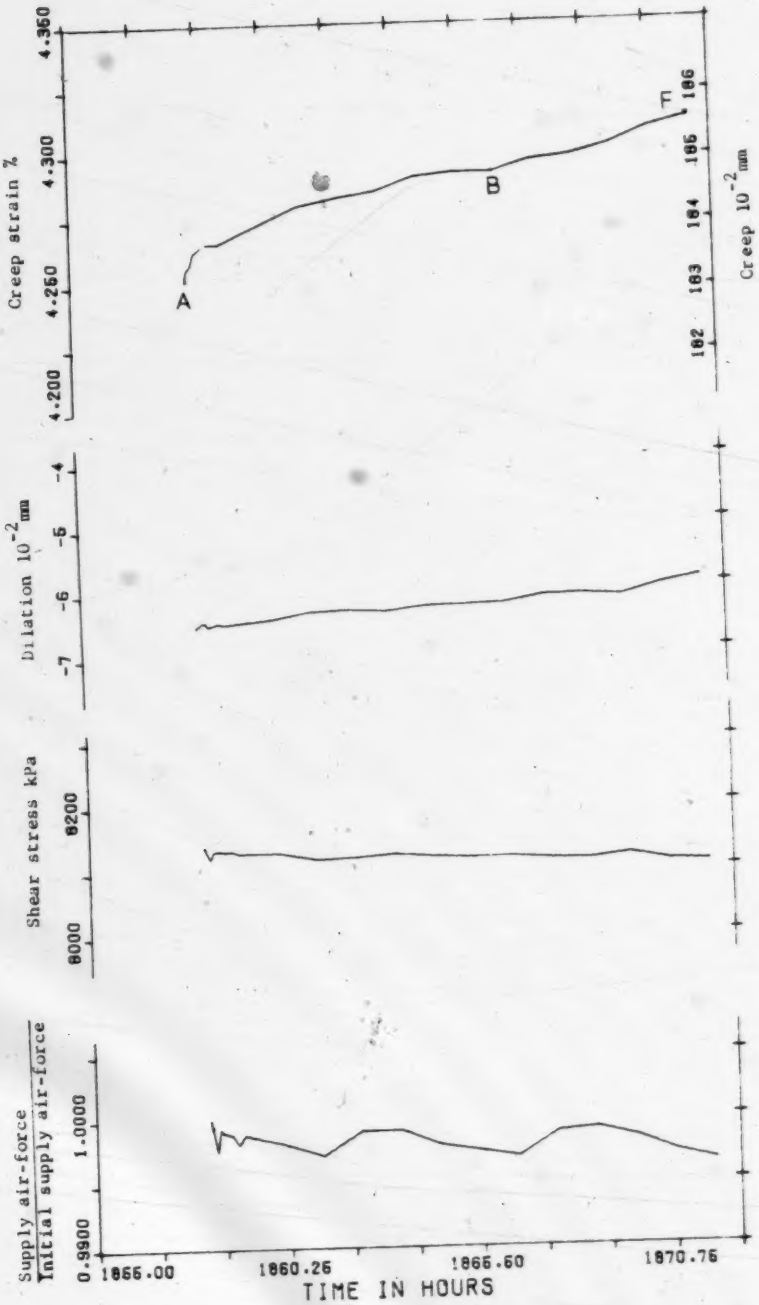

Figure 4.18 Results of creep test #4 (final stage)

possible explanation was due to seating errors of the specimen. During the creep, continuous further contractions were measured and a total value of 0.004 mm contraction had occurred at the end of stage 1.

Even at this low constant stress level, fluctuations were measured in the dilation, shear stress and supply load curves. The percentage variations were measured to be ±0.92% and ±0.42% above the mean values of shear stress and supply shear load respectively. Even though it could be assumed that the variations in shear stress were primarily results of fluctuations in the supply load, yet the difference in their percentage variations plus their out of phase characteristics (third and bottom diagrams) suggested additional causes of the variation in shear stress as indications of certain internal instabilities (more discussions in section 4.4.5).

As the shear force was increased to the next stage (figure 4.16), an additional apparent elastic strain of 0.44% was obtained when the shear force was raised by 20%. During this stage the dilation continued to contract and had reached a value of 0.004 mm. at the end of creep. However, the shear stress in general increased during creep despite of some fluctuations. The creep curve showed distinct features of a decelerating creep zone. At a total elasped time of 1365 hours, the creep rate began to increase slightly for the next 13 hours and thereafter resumed its

normal decreasing rate. About the same moment at about 1378 hours, the dilation showed a small jump (point K in diagrams) and accompanied a small decrease in the shear resistance. The physical implication might be the results of brittle failure of some steep asperities. The total amount of creep measured was 0.072% which represented 16.40% of the apparent elastic strain obtained in this stage.

Further increase in shear force (stage 3, figure 4.17), brought another additional apparent elastic strain of 0.488% when the shear force was raised by 19.50%. These values were quite similar to that of stage 2 (0.44% and 20.00% respectively) indicating not much change in apparent shear stiffness during the stage-loading. Extra specimen contractions were induced during the loading; a total of 0.05 mm contraction had resulted at the beginning of creep. Subsequently, further contractions were observed as the creep progressed but at the end of 1643 hours, it tended to have a fairly steady value of -0.057 mm. The shear stress plot indicated variaticns in stress. It appeared that there were 4 major "humps" along the entire curve. When it was aligned with the creep curve (top diagram). These humps reflected the 4 distinct stepping up sections along the creep curve. The total amount of creep was 0.089% which represented 18.24% of the stage's apparent elastic strain.

The final stage (figure 4.18) was reached when the shear force was raised by 7.85% to give ancther additional

apparent elastic strain of 0.144%. Not like the preceding stage-loading tests, both shear stress and dilation versus time plots resembled smooth curves without any dramatic "jump" events along the curves. During the loading, a total contraction of 0.065 mm had resulted but once the creep progressed, continuous dilations were observed. Its rate behaved quite steadily covering the range of decelerating creep (AB) zone. Upon reaching the onset of accelerating creep, point B, the dilation rate increased much further until creep failure. This again presented sufficient warning concerning creep rupture at point F. Noticed in the last two diagrams (shear stress and supply load curves), their general appearances suggested that they were in phases with each other. This exact characteristic could not be found in any other stage-loading tests performed. The physical implication was that the major cause of variations in shear resistance was due to the fluctuations of supply load through its bellofram. The agreement in the percentage variations, approximately ±0.19% and ±0.18% above the mean values of shear resistance and supply load respectively, reinforced this conclusion.

As for the creep curve, again two stages of creep zone could be observed; decelerating creep (AB) and accelerating creep (BF). However, the accelerating creep did not show any dramatic increase in strain rate. Moreover no obvious warning was present as to where the onset of rupture point F would be.

The total amount of creep strain obtained in this stage was 0.06% which represented approximately 41.66% of the final stages apparent elastic strain. By ignoring the effects due to stress history, the lifetime T for this final stage under the particular constant shear force (99.04%) was measured to be 13.72 hours which corresponded to the difference in time between points A and F.

4.4.5 Variations of Shear Resistance

In all the shear creep test results, the shear stress versus time plots showed fluctuations. Moreover certain variations in the supply air line were also encountered. It was believed that the variations in resistance could be explained by the feed fluctuations since it seemed quite reasonable to expect the forces as supplied by belloframs to be picked up by load cells. However one could argue that there existed friction within the shear box arrangement so that the driving force could not be transmitted completely across to the shearing plane and then to the load cell. As a matter of fact, calibration records did show approximately 1% of shear force overcome by friction. Despite this, any change in the feed should be reflected by a similar change in shear resistance shortly afterwards.

The above argument was employed for the investigation of causes of variations. First of all, phase shifts were observed in some of the stage tests. They might be due to

the loading shedding too fast for the machine to handle; that was the interaction between the machine and deformation rate process or perhaps, there might be possibility of other major causes. In order to check whether the feed were responsible for the variation, statistical analysis was employed. To do this, percentage ranges of variation were computed for each pair of shear stress and supply air-load curves and the results are tabulated in table 4.2. The following conclusions could be made from this table.

(1) Degree of fluctuation in the feed was not the same for different stage of tests; they ranged from 0.27% to 0.84%.

(2) Area corrections applied to the shear stress did not appear to make any significant difference in the percentage ranges of shear resistance.

(3) The results of percentage change of the feed for the final stages of creep tests 2 and 4 reflected close agreement with the corresponding percentage changes in shear stress. In the other stages, differences in ranges were significant; therefore, other possible causes of variation in resistance had to be found.

Another explanation could be due to the increase in normal stress during the course of creep. As the specimen was creeping, dilation occurred in some experiments. When this happened, the friction between the upper shear box and walls of the upper half rock surface would introduce additional normal load to the sample thus increased the

		CREEP TEST 1 final stage	CREEP TEST 2 first stage	CREEP TEST 2 final stage	CREEP TEST 3 final stage	CREEP TEST 4 first stage	CREEP TEST 4 final stage
Air-load from bellofram	Mean ratio	0.9983	1.0000	0.9634	0.9997	1.0007	0.9985
	Maximun ratio	1.0000	1.0022	1.0005	1.0021	1.0044	1.0000
air-load / initial air-load	Minimun ratio	0.9973	0.9982	0.9977	0.9964	0.9960	0.9965
% change in air-load		0.27%	0.40%	0.28%	0.57%	0.84%	0.35%
Measured shear resistance with no shear area correction	Mean ratio	0.8935	0.8555	0.9007	0.9949	0.5041	0.9464
	Maximun ratio	0.8959	0.8565	0.9354	1.0013	0.5162	0.9483
shear resistance / predicted peak	Minimun ratio	0.8924	0.8541	0.9329	0.9913	0.4985	0.9439
% change in shear resistance		0.35%	0.24%	0.25%	1.00%	1.77%	0.44%
Measured shear resistance with shear area correction	Mean ratio	0.9749	0.8969	0.9463	1.0786	0.5196	0.9887
	Maximun ratio	0.9775	0.8979	0.9828	1.0859	0.5321	0.9904
shear resistance / predicted peak	Minimun ratio	0.9733	0.8956	0.9801	1.0746	0.5136	0.9865
% change in shear resistance		0.42%	0.23%	0.27%	1.13%	1.85%	0.39%

Table 4.2 Comparison between the% fluctuation of supply air-load from the bellofram and the % fluctuation in the measured shear resistance for creep tests

shearing resistance. This explanation needed experimental justification before one were certain the real physical shear creep mechanism.

As mentioned earlier, another possible cause of jump like events in shear stress could be results of brittle failure of steep irregularities subjected to fatigue shear loading. However, this kind of jump phenomenon was not the same as observed in the ultimate stress-loading path (figure 2.17) in direct shear strength tests where the rock surface were riding on some uneven broken shear asperities or alike. As in creep tests, surfaces would have been in peak to peak contacts when the sheared asperities stayed in valleys or troughs of the lower half surfaces.

In summing up, results from the above discussions had indicated that the causes of variation in shear stress would have been in some cases primarily due to fluctuations of the supply air system and some cases in combination of effects of (a) increase in normal load during creep and (b) fatigue ruptures of some steep asperities.

4.4.6 Increment Versus Single Creep Tests

Conventional direct shear strength tests had shown (chapter 2) that stage- loading tests on rough rock surfaces would have apparent peak strengths some where between the peak and ultimate strengths i.e. the peaks could have been underestimated.

There is an important difference between stage-loading tests and staged creep tests. In the stage-loading tests the rock surface is taken to failure at every stage, there is a large amount of non recoverable damage to the surface resulting from a failure. Thus the specimen gets severely damaged even after one stage, nearly all the asperities wiped out. In creep tests the amount of damage due to creep is small compared to the deformation associatd with loading. The asperities damaged in creep are those with strengths only slightly above the stresses imposed by the present loading. If these fail in creep, they are not available to fail when the shear load is increased and so the rock surface appears stiffer. Notice that the aforementioned shear creep results showed a relatively small amount of apparent elastic strain when the shear force was stage-increased. The elastic strain values in table 4.3 indicated this phenomenon. Thus, this led to a situation where the shear stiffness of a rock surface increased in a stage-loading creep test. Further creep specimens showed relatively high time-dependent strengths in stage-loading creep.

In figure 4.23, the 3 stage-loading creeps appeared to have higher time-dependent shear strengths than that of single-loading creep. These experiments do not mean that the specimens were strengthened against creep rupture but simply prolonged their lifetimes instead.

The results of complete loading-displacement history for 4 creep tests are illustrated in figures 4.19 to 4.22 respectively. Two curves were drawn for each figure. The lower one was without area corrections. The following conclusions could be drawn from these figures.

(1) The initial shear stiffness obtained from slopes of the approximated straight line underestimated the true stiffness.

(2) Judging from the inclinations of straight line to the strain axis, the elastic portions divided into 2 groups: first being creep tests 1 and 3 and second being creep tests 2 and 4. This might be due to testing them in two creep machines of different machine stiffness since group 1 was performed in one machine and group 2 in the other.

(3) The elastic portions of the curves were concave downward.

(4) Curves where the shear resistance underwent area corrections would not have dramatic difference in curvature from that of no area corrections. The difference was marked as the strain increased.

(5) Regardless the trend of curves, the slopes (shear stress/strain) along them in each figure (creep tests 2 to 4) were much less than that of the apparent slopes between two adjacent creep stages; which indicated the rock specimens increased their shear stiffness during stage-loading creep tests.

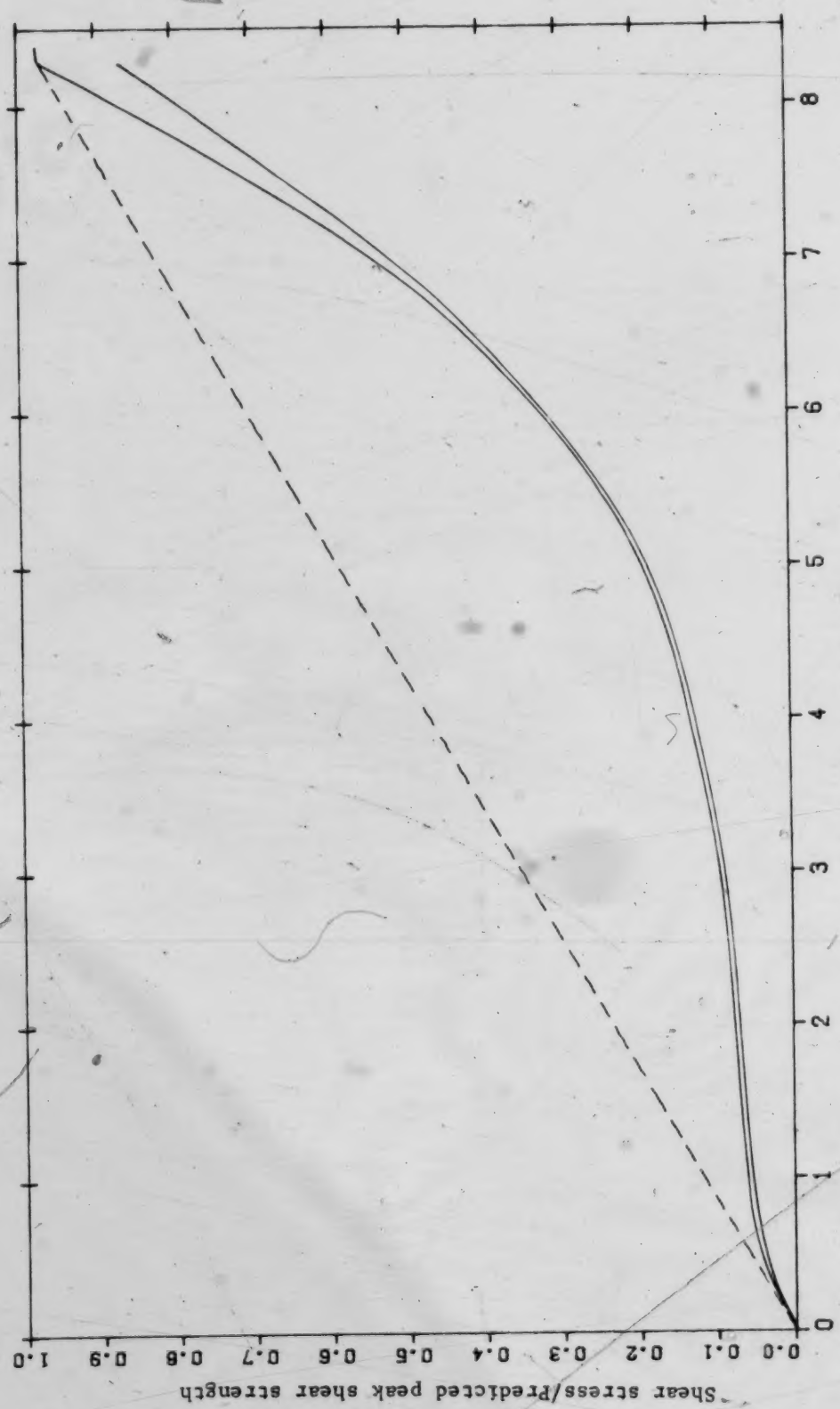

Figure 4.19 Complete shear stress-displacement history for creep test #1

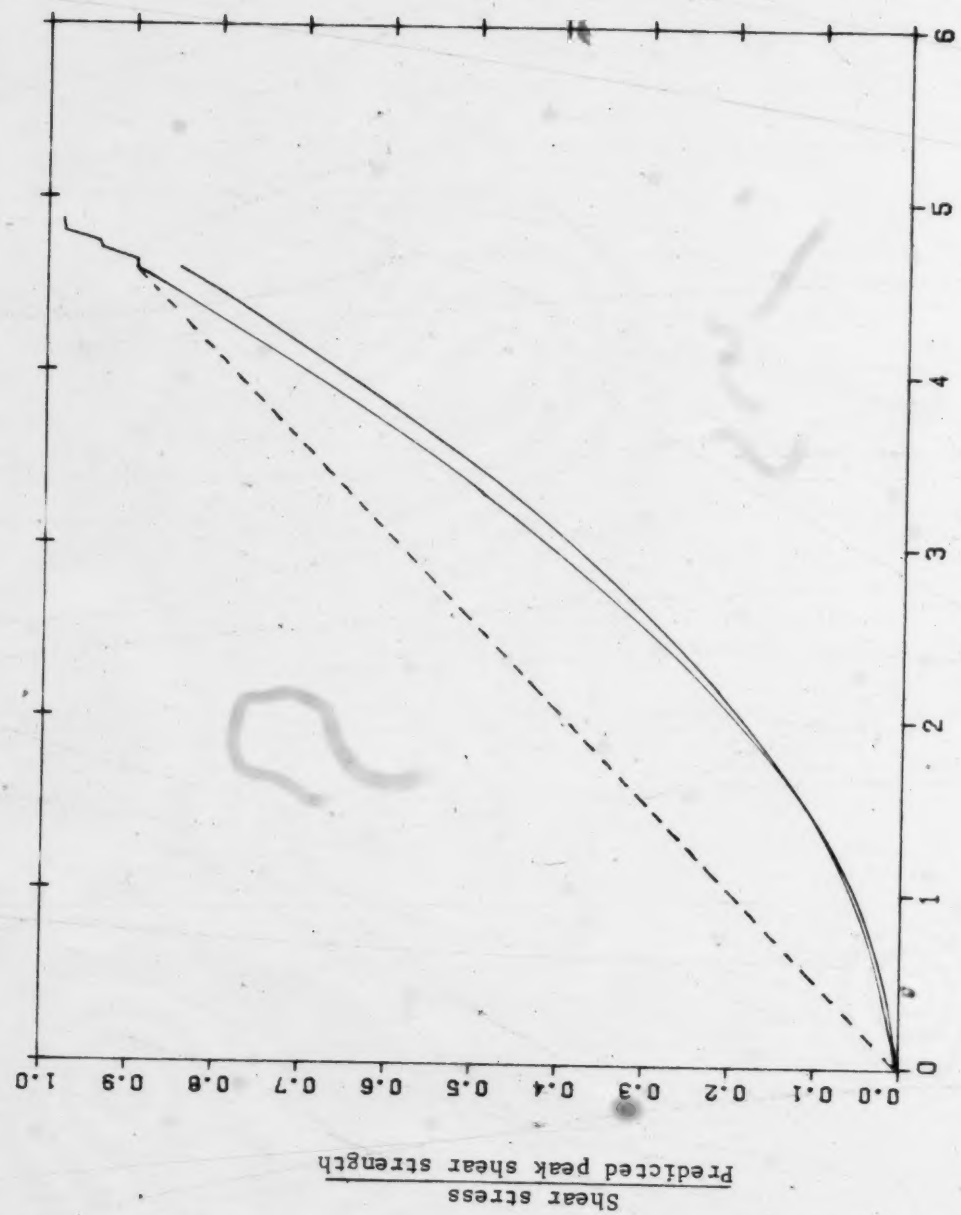

Figure 4.20 Complete shear stress-displacement history for creep test #2

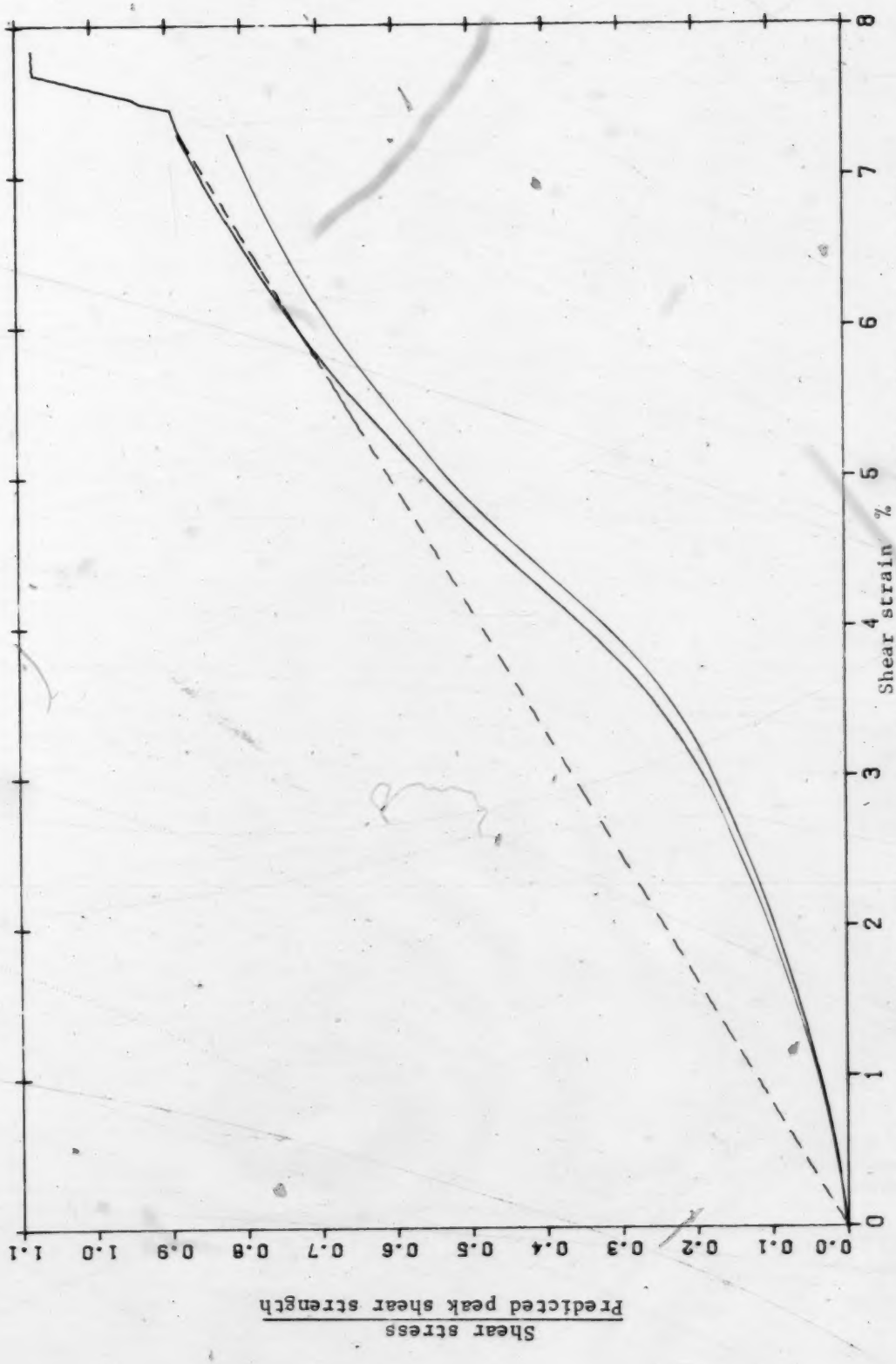

Figure 4.21 Complete shear stress-displacement history for creep test #3

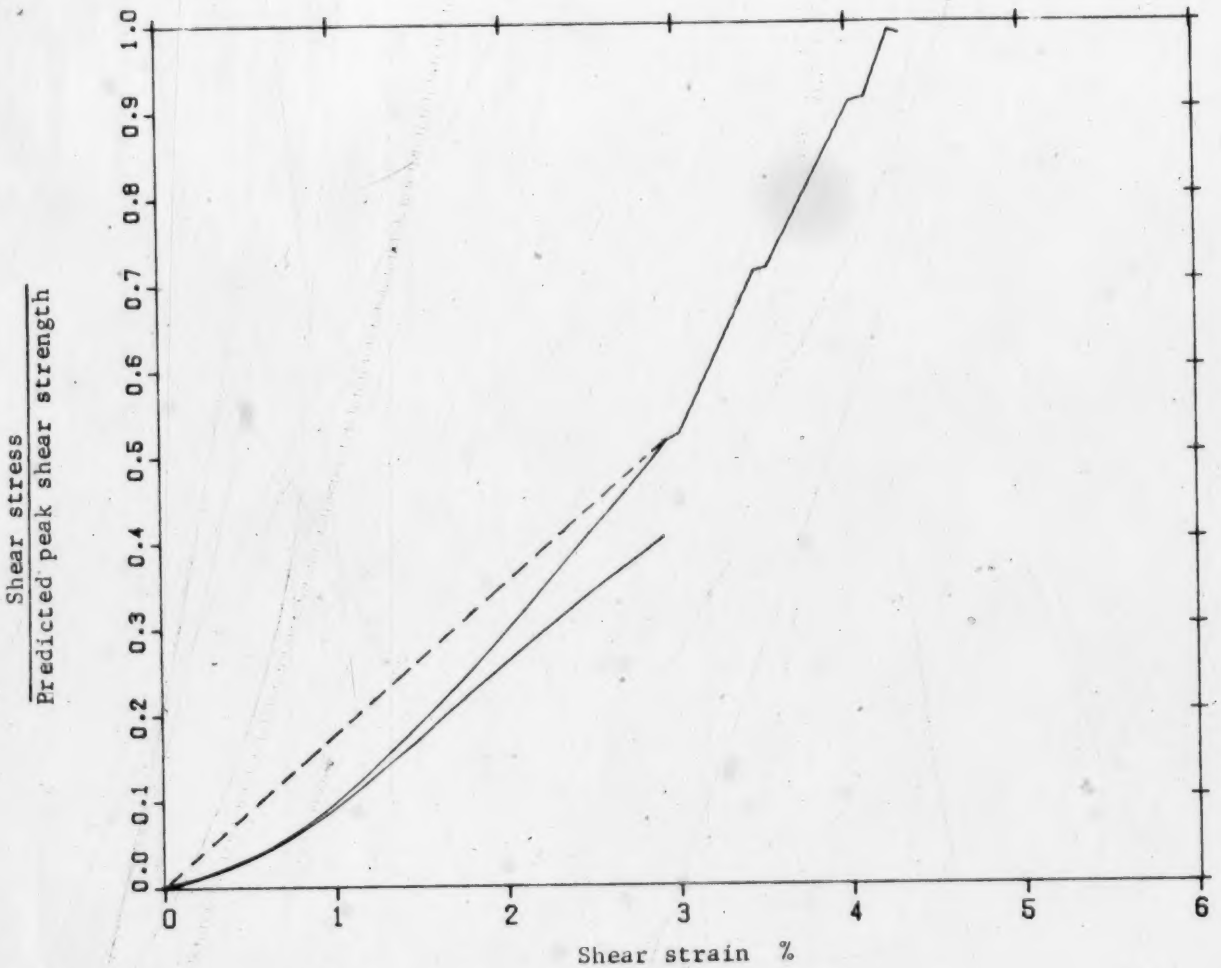

Figure 4.22 Complete shear stress-displacement history for creep test #4

One hypothesis is that when a rock surface crept, some asperities failed; upon loading to the next creep stage, say from a 95% to a 97% shear force, there were no "97% asperities" to fail during loading as they had been already used up in creep at the 95% level. Thus, this would associate with reduction of surface roughness and decrease in the strain rate with a strengthened specimen. In other words, if a rock surface subjected to shearing were stopped on its way up, it could have been stabilized. When this occurred, the apparent time-dependent strength was strengthened and the lifetime,T extended. This might be the reason why in test 3 where strength as high as 107.72% of the predicted peak strength had been obtained. Perhaps another hypothesis is a rate deformation dependency where failure of the rock surface occurs when deformation exceeds a critical rate. If the asperity failures which would contribute to that critical rate have already occurred in creep at a lower level, creep failure may be delayed as seen in test 3.

The results of 4 aforementioned shear creep tests are recapitulated in table 4.3. Figure 4.23 attempts to show the crude relationship between the aforesaid percentage of constant shear strengths and their lifetimes, T of the tested specimens regardless of different Z2 values, normal stress levels and stage-loading criteria. Noted that the distribution of the data suggested that the general trend of shear strength decreased with time. Its shape resembled the

Rock surface number	Z2	L cm	W cm	σ_n kPa	i angle degree	τ kPa	τ' %	Creep stage	ϵ_o %	Decelerating creep	Accelerating creep	ϵ_p %	Duration of test hours
	creep test 1												
53121	0.46750	4.305	2.413	1035	53.10	9227.62	97.41	final	8.310	yes	yes	0.075	82.42
	creep test 2												
53361	0.45201	4.290	2.347	1035	51.54	7409.07	89.67	1	4.580	yes		0.057	63.46
							93.82	2	0.069	yes		0.039	366.45
							98.11	final	0.057	yes	yes	0.065	93.14
	creep test 3												
53222	0.50122	4.390	2.500	690	51.55	4942.97	(80.60)	1	7.286	yes		0.156	1125.13
							(85.43)	2	0.042	yes		0.031	504.25
							(98.40)	final	0.163	yes	yes	0.050	72.37
	creep test 4												
53291	0.55241	4.310	2.040	690	54.70	8216.99	51.36	1	2.920	yes		0.099	1175.65
							71.30	2	0.440	yes		0.072	285.23
							90.80	3	0.488	yes		0.089	317.23
							99.04	final	0.144	yes	yes	0.060	13.72

L =the length of shearing plane
σ_n =the normal stress level
τ^n =the predicted shear peak strength
ϵ_o =the initial or the apparent elastic strain
ϵ_p =the plastic or creep strain
W =the width of shearing plane
i =the predicted i-angle
τ' =the percentage of predicted peak strength substained during creep test

Table 4.3 Summary of 4 shear creep test results

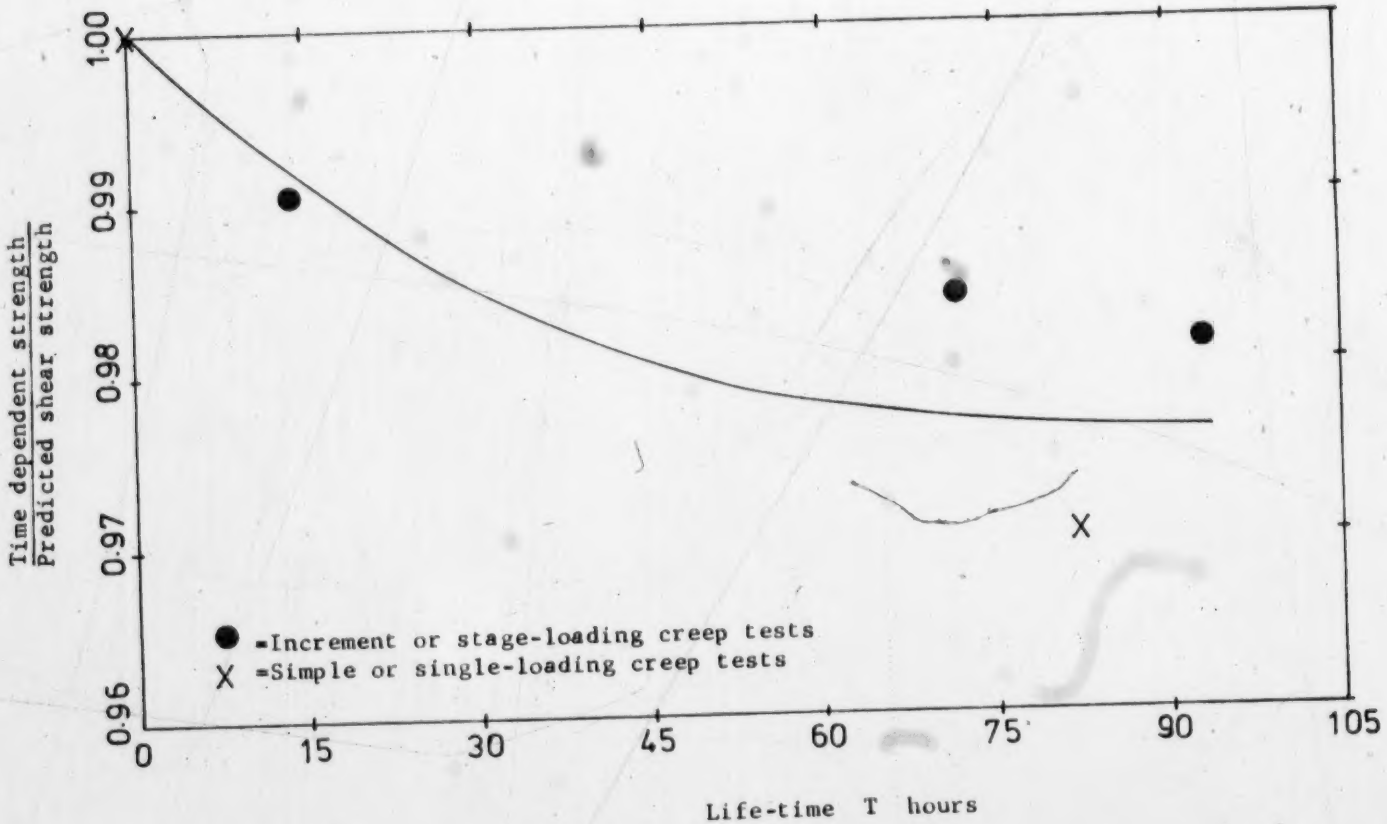

Figure 4.23 Shear strength-time plot of rough Standstead Granite surfaces

characteristics of figure 4.1c. So these limited shear creep results suggest the friction of rough rock surfaces is time-dependent. However,an alternative hypothesis explaining the deformation by fluctuations in the shear loads can not be excluded by these experiments.

4.5 Summary of Chapter 4

(1) The objective of this chapter was devoted to the investigation of shear creep hypothesis that the friction of highly dilatant surfaces are time-dependent in nature. Two shear creep machines were modified from two conventional direct shear machines to undertake this investigation. Under a certain normal stress, a shear creep experiment was carried out by substaining a particular predetermined constant shear force on the shearing plane of a granite specimen. The force was regulated by compressed air diaphragm - the bellofram. The test was run in a temperature and humidity controlled environment. Electronic measuring devices were used and the sampled data were processed by computer programs to yield graphical outputs.

(2) Based on the findings of rock surface roughness studies in chapter 3 and the evaluation of these findings through shear strength results in chapter 2, certain percentages of shear peak could be estimated

for the constant forces substained in creep tests; thus, the ability of stopping a direct shear test and starting a shear creep experiment was possible.

(3) A total of 4 shear creep experiments (three of them shear stage-loading tests) were performed and all of which eventually ended up in creep failure. The resulting failed creep curves could be divided into 2 creep zones; decelerating creep and accelerating creep. However, the rest of the staged creep curves covered portions of decelerating creep only.

(4) Also plotted were dilation, shear stress and supply air-pressure versus time curves. Fluctuations in these quantities were measured. The major cause of variations in shear stress was believed to be the feed fluctuations but other causes may be increase in normal stress during creep and fatigue failures of some steep asperities. These causes introduced internal instability and uneven distribution of stresses along the rock surfaces.

(5) Of all the creep tests, sufficient warning concerning failure was usually present since regardless of the type of test (incremental or simple) and shear stress level, on the onset of accelerating creep rapid increase in creep strain and dilation rate plus reduction in shear resistance were observed.

(6) Results from incremental creep tests or the stage-loading creep showed that the specimens were

strengthened and stabilized to certain degree between stages. The manifestation of this behavior was the occurrence of high apparent shear stiffness and extended lifetimes T.

(7) Results of the shear creep tests may suggest not only that the static friction of dilatant rock surfaces decreased with time (this is what one would expect from uniaxial compression and tension tests) but also show direct shear machines can be modified into shear creep machines plus the proof of hypothesis of time-dependent frictional behavior of rough Standstead Granite surfaces. Dieterich (1971) however showed that the static friction of non-dilatant rock surfaces increased with time. The differences between the two were (a) rock surfaces with different degree of irregularity, (b) normal stress levels (0.7-1.0 MPa and 2-88 MPa for this thesis work and Dieterich's work respectively), and (c) different shear creep mechanism; here the rock surfaces were in the peak to peak mode during the course of creep while the other were in gouge contacts which were similar to "soil creep behavior".

CHAPTER V

Concluding Remarks

The objective of this thesis was to investigate the shear strength characteristics of two artificially fractured rough rock surfaces (Tyndall Stone and Standstead Granite) with emphasis on the time-dependent frictional behavior of these surfaces in shear. In the light of the results presented in the previous chapters, the following concluding remarks may be made.

In connection with the investigation of time-dependent rock friction, the prediction of peak shear strength of rock surfaces was a crucial step.

An investigation was conducted in to the possibility of numerically characterizing the macroscopic surface roughness of prepared rough rock surfaces and then correlating these with the effective i-angle through Barton's expression for i-angles. The Z2 surface parameter gave a useful correlation with the joint roughness coefficient (JRC) parameter.

Using the correlation, the predetermined surface profile and its appropriate surface parameter one could predict, with a reasonable degree of certainty, the peak shear strengths of rough rock surfaces. This has been verified by the corresponding measured peak values obtained from extensive laboratory direct shear strength tests on

both types of rock surface.

The results from the shear strength tests yield not only the necessary strength parameters for the verification of the peak strength prediction criterion but also shed some new light on the shear strength behavior of rough rock surfaces and the criterion for setting up a shear creep experiment. The following characteristics can be drawn from the strength tests .

(a) The artificially fractured rock surface exhibited high dilatancy.

(b) The ϕ_b plus i concept was very successful in the shear strength analysis of rock surfaces. The magnitude of effective i-angle depends upon the degree of surface roughness, material strength of surface walls and stress level encountered.

(c) In addition to Barton's criterion of peak shear strength, the power law fit could be used to describe the experimental observations of shear strength data. Changes in the slope of the shear strength envelope reflected the changes in the mode of asperity failure.

(d) The shear stiffness and stress drop after peak of the rock surfaces increased with normal stress level and strength of the material.

(e) Shear strengths derived from stage-loading tests were not reliable because of the unknown stress history involved and asperity damage. They tended to have higher values than that of single specimen loading

tests for the non-dilatant surfaces but between peak and ultimate values for the dilatant surfaces.

(f) For a given type of rock surface, the ultimate friction angle was not a unique value but depended upon the initial surface conditions and post peak characteristics. In this study, the estimated average ultimate friction angles for both rock surfaces were higher than the basic friction angles of the same rocks.

A hypothesis of shear creep in rock has been presented: shear strengths of rough rock surfaces decrease with time. An investigation was conducted into the validity of the hypothesis. A total of 4 granite surfaces were tested for this purpose, employing the modified creep machines. All the samples ended up in creep failure. Results of the tests showed not only the possibility of having creep in shear on rough surfaces, but also indicated the applicability of the designed apparatus in creep studies and confirmation of peak strength prediction analysis.

The supply air pressure in creep experiments, varied within 1%, but this was enough to affect the result of the shear resistance records and complicate the interpretation of creep characteristics. Therefore, these tests also demonstrated the importance of having accurate, constant supply air pressure.

Incremental creep tests i.e. stopping shearing on the

way up have proved to strengthen the transient shear strength of creep specimens. This would introduce high apparent shear stiffness and extend the creep failure time.

With regard to future research in the area of shear creep in rocks, further research is needed to

(1) Establish the form of the static fatigue law

$ST = f(T, So)$

ST, the shear strength at time T and So the initial shear strength

(2) Establish the form of the creep law in shear, particularily the time for the onset of accelerating creep

(3) Investigate creep on other types of surface and in other materials

(4) Investigate creep in water saturated rocks

(5) Investigate creep in rock subjected to a freeze-thaw condition

REFERENCES

Acton, F.S., 1959. "Analysis of straight line data." Wiley, New York.

Afrouz, A. and Harvey, J.M., 1974. "Rheology of rocks within the soft to medium strength range." Int. J. Rock Mech. Min. Sci., Vol. 11., pp. 281-290.

Ampferer, O., 1939. "Uber linige Formen der Bergzerrei Bung Siztungsber." Akad. d. Wiss. Wien, Math. -nat. Kl., Abt. 1, 148., pp. 1-14.

Am. Standards Assoc., 1955., "Surface roughness, waviness and lay.", ASA B46.1.

Andersland, O.B. and Akili, W., 1967. "Stress effect on creep rates of a frozen clay soil." Geotechnique, Vol. 17, No. 1., pp. 27-39.

Barton, N.R., 1970. "Alow strength model material for simulation of the mechanical properties of intact rock in rock mechanics models." Pro. of 2nd Cong. of the Int. Soc. for Rock Mech., Belgrade, Vol. 2.

Barton, N.R., 1971. "Estimation of insitu shear strength from back analysis of failed slopes." Proc. of the Int. Symp. on Rock Mech., Nancy, France., pp. 2-27.

Barton, N.R., 1971. "A relationship between joint roughness and joint shear strength." Rock Fracture, Pro. of Int. Symp. on Rock Mech., Nancy, France.

Barton, N.R., 1973. "Review of a new shear strength criterion for rock joints." Engineering Geology, Elsevier, Vol. 7., pp. 287-332.

Barton, N.R., 1976. "The shear strength of rock and rock joints." Int. J. Rock Mech. Min. Sci. and Geomech. Abst., Vol. 13., pp.255-279.

Barton, N. and Choubey, V., 1977. "The shear strength of rock joints in theory and practice." Rock Mechanics,

Vol.10, Springer., pp. 1-54.

Bendat, J.S. and Piersol, A.G., 1971. "Random data: analysis and measurement procedures." Wiley Interscience, Toronto.

Benjamin, J.R. and Cornell, C.A., 1970. "Probability, statistics and decision for civil engineers." McGraw Hill.

Beiniawski, Z.T., 1970. "Time-dependent behavior of fractured rock." Rock Mechanics, Vol.2, pp. 123-137.

Bishop, A.W., 1966. "The strength of soils as engineering materials." Sixth Rankine Lecture, Geotechnique, Vol.16, No. 2., pp. 91-128.

Boresi, A.P. and Deere, D.U., 1963. "Creep closure of a spherical cavity in a finite medium (with special application to Project Dribble, Tatum Salt Dome, Mississippi) for Holmes Narver, Inc., Las Vegas, Division."

Broch, E. and Frankin, J.A., 1972. "The point-load strength test." Int. J. Rock Mech. Min. Sci. Vol. 9., pp. 669-697.

Bruce, I., 1978. Ph.D. Thesis, Univ. of Alta., Edmonton, Alberta.

Campanella, R.G. and Vaid, Y.P., 1974. "Triaxial and plane strain creep rupture of an undisturbed clay." Can. Geot. J., Vol. 11, pp. 1-10.

Christensen, R.W. and Wu, T.H., 1964. "Analysis of clay deformation as a rate process."J. Soil Mech. Fnd. Div., ASCE, 90, SM6., pp.125-157.

Coates, D.F., 1970. "Rock mechanics principles." Mines Branch Monograph 874, Revised.

Coulson, J.H., 1970. "The effects of surface roughness on the shear strength of joints in rock." Ph.D. Thesis,

Univ. of Illinois.

Coulson, J.H., 1972. "Shear strength of flat surfaces in rock." ASCE, 13th Symp. on Rock Mech., pp. 77-105.

Cruden, D.M., 1970. "A theory of brittle creep in rock under uniaxial compression." J. Geophys. Res., 75, p.3431.

Cruden, D.M., 1971. "The form of the creep law for rock under uniaxial compression." Int. J. Rock. Mech. Min. Sci., Vol. 8., pp. 105-126.

Cruden, D.M., 1971. "Single-increment creep experiments on rock under uniaxial compression." Int. J. Rock. Mech. Min. Sci., Vol. 8., pp. 127-142.

Cruden, D.M., 1971. "The recovery of Pennant Sandstone from a uniaxial compressive load." Can. J. Earth Sci., 8., p. 518.

Cruden, D.M., 1974. "The static fatigue of brittle rock under uniaxial compression." Int. J. Rock Mech. Min. Sci. and Geomech. Abst., Vol. 11., pp. 67-73.

Cruden, D.M., 1976. "The influence of discontinuities on the stability of rock slopes." Pro. 4th Guelph Symp. on Geomorphology., pp. 57-67.

Deere, D.U., 1963. "Technical description of rock cores for engineering purposes." Rock Mech. and Eng. Geology., Vol. 1, No. 1.

Deere, D.U. et al, 1967. "Design of surface and near-surface construction in rock." Proc. 8th Symp. on Rock Mech., Minnesota, AIME., pp. 232-302.

DeFreitas, M.H. and R.J. Watters, 1973. "Some field examples of topping failure." Geotechnique, 23, pp. 495-514.

Dieterich, J.H., 1972. "Time-dependent friction in rocks." J. of geophys. Res., Vol. 77, No. 20., p. 3690.

Dixon, W.J. and F.J. Massey, 1969. "Introduction to statistical analysis." McGraw Hill.

Emery, J.J., 1971. "Finite element analysis of creep problems in soil mechanics." Ph.D. Thesis, Univ. of British Columbia.

Evdokimov, P.D. and D.D. Sapegin, 1967. "Stability, shear, and sliding resistance and deformation of rock foundations." Jeruselem: Israel program for scientific translation.

Eyring, H., 1936. "Viscosity, plasticity and diffusion as examples of absolute reaction rates." J. Chem. Phys. 4., pp. 283-291.

Fairhurst, C., 1964. "On the validity of the Brazilian test for brittle materials." Int. J. of Roch Mech. and Min. Sci., Vol. 1., pp. 535-546.

Farmer, I.W., 1968. "Engineering properties of rocks." Spon, London.

Fecker, E. and N. Rengers, 1971. "Measurement of large scale roughness of rock planes by means of prolilograph and geological compass." Rock Fracture, Pro. of Int. Symp. on Rock Mech., Nancy, France.

Feld, J., 1966. "Rock as an engineering material." Soil Test, Inc., Evanston, Illinois.

Gocdman, R.E., R.L. Taylor and T.L. Brekke, 1968. "A model for the mechanics of jointed rock." Pro. ASCE, SM.3, 94., pp. 637-659.

Goodman, R.E., 1970. "The deformability of joints. Determination of the insitu modulers of deformation of rock." Sym. Denver, Co., 1969. ASTM, Spec. Technical publ. 477, pp. 174-196.

Goodman, R.E. and Y. Ohinishi, 1973. "Undrained shear testing of jointed rock." Rock Mechanics, Vol. 5., p. 129.

Goodman, R.E., 1976. "Methods of geological engineering in discontinuous rocks." West Publishing Company.

Griggs, D.T., 1936. "Deformation of rocks under high confining pressures." J. Geol. 44, No. 5., p. 541.

Griggs, D.T., 1939. "Creep of rocks." J. Geol. 47, No. 3., p.225.

Griggs, D.T., 1940. "Experimental flow of rocks under conditions favoring recrystallization." Bull. Geol. Soc. Amer. 51., p. 1001.

Haefeli, R., 1953. "Creep problems in soils, snow and ice." Proc. 3rd ICOSOMEF, Vol. 3., Zurich., pp. 238-251.

Hald, A., 1952. "Statistical theory with engineering application." John Wiley and Sons, Inc.

Heim, A., 1882. "Uber Bersturze." Neujahrsblatt der Naturforschenden Gesellschaft, Zurich.

Hobbs, D.W., 1970. "Stress-Strain-Time behavior of a number of coal measure rocks." Int. J. of Rock Mech. and min. Sci. Vol. 7., pp. 149-170.

Hobbs, D.W., 1970. "The behavior of broken rock under triaxial compression." Int. J. Rock Mech. and Min. Sci. 7., pp. 125-148.

Hoek, E., 1968. "Brittle failure of rock." Rock Mechanics in Engineering Practices; Edited by K.G. Stagg and O.C. Zienkienwicz., Published by J. Wiley, London., pp. 99-124.

Hoek, E., 1970. "Estimating the stability of excavated slopes in open cast mines." Trans. Inst. Min. Metall. Section A., Vol. 79., p. 109.

Hoek, E., 1976. "Rock slopes." Pro. of a Specialty Conference, ASCE, Rock Engineering for Foundations and Slopes., Vol. 2., p. 157.

Hoek, E. and J.W. Bray, 1977. "Rock slope engineering." The Institution of min. and Metall., London.

Horn, H.M. and D.U. Deere, 1962. "Frictional characteristics of minerals." Geotechnique, Vol. 12., p. 319.

Jaeger, J.C., 1972. "Rock mechanics and engineering." Cambridge University Press, London.

Jaeger, J.C., 1971. "Friction of rocks and stability of rock slopes." Geotechnique, 21., pp. 97-134.

Kenty, J.D., 1970. "Suggested method of test for direct shear strength of rock core specimens." ASTM, Special Technical Publication, No. 479.

Krahn, J., 1974. "Rock slope stability." Ph.D. Thesis, Univ. of Alberta, Edmonton, Alberta.

Krsmanovic, D. and Z. Langof, 1964. "Large scale laboratory tests of the shear strength of rocky materials." Rock Mech. and Eng. Geol. Supplement 2, p. 20.

Kutter, H.K., 1971. "Stress distribution in direct shear test samples." Rock Fracture, Proc. of Symp. on Rock Mech., Nance, France.

Ladanyi, B. and G. Archambault, 1970. "Simulation of shear behavior of a jointed rock mass." Proc. 11th Symp. on Rock Mech., (AIME), p.105.

Lajtai, E.Z., 1969. "Shear strength of weakness planes in rock." Int. J. Rock Mech. and Min. Sci., 6., pp. 499-515.

Lane, K.S., 1975. "Field test sections save cost in tunnel support." Report from Underground Construction Research Council, ASCE.

Lo, K.Y. and Morton, 1975. "Tunnels in bedded rock with high horizontal stresses." 28th Can. Geotechnical Conference, Montreal.

Maslov, N.N. and T.V. Pavlisheva, 1974. "Creep and pseudocreep of rocks and their effect when estimating the stability of jointed rock masses." 3rd Cong. Int. Soc. Rock Mech., Denver., Vol. 2, Part A., p. 271.

Maurer, W.C., 1965. "Shear failure of rock under compression." J. Soc. Petrol. Engrs. (AIME) 5, pp. 167-176.

Michelson, A.A., 1917. "The laws of elastico-viscous flow." Int. J. Geol., 25, No.5, pp. 405-410.

Miller, R.P., 1965. "Engineering classification and index properties for intact rock." Ph.D. Thesis, U. of Illinois.

Mitchell, J.K., 1976. "Fundamentals of soil behavior." Series in Soil Engineering. John Wiley and Sons, Inc.

Mitchell, J.K., R.G. Campanella and A. Singh, 1968. "Soil creep as a rate process." J. Soil Mech. Fdn. Div. ASCE, 94, SM. 1., pp. 231-253.

Moore, D.F., 1969. "A history of research on surface texture effects." Wear, 13., pp. 381-412.

Murayama, S. and T. Shibata, 1961. "Rheological properties of clays." Proc. 5th Int. Conf. Soil Mech., Paris, 1., pp. 269-273.

Murrel, S.A.F., 1965. "The effect of triaxial stress systems on the strength of rocks at atmospheric temperature." Geophysics J. 10., pp.231-281.

Murrell, S.A.F. and A.K. Misra, 1962. "Time-dependent strain or creep in rocks and similar non-metallic materials." Bull. Inst. Min. Met., Vol. 71, Part 7, p. 353.

Myers, N.O., 1962. "Characteristics of surface roughness." Wear, pp. 182-189.

Nair, K., C.Y. Chang, R.D. Singh and A.M. Abdullah, 1973. "Time-dependent analysis to predict closure in salt cavity." 4th Symp. on Salt, Ohio., Vol. 2., pp. 129-139.

Noonan, D., 1972. "Fractured rock subjected direct shear." M.Sc. Thesis, Univ. of Alta., Edmonton, Alberta.

Obert, L. and W.I. Duvell, 1967. "Rock mechanics and the design of structures in rocks." John Wiley and Sons Inc., New York.

Ohnaka, M., 1975. "Friction characteristics of typical rocks." J. Phys. Earth, 23., pp. 87-112.

Osborn, 1975. "Advancing rock glacier in Lake Louise area, Banff." Can. J. of Earth Sci., Vol. 12, A, 75., pp. 1060-1062.

Patton, F.D., 1966. "Multiple modes of shear failure in rock." Proc. 1st Congress Int. Soc. Rock Mech., pp. 509-513.

Patton, F.D., 1966. "Multiple modes of shear failure and related materials." Ph.D. Thesis, Univ. of Illinois, Urbana.

Paulding, B.W., 1970. "Coefficient of friction of natural rock surfaces." Pro. ASCE, 96, SM. 2., 385-394.

Pearson, E.S. and H.O. Hartley, 1966. "Biometrika tables for statisticians." Vol.1.

Rengers, N., 1970. "Influence of surface roughness on the friction properties of rock planes." Pro. of 2nd congress of the Int. Soc. for Rock Mech., Vol. 1., pp.

229-234.

Renger, N., 1971. "Unebenheit under Reibungswiderstand Von Gesteinstrenrflachen." Diss. Tech. Hochschule Fridericiana Karsruhe, Ins. Bodenmech. Felsmech Veroff, 47., p. 129.

Ripley, C.F. and K.L. Lee, 1961. "Sliding friction tests on sedimentary rock specimens." 7th Int. Cong. Large Dams, Rome., Vol. 4, pp. 657-671.

Robertson, E.C., 1963. "Viscoelasticity of rocks." Int. Conf. on the State of Stress in the Earth's Crust, Santa Monica, California, pp. 181-220.

Ruiz, M.D. and F.P. Camarogo, 1966. "A large scale field shear test on rock." Proc. 1st Congress Int. Soc. for Rock Mech., Vol. 1, pp. 257-262.

Ruiz, M.D., et al, 1968. "Some consideration regarding the shear strength of rock masses." Proc. Int. Symp. on Rock Mech., Madrid, p. 159.

Sayles, R.S. and T.R. Thomas, 1976. "A stochastic explanation of some structural properties of a ground surface." Int. J. Prod. Res., 14., p. 641.

Sayles, R.S. and T.R. Thomas, 1977. "The spatial representation of surface roughness by means of the structure functions: a practical alternative to correlation." Wear, 42., pp. 263-276.

Schneider, H.J., 1974. "Rock friction - a laboratory investigation." 3rd Congress of Int. Rock Mech. Denver., pp. 311-315.

Schneider, H.J., 1976. "The friction and deformation behavior of rock joints." Rock Mech. 8., pp. 169-184.

Scholz, C.H., 1968. "Mechanism of creep in brittle rock." J. Geophys. Res. 73., pp. 32-95.

Scholz, C.H., 1972. "Detailed studies of frictional sliding

of granite and implication for the earthquake." J. of Geophysical Research., Vol. 77.

Scott, R.F. and H.Y. Ko, 1969. "Stress-deformation and strength characteristics." Proc. 7th Int. Conf. Soil Mech., Mexico State-of-the-Art., pp. 1-47.

Selwood, A., 1962. Wear, 5, p. 148.

Semple, R.M., A.J. Hendron and G. Mersi, 1973. "The efforts of time-dependent properties of altered rock on tunnel supported requirement." Federal Railway Administration, Department of Transportation, Washington, D.C.

Suklje, L., 1969. "Rheological aspects of soil mechanics." London: Wiley-Interscience.

Ter-Stepanian, G., S.R Meschian and R.R. Galstian, 1973. "Investigation of creep of clay soils at shear." Proc. 8th Int. Conf. Soil Mech. Moscow, 1-2., pp. 433-438.

Ter-Stepanian, G., 1975. "Creep of a clay during shear and its rheological model." Geotechnique, Vol. 25, No. 2., pp. 299-320.

Terzaghi, K. 1931. "The static rigidity of plastic clays." J. Rheology, 2, No. 3., pp. 253-262.

Terzaghi, K., 1946. "Rock defects and loads on tunnel supports, in rock tunnelling with steel supports." Commercial Shearing and Sampling.

Terzaghi, K., 1953. "Discussion on earth pressure, retaining walls, tunnels and shafts in soil." proc. 3rd Int. Conf. on Soil Mech. and Fnd. Engineering, Zurich, pp. 205-206.

Tsytovich, N.A., S.B. Ukhov and V.N. Burlakov, 1970. "Failure mechanism of a fissured rock base upon displacement of a loading plate." Proc. 2nd Cong. Int. Soc. Rock Mech., Belgrade., paper 3-13., Vol. 2.

Tsytovich, N.A., 1973. "Soil mechanics." (2nd ed.) Moscow:

Jzd "Vysshaya shkola".

U.S. Army Corps. of Engineers, 1963. "Project dribble petrographic examination and physical tests of cores, Tatum Salt Dome, Mississippi." Tech. Report No. 6-614, Vicksburg, Mississippi.

Vyalov, S.S., 1959. "Rheological properties and bearing capacity of frozen soils." Moscow: Acad. Sci. USSR.

Warwersik, W.R., 1972. "Time-dependent rock behavior in uniaxial compression." 14th Symp.Rock Mech., Penn.State, AIME.

Winkle, B.V., 1970. "Time-dependent analysis of rock mechanics problems." PhD. Thesis, Univ. of Colorado.

Zeigler, T.W., 1972. "Insitu tests for the determination of rock mass shear strength." U.S. Army Eng. Waterways Expt. Station, Tech. Report, S-72-12.

Appendix A

Design of load cells

Requirement: 5 load cells (1 of 4.5 kN; 2 of 11.12 kN and 2 of 22.24 kN capacity)

Material: Aluminum alloy 6061-T6 (extruded)

Properties: E (Young's modulus) = 6.9×10^{10} N/m^2 (10.0×10^6psi), 0.2% yield strength (tension) = 24×10^7 N/m^2 (35×10^3spi), ultimate strength (tension) = 26×10^7 N/m^2 (38×10^3psi), weight = 2.713×10^3 Kg/m^3 (0.098 lb/in^3).

Assumption made: Yield strength in compression = yield

Configuration of load cell:

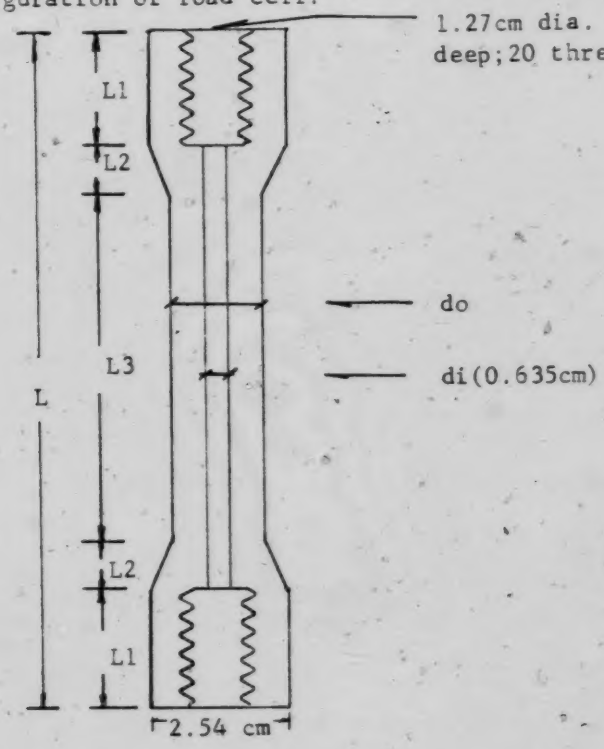

L = Total length of the load cell, 12.70 cm. This is the maximum available in the shear machine.

L1 = Allowable length of threaded portion on male connector.

L2 = Portion of load cell transiontal between regions L and L3. Its shape is such as to minimize stress concentrations due to difference in section in regions L1 and L3.

L3 = Working area of load cell. Strain gages are installed in this regicn.

d1 = The inner diameter. It is held constant, in all cases for ease of machining.

d0 = The outer diameter in the region L3. It varies with the design load.

Design procedure:

yield strength (factor of safety=2) = 12×10^4 kN/m^2

design load capacity = Y kN

required cross-sectional area, A = $Y/12 \times 10^4$ m^2

where:

$A = (d0^2 - d1^2)\ \pi/4$

$= (d0^2 - 0.635^2)\ \pi/4$ cm^2

Therefore, for a given load, y the unknown do can be found employing the following expression

$$(Y/12 \times 10^4)\ (100\ \text{cm})^2 = (d0^2 - 0.635^2)\ \pi/4\ \text{cm}^2$$

For an elastic column of length L3, the Euler buckling load is given by the formula

$$Pb = A\pi^2 E / (L3/r)^2$$

(Reference: Engineering Mechanics of Deformable Bodies by Byars and Snyder)

where Pb = buckling load

r = The radius of gyration about the bending or buckling axis of the load cell. It has the expression of $(d0^2-d1^2)^{0.5}$.

Dimensicns of load cells			
Y (kN)	4.5000	11.1200	22.2400
d0 (cm)	0.9385	1.2582	1.6622
d1 (cm)	0.6350	0.6350	0.6350
L (cm)	12.7000	12.7000	12.7000
L1 (cm)	2.5400	2.5400	2.5400
L2 (cm)	1.9100	1.2700	1.2700
L3 (cm)	3.8000	5.0800	5.0800
A (cm2)	0.3751	0.9266	1.8532
r (cm)	0.1728	0.2716	0.3840
pb (kN)	52.8200	180.3700	721.1200

Delocalization of stress concentrations in load cells resulting from maching:

To remove any stress concentrations, the following procedure was adopted:

(a) In a compression test machine,[1] the load cell was subjected to 110% of the design load, unload and reload manually to the same stress level.

(b) Upon unloading for a second time, 100% of the design load was applied for the first 5 minutes.

(c) The load was then reduced to 50% of the design load and maintained for half an hour after which time it was removed completely.

Strain Gages:

The following steps outline a procedure for the selection of strain gages and bonding them to load cells.

(1) Strain gage selection:

The installation procedure and operating characteristics of a particular type of strain gage are determined by the native of the

(i) strain-sensitive alloy

---

[1] The TINIUS OLSEN Testing Machine Co. Willow Grove, Pa., U.S.A.

(ii) backing (carrier) material

(iii) gage pattern (number, arrangement, and orientation of grids; grid width; solder tab type and configuration; etc.)

and (iv) self-temperature compensation number grid resistance (S-T-C)

One then selects the available strain gage combining parameters most compatible with the environmental and other operating constraints. These constraints are generally expressed in the form of requirements such as

- accuracy
- stability
- maximum elongation or contraction
- test duration
- cyclic endurance
- simplicity and ease of installation

CEA series strain gages were chosen for the present work. These gages are manufactured by Intertechnology LTD., Don Mills, Ontario. They have a gage designation of CEA-13-250 UW-350 (CEA, the coding symbol; 13, the S-T-C number; 250, the active gage length in mm; UW, the grid and tab geometry and 350, the resistance in ohms). The CEA gages are primarily used for general-purpose static and dynamic stress analysis. The constantan grids are completely encapsulated in polyimide, with large, integral, copper-coated terminals. (Reference: Strain gage selection TN-132, Micro-Measurments,

Vishay Intertichnology, Inc; Romulus, Michigan)

Each load cell was equipped with 4 CEA strain gages. The arrangement is shown below

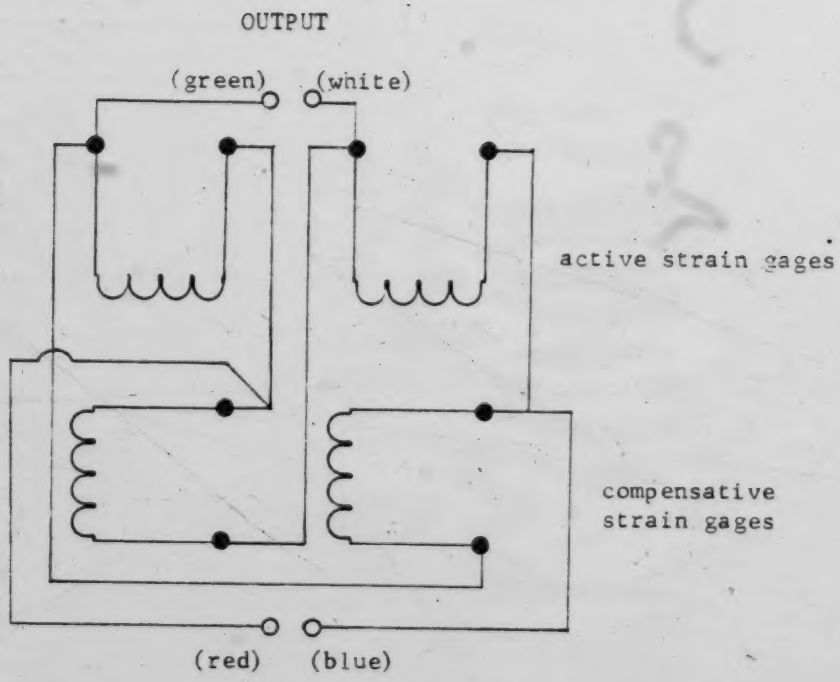

(2) Surface preparation for strain gage bonding:

The purpose of surface preparation of a load cell is to develop a chemically clean surface having a roughness appropriate to the gage installation requirements, a surface alkalinity corresponding to a ptt of 7 or 50, and visible gage layout lines for locating and orienting the strain gage. Listed below in the usual order of execution are the five basic steps:

(i) solvent degreasing - to remove oils, grease, organic contaminants, and soluble chemical residues

(ii) abrading - to remove any loosely bonded adherents and to develop a surface texture suitable for bonding

(iii) application of gage layout lines - to layout reference lines for strain gage placement

(iv) conditioning - to condition the surface with Conditioner A (Bulletin B-129 Vishay Intertechnology, Inc., Michigan)

(v) neutrlizing - to bring the surface condition back to an optimum alkalinity of 7.0 to 7.5 pH which is suitable for the strain gage adhesive system.

(3) Strain gage installation with adhesive:

Once the surface has been cleaned, the next step is to stick the strain gages on the surface with M-Bond 200

adhesive (manufactured by the Vishay Intertechnology, Inc. Michigan). It is an excellent general purpose laboratory adhesive.

(4) Protective coatings for strain gage application:

Strain gage installations require various degrees of protection to avoid gage instability and mechanical damage. Gages are easily degraded by an chemical attack. Moisture, fingerprints, etc. are all detrimental. While it is often practical, in the labortory, to operate fully encapsulated gages without additional protection, open faced gages should always have a suitable coating applied as soon as possible after installation. The M-coat D compounds manufactured by Intertechnology LTD. Don Mills Ontario, will handle the majority of gage protection requirements in this work. It serves as a moisture barrier and contaminant free cover.

Before applying the coating to an unprotected surface, dry the surface (region L3) throughly by heating. When cool, apply a coating of M-coat D on the surface. Generally, a thick coating offers a more difficult path for moisture absorption by strain gages than a thin one. Once coating is done, the protected load cell is then put into an oven for curing at an elevated temperature to ensure a permanent dry cover.

Delocalization of stress concentration in protected load cells resulting from strain gage installation:

The same compression machine as used in delocalization of stress concentration resulting from machining was employed. The loading pattern was also identical to that used previously except that in the first two sequences of loading 100% rather than 110% of the design load was applied.

The final stage in the preparation of load cells was their calibration. This was carried out in the direct shear box and creep machines using a "dead weight scale loader". The load cell was loaded to a known weight corresponding to a certain amount of "travel" in cm, on the x-y-y' plotter (in case of the shear box tests) or a certain "increment" in mili-volts on the data acquisition system (in case of the creep machine). The calibration factor was taken to be the unit weight per "travel", in N/cm and per "increment", in N/mv for the shear strength and creep tests respectively.

Appendix B

Derived results of direct shear strength test on artificially prepared Tyndall Stone and Standstead Granite surfaces

Rock sample	Stress drop kPa	Failure time t_f (min)	Shear stiffness K_s (kPa/cm)	Total friction angle (ϕ)
51842	916.04	1.7	13433.77	81.77
51421	863.40	2.3	9559.75	81.45
51111	584.98	0.8	21714.11	79.23
51112	868.85	4.8	5164.00	75.07
51662	1155.54	3.5	8775.25	77.85
511312	717.46	3.0	8105.98	74.79
51681	2598.95	2.9	21088.19	80.79
51561	1656.69	1.1	40575.56	77.48
51792	1046.45	2.1	14942.05	72.47
51632	2870.19	1.1	58543.99	81.25
51672	2394.51	2.9	23554.25	79.05
51742	1937.04	2.1	24914.33	75.82
51152	1626.95	2.4	20165.27	74.72
51841	2723.50	3.5	21010.52	74.91
51562	1822.63	1.3	42271.80	70.16
51791	3347.74	4.2	19921.57	76.67
51151	2746.55	2.3	31523.66	74.70
511022	467.20	1.2	24389.34	55.88
51451	939.85	1.2	36441.91	58.84
51342	1027.82	3.2	15303.24	61.64
51381	2146.18	2.0	33248.82	68.32
51692	2339.31	3.2	19847.74	67.40
51642	2380.02	3.0	25256.51	66.43
51641	2493.18	4.1	17593.72	65.39
51771	2517.81	3.6	19942.93	65.28
511242	3079.33	5.6	15990.45	66.11
51482	1629.02	5.5	14850.16	64.10
51782	2147.35	2.8	26147.49	61.56
51781	3118.45	3.6	27288.00	61.71
51632	2839.49	5.5	17499.27	61.22
51772	2577.98	3.4	27343.83	60.37
511021	4723.81	3.1	49136.88	66.54
519320	5986.02	4.3	41826.94	69.82
511042	6934.91	3.0	63919.90	70.98
51262	1995.82	4.3	28833.13	57.39
51331	5944.21	3.4	55015.82	67.02
511152	4063.27	3.2	51510.10	64.30
51712	3034.97	3.2	47835.99	58.85
51852	7947.90	3.8	63134.68	68.91
511041	5348.39	3.2	55276.33	62.38
51671	6140.86	3.7	50165.26	60.33
51422	6908.90	5.2	45873.26	66.09
511151	949.78	3.2	41600.68	48.21
51711	1292.02	3.3	44224.51	50.81
51831	4505.77	4.0	54535.28	58.78
51842	6271.55	3.4	70163.38	61.01

Derived results of direct shear strength test on artificially prepared Tyndall Stone surfaces

Rock sample	Stress drop kPa	Failure time t_f (min)	Shear stiffness K_s (kPa/cm)	Total friction angle (∅)
5392	1523.80	1.3	25458.05	84.30
53281	4515.70	2.9	31272.86	87.91
53211	1134.36	1.1	23688.71	82.77
53352	1546.77	1.6	20580.57	84.27
53332	3848.06	3.2	25788.08	85.42
53151	3198.56	1.9	36212.13	84.51
53331	1930.34	1.8	25999.14	81.96
53162	1946.97	3.0	14535.77	81.38
53161	1286.64	2.0	18346.87	74.88
53181	2888.34	1.3	54271.74	82.00
53182	1678.91	1.3	31637.49	76.45
53152	6745.02	2.2	76727.50	86.64
53322	3809.15	1.6	53318.63	81.19
5321	5022.09	1.6	68485.13	83.12
5322	7018.75	2.1	69960.13	84.86
53302	9611.97	3.4	59392.52	84.39
53342	6875.78	4.2	35528.99	82.43
53341	5588.03	2.4	51224.76	80.84
53132	4524.40	1.5	71224.75	76.10
5382	6391.81	1.9	77444.00	79.81
53351	8150.90	2.7	65924.38	81.55
53242	3993.72	3.1	33765.56	72.48
53241	7254.80	2.3	72470.25	78.79
5361	6545.96	2.0	76548.13	77.82
53132	6295.83	2.1	70490.19	75.00
53131	4143.31	1.8	65826.94	71.49
5381	10161.84	4.2	54729.81	80.21
5351	5791.86	2.1	71599.94	70.62
5352	7017.50	2.4	72215.63	73.03
53172	9235.03	2.9	75709.69	76.46
53171	7582.55	3.1	64584.54	71.73
5341	9790.27	2.8	85630.38	74.59
5342	8964.27	3.1	74118.06	73.95
53272	8241.08	3.0	72054.50	69.85
53271	9197.94	2.4	78582.31	67.19
5371	9199.70	4.9	50251.13	72.15
53141	8864.50	4.6	52378.58	68.99
5332	5953.66	2.8	68378.38	64.20
5372	7486.64	4.3	54203.14	68.35
53252	10540.23	3.6	75811.81	71.27
53311	8735.88	3.6	71635.31	67.70
53312	5475.29	5.1	39837.59	62.50
53321	8066.23	4.6	49934.50	65.28
5331	11868.14	4.0	79051.50	71.51
5391	9877.00	4.0	66623.19	65.94
53191	9927.72	5.9	43926.80	65.34
53192	12218.93	4.5	73733.50	68.28
53142	9009.26	7.6	35678.14	64.01

Derived results of direct shear strength test on artificially prepared Standstead Granite surfaces

Appendix C

Results of two surface characterizations (Z2 and SF)
for the surface profiles of Tyndall Stone
and Standstead Granite surfaces

Rock surface number	Maximun value of ZZ	Maximun value of SF	Average value of ZZ	Average value of SF
51842	0.4969	0.0189	0.4394	0.0162
51421	0.4142	0.0152	0.3833	0.0125
51111	0.5576	0.0120	0.4121	0.0110
51112	0.4733	0.0160	0.4102	0.0142
51662	1.1187	0.0160	0.8673	0.0131
511312	0.4081	0.0146	0.3640	0.0120
51681	0.4064	0.0141	0.3793	0.0126
51561	0.4027	0.0152	0.3967	0.0133
51792	0.3643	0.0117	0.3616	0.0112
51632	2.6183	0.0172	1.1508	0.0157
51672	0.3378	0.0109	0.3305	0.0104
51742	0.3705	0.0117	0.3347	0.0102
51152	0.7583	0.0216	0.4986	0.0156
51841	0.3560	0.0120	0.3352	0.0104
51562	0.4536	0.0192	0.3563	0.0126
51791	0.2982	0.0086	0.2739	0.0074
51151	0.4370	0.0156	0.3628	0.0115
511022	0.4218	0.0160	0.3889	0.0137
51451	0.6953	0.0190	0.5338	0.0168
51342	0.8512	0.0255	0.5922	0.0208
51381	0.7440	0.0279	0.5087	0.0183
51692	0.6227	0.0292	0.5559	0.0252
51642	0.5117	0.0268	0.4728	0.0232
51641	0.5991	0.0339	0.5673	0.0303
51771	0.4754	0.0215	0.4588	0.0194
511242	0.5768	0.0317	0.5531	0.0266
51482	0.4684	0.0170	0.4079	0.0137
51782	0.9537	0.0263	0.7108	0.0256
51781	0.5686	0.0279	0.4750	0.0203
51632	0.6046	0.0308	0.5778	0.0274
51772	0.5798	0.0286	0.5491	0.0249
511021	0.4116	0.0154	0.3385	0.0108
51932	0.4680	0.0162	0.4014	0.0135
511042	0.6866	0.0096	0.4309	0.0086
51262	0.4253	0.0159	0.3864	0.0131
51331	0.5846	0.0139	0.4409	0.0128
511152	0.6449	0.0227	0.5119	0.0173
51712	0.4256	0.0141	0.3778	0.0118
51852	0.4032	0.0149	0.3822	0.0130
511041	0.6063	0.0231	0.5191	0.0196
51671	0.4690	0.0174	0.4017	0.0139
51422	0.4161	0.0160	0.3735	0.0130
511151	0.3700	0.0133	0.3612	0.0121
51711	0.4240	0.0157	0.3928	0.0127
51831	0.4533	0.0177	0.3872	0.0140
51842	0.4097	0.0146	0.3903	0.0135

Results of two surface characterizations(Z2 and SF)for the surface profiles of Tyndall Stone fractures

Rock surface number	Maximun value of Z2	Maximun value of SF	Average value of Z2	Average value of SF
5392	0.5002	0.0206	0.4697	0.0172
53281	0.5316	0.0218	0.5038	0.0196
53211	0.4588	0.0212	0.4895	0.0199
53352	0.4921	0.0184	0.3883	0.0151
53332	0.9188	0.0203	0.3708	0.0131
53151	0.6118	0.0272	0.6072	0.0152
53331	0.4588	0.0155	0.5017	0.0205
53162	0.3884	0.0145	0.4137	0.0137
53161	0.4280	0.0157	0.7275	0.0236
53181	0.5310	0.0217	0.4031	0.0135
53182	0.4758	0.0183	0.4534	0.0157
53152	0.8271	0.0268	0.4952	0.0198
53322	0.4538	0.0202	0.6532	0.0189
5321	0.4546	0.0196	0.4196	0.0164
5322	0.9667	0.0204	0.3960	0.0153
53302	1.1768	0.0361	0.7717	0.0310
53342	0.5308	0.0257	0.4695	0.0207
53341	0.4786	0.0211	0.4431	0.0180
53132	0.4522	0.0194	0.4086	0.0159
5382	0.4703	0.0213	0.4672	0.0209
53351	0.4913	0.0228	0.4159	0.0165
53242	0.4451	0.0191	0.5349	0.0239
53241	0.6246	0.0314	0.3848	0.0143
5361	0.5261	0.0233	0.4244	0.0167
53132	0.4919	0.0218	0.3825	0.0130
53131	0.4297	0.0155	0.4344	0.0176
5381	0.5384	0.0247	0.4617	0.0196
5351	0.4818	0.0222	0.4952	0.0210
5352	0.5060	0.0195	0.4760	0.0175
53172	0.5690	0.0259	0.4507	0.0192
53171	0.5024	0.0209	0.4542	0.0184
5341	0.5596	0.0272	0.5199	0.0235
5342	0.5537	0.0276	0.5022	0.0230
53272	0.5054	0.0232	0.4246	0.0178
53271	0.4325	0.0187	0.4809	0.0212
5371	0.5562	0.0252	0.4802	0.0187
53141	0.4837	0.0177	0.4162	0.0147
5332	0.4453	0.0170	0.4297	0.0154
5372	0.4471	0.0168	0.4954	0.0194
53252	0.5672	0.0229	0.4076	0.0131
53311	0.6757	0.0341	0.3840	0.0124
53312	0.4104	0.0138	0.4376	0.0147
53321	0.4635	0.0170	1.2966	0.0154
5331	3.1300	0.0243	0.5925	0.0278
5391	0.4969	0.0192	0.4830	0.0182
53191	0.4311	0.0135	0.3867	0.0114
53192	0.4771	0.0178	0.4023	0.0133
53142	0.4595	0.0164	0.4272	0.0147

Results of two surface characterizations(Z2 and SF)for the surface profiles of Standstead Granite fractures

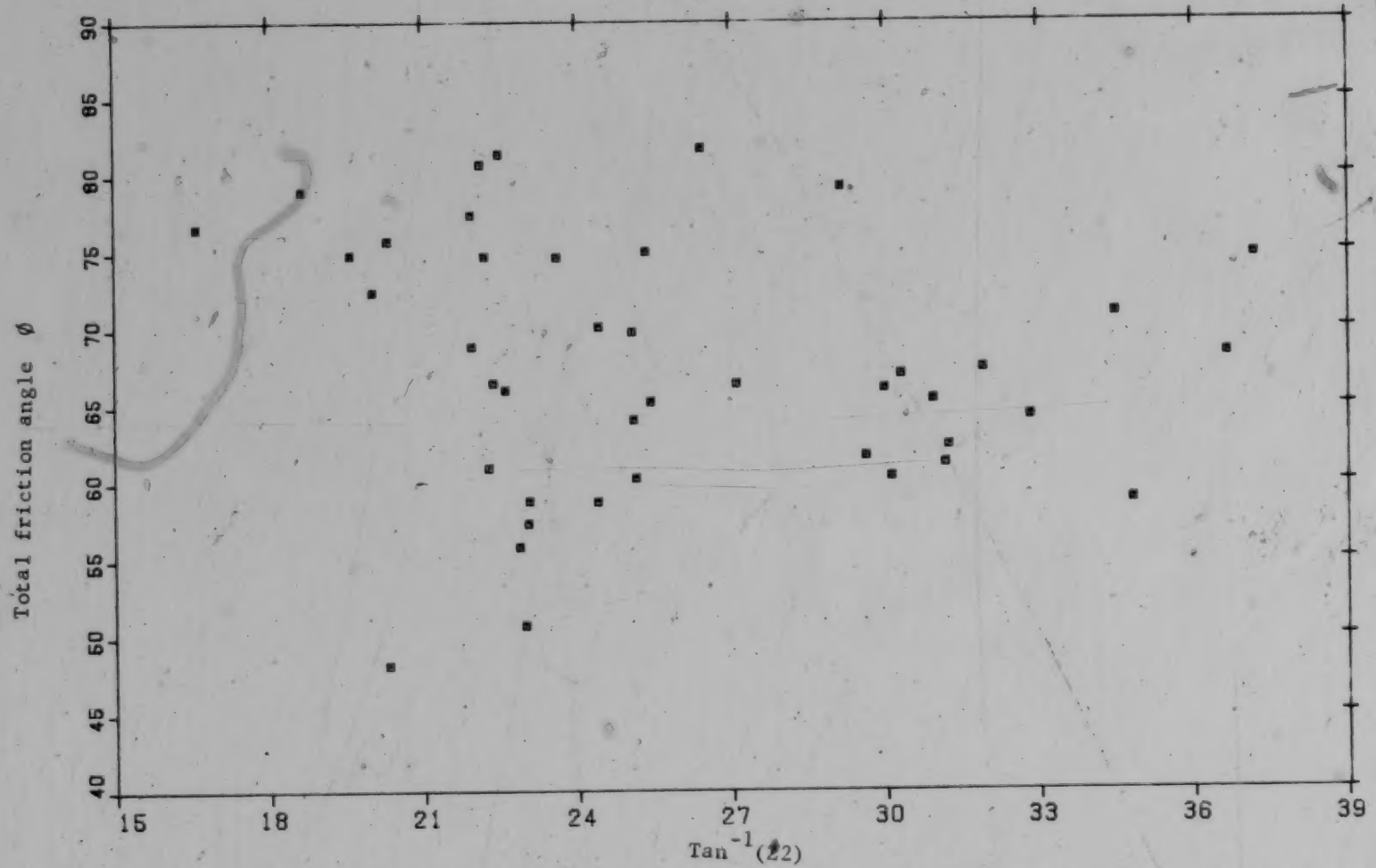

The total friction angle, arctan(peak/normal stress) versus the largest value of arctan(Z2) measured on the rock surface(Tyndall Stone).

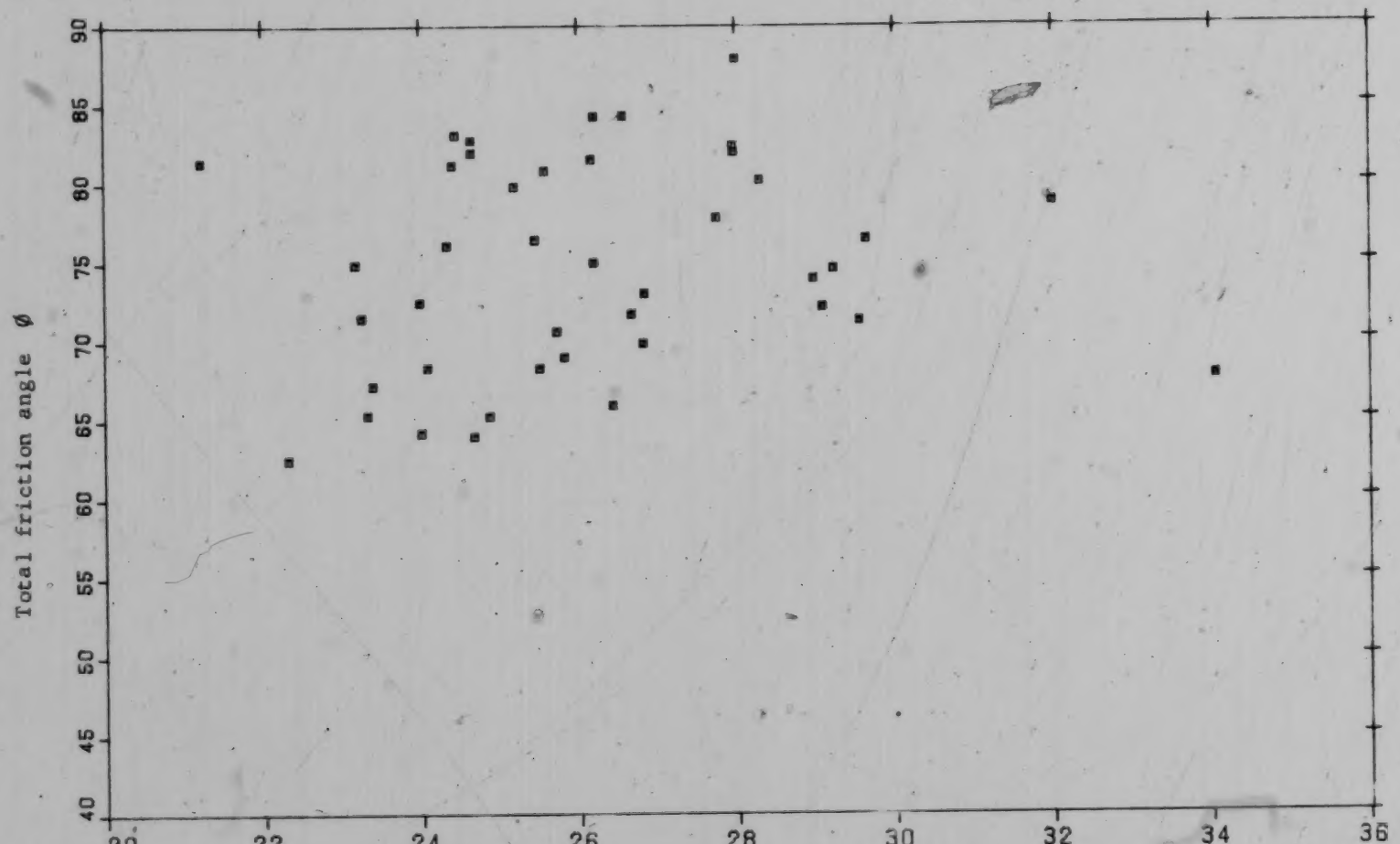

The total friction angle,arvtan(peak/normal stress)versus the largest value of arcatn(Z2) measured on the rock surface(Standstead Granite).